Department of Molecular & Clinical Cancer Medicine
Institute of Translational Medicine

Tumour Metabolism in Squamous Cell Carcinoma of the Head & Neck: Consequences & Potential Therapeutic Implications of *TP53* Mutation

Thesis submitted in accordance with the requirements
of the University of Liverpool for the degree of Doctor in Philosophy

by

Mark David Wilkie

November 2017

Table of Contents

I. Abstract

Survival outcomes for traditional Human papillomavirus (HPV)-negative squamous cell carcinoma of the head and neck (SCCHN) have not improved significantly over the last 20-30 years. In contrast, HPV-positive oropharyngeal SCC is associated with favourable survival outcomes, but patients often suffer long-term functional ramifications from the toxicity of their treatment. Therefore, in the context of HPV-negative SCCHN there is a need to improve treatment efficacy to enhance survival outcomes, while for HPV-positive oropharyngeal SCC there is a need to minimise treatment-associated toxicity. Fundamental to this is to identify novel radiosensitising therapeutic approaches given that radiotherapy (RT) remains a mainstay of treatment for all SCCHN patients. Cancer cell metabolism is an attractive putative target in this regard, yet has received relatively little attention in the context of SCCHN. p53 is known to be a potentially important metabolic mediator, while *TP53* mutation is central to SCCHN oncogenesis and is associated with poorer clinical outcomes. Consequently, the primary of aims of thesis these were to examine the metabolic phenotype exhibited by SCCHNs, whether this was related to *TP53* status, and to determine whether tailored anti-metabolic treatment might have potential therapeutic value, specifically in enhancing the effects of ionising radiation (IR). Secondary aims were to explore the mechanistic basis underlying any metabolic alterations and any observed anti-metabolic therapeutic effects.

Microplate-based extra-cellular flux analysis revealed that mutant *TP53* SCCHN cell lines exhibited a distinct metabolic phenotype to that of wild-type *TP53* cell lines. Wild-type *TP53* cells maintained metabolic diversity, while mutant *TP53* cells exhibited a specific survival dependence on glycolysis. This correlated with radiation response following glycolytic inhibition with 2-deoxy-D-glucose (2-DG), which potentiated IR effects in mutant *TP53* cells only. In line with their more diverse metabolic phenotype, in wild-type *TP53* cells (HPV-positive SCCHN cells included) a broader anti-metabolic approach, comprising both 2-DG and metformin (inhibitor of mitochondrial respiration), was required to achieve a similar effect.

The potentiating effects of glycolytic inhibition on IR in mutant *TP53* SCCHN cells were reversed by the addition of N-acetylcysteine (free radical scavenger). Consistent with this, flow cytometry demonstrated a marked increase in reactive oxygen species (ROS) following IR + 2-DG, and also increased levels of apoptosis, implicating oxidative stress-

mediated activation of apoptotic signalling as the mechanism underlying the radiosensitising effects of 2-DG. That oxidative stress was centrally involved in the mechanism underlying glycolytic inhibition in SCCHN also suggested that the impetus driving mutant *TP53* SCCHN cells towards glycolysis was at least partly to regulate cellular redox status and evade excessive ROS accumulation. In accordance with this, pentose phosphate pathway (PPP) enzyme expression and intracellular NADPH/NADP ratios were greater in mutant *TP53* SCCHN cells, indicative of increased PPP flux. This appeared to be mediated by de-regulated TIGAR overexpression in those cells with loss of p53 function. Therapeutically, the addition of the PPP inhibitor 6-aminonicotinamide further potentiated IR effects in mutant *TP53* cells over and above glycolytic inhibition.

Ultimately, the findings described in this thesis present the opportunity for a novel, tailored anti-metabolic therapeutic approach in SCCHN, which not only carries a selective therapeutic index, but is also informed by *TP53* status as a predictive biomarker. Specifically, we propose that in mutant *TP53* SCCHNs glycolytic inhibition with 2-DG, possibly in combination with 6-AN-induced PPP inhibition, would result in significant radiosensitisation. This strategy would be applicable in upwards of 60-85% of SCCHN tumours and would be preferentially effective in targeting the treatment-resistant disease typically associated with *TP53* mutation. For SCCHNs harbouring wild-type *TP53* (HPV-positive disease included) we suggest the combination of 2-DG with metformin. This strategy may also provide an attractive platform for the treatment de-intensification of carefully selected HPV-positive cases by facilitating RT dose reduction to minimise the impact of treatment on long-term function. The efficacy and safety of these strategies will require further validation in pre-clinical models prior to translation into the clinical setting, and future work will be directed in this regard.

II. Acknowledgements

I would like to thank my supervisors Professors Mark Boyd and Terry Jones, and Dr. Nikolina Vlatkovic for their guidance and support throughout my PhD studies.

Thanks are due to all those who assisted or advised me during the project from the Department of Molecular and Clinical Cancer Medicine. Special mentions are due to Dr. Jane Armstrong of the Pancreas Biomedical Research Unit for her expertise with the Seahorse XF24 instrument and Dr. Kathy Till who assisted with use of the flow cytometers.

I would also like to express my appreciation to all the members of the laboratory for providing a friendly work environment, especially to my friend Andrew Lau, from whom I learnt a lot and who supported me during my studies.

I am grateful for the support of Cancer Research UK and The Royal College of Surgeons of England. Their support, both financial and practical, has been invaluable in driving this research.

Finally, to my family I owe everything. Specifically, to my beautiful daughter Madeleine; you always give me perspective, to my wife Kate; for your constant love and support and for never ceasing to be there for me, and to my parents, Maureen and David; for your enduring support, without which I would have never made it this far. Last but not least, no family acknowledgement would be complete without mention of my dog, Fabio, who has provided welcome distraction and entertainment throughout!

III. Declarations

The studies described in this thesis are my own work performed during the course of my PhD studies at the University of Liverpool between August 2013 and July 2016 inclusive.

All the experiments described were performed by me with the exception of some of the STR profiling and mycoplasma testing experiments. Verification and optimisation of the cell lines used in our laboratory was the combined work of myself and another PhD student (Mr. Andrew Lau), with the assistance of Dr. Carolyn Rainer (University of Liverpool).

This thesis was written entirely by me under the valued guidance of my supervisors, Professors Mark Boyd and Terry Jones, and Dr. Nikolina Vlatkovic.

IV. List of Figures

1. Introduction:

2. Materials and Methods:

3. Results:

5. Appendix:

V. List of Tables

2. Materials and Methods:

VI. Abbreviations

2-DG 2-deoxy-D-glucose

3-BP 3-bromopyruvate

6-AN 6-aminonicotinamide

6-PGD 6-phosphogluconate dehydrogenase

^{18}F-FDG 2-deoxy-2-(^{18}F)fluoro-D-glucose

µL Microlitre (10-6 litre)

µg Microgram (10-6 gram)

µm Micrometer (10-3 meter)

ADH1B Alcohol dehydrogenase 1B

ADP Adenosine diphosphate

AJCC American Joint Committee on Cancer

AMP Adenosine monophosphate

AMPK AMP-activated protein kinase

Apaf-1 Apoptosis protease activating factor-1

APS Ammonium per sulphate

ATM Ataxia telangiectasia mutated

ATP Adenosine triphosphate

ATR ATM-related

BH Bcl-2 like homology

BSA Albumin from bovine serum

cDNA Complementary DNA

CDK Cyclin-dependent kinase

Chk Checkpoint kinase

CI Confidence interval

CISH Chromogenic in-situ hybridisation

COX Cytochrome c oxidase

CPT1C Carnitine palmitoyltransferase 1C

CRT Chemoradiotherapy

CT Computed tomography

DCA Dichloroacetic acid

DCF 2′,7′-di-chlorofluorescein

DCF-DA 2'-7'-Dichlorodihydrofluorescein diacetate

DISC Death-inducing-signalling-complex

DMEM Dulbecco's modified Eagle's medium

DMSO Dimethyl sulphoxide

DNA Deoxyribonucleic acid

ECAR Extracellular acidification rate

ECS Extra-capsular spread

EDTA Ethylenediaminetetraacetic acid

EGTA Ethylene glycol-bis(β-aminoethyl ether)-N,N,N',N'- tetracetic acid

EGF Epidermal growth factor

EGFR Epidermal growth factor receptor

ETC Electron transport chain

FADD Fas-associated death domain protein

FAD(H_2) Flavin adenine dinucleotide (reduced)

FASN Fatty acid synthase

FasR Fas receptor

FCCP Trifluoromethoxy carbonyl cyanide phenylhydrazone

FBS Foetal bovine serum

FITC Fluorescein isothiocyanate

FS Forward scatter

G6PD Glucose-6-phosphate dehydrogenase

GADD45 Growth arrest and DNA-damage-inducible protein 45

GFP Green fluorescent protein

GLUT Glucose transporter

GOF Gain-of-function

GPX 1 Glutathione peroxidase 1

GSH Glutathione (reduced)

Gy Gray

HIF-1α Hypoxia inducible factor 1 alpha

HPV Human papillomavirus

HRP Horseradish peroxidase

IGFBP3 IGF-binding protein-3

IMRT Intensity-modulated radiotherapy

IMS Intermembrane space

IR Ionising radiation

ISH In-situ hybridisation

LDH Lactate dehydrogenase

LOH Loss of heterozygosity

MAS Mitochondrial assay solution

MAS NMR Magic angle spinning nuclear magnetic resonance

MCT-1 Monocarboxylate transporter-1

MCT-4 Monocarboxylate transporter-4

MDM2 Murine double minute 2

MDMX Murine double minute X

Mieap Mitochondria-eating protein

MOM Mitochondrial outer membrane

MOMP Mitochondrial outer membrane permeabilisation

MRI Magnetic resonance imaging

mRNA Messenger ribonucleic acid

mTOR Mammalian target of rapamycin

MTT N,N-dimethylformamide 3-(4,5-dimethylthiazol-2-yl)-2,5-diphenyl tetrasodium bromide

NAC N-acetyl cysteine

NAD(H) Nicotinamide adenine dinucleotide (reduced)

NADP(H) Nicotinamide adenine dinucleotide phosphate (reduced)

NF-κB Nuclear factor-κB

NMR Nuclear magnetic resonance

NS Not significant

OCR Oxygen consumption rate

OR Odds ratio

PAGE Polyacrylamide gel electrophoresis

PBS Phosphate buffered saline

PCNA Proliferating cell nuclear antigen

PCR Polymerase chain reaction

PDC Pyruvate dehydrogenase complex

PDK Pyruvate dehydrogenase kinase

PE Plating efficiency

PET Positron emission tomography

PFK-1 Phosphofructokinase-1

PGAM Phosphoglycerate mutase

PI Propidium iodide

PI3K-AKT Phosphatidylinositol 3-kinase/protein kinase-B

PIDD p53-induced protein with a death domain

PIGs p53-induced genes

PKM1 Pyruvate kinase M1

PKM2 Pyruvate kinase M2

PMP Plasma membrane permeabiliser

PMSF Phenylmethylsulphonyl fluoride

PPP Pentose phosphate pathway

PS Phosphatidylserine

PTEN Phosphatase and tensin homologue

Rb Retinoblastoma

RE Response element

RNA Ribonucleic acid

RNase Ribonuclease

ROS Reactive oxygen species

RR Relative risk

RT Radiotherapy

SA-βgal Senescence-associated β-galactosidase

SCCHN Squamous cell carcinoma of the head and neck

SCID Severe combined immunodeficiency

SDS Sodium dodecyl suphate

SEM Standard error of the mean

SESN1 Mammalian sestrin homologue

SF Surviving fraction

SH3 Src homology 3 domains

shRNA Short-hairpin RNA

SLIP Stuart Linn immunoprecipitation

SS Side scatter

STI Trypsin inhibitor from soybean

STR Short tandem repeat

TCA Tricarboxylic acid

TEMED N, N, N', N'-tetramethylenediamine

TIGAR TP53-inducible glycolysis and apoptosis regulator

TGF-α Transforming growth factor-α

TKTL1 Transketolase-like protein

TMPD *N,N,N′,N′*-tetramethyl-*p*-phenylenediamine dihydrochloride

TNF Tumour necrosis factor

TNF-R Tumour necrosis factor receptor

TSC2 Tuberous sclerosis protein 2

UICC Union for International Cancer Control

UK United Kingdom

US United States

UV Ultraviolet

XF Extracellular flux

X-gal 5-Bromo-4-chloro-3-indolyl β-D-galactopyranoside

1. Introduction

1.1. Squamous cell carcinoma of the head and neck

1.1.1. Definition and regional anatomy

The broad terms "head and neck cancer" and "squamous cell carcinoma of the head and neck" (SCCHN) are used interchangeably to describe collectively malignant tumours arising from the epithelial lining of the upper aerodigestive tract, which encompasses the oral cavity, pharynx, and larynx(1, 2). Although cancers of other histopathological types may arise from this anatomical region, squamous cell carcinomas account for the overwhelming majority (>90%)(1, 2), and are thus the exclusive focus of this thesis. It is also important to note that other cancers occurring in the head and neck region, such as salivary gland, thyroid, intra-cranial, and cutaneous malignancies are excluded from this definition.

Although SCCHN is often considered as one disease, tumours can be stratified on the basis of their anatomical subsite of origin (figure 1.1.1.1), which influences biological behaviour and from a clinical perspective has implications for diagnosis, staging, treatment, and prognosis(1, 3, 4). The four common subsites of SCCHN are as follows: oral cavity, oropharynx, larynx, and hypopharynx, with oral cavity being the most common site of origin (≈40%)(5). Although the nasopharynx is also technically an SCCHN subsite, nasopharygeal carcinoma is generally regarded as a separate clinicopathological entity given its distinct clinical behaviour(1, 6) and is not considered further here. The oral cavity extends from the lips anteriorly to the junction of the anterior 2/3 and posterior 1/3 of the tongue posteriorly, the palatoglossal arch posterolaterally, and the hard palate superiorly(5). Posteriorly, the oral cavity then communicates with the oropharynx, which is bounded by the soft palate superiorly, the base of the tongue (posterior 1/3 of the tongue) to the level of the epiglottis inferiorly, the palatoglossal and palatopharyngeal arches laterally, and the posterior pharyngeal wall posteriorly(5). Particularly important constituent parts of the oropharynx in relation to Human papillomavirus (HPV)-positive SCCHN (discussed in section 1.1.2.) are the collections of lymphoid tissue at the base of tongue and on either side of the oropharynx in the cleft between the palatoglossal and palatopharyngeal arches – the lingual and palatine tonsils respectively(5). These areas, particularly the palatine tonsils, seem to be disproportionally affected by HPV-related disease, although the reasons for

this remain to be fully elucidated. Inferior to the oropharynx lies the larynx, which communicates with the pharynx through the laryngeal inlet. The larynx extends from the laryngeal surface of the epiglottis superiorly to the inferior edge of the cricoid cartilage inferiorly, is bounded anteriorly by the thyrohyoid membrane and anterior laryngeal cartilages, and posterolaterally by the aryepiglottic folds, the arytenoid region, and the posterior aspect of the cricoid cartilage(5). The remainder of the pharynx, which surrounds the larynx posteriorly and laterally, extends inferiorly from the oropharynx (specifically from the level of the superior aspect of the hyoid bone) to the level of the inferior border the cricoid cartilage and constitutes the hypopharynx(5).

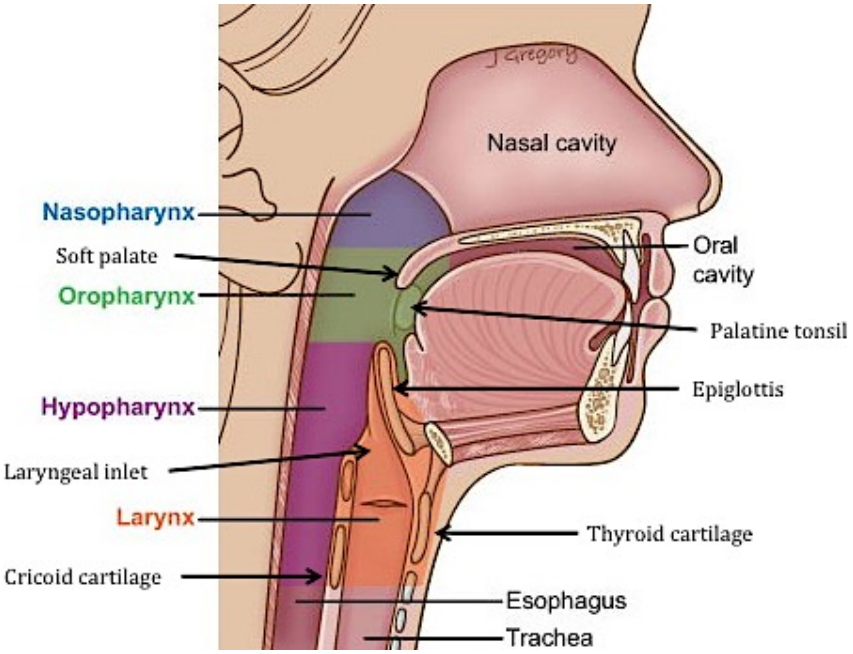

Figure 1.1.1.1: Anatomical sub-sites of the head and neck. A diagrammatic representation of the different anatomical sub-sites of the head and neck relevant to SCCHN including pertinent regional anatomy. Figure adapted from (7).

As would be expected on the basis of regional anatomy, the upper aerodigestive tract plays critical functional roles in mastication, speech, voice, and swallowing. Clinical presentation often reflects this and significant functional ramifications can result from both the tumour itself and subsequent cancer treatment. In general, for tumours of the oral cavity and oropharynx more anterior lesions tend to alter speech and mastication to a larger extent, while more posterior lesions result in greater swallowing impairment(8, 9). More distal tumours affecting the larynx and hypopharynx tend to carry both voice and swallowing functional morbidity(1, 2).

1.1.2. Epidemiology and risk factors

SCCHN is the sixth most common cancer globally and represents around 6% of all cancer cases, with an estimated incidence of 800,000 cases per year, approximately 11,000 of which arise in the United Kingdom (UK)(10, 11). Although subtle differences exist between SCCHN subsites, the incidence of SCCHN is strongly and directly related to age: the median age at diagnosis is over 60 years old, and 98% and 50% of patients in Europe are over 40 and 60 years old at diagnosis respectively(12). There is also a significant male preponderance, particularly for laryngeal cancer, with a male:female gender ratio of approximately 10:1 in developed countries(10, 11). These demographic patterns are depicted clearly in the context of the UK population in figure 1.1.2.1.

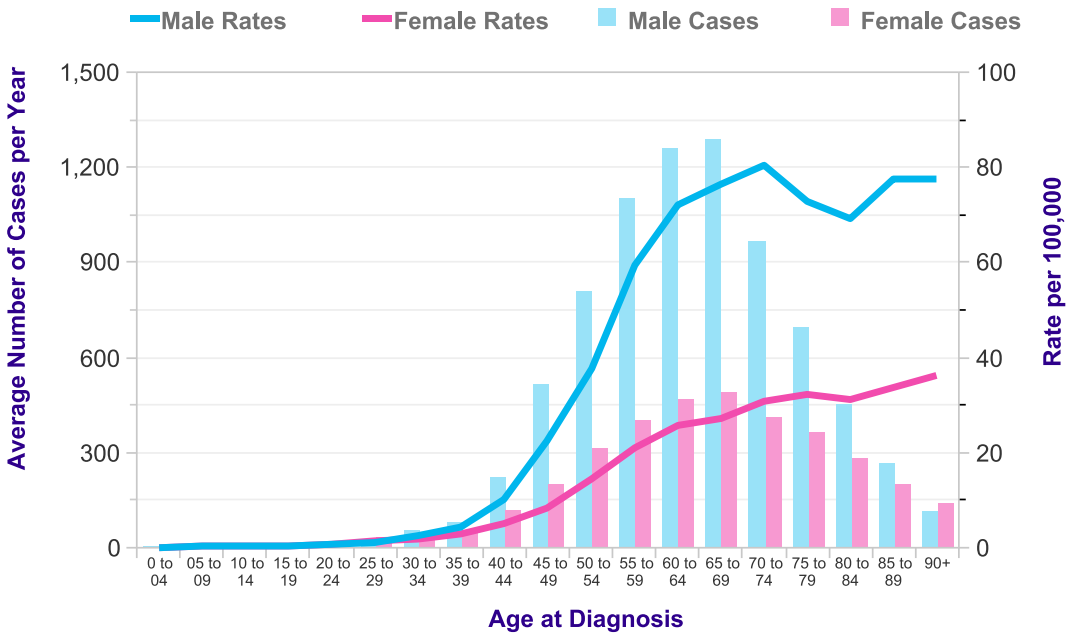

Figure 1.1.2.1: Age-specific incidence rates of SCCHN in the UK. Graphs illustrating both the average number of new cases/year, and the age-specific incidence rates in the UK in 2012-2014 for SCCHN. There is a clear increase in incidence from the age around 40 with a peak in the sixth decade, and a marked male preponderance in this age group. Figure reproduced from Cancer Research UK website(11).

The incidence of SCCHN varies quite considerably around the world(10, 12), indicative of a strong environmental component to disease pathogenesis and geographical differences in the prevalence of risk factors. With respect to oral cavity cancer, high-risk areas include Melanesia (a sub-region of Oceania, northeast of Australia) and south-central Asia, western and southern Europe, and southern Africa. In contrast, for

laryngeal cancer, prevalence is highest in southern and eastern Europe, South America, and western Asia(10, 12). However, it is also important to note that this may also partly reflect varying data quality worldwide.

The major risk factors in the development of SCCHN are consumption of tobacco and alcohol, which have a synergistic effect and together are implicated in 75% of all SCCHNs(13). Both tobacco and alcohol increase the risk of developing SCCHN in a dose-dependent manner, and the combination of tobacco and alcohol confers an estimated relative risk (RR) of 22 (95% confidence interval [CI]: 12.9-37.8)(14). The fact that many tobacco and alcohol users tend to consume both substances has made distinguishing the independent associations of these individual agents challenging. Nonetheless, tobacco smoking has been reported to increase the risk of SCCHN at all anatomical subsites with a RR of 8.4 for current smokers (95% confidence interval [CI]: 5.8-12.2)(15), while the risk decreases gradually after stopping smoking, with no excess risk after more than 20 years of cessation(15). Similarly, smokeless forms of tobacco, such as oral snuff or the chewing of betel quid (a preparation of various ingredients, including tobacco and the seeds of the betel palm wrapped in a betel leaf), also carry an increased risk of SCCHN, specifically oral cavity cancer, which has been estimated as high as a RR of 2.6 (95% CI: 1.3-5.2)(reviewed in(16)). In relation to alcohol consumption, a pooled analysis of 15 case-control studies revealed that non-smokers who consume three or more alcoholic drinks a day have approximately double the risk of developing SCCHN compared with non-drinkers (odds ratio [OR] = 2.04, 95% CI: 1.29-3.21)(17), with the relative effect being strongest for pharyngeal cancers, reported to be as high as 8.5 (95% CI: 4.0-18.2) in an individual study(15).

Interestingly, selected genetic polymorphisms in genes encoding enzymes involved in the metabolism of tobacco and alcohol can influence individual susceptibility to these risk factors. For instance, the gene that encodes the alcohol metabolising enzyme alcohol dehydrogenase 1B (ADH1B) (involved in oxidation of ethanol to acetaldehyde in the liver) has a polymorphism that enhances alcohol-oxidising capability, known as allele ADH1B*2, which has been reported to confer a significant protective effect in the risk of SCCHN development in moderate and heavy drinkers (ORs of 0.57 [95% CI: 0.36-0.91] and 0.36 [95% CI: 0.17-0.77] respectively)(18). In contrast, a polymorphism in the gene encoding aldehyde dehydrogenase 2, the major enzyme that converts acetaldehyde into acetate, results in inactivation of the enzyme and increased accumulation of acetaldehyde, which significantly heightens the risk of SCCHN development in the

context of alcohol consumption(19). Similarly, in relation to tobacco, a polymorphism in the gene encoding glutathione-S-transferase, which is involved in the detoxification of carcinogenic metabolites, is associated with a 1.23 fold (95% CI: 1.06-1.42) increased risk of developing SCCHN(13).

Whilst tobacco and alcohol consumption are the traditional risk factors, there is now a considerable body of evidence implicating HPV as a cause of SCCHN, in particular of oropharyngeal SCC affecting the base of tongue and tonsils, which according to the International Agency for Research on Cancer monograph fulfils the criteria for causality(20). More than 170 different HPV types have been identified to date, of which types 16, 18, 31, 33, 35, 39, 45, 51, 52, 56, 58, 59, 68, 73, and 82 are considered "high-risk" and carcinogenic(21). Such oncogenic HPVs have long been recognised as the major cause of cervical cancer(21), and nearly 30 years ago it was first suggested that certain high-risk HPVs may also be involved in the pathogenesis of SCCHN(22). Numerous observational case-series published throughout the 1990s and early 2000s evaluated the point prevalence of HPV infection in SCCHN with varying results. This culminated in a large-scale systematic review in 2005 of over 5,000 SCCHN specimens from 60 studies, which concluded that overall prevalence of HPV infection was 25.9% (95% CI: 24.7-27.2%), with the overwhelming majority (86.7% of oropharyngeal SCC, 95% CI: 82.6-90.1%) being associated with HPV-16(23). Type 18 was also found to account for a significant minority (2.8% of oropharyngeal SCC, 95% CI: 82.6-90.1%), while other HPV types were rarely implicated(23). A further prominent finding from this study was the propensity for HPV infection to affect tumours arising in the oropharynx, with over one third (35.6%, 95% CI: 32.6-38.7%) of oropharyngeal SCCs containing HPV DNA (87% of which were HPV-16)(23). Similarly, a subsequent meta-analysis demonstrated a strong association between HPV-16 and tonsillar SCC specifically (OR = 15.1, 95% CI: 6.8-33.7), a moderate association with other oropharyngeal SCCs (OR = 4.3, 95% CI: 2.1-8.9), and weak association for oral cavity and laryngeal SCCs (OR = 2.0, 95% CI: 1.2-3.4; and OR = 2.0, 95% CI: 1.0-4.2 respectively)(24). Consistent with this, a more recent meta-analysis from 2013 seeking primarily to determine the chronology of HPV prevalence in SCCHN reported a prevalence of 72.2% (95% CI: 52.9–85.7%) in oropharyngeal SCCs between 2005 and 2009, while only 6.1% (95% CI: 0.7-39.0%) of SCCHNs outside of the oropharynx were found to be attributable to HPV-16 infection during the same time period(25). In addition to viral DNA presence, several studies have corroborated a causal relationship in these tumours, demonstrating localisation of HPV DNA to the cell nucleus(26), viral

DNA integration(26, 27), elevated viral copy number in malignancy(28), and most importantly evidence of viral oncogene expression(29). Such supporting evidence for causality remains lacking for SCCHNs outwith the oropharynx. The biological reasons underlying these anatomical subsite differences remain unclear. Interestingly, HPV-related SCCHN also tends to affect younger patients often in the absence of the traditional risk factors of tobacco and alcohol consumption, another demographic aspect of the disease that is poorly understood(30).

Although contentious, HPV-positive SCCHN is increasingly considered as sexually transmitted. A relatively recent pooled analysis of eight multi-national observational studies demonstrated that the risk of developing oropharyngeal SCC was associated with a history of six or more lifetime sexual partners (OR = 1.25, 95% CI: 1.01-1.54), four or more lifetime oral sex partners (OR = 3.36, 95% CI: 1.32-8.53), and for men an earlier age at sexual debut (OR = 2.36, 95% CI: 1.37-5.05)(31).

In addition to the major risk factors of tobacco, alcohol, and HPV infection, epidemiological studies have also identified more minor risk factors. Consumption of fruits and vegetables, particularly carotene-rich vegetables, has been consistently associated with a reduced risk of SCCHN(32), while several other dietary factors such as salted meat and fish and charcoal-grilled or deep-fried foods have been linked with an elevated risk(33). Factors relating to oral hygiene have also been associated with increased risk of SCCHN, specifically frequent gum bleeding, no dental check-ups, no tooth brushing, and frequent use of mouthwash(34). Occupational factors are also implicated, with approximately 4-10% of all SCCHN in western countries estimated to result from occupational exposures(35). Asbestos exposure has been reported to increase the risk of laryngeal cancer in a dose-dependent manner, exposure to welding fumes has been linked with an elevated risk of pharyngeal and laryngeal cancers, and exposure to wood dust has been associated with a strongly increased risk of SCCHN of all anatomical subsites(36).

The patterns of SCCHN incidence over time and by geography are intriguing, carry important public health implications, and reflect closely the changing prevalence of the aforementioned major risk factors. Although rates of oral and laryngeal cancers are stable or decreasing slightly in developed countries (figure 1.1.2.2.), primarily because the population is smoking less, the worst of the tobacco epidemic has yet to manifest in developing countries because of the ≈40 year temporal gap between changes in

population tobacco use and resulting epidemiological effects(12). Indeed, World Health Organisation projections estimate that whilst mortality in Europe is expected to remain stable, figures are projected to rise markedly in South East Asia, with modest rises also predicted in Africa, the Americas, and the Middle East(37). In contrast, there has been a dramatic upsurge in the incidence of oropharyngeal cancer in the developed world in recent years. In the United States (US), the incidence of oropharyngeal SCC increased by 22% between 1999 and 2006, after no change between 1975 and 1999(38), and the UK has seen a doubling in incidence from 1/100,000 population to 2.3/100,000 in just over a decade (figure 1.1.2.2.)(39). This rapid increase has been widely attributed to an exponential rise in the incidence of HPV-related disease, a consensus corroborated by several prevalence studies. Scandinavian data showed a progressive proportional increase in HPV detection in oropharyngeal SCCs, specifically of the tonsil, over the past three decades: 23% in the 1970s, 29% in 1980s, 57% in 1990s, 68% between 2000 and 2002, 77% between 2003 and 2005, and 93% between 2006 and 2007(40). Similarly, the 2013 meta-analysis of HPV prevalence mentioned above demonstrated an increase in HPV point prevalence in oropharyngeal SCCs in Europe from 35.3% (95% CI: 28.7-42.5%) before 2000 to 73.1% (95% CI: 39.4-91.9%) between 2005-2009, and in the US from 50.7% (95% CI: 42.6-58.7%) to 69.7% (95% CI: 46.8-85.7%) during the same time periods(25). Interestingly, however, a recent UK study showed that the prevalence of HPV-positive oropharyngeal SCC has been stable at 51.8% (95% CI: 49.3–54.4%) between 2002 and 2011 despite an increase in incidence, suggesting an increase in both HPV-positive and HPV-negative disease(41). The reasons for this parallel increase as yet remain unclear.

A

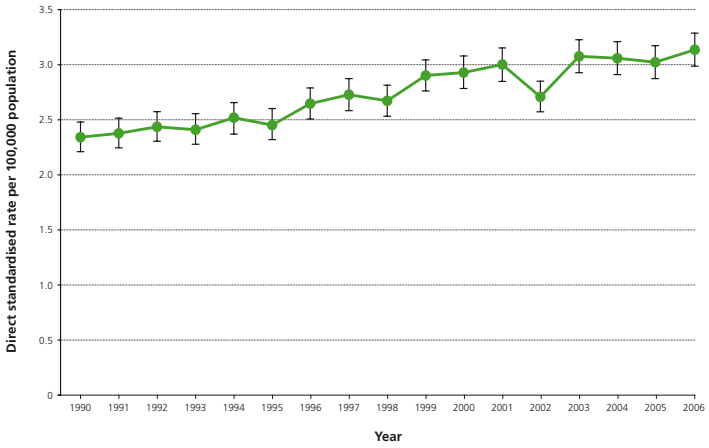
Direct standardised rate per 100,000 population
3.5
3.0
2.5
2.0
1.5
1.0
0.5
0
1990 1991 1992 1993 1994 1995 1996 1997 1998 1999 2000 2001 2002 2003 2004 2005 2006
Year

B

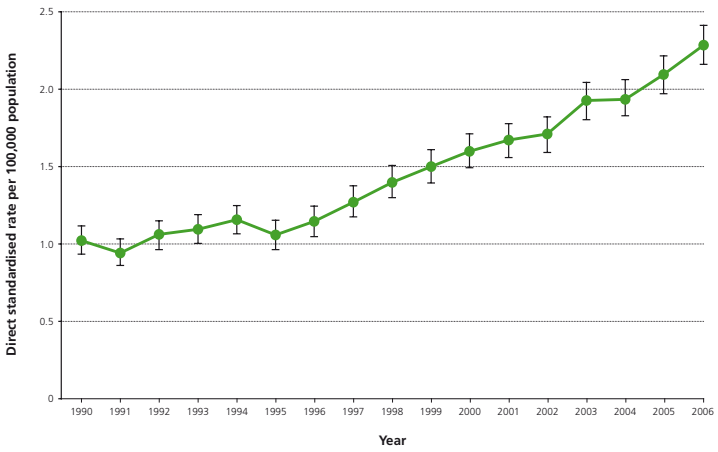
Direct standardised rate per 100,000 population
2.5
2.0
1.5
1.0
0.5
0
1990 1991 1992 1993 1994 1995 1996 1997 1998 1999 2000 2001 2002 2003 2004 2005 2006
Year

C

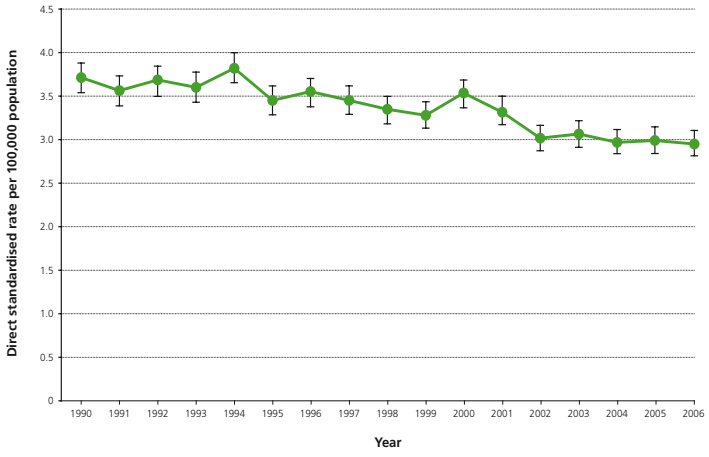
Direct standardised rate per 100,000 population
4.5
4.0
3.5
3.0
2.5
2.0
1.5
1.0
0.5
0
1990 1991 1992 1993 1994 1995 1996 1997 1998 1999 2000 2001 2002 2003 2004 2005 2006
Year

D

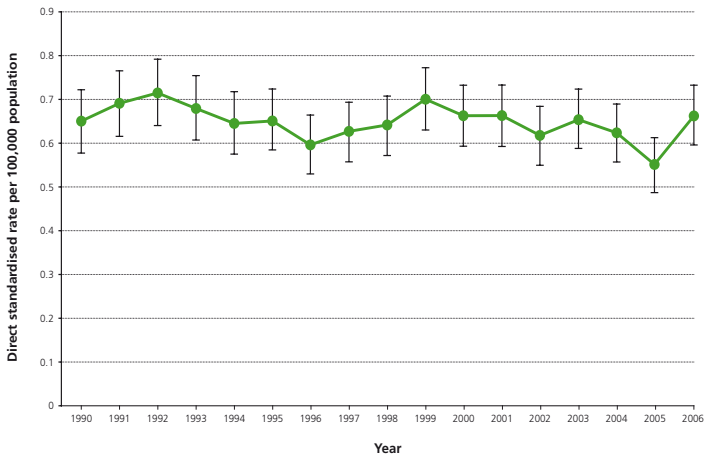

Figure 1.1.2.2: Trends in incidence rates of SCCHNs in the England from 1990-2006. Graphs illustrating incidence rates in England year by year from 1990-2006 for oral cavity (A), oropharyngeal (B), laryngeal (C), and hypopharyngeal (D) SCCs. There is a marked increase in incidence of oropharyngeal SCCs with a doubling of incidence on just over a decade, while the incidence rates for the other subsites have remained relatively unchanged. Figures reproduced from the National Cancer Intelligence Network website(39).

1.1.3. Molecular carcinogenesis

As with most types of human cancer, SCCHN arises as a result of the accumulation of numerous genomic changes, secondary to exposure to the carcinogenic risk factors detailed in the previous section(42). Such accumulation of genomic alterations, which provide a selective advantage, results in the acquisition of characteristic cancer-related phenotypes, termed the hallmarks of cancer by Hanahan and Weinberg(43), and thus malignant transformation of normal cells. These hallmarks were originally described as limitless replicative potential, self-sufficiency in growth signals, insensitivity to anti-growth signals, ability to evade apoptosis, invasion and metastasis, and sustained angiogenesis(43), but more recently the additional hallmarks of evading immune destruction and deregulating cellular energetics have been proposed(44).

At the molecular level, SCCHN carcinogenesis is a complex process involving a plethora of potential genetic and epigenetic abnormalities in DNA repair, cell signalling, cellular differentiation, angiogenesis, apoptosis, and cell cycle regulation, which has led to publication of countless studies on the identification of candidate cancer genes in SCCHN(42). To complicate matters further, despite a common origin in the squamous mucosa of the upper aerodigestive tract, as alluded to in previous sections, there are

several sources of heterogeneity that hinder consideration of SCCHN as a single disease entity. In addition to anatomical subsite differences, molecular analyses have revealed biological heterogeneity independent of subsite, identifying distinct subclasses of SCCHNs with particular mRNA expression profiles or patterns of DNA copy number alterations predictive of clinical behaviour(45-47). The most clear-cut differences, however, relate to HPV status(48, 49) and there is now a general consensus that HPV-related disease should be considered as distinct molecular entity within SCCHN(42), something which has now been recognised in the most recent edition of the TNM classification system(50).

Despite such heterogeneity, genetic alterations in particular cancer-associated signalling pathways are frequently observed in SCCHN, and these will form the focus of discussion in the remainder of this section. Findings from three recent independent and comprehensive sequencing studies, conducted on over 350 SCCHN specimens collectively, provided significant advances in our understanding of the molecular pathogenesis of SCCHN(51-53). Interestingly, this work highlighted the relative paucity of classical proto-oncogenes, such as *RAS* and *MYC*, targeted by activating mutations, and the importance of mutational "knock-out" of tumour suppressor pathways including p53, retinoblastoma (Rb), and Notch in SCCHN pathogenesis(51-53).

Of the various molecular alterations found in SCCHN, and indeed in most human cancers, the inactivation of the p53 tumour suppressor pathway, best known for its complex and critical roles in the regulation of processes including cell proliferation, death, and responses to exogenous stress (discussed in section 1.2.), seems to be paramount in tumour development(42). Mutation of the *TP53* gene is the most common genetic alteration in SCCHN by some margin, harboured in 60-85% of all cases(51-53). As in other human cancers, the majority of mutations (≈75%) are missense point mutations occurring primarily within the central DNA binding domain of the p53 protein(54), which typically exert dominant-negative regulation over any remaining wild-type p53, and may exhibit oncogenic gain-of-function (GOF) properties (discussed in more depth in section 1.2.7.)(55). Furthermore, *TP53* mutation also contributes to the clinical behaviour of SCCHNs, correlating with reduced survival following treatment with primary surgery with or without adjuvant radiotherapy (RT), as well as treatment resistance(56-58). Interestingly, the majority of this association was specific to truncating and function-disrupting *TP53* mutations (discussed in more depth in section 1.2.7.)(56, 58).

Although contentious, *TP53* mutation is thought to be one of the earliest genetic alterations in SCCHN carcinogenesis, based on the fact that mutations frequently occur in precursor lesions prior to conversion to the invasive state, and also in surrounding mucosa(59, 60). Furthermore, sequencing of primary SCCHNs and matched nodal metastatic lesions revealed no differences in *TP53* mutations(61). Such findings have also led to proposals of a "patch-field" progression model of SCCHN development, in which the invasive carcinoma, as well as any local recurrences or metachronous tumours, develop from a field of genetically abnormal mucosa, in turn the result of expansion of a clonal patch originating from a putative stem cell containing a *TP53* mutation(62).

Yet further evidence that attests to the importance of p53 inactivation in SCCHN carcinogenesis comes from the mechanisms of HPV-mediated oncogenesis, which are predominantly a function of the two viral oncoproteins E6 and E7(63). In HPV-driven SCCHNs, in which p53 is typically wild-type(64), the HPV E6 oncoprotein specifically inactivates wild-type p53, providing an alternative pathway to the classical mutational "knock-out" of p53-regulated pathways. E6 forms a trimeric complex with the cellular E3 ubiquitin ligase, termed E6-associated protein, and host cell wild-type p53, which results in ubiquitylation of p53 and its rapid proteasomal degradation(65). Furthermore, E6 can inhibit p53-mediated gene transcription through direct binding(66).

The other major HPV viral oncoprotein, E7, acts to inactivate another important tumour suppressor pathway, the Rb pathway, which plays a key role in the regulation of the cell cycle(63). Rb activity is regulated through its phosphorylation status, which is dependent on cell cycle regulators such as p16 and cyclin D1(67, 68). Underphosphorylated Rb forms a complex with the transcription factor, E2F, which prevents the transcription of genes essential for transition from G1 to S phase, resulting in inhibition of the cell cycle at the G1-S checkpoint(67). In contrast, Rb phosphorylation, which is initiated by the binding of cyclin-dependent kinase (CDK)4/6 and cyclin D1 to form an active protein complex, leads to E2F dissociation, activation of S phase genes, and cell cycle entry(67). The tumour suppressor p16 is also intricately linked here and binds to the CDKs, thus interfering with the interaction between cyclin D1 and CDK4/6 and preventing Rb phosphorylation(69). The viral oncoprotein, E7, causes destabilisation of Rb through a ubiquitin/proteasome-dependent mechanism,

allowing E2F to induce transcription of S phase promoting genes(63). This results in an overexpression of p16 in an attempt to block cell cycle progression, and consequently assaying of p16 expression in tumour cells by immunohistochemistry is often utilised clinically to determine HPV status, either alone or in combination with other detection techniques(70) (discussed in section 1.1.4.). Inactivation of the Rb pathway is also a crucial molecular event in SCCHN carcinogenesis more widely. In HPV-negative disease the *CCND1* gene, which encodes cyclin D1, has been shown to display copy number gains/amplification in more than 80% of cases(47), and has been consistently associated with poor prognosis(71). Furthermore, although mutations in *CDKN2A*, which encodes p16, were observed in only approximately 7% of tumours in the aforementioned sequencing studies, copy number losses were noted in another 20–30%(51-53) and previous data suggest that overall inactivation of *CDKN2A*, (through mutation, deletion, or epigenetic inactivation) occurs in up to 75% of SCCHNs(46, 72). The resulting loss of p16 expression has also been associated with decreased disease-specific survival and early recurrence(73).

Perhaps the most novel finding to emerge from the whole-exome sequencing studies was the relatively high frequency of mutations within the *NOTCH* genes, in particular *NOTCH1*, present in 20–25% of cases(51-53). Although previous work in certain haematological malignancies demonstrated predominantly activating mutations and translocations in the genes involved in Notch signalling, suggestive of a pro-tumorigenic role(74, 75), mutations observed in SCCHN were generally inactivating mutations, implying tumour suppressor function. Interestingly, Notch activity has been linked to suppression of HPV E6 and E7 oncoprotein expression(76), which intuitively would provide selective pressure for inactivation of Notch in HPV-driven disease. Otherwise, Notch signalling has been linked to regulation of self-renewal capacity, cell cycle exit, and cell survival(77, 78). Additionally, in stratified epithelia Notch activity plays a central role in promoting squamous differentiation, suggesting that dysregulation of this may be involved in SCCHN carcinogenesis(79). Consistent with this notion, the whole-exome sequencing studies demonstrated that at least 30% of cases harboured mutations in either *NOTCH* genes or other genes that regulate squamous differentiation(51-53).

Another dysregulated pathway involved in SCCHN pathogenesis, and the target of one of the first molecularly targeted therapies that has been approved for clinical use for SCCHN, is the epidermal growth factor (EGF) signalling pathway(1, 80, 81). Epidermal growth factor receptor (EGFR) is overexpressed in many SCCHNs(82), which has also

been linked with shorter overall and relapse-free survival, more advanced stage disease, and increased lymph node metastasis(83). EGFR is a transmembrane glycoprotein that belongs to the ErbB family of receptor tyrosine kinases and can bind multiple ligands, most importantly EGF and transforming growth factor α (TGF-α)(84). Ligand binding results in a conformational change in EGFR, promoting homo- or hetero-dimerisation with other ErbB/HER family members(84). This triggers internalisation and tyrosine kinase induced autophosphorylation of its cytoplasmic domain, which in turn initiates a mitogenic signalling cascade through Ras-Raf and phosphatidylinositol 3-kinase/protein kinase-B (PI3K-AKT)(84). Furthermore, when bound to EGF, it has been proposed that EGFR can translocate to the nucleus, where it can function as a transcription factor to promote cyclin D1 expression, and thus stimulate cell cycle progression as described above(85). Interestingly, dysregulation of EGFR expression is considered to be an early event in SCCHN carcinogenesis. As with *TP53* mutations, seemingly normal mucosa surrounding SCCHNs tend to display moderately increased EGFR expression and when cells become dysplastic there is a further marked increase in expression(82, 86), findings which also support the "patch-field" progression model of SCCHN discussed above.

Because of its prevalence and important role in SCCHN pathogenesis, therapeutic targeting of EGFR has been the subject of intensive study. In 2006, cetuximab, a monoclonal antibody against EGFR, became the first molecularly targeted agent to be approved and introduced into clinical practice for the treatment of SCCHN(87). Cetuximab was approved for use primarily in combination with RT in the context of loco-regionally advanced SCCHN following on from a landmark multi-national clinical trial that demonstrated that the addition of cetuximab significantly increased five-year overall survival from 36.4% to 45.6% compared with RT alone in this patient group(88). Additionally, cetuximab was approved for single agent use for the treatment of patients with recurrent or metastatic SCCHN refractory to platinum-based therapy(87), and more recently cetuximab has been shown to improve the outcome of palliative chemotherapy in a large randomised phase III study(89).

1.1.4. Diagnosis and staging

Diagnosis of early-stage SCCHN or pre-malignant lesions, such as oral or laryngeal dysplasia, is typically hindered by an absence of symptoms, compounded by the fact that such lesions are frequently overlooked by both patient and examiner, if indeed medical or dental consult is sought(1, 2). As such, there is often a delay of up to a year in

diagnosis(5). When patients do become symptomatic, SCCHNs can manifest in a variety of ways, often depending on the function of the site where they originate, as alluded to in section 1.1.1. Laryngeal cancers commonly present with dysphonia (particularly hoarseness), while pharyngeal cancers frequently present late with dysphagia(1, 2, 5). However, seemingly non-specific and benign symptoms, such as sore throat or ear pain (referred pain owing to the complex innervation of regional anatomy), are also common presentations, and others may first present simply with a painless neck lump as a manifestation of regional lymph node metastases(1, 2, 5). Such symptoms and signs are reflected in current practice guidelines for specialist referral (figure 1.1.4.1.), which have been developed to expedite specialist assessment, with UK guidelines specifying that patients meeting these criteria warrant a specialist consultation within two weeks(90).

- Hoarseness persisting for more than six weeks
- Ulceration of oral mucosa persisting for more than three weeks
- Oral swellings persisting for more than three weeks
- All red or red and white patches of the oral mucosa
- Dysphagia persisting for more than three weeks
- Unilateral nasal obstruction, particularly when associated with purulent discharge
- Unexplained tooth mobility not associated with periodontal disease
- Unresolving neck masses for more than three weeks
- Cranial neuropathies
- Orbital masses

(The level of suspicion is further increased if the patient is a heavy smoker or heavy alcohol drinker and is aged over 45 years and male. Other forms of tobacco use and/or chewing betel (areca nut) should also arouse suspicion.)

Figure 1.1.4.1: Urgent specialist referral guidelines for SCCHN in England. Reproduced from reference (90).

Initial assessment of any lesion of the head or neck is centred on physical examination and should include palpation of the entire neck for lymph nodes, visual inspection of the oral cavity and oropharynx, and flexible nasolaryngoscopy, which allows proper examination of the nasal cavities, postnasal space, base of the tongue, larynx, and hypopharynx(1, 2, 5). If such examination confirms the presence of a suspicious looking lesion a diagnosis of cancer is confirmed or refuted with biopsy and subsequent histopathological examination. In the case of epithelial primary site biopsies, these are usually performed during an examination under general anaesthetic, while in the case of enlarged cervical lymph nodes with no identifiable primary lesion fine needle

aspiration, typically under ultrasound guidance, and subsequent cytological evaluation is usually performed(5, 90).

Following confirmation of a SCCHN diagnosis, accurate staging is one of the most important factors that guides therapeutic decision-making. Pre-treatment disease staging is formulated on the aforementioned clinical examination in combination with radiological assessment that usually entails imaging of the neck with computed tomography (CT), magnetic resonance imaging (MRI), or both to evaluate the extent of invasion of surrounding anatomy and detection of regional lymph node involvement. In cases where there is a high index of suspicion of SCCHN based on clinical examination such radiological evaluation is often undertaken prior to biopsy to avoid upstaging of the disease. In addition, thoracic and abdominal imaging (typically CT) should be performed to exclude the presence of a synchronous primary bronchogenic carcinoma or distant metastases(2, 5, 90). Indeed, up to 36% of SCCHNs metastasise to distant sites, with the risk being higher for locally advanced disease with nodal involvement(91), and in approximately 4-5% of cases a synchronous pulmonary tumour will be detected(92). The relatively new technique of positron emission tomography (PET), which detects uptake of the glucose analogue 2-deoxy-2-(^{18}F)fluoro-D-glucose (^{18}F-FDG) and is described in detail in section 1.3.3., fused with normal CT imaging for anatomical detail, has also become an important diagnostic and staging adjunct to help identify occult primary tumours not detectable by examination and conventional imaging(93). This information is then assimilated using TNM classification and the Union for International Cancer Control (UICC)/American Joint Committee on Cancer (AJCC) staging systems(50). Staging criteria vary according to the primary site of origin, and account for the anatomical extent of disease, and following recent revisions now incorporate certain pathological and biological aspects of tumour behaviour, such as extra-capsular spread (ECS), HPV-status, and depth of invasion(50).

The now widespread consensus that HPV-related oropharyngeal SCC represents a separate disease entity from HPV-negative disease, conferring favourable survival(94-96) (discussed in section 1.1.5.), has led to the introduction of HPV-16 testing in the diagnostic work-up and staging process for SCCHN. Specifically, several recently published evidence-based clinical management guidelines recommend such testing for SCCHNs arising in the oropharynx and also in the case of metastatic SCC of unknown origin(97). However, a variety of laboratory detection methods are available, each with particular benefits and detractions, and currently there is insufficient evidence to

recommend one particular testing regime over another to establish HPV status(97, 98). Nonetheless, the combination of immunohistochemical testing for p16 expression, a downstream product of HPV DNA transcription (discussed previously in section 1.1.3.), with either an HPV DNA directed polymerase chain reaction (PCR) amplification technique or detection of HPV DNA using signal amplification in-situ hybridisation (ISH) have been proposed(98). One such tiered diagnostic algorithm published by the John Hopkins Institution and commonly utilised in clinical practice, including in our regional head and neck network, is illustrated in figure 1.1.4.2.

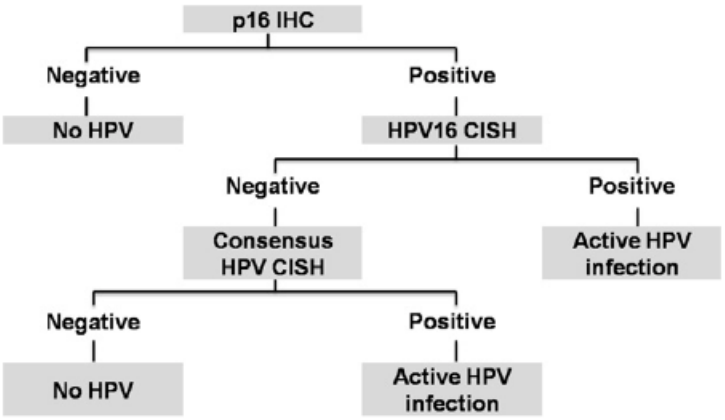

Figure 1.1.4.2: Diagnostic algorithm for the detection of biologically relevant HPV infection. This tiered diagnostic algorithm proposed by Westra(99) uses p16 immunohistochemistry (IHC) for initial screening of cases, because it has high sensitivity, followed by HPV-16 type specific ISH, which is highly specific. In equivocal cases (p16 positive/ HPV-16 negative) a consensus HPV in-situ probe is used to detect a broader range of oncogenic HPVs. (CISH = chromogenic in-situ hybridisation). Reproduced from reference(98).

1.1.5. Treatment and prognosis

As the recognition of HPV-related oropharyngeal SCC as a distinct disease entity has evolved, its prognostic importance has also been revealed. Initial indications that HPV status influenced survival came from a single-institution case series of tonsillar SCCs, in which risk of disease relapse at three years was less in HPV-positive cases (OR = 4.18) and respective three-year overall survival rates of 65.3% and 31.5% were observed in the HPV positive and negative groups(100). This initial association was subsequently corroborated by a meta-analysis of individual retrospective case series(101), and further by the landmark HPV status specific analysis of outcomes in the Eastern Cooperative Oncology Group 2399 phase II trial, which demonstrated a 73% (HR = 0.27,

95% CI: 0.1–0.75) reduction in risk of disease progression and a 64% (HR = 0.36; 95% CI: 0.15–0.85) reduction in risk of mortality for patients with HPV-positive disease(94). Moreover, the differential survival benefit appears to hold true irrespective of treatment modality employed, with similar results demonstrated in surgically treated patients with or without postoperative RT(96), following treatment RT alone(102), and in those treated with primary chemoradiotherapy (CRT)(95). Interestingly, further prognostic stratification combining HPV status and tobacco exposure has been suggested. Results from the Radiation Therapy Oncology Group 0129 trial demonstrated that tobacco smoking was independently associated with overall survival and progression-free survival in both HPV positive and negative subgroups, with a similar magnitude of effect in both groups, which led the authors to propose a survival classification (high, intermediate and low risk categories) based on HPV status, tobacco consumption, and tumour stage(95).

HPV status notwithstanding, the strongest, and indeed traditional, prognostic factors include tumour site of origin, disease stage, and the presence of ECS in cervical lymph node metastases(80, 103). As would be expected, tumours that are larger and have spread to cervical lymph nodes and other tissues are associated poorer survival(80, 103). ECS has shown to confer poorer oncological outcomes in numerous retrospective case series of SCCHNs from different subsites, and in a large-scale study of 400 patients with oral SCC ECS was observed to be the most significant adverse prognostic indicator, doubling the incidence of local recurrence and distant metastases, and tripling the risk of regional failure(104). Furthermore, a meta-analysis including all SCCHN subsites showed that ECS more than halved the chances of surviving for five years (OR = 2.7, 95% CI: 2.1-3.7)(105). Other prominent prognostic factors have been reported, such as histological grade, pattern of invasion, and proximity of carcinoma to surgical resection margins, all of which are included as accepted features related to clinical outcome in the UK Royal College of Pathologists guidelines(106).

The treatment of SCCHN is typically complex and often multi-modal, comprising various combinations of surgery, RT, and chemotherapy, and as such is increasingly delivered by multi-disciplinary teams of health professionals(1, 80). The specifics of treatment depend largely on the primary site of the tumour and the stage of disease, as well as patient performance status and preference. In the broad context of SCCHN, RT and surgery are the most common treatment modalities, with the former indicated in 74% of all cases at some point during the treatment pathway, either as primary or adjuvant

therapy, if current treatment guidelines are followed(107). Patients with early stage SCCHN are generally treated with single modality therapy, either surgery or RT, with curative intent(1, 80, 81). In early stage oral cavity SCC, although efficacy of surgery and RT appear equitable, surgery is usually preferred to avoid late toxic effects of radiation and to enable more accurate pathological staging from surgical resection specimens(108). Similarly, in terms of oncological control RT and surgery stand in clinical equipoise for early stage oropharyngeal and laryngeal SCC, with the treatment choice largely dependent on the treating centre's expertise and patient preference(109-111). There is an increasing body of evidence, however, that use of contemporary, endoscopic surgical techniques may be associated with favourable functional outcomes(112-114). For advanced SCCHN, which represents approximately two-thirds of all SCCHN cases(1, 81), single modality treatment is generally associated with poorer outcomes, and several seminal studies have demonstrated that combined use of surgery and adjuvant RT, or combined post-operative platinum-based CRT, or perhaps most commonly primary CRT, offer the most favourable disease control rates and survival(115-119). Unfortunately, however, such multi-modality treatment also comes with considerable toxicity and carries significant functional morbidity for the majority of patients(120, 121).

In addition to treating the primary tumour, it is typically considered mandatory to electively treat the neck, either surgically or with RT, even in the absence of clinical and radiological evidence of lymph node involvement when the estimated likelihood of occult metastasis is more than 15-20%(122). This assessment is based predominantly on disease stage and the lymphatic drainage of the primary tumour site(122).

As alluded to above, a major advancement in the treatment of SCCHN has been the advent, and more widespread adoption, of organ preserving surgical techniques, specifically transoral laser microsurgery and transoral robotic surgery. These minimally invasive approaches obviate the need for an external skin incision and limit the extent of tissue dissection, disruption to speech and swallowing muscles, damage to major neurovascular structures, and injury to normal tissue(123). Furthermore, these techniques allow for intraoperative microscopic evaluation of the tumour resection, which can be undertaken in a transtumoural manner, maximising appreciation of three-dimensional orientation(123). Another major recent advancement has been the introduction of intensity-modulated RT (IMRT), which represents an advanced form of radiation in three dimensions(124). Computer-driven linear accelerators are used to

produce multiple RT beams, in which the intensity is optimised to deliver a high dose of radiation to specified tissues, while reducing the dose to adjacent non-target tissues(124). IMRT, therefore, allows for better control of radiation dose delivery and has been shown in a recent phase III multi-centre randomised controlled trial to significantly reduce radiation-induced xerostomia (the main long term side effect of standard RT) from 74% (95% CI: 56-87%) to 39% (95% CI: 23-55%) and from 83% (95% CI: 63-95%) to 29% (95% CI: 14-48%) at one and two years after treatment respectively(125). Other advancements in RT relate to delivery schedules, such as accelerated RT (radiation delivered over a shorter time period) or hyperfractionated RT (delivery of a higher dose of radiation in two to three low dose fractions a day)(126). Use of concomitant chemotherapy, as discussed above, is a relatively recent development in SCCHN treatment, having evolved from the palliative care setting, and more recently the concurrent administration of cetuximab has been shown to be beneficial in specific therapeutic contexts (see section 1.1.3.)(81).

Despite such advances in therapeutic strategies, as well as recent developments in diagnostics, overall survival outcomes for HPV-negative SCCHN have not improved significantly over the last 20-30 years (figure 1.1.5.1. shows UK data), still accounting for nearly 350,000 deaths annually worldwide(10-12, 38, 127). To a large extent, this reflects the failure of currently available treatment regimes to achieve loco-regional and long-term distant control in advanced disease, and overall survival rates for such patients remain as low as 35%(38, 127). Furthermore, it is generally not a feasible option to escalate RT and/or chemotherapy dosage in these patients owing to concerns over normal tissue toxicity(128, 129). In contrast, HPV-driven oropharyngeal SCC is associated with favourable survival outcomes, as discussed above, which together with the fact that HPV-related disease tends to affect younger and generally medically fitter patients(30), who are therefore likely to experience the functional ramifications of their treatment long-term, has led many to propose treatment de-intensification for these patients in order to avoid potential overtreatment with associated toxic effects(130, 131). Despite this apparent clinical paradox of the need for treatment escalation versus de-escalation in HPV-negative and HPV-positive disease respectively, there remains a common goal from a translational research perspective: to identify more effective treatment strategies, and a major focus for this includes to identifying ways of sensitising these tumours to the effects of existing treatments, not only to improve efficacy, but also to minimise the substantial toxic effects. Fundamental to this is to elucidate the cellular processes that may determine radio- and chemo-sensitivity to

facilitate therapeutic targeting of the key pathways that may impinge on these processes.

A

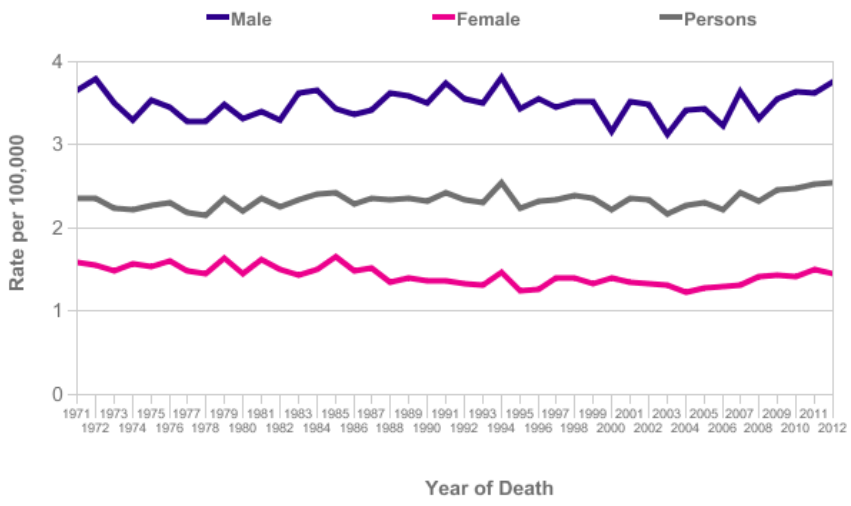

B

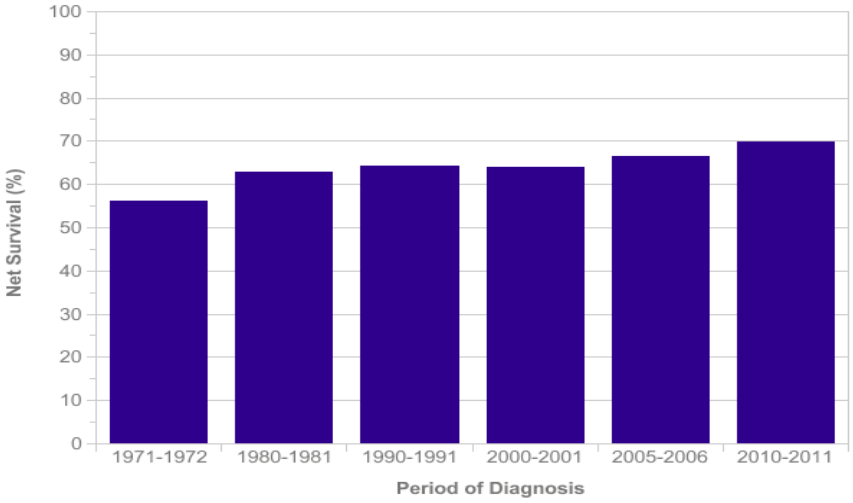

Figure 1.1.5.1: SCCHN survival/mortality trends in the UK over time. Graphs illustrating the mortality rates in the UK from 1971-2012 for oral cavity and pharyngeal cancers combined (A), and the five-year overall survival rates from 1971-2011 for laryngeal cancer alone (B). Figures reproduced from Cancer Research UK website(11).

1.2. The p53 tumour suppressor protein

The *TP53* tumour suppressor gene, which encodes the p53 protein, plays a critical role in orchestrating cellular damage control pathways that suppress the development of

cancer(132). The fact that *TP53* has the greatest number of cancer-associated mutations of any known gene, mutated directly in approximately half of all human cancers(133), attests to the importance of this role, which, as touched on previously in section 1.1.3., is also evident specifically in SCCHN.

1.2.1. Structural organisation of p53

The *TP53* tumour suppressor gene is 20 kilobase pair gene comprising 11 exons and is located on the short arm of chromosome 17(134). The resulting p53 protein consists of 393 amino acid residues and functions as a tetramer(135). From a structural perspective, the p53 protein is divided into three regions: the N-terminal domain, the central core domain, and the C-terminal domain (figure 1.2.1.1.)(135).

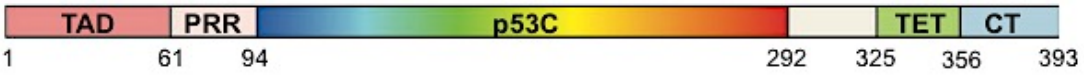

Figure 1.2.1.1: Domain structure of full-length p53 protein. The p53 protein consists of 393 amino acid residues and contains an N-terminal transactivation domain (TAD), followed by a proline-rich region (PRR), the central DNA-binding domain (p53C), the tetramerisation domain (TET), and the extreme C terminus (CT) containing the regulatory region. Figure reproduced from reference (135).

The N-terminal domain is natively unfolded, encompasses residues 1-93, and contains an acidic transactivation domain (this can be further subdivided into two ill-defined subdomains) and a proline-rich region(136, 137). The transactivation domain is a binding site for numerous interacting proteins, including general transcription factors(138, 139), transcriptional co-activators(140), and the negative regulators murine double minute (MDM)2/MDMX (see section 1.2.2.)(141, 142). Notably, the residues F19, L22, and W23 are thought to be essential for transcriptional activation by p53 as they interact directly with the components of the transcriptional machinery(143). The precise role of the following proline-rich region, which links the transactivation domain to the central core domain, is poorly understood. However, the region contains five PXXP motifs (where P represents proline and X any amino acid), which are generally known to mediate protein-protein interactions in signal transduction through binding to Src homology 3 domains (SH3), and it has been suggested that this may play a role in the transmission of anti-proliferative signals down-stream of the p53 protein(137).

The central core region consists of residues 102-292, and is made up of a β-sandwich that serves as a scaffold for two large loops and a loop-sheet-helix motif, which form the α-helical sequence-specific DNA-binding element of the p53 protein(135, 144). The two loops, which are held together by a tetrahedrally coordinated zinc atom, and the loop-sheet-helix motif contain the evolutionarily conserved regions of the core domain: region II 117-142; III 171-181; IV 234- 258; and V 270-286(144, 145). Residues from the loop-sheet-helix motif interact in the major groove of the DNA, while arginine from one of the two large loops interacts in the minor groove(135, 144). Residues K120, S241, R273, A276, and R283 are also involved in the sequence-specificity of p53 as they make direct contact with the phosphate backbone in the major grove of DNA, while residues K120, R248, C277 and R280 form hydrogen bonds with DNA bases in the minor grove of DNA(144). Importantly, the majority of *TP53* mutations identified in human cancers affect the central core domain, particularly the highly conserved regions, resulting in the loss or alteration of sequence-specific DNA binding(54, 145).

The C-terminal domain, consisting of residues 300-393, is multi-functional and is further subdivided into three regions: a flexible linker (residues 300-320), a tetramerisation domain (residues 325-356), and a regulatory domain (residues 363-393)(135). The monomeric tetramerisation domain consists of a short β-strand and an α-helix linked by a sharp turn, which can homodimerise to form a primary dimer, which can in turn associate with another such primary dimer through their helices to form the functional p53 tetramer (figure 1.2.1.2.)(146, 147). The tetramer interface is stabilised largely by strong hydrophobic interactions between the surfaces of each helix pair(146, 147). At the extreme C terminus of p53 lies the regulatory domain, which is a natively unfolded region, is rich in basic amino acids (mainly lysines), and is capable of binding DNA non-specifically(135, 145). Additionally, this region has been reported to bind damaged DNA and to promote re-annealing of complementary DNA or RNA strands(135).

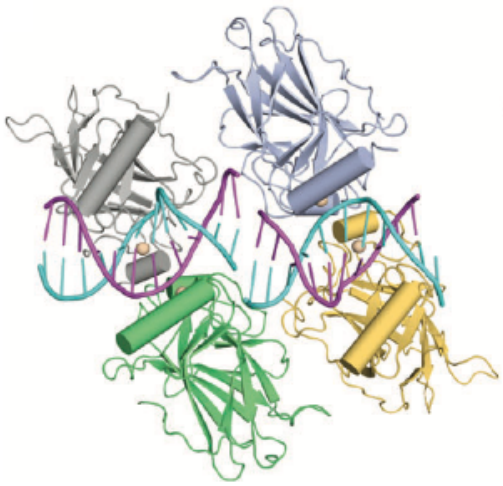

Figure 1.2.1.2: Structure of the tetrameric DNA-binding domain of p53 binding to DNA. p53 core domains bound to two consecutive DNA half-site motifs (purple and turquoise chains). The grey and green subunits form one dimer, and the blue and yellow subunits form the other. Zinc atoms are depicted as beige spheres. Figure reproduced from reference (135).

1.2.2. Regulation of p53

Given that p53 regulates such a large number of cellular processes and is a potent inhibitor of cell growth, its activity has to be tightly regulated during development and normal growth(148, 149). Under normal conditions, p53 is maintained at low, often undetectable levels, predominantly due to the function of its negative regulators MDM2 and MDMX (also known as MDM4)(148, 149). MDM2 is the main negative regulator of p53, acting both to promote its degradation and inhibit its transcriptional activity(148). Perhaps most importantly, as a RING-finger E3 ubiquitin ligase, MDM2 binds to and ubiquitylates p53, ultimately targeting it for proteasomal degradation(150). Such ubiquitylation can also hamper the transcriptional activity of p53 through control of sub-cellular localisation. The transcriptional activity of p53 relies on its nuclear localisation, and ubiquitylation of p53 by MDM2 can cause exposure of the C-terminus nuclear export sequence within the tetramerisation domain of p53, resulting in p53 export from the nucleus to the cytoplasm(151). MDM2 can also negatively regulate the transcriptional activity of p53 more directly by binding to the p53 N-terminal transactivation domain, which prevents binding of the components of the transcription machinery(152). A further mechanism by which MDM2 can inhibit p53 transcriptional activity is through inhibition of histone acetyltransferase-mediated p53 acetylation, which normally enhances the DNA-binding capacity(153). Importantly, p53 and MDM2 are engaged in an auto-regulatory feedback loop, which titrates the levels of both p53

and MDM2(150). p53 stimulates the expression of MDM2 by binding to the MDM2 P2 promoter, with MDM2 then inhibiting p53 function, while on the other hand, low p53 activity leads to decreased steady state levels of MDM2(150). Moreover, MDM2 can also target itself for degradation, ensuring it is not present at excessive levels(150).

The function of MDMX, a homologue of MDM2, in regulating p53 stability is less well understood. MDMX lacks the robust E3 ubiquitin ligase function of MDM2 but is thought to regulate p53 stability indirectly (328), primarily by interacting with and stabilising MDM2, hence stimulating the ability of MDM2 to inhibit p53 function(154). It has also been suggested that in a similar manner to MDM2, MDMX can negatively regulate p53 through inhibition of its acetylation by the histone acetyltransferase p300/CBP(155).

p53 can become activated in response to a wide variety of stimuli including genotoxic stress, hypoxia, and aberrant growth signalling(149). Such activation in response to these stress signals is almost always accompanied by stabilisation, leading to a rapid increase in p53 levels(148, 149). This largely results from a disruption of the interaction between p53 and its negative regulators, MDM2 and MDMX, thereby liberating p53, rather than through *de novo* synthesis(148, 149). Indeed, transcriptional activation of p53 would create a delay in the DNA-damage response, which would also carry a risk of producing a mutated and non-functional p53 protein as the DNA may be damaged(148). One of the main mechanisms of abrogating the interaction between p53 and MDM2 is post-translational modification of both proteins(149). In response to ionising radiation (IR), p53 is phosphorylated at serine 15 by ataxia telangiectasia mutated (ATM) kinase and at serine 20 by checkpoint kinase 2 (Chk2), and in response to ultra-violet (UV) radiation ATR (ATM-related) kinase causes phosphorylation at serines 15 and 37, all of which prevent MDM2 from binding to the transactivation domain of p53(156-158). ATM kinase and ATR kinase can also phosphorylate MDM2, resulting in its functional inactivation and/or destabilisation(159, 160). Additionally, acetylation of p53 at lysine residues clustered around the C-terminus can also compete with MDM2 ubiquitylation of the same lysine residues, enhancing the stability of p53(161)

Another mechanism by which the p53-MDM2 interaction can be abrogated is through the binding of p14ARF to MDM2, which results in the inhibition of MDM2-mediated p53 nuclear export, thus preventing ubiquitylation of p53(162). p14ARF is an alternative reading frame product of the *CDKN2A* gene and is activated in response to aberrant growth signals secondary to oncogene activation(163). The mechanistic basis of the

interaction between p14ARF and MDM2, however, is not fully understood and may involve sequestration of MDM2 into the nucleolus, formation of ARF-MDM2-p53 ternary complexes in the nucleoplasm, or inhibition of MDM2 nuclear ubiquitin ligase activity (162).

In addition to mechanisms liberating p53 from the negative regulation of MDM2, a number of post-translational modifications of p53, including acetylation, adenosine diphosphate (ADP)-ribosylation, ubiquitination, NEDDylation, or SUMOylation, have been suggested to enhance the sequence-specific DNA-binding and transcriptional activities of p53 in response to stress(164). These modifications may result in a conformational change of the protein, and whilst the precise details of how all of these promote p53 function remain to be clarified, it appears that modification, in particular acetylation, of p53 near the C-terminus can interfere with the folding of this region of the protein(164). In the unmodified protein the C-terminus usually folds back inhibiting the DNA-binding domain in the central core region, with the modifications therefore enhancing the DNA-binding capacity of p53(164).

1.2.3. Functions of p53

Following activation and stabilisation in response to stress signals, the p53 protein integrates numerous signals that function ultimately to control decisions between cellular life and death, which together act to prevent errors in the duplication process of a cell that is under stress and thus prevent cancers from arising(165). For instance, p53-mediated induction of cell cycle arrest in response to acute DNA damage signals allows time for DNA repair before further cellular proliferation, which prevents the propagation of potentially deleterious mutations, while induction of apoptosis by p53 directly eliminates abnormal cells harbouring mutations that would otherwise contribute to genomic instability(166). The outcome of p53 activation depends on a wide range of factors, including the tissue type, the state of the cell, the presence of other oncogenic changes in the cell, whether p53-independent death or survival signals that cooperate with p53 are present, and the type and severity of the stress stimuli(166).

p53 functions predominantly as a sequence-specific transcription factor that can regulate the expression of a large and disparate group of responsive genes. Indeed, it has been suggested that there may be as many as 4000 such human genes, covering various functions involved in cell cycle regulation, apoptosis, senescence, DNA repair

after genotoxic stress, oxidative stress, angiogenesis, differentiation, cell adhesion, cell migration, extracellular matrix and cytoskeleton organisation, and metabolic homeostasis(167-169). These p53 responsive genes either contain a p53 response element (RE) or are situated close to DNA harbouring such a RE(167, 169). These p53 REs are composed of a consensus DNA sequence to which p53 binds with high affinity and specificity, which has striking internal symmetry and consists of two copies of a 10 base pair motif 5′-RRRCWWGYYY-3′, where R is a purine, Y is a pyrimidine, W is either adenine or thymine, G is a guanine, and C is cytosine, separated by 0-13 base pairs(167, 170). Whilst the binding of p53 to the majority of p53 REs is associated with transcriptional activation of gene expression, a considerable number of REs (approximately 15%) are linked to transcriptional repression(167). At present it remains unclear what differentiates a RE from being a transcriptional-activator site versus a transcriptional-repressor site. p53-mediated transcriptional activation is typically achieved through direct, sequence-specific DNA binding, whereas there are several generally accepted direct methods of repression: binding-site overlap that interferes with another transcriptional activator; inactivation of other transcriptional activators through protein-protein interactions; and recruitment of histone deacetylases(167). Indirect p53-mediated repression may also occur through binding to another transcription factor and, together, repressing a gene without a p53-specific RE, or in the instance of activation of CDKN1A (otherwise known as $p21^{Cip1/Waf1}$, and from hereon referred to simply as p21), which inhibits formation of the CDK4/6-cyclin D1 complex and ultimately repression of S phase genes (see section 1.1.3.)(167).

In addition to the importance of transcriptional regulation, p53 also exerts some of its downstream effects by transcriptionally independent means, chiefly related to its apoptotic activity(165). The details of these effects remain to be clarified but may include the relocalisation of death receptors to the cell surface(171), a direct cytoplasmic function of p53 in the regulation of mitochondrial membrane permeabilisation(172), and direct regulation of translation by p53 binding to the 5′ untranslated region of certain mRNAs(173).

Perhaps the best characterised functions of p53 are induction of cell-cycle arrest, apoptosis, and more recently senescence in response to acute DNA-damage signals(165), and as such will be discussed in more detail in the subsequent sections of this chapter (sections 1.2.4-5.). In addition, and of particular relevance to the topic of this thesis, recent studies have revealed that p53 also plays a central role in metabolic

homeostasis, balancing glycolytic activity and mitochondrial respiration(174), and this will be discussed further in section 1.3.2.

1.2.4. Cell cycle regulation

The cell cycle comprises a coordinated series of events, which results in the duplication of all cell components and division to produce two cells, a mother and a daughter cell. Although cell proliferation is a continuous process, DNA synthesis and mitosis can be divided into distinct phases as follows: G1 (pre-synthetic gap); S phase (DNA synthesis); G2 (post-synthetic gap); and M phase (mitosis) (figure 1.2.4.1.)(175). Progression through the cell cycle depends on a series of regulatory events, principally the sequential activation and inactivation of the CDKs, which are active in facilitating successful progression through the cell cycle only when bound in complexes with the cyclins(175, 176). Progression through G1 is dependent on CDKs binding to cyclins D and E, while S and M phase progression relies upon CDKs binding to cyclins A and B(176). G1/S and G2/M cell cycle checkpoints maintain an accurate sequence of events by ensuring the next phase of the cell cycle is not initiated until completion of the current phase(175), and enable induction of temporary cell cycle arrest, allowing damaged DNA to be repaired before allowing the cell to continue replication of the DNA or subsequent division(175, 176).

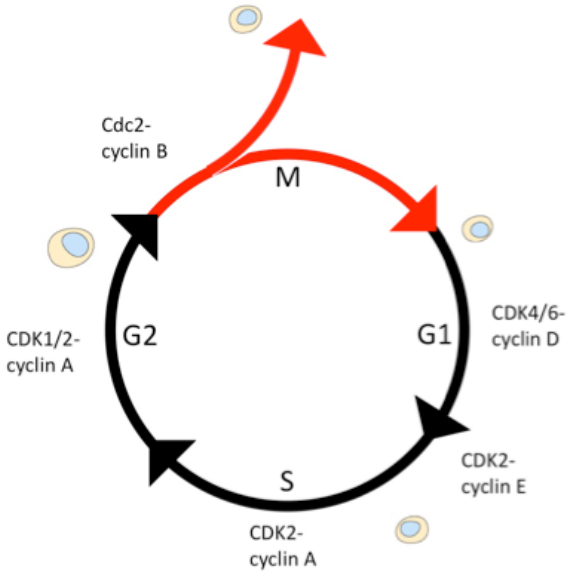

Figure 1.2.4.1: Diagrammatic representation of the cell cycle. The distinct phases of the cell cycle include G1 (pre-synthetic gap), S phase (DNA synthesis), G2 (post-synthetic gap), and M phase (mitosis). Progression through G1 is dependent on CDKs binding to cyclins D and E, while S

and M phase progression relies upon CDKs binding to cyclins A and B. Figure reproduced from reference (177).

One of the principal functions of p53 in the majority of mammalian cells is induction of cell cycle arrest, a function which p53 executes via a number of pathways. p21 was the first p53 target discovered with a role in cell cycle arrest(178), and is the main downstream target of p53 for G1/S cell cycle arrest in response to DNA damage(179). p53 transcriptionally activates the expression of p21, which results in potent inhibition of the CDKs(179). At high concentrations of p21 (as would be induced upon p53 activation), p21 binds to and inhibits a wide range of cyclin-CDK complexes, including cyclin D1–CDK4 or 6, cyclin E–CDK2, cyclin A–CDK1 or 2, and cyclin B1–CDK1, thereby blocking cell cycle progression at both G1/S and G2/M checkpoints(179). Furthermore, p21 is also able to bind and inhibit the activity of proliferating cell nuclear antigen (PCNA), a DNA polymerase activator in DNA replication, contributing to G1/S arrest(180). In addition to p53, several other factors can regulate the transcription of p21 in a p53-independent fashion and thus influence cell cycle progression (reviewed in (179)).

The ability of p53 to induce cell cycle arrest also involves the gene *GADD45* (growth arrest and DNA-damage-inducible protein 45)(181). Following certain genotoxic stresses, p53 transcriptionally activates GADD45, which is implicated in the induction of G2/M arrest through inhibition of the activity of the cyclin B1–CDK1 complexes(181). Inhibition of cyclin B1–CDK1 complexes also underlies another of the pathways by which p53 can achieve cell cycle arrest – up-regulation of 14-3-3σ(182). 14-3-3σ promotes cell cycle arrest in the G2 phase by sequestering cyclin B1-CDK1 complexes in the cytoplasm preventing their nuclear import and entry into mitosis(182). Akin to 14-3-3σ and GADD45, *Reprimo,* a candidate tumour-suppressor gene, is a further potential mediator of p53-dependent cell cycle arrest in the G2 phase by interfering with cyclin B1–CDK1 complex activity(183). Although there is currently no evidence for the presence of a p53 consensus binding site within the promoter region of *Reprimo*, its induction upon p53 expression suggests that Reprimo expression is positively regulated by p53(183).

1.2.5. Apoptosis

Apoptosis, or programmed cell death, is crucial to the maintenance of healthy multi-cellular organisms, occurs in response to a wide variety of stimuli, and is tightly

controlled by a numerous pro- and anti-apoptotic proteins(184, 185). As mentioned in section 1.1.3., the inactivation of apoptosis is central to the development of cancer such that it is considered to be one of the fundamental hallmarks of cancer(43, 44). It is perhaps unsurprising then, that traditional thinking dictates that anti-cancer therapies work by triggering cancer cells to undergo apoptosis, and that cells resistant to apoptosis will be resistant to therapy(186).

Cells undergoing apoptosis are conspicuous by the following morphological features: the cell shrinks, its chromosomes condense, the nucleus fragments, the cellular membranes bleb and form small apoptotic bodies, which are then removed by phagocytes(185). It is the organised removal of cell debris and the prevention of an unwanted immune response that distinguishes apoptosis from necrotic cell death(187). There are currently three recognised pathways that result in the initiation of apoptosis: the extrinsic apoptotic pathway, the intrinsic apoptotic pathway, and the granzyme B pathway (detailed in figure 1.2.5.1.). The extrinsic and granzyme B pathways are initiated by extracellular signals, while the intrinsic pathway is initiated by intracellular signals. Regardless, all three pathways converge at the mitochondrial outer membrane (MOM), where members of the Bcl-2 protein family interact to control the release of cytochrome C, which triggers the caspase cleavage cascade, in turn leading to the destruction of structures within the cell(185).

The Bcl-2 family of proteins is divided into three broad subclasses based on their areas of Bcl-2 like homology (BH domains) and function(184, 185). The anti-apoptotic members include Bcl-2, Bcl-w, Bcl-xL Mcl-1, Bfl-1/A1, and Bcl-B, and contain all four BH domains(184, 185). The pro-apoptotic members comprise multi-BH domain members (Bax, Bak, and Bok), which contain BH domains 1-3, and a separate group of BH3-only members, including Bid, Bim, Puma, Hrk, Noxa, Bad, Bmf, and Bik(184, 185).

Under normal conditions at the MOM, the anti-apoptotic Bcl-2 family members inhibit apoptosis by preventing the oligomerisation of Bax and Bak(188). In response to a death-inducing signal, however, the pro-apoptotic proteins Bax and Bak can be activated to oligomerise. As homodimers they can become inserted into the MOM and create channels that allow the release of cytochrome c, and other pro-apoptotic proteins, from the intermembrane space (IMS), so-called MOM permeabilisation (MOMP)(188). It is thought to be the balance of Bcl-2 pro- and anti-apoptotic family members on the MOM that determines whether to prevent or to allow MOMP(188). Subsequently, released

cytochrome c interacts with apoptosis protease activating factor-1 (Apaf-1), which then recruits pro-caspase-9 to form the apoptosome(184, 185). Pro-caspase-9, an initiator caspase, is then cleaved and auto-activated within the apoptosome, and can then proceed to cleave and activate the executioner caspases-3 and -7, which triggers the caspase cascade, ultimately resulting in the demolition of the cell(184, 185) (figure 1.2.5.1.).

The intrinsic apoptotic pathway is initiated exclusively by signals from within the cell, independent of any extracellular signalling, and such signals include but are not limited to growth factor deprivation, DNA damage, cytokine deprivation, and hypoxia(184, 185). Intrinsic apoptosis is mediated by the BH3-only family of pro-apoptotic proteins, which are signalled to undergo post-translational modifications or are up-regulated in response to pro-apoptotic stimuli(184, 185). For instance, Noxa and Puma are up-regulated by increased transcription, Bid is cleaved into its active form, tBid, and Bad requires activation by de-phosphorylation(189). Following this, these BH3-only proteins can promote Bax and Bak activation and apoptosis then proceeds as described above (figure 1.2.5.1.).

The extrinsic apoptotic pathway is initiated by transmembrane receptor and ligand interactions involving death receptors of the tumour necrosis factor receptor (TNF-R) family and Fas receptor (FasR)(184, 185). Both TNF-R and FasR are characterised by the presence of a common cytoplasmic region termed the death domain, an 80–100 amino acid motif involved in the transduction of the apoptotic signal(190). Upon TNF-R and FasR binding with their ligands, TNF-α and FasL respectively, the death domain binds and activates an associated protein, FADD (Fas-associated death domain protein)(190). The resulting complex, the death-inducing-signalling-complex (DISC), then activates pro-caspases-8 and -10, which then go on to activate the executioner caspases independently of the intrinsic mitochondrial pathway, and the caspase cascade that leads to apoptosis ensues (figure 1.2.5.1.)(184). Caspase-8 also cleaves the BH3-only domain protein Bid into its active form, tBid, which then translocates to and inserts into the MOM, resulting in activation of Bax and Bak and leading to apoptosis as described previously (figure 1.2.5.1.)(184).

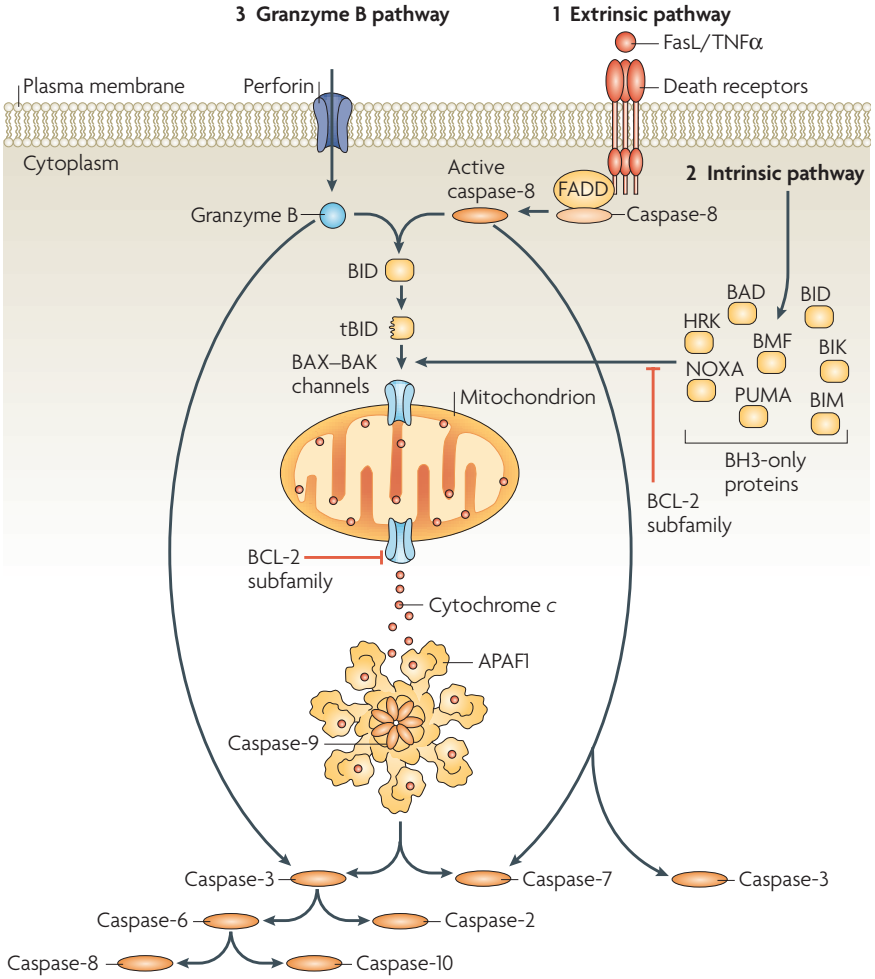

Figure 1.2.5.1: Apoptotic pathways. The caspase cascade and apoptosis can be triggered in three, not necessarily exclusive, ways: 1) The intrinsic pathway; 2) the extrinsic pathway; and 3) the granzyme B pathway. Importantly, the intrinsic pathway is dependent on Bax/Bak oligomerisation and the resultant mitochondrial outer membrane permeabilisation, release of cytochrome c, and formation of the apoptosome to trigger the caspase cascade, whereas the extrinsic and granzyme B pathways can also activate the executioner caspases independently of the mitochondria. Figure reproduced from reference (184).

The third apoptotic pathway is the granzyme B pathway, through which cytotoxic T-lymphocytes are able to eliminate transformed tumour cells or virally infected cells by delivering granules containing a pore forming protein called perforin and serine proteases called granzymes(184). Perforin can form pores in the plasma membrane of the target cells, permitting entry of granzyme B, which can cleave and activate caspase-3 and the BH3-only protein Bid, both leading to apoptosis as detailed above(184).

In addition to the three described apoptotic pathways, reactive oxygen species (ROS) can also be involved in the initiation of apoptosis(191). Mitochondrial integrity may be influenced by the redox status of the cell, with excessively high levels of ROS resulting in significant damage to mitochondria(191). This can cause leakage of calcium and mitochondrial proteins, including cytochrome c, into the cytoplasm, in turn resulting in activation of the caspase cascade(191). Furthermore, the pro-apoptotic activity of cytochrome c itself can be influenced by its redox state. Under normal conditions cytochrome c has been shown to be reduced and held inactive by intracellular antioxidant systems, whereas under conditions of oxidative stress it is oxidised and becomes active in driving cytochrome c-mediated apoptosis(192).

p53 plays a central role in mediating the induction of apoptosis, which it can influence through numerous mechanisms. Importantly, however, these are highly dependent on the nature of pro-apoptotic stimulus and the tissue type involved (reviewed in(193)). As described previously, p53 functions predominantly as a transcription factor and can promote the transcription of the pro-apoptotic protein Bax(194), as well as the BH3-only pro-apoptotic family members Noxa(195) and Puma(196), all of which are key players in promoting initiation of apoptosis at the mitochondria. Furthermore, another transcriptional target of p53, p53-regulated apoptosis-inducing protein-1, which is a non-Bcl-2 family member, can localise to the mitochondria and through binding to Bcl-2 stimulate MOMP(197). p53 can also promote the up-regulation of proteins involved in the extrinsic apoptotic pathway as follows: the cell surface death receptor FasR(198) and its ligand FasL(199); DR5/KILLER (a TNF-R family death receptor)(200); and p53-induced protein with a death domain (PIDD), which is a cytoplasmic protein that upon binding an adaptor protein RAIDD activates caspase-2, triggering the caspase cascade(201). p53 has also been reported to transcriptionally activate the expression of Apaf-1(202) and caspase-6(203), further contributing to the stimulation of the caspase cascade.

A collection of genes termed p53-induced genes (PIGs) have also been identified, which encode proteins with activities related to the increase of cellular ROS levels, and as such are implicated in ROS-mediated apoptosis(191). p53 promotes the induction of such pro-oxidant genes when at hyper-physiological levels, which is in contrast to its role in under basal conditions(204). At basal levels, p53 induces the expression of several genes encoding proteins with anti-oxidant activities, including mammalian sestrin homologues 1 and 2 (SESN1 and SESN2), glutathione peroxidase 1 (GPX1), and TP53-

inducible glycolysis and apoptosis regulator (TIGAR), which act to maintain ROS at a non-toxic levels(204, 205). This dual action of p53 in relation to ROS ensures that in unstressed cells the levels of ROS are controlled, preventing DNA damage and genetic instability, while in the context of cellular stress ROS up-regulation results in induction of apoptosis(204).

In addition to transcriptional activation, p53 can also repress the transcription of the anti-apoptotic protein Bcl-2 through a transcription repressing p53 RE in the promoter of the *BCL-2* gene(206). A role for the direct, transcription-independent involvement of p53 in eliciting an apoptotic response has also been described. It is thought that cytosolic p53 can translocate to the mitochondria where it can directly activate Bax(207), or form an inhibitory complex with the anti-apoptotic proteins Bcl-XL and Bcl-2(208).

The undoubted role of p53 as a critical mediator of apoptosis, together with the importance of apoptosis in determining responses to anti-cancer therapies, has led to the assumption that cells deficient in wild-type p53 (through mutation for example) would be resistant to apoptosis, and by extension such anti-cancer therapies(186). However, a number of studies have revealed that apoptosis can also be induced independently of p53, and the study of many cancer cell lines has shown that p53-mutated cells do not lose their ability to undergo apoptosis(209). For instance, several relatively recent studies have shown that the induction of the pro-apoptotic proteins Puma, Noxa, Fas, and DR5 can be orchestrated in p53-independent manner(210-213). The check-point kinases Chk1 and Chk2, along with E2F and p73, have also been reported to function in a pathway controlling p53-independent apoptosis induced by cytotoxic drugs(214), and p53-independent apoptosis, involving p73 and caspase-2 signalling, has been observed in melanoma cells following treatment with a DNA topoisomerase I inhibitor(215). A further mechanism implicated in p53-independent apoptosis involves nuclear factor-κB (NF-κB), which although typically anti-apoptotic, can display pro-apoptotic activity in certain contexts(209). To this end, ROS have been shown to induce apoptosis through NF-κB-mediated transcription of FasL(216). Finally, another factor implicated in p53-independent apoptosis involves degradation of the anti-apoptotic protein Bcl-2, although the mechanistic basis of this still remains to be clarified(209).

1.2.6. Senescence

Cellular senescence is another fail-safe mechanism involved in preventing the development of cancer, and is becoming increasingly recognised as an important alternative means by which anti-cancer treatments act in some cell types(217, 218), SCCHN cells included(57). Cellular senescence is a type of irreversible cell cycle arrest, where the cell remains metabolically active but can no longer divide and proliferate, and which is characterised by a number of specific phenotypic changes that differentiate it from quiescence (reversible cell cycle arrest)(218). Such features include an enlarged and flattened morphology, condensed chromatin, and senescence-associated β-galactosidase (SA-βgal) activity (described in more detail in section 2.7.1.)(218, 219). Senescence was first formally identified in normal cells as a physiological process related to ageing and replicative stress(220). Most somatic cells have a limited replicative lifespan related to telomere (the repetitive DNA sequence at the ends of chromosomes) shortening. Every cell cycle is accompanied by a shortening of telomeres, and in cells that lack endogenous telomerase (an enzyme which can extend the telomeres) it is this telomere erosion that results in so-called replicative senescence(218). Cell ageing is associated with the accumulation of mutations that could result in genetic instability and eventually lead to malignant transformation, and consequently senescence is now recognised to be an important tumour suppressive response(218). In keeping with this, a senescent state can also be induced by other distinct stress signals such as oncogene activation, excessive DNA damage, and oxidative stress(218).

It comes as no surprise, therefore, that p53 plays an important role as an effector in the induction of cellular senescence(221). p53 is activated in response to the senescence-inducing signals of telomere erosion, DNA damage, and oncogenic signalling (discussed previously in section 1.2.3.), and subsequently promotes the transcription of p21, which can inhibit cell cycle regulators to induce senescence(221). Although stimuli that generate a DNA damage response induce senescence primarily through this p53-dependent pathway, senescence can also be induced through the p16–Rb pathway(218). Senescence signals can induce the expression of p16, which, by binding and inhibiting the CDKs, prevents Rb phosphorylation and cell cycle progression (discussed previously in section 1.1.3.)(218). Whilst there is cross-talk between the p53 and p16–Rb pathways, these pathways can both independently halt cell cycle progression and give

rise to a senescent phenotype(218). Moreover, other examples of senescence that appear to be independent of these pathways have also been reported(222, 223).

As with apoptosis, cellular redox status appears to play an important role in cellular senescence(224). High levels of ROS appear to be involved, not only as inducers of DNA damage and thus senescence, but also in maintaining a senescent phenotype. Persistent activation of p21 has been shown to induce mitochondrial dysfunction and production of ROS, which in turn propagates the DNA damage response, thereby setting up a positive feed-back loop that is necessary for establishing a stable senescent phenotype(225, 226). Similarly, activation of the other major senescence-inducing pathway, the p16-Rb pathway, has been shown to induce elevated intracellular ROS levels, which activate protein kinase Cδ, in turn promoting further generation of ROS and thus establishing a positive feed-back loop(227). The resulting sustained activation of ROS-protein kinase Cδ signalling was reported to irreversibly block cytokinesis and lock the cell into an actively maintained state of "deep" cellular senescence(227).

1.2.7. TP53 mutation in cancer

As discussed in section 1.1.3., the most common molecular alteration found in human cancers, SCCHN included, is inactivation of the p53 tumour suppressor pathway. Typically, this is achieved through mutation of the *TP53* gene itself, which is found in ~50% of all human cancers(133) and in 60-85% of SCCHNs(51-53), but may also result from defects preventing p53 activation, altered subcellular localisation of the p53 protein, defects in the signalling pathways downstream of p53(174), and, in the case of HPV-related SCCHN, viral oncoprotein-induced inactivation of p53 (see section 1.1.3.).

It is interesting to note the mutational spectra of *TP53*, which differs markedly from that of other tumour suppressor genes. For most tumour suppressor genes, such as *APC* or *RB*, nonsense point mutations and frameshift mutations, which result in the production of a truncated protein or no protein expression at all, predominate(228). In contrast, the vast majority of *TP53* mutations (≈75%) are missense mutations, resulting in the production of a full-length protein with single amino acid substitutions(54). This suggests that there is a selective advantage of the mutant p53 protein over the truncation, which can be explained by considering Knudson's two-hit hypothesis together with the fact that p53 functions as a tetramer (see section 1.2.1.). Knudson's two-hit hypothesis dictates that most tumour suppressor genes are recessive, with inactivation of both alleles, so-called loss of heterozygosity (LOH), therefore required for

loss of tumour suppressor function and initiation of cancer development(229). Accordingly, whilst the presence of a nonsense mutation in one *TP53* allele would potentially result in no protein expression or expression of a truncated protein, the remaining wild-type protein expressed from the second allele would retain p53 transcriptional activity and suppress tumour formation. In the context of missense mutation, however, hetero-oligomerisation can occur between such mutants and the remaining wild-type p53, which prevents p53 from functioning as a tetramer and thus neutralises the wild-type protein(230, 231). This phenomenon is known as a dominant-negative effect and less competent sequence-specific DNA binding of the mutant/wild-type p53 hetero-oligomer has been implicated as the underlying mechanism(231). Furthermore, It has also been suggested that in these complexes mutant p53 is capable of shifting the wild-type p53 into a mutant conformation(232). In support of this concept of negative dominance, mice that are heterozygous for a dominant-negative p53 mutant still have a tendency to develop tumours(230). Interestingly, however, LOH is still frequently observed in cancers harbouring *TP53* mutations, suggesting that the dominant-negative effects of the mutants may not lead to complete loss of p53 function(233).

The overwhelming majority of tumour-derived *TP53* mutations affect the conserved regions within the central DNA-binding domain of the protein, most of which exert a dominant-negative effect resulting in loss of wild-type p53 transcriptional activity(135, 144, 234). Furthermore, although the spectrum of missense mutations within DNA-binding domain is wide, certain codons have a particularly high frequency of mutation, with more than 40% of all mutations found at only six p53 residues – 175, 245, 248, 249, 273 and 282 – the so-called mutational hotspots(54, 135) (figure 1.2.7.1.).

A

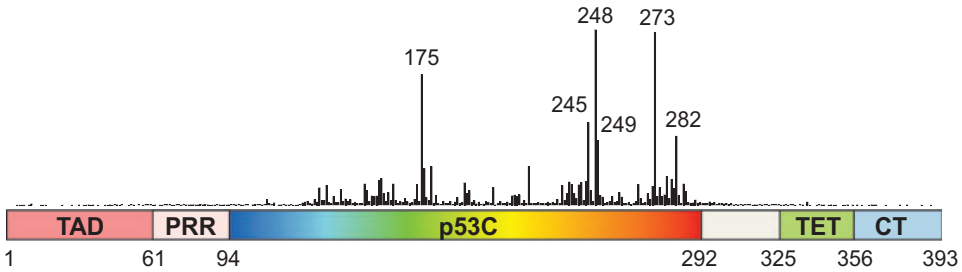

B

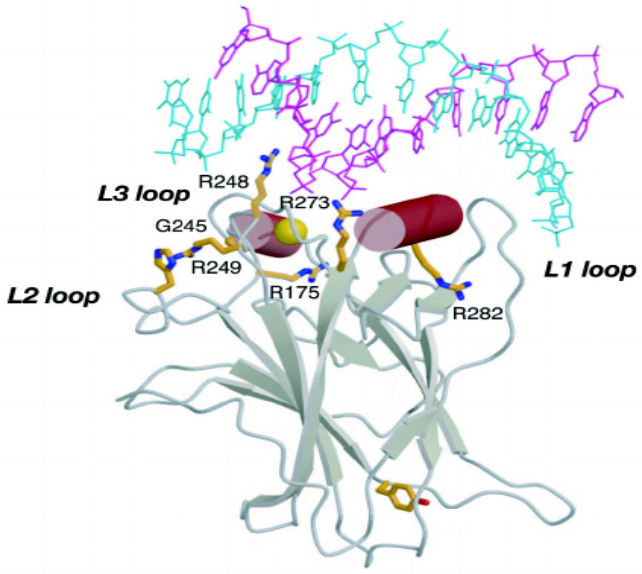

Figure 1.2.7.1: Mutational hotspots in the p53 protein. The majority of p53 mutations are found in the DNA-binding domain of the protein (p53C) with six mutational hot-spots at residues 175, 245, 248, 249, 273 and 282. These are depicted on a schematic of the domain structure of the full-length p53 protein in A, and on a ribbon diagram of DNA bound core p53 domain. In B, the two strands of bound consensus DNA are shown in blue and magenta, and the bound zinc ion is shown as a golden sphere. Figures adapted from reference (135).

It is now widely recognised that different p53 mutants, even within the DNA-binding domain, confer varying oncogenic potency(235), which has led to the classification of p53 mutants. On the basis of the crystal structure of the core domain of p53, mutations can be divided into two main classes – contact and structural mutations(144). The contact mutations affect residues that make direct contact with DNA, the two most common of which are found at residues R248 and R273, with frequencies of 8% and 7.5% respectively(54). In contrast, the structural mutations disrupt the folding of the p53 protein and most commonly occur at residues R175 (5.5%), G245 (3.5%), R249 (3%) and R282 (3%)(54). It has been suggested that structural mutations confer greater

oncogenic potency than contact mutants(235), which is thought to relate to the degree of the dominant-negative effect. Structural mutants can shift the remaining wild-type p53 into a mutant conformation upon hetero-oligomerisation, resulting in complete loss of p53 function, whereas contact mutants are more likely to retain a native conformation and when incorporated into tetramers with wild-type p53 would therefore retain some residual wild-type activity(236). Consistent with this, 100% LOH has been observed with expression of contact p53 mutants in SCCHN, while expression of structural mutants has been associated with LOH in only 50% of cases, implying a stronger dominant-negative effect on wild-type p53, and by association a lesser selective pressure for losing the wild-type allele(237). Interestingly, however, contact mutations were associated with higher tumour stages, higher propensity for lymph node metastasis, and shorter recurrence-free and overall survival than structural mutations in this study, suggesting that dominant-negative inhibition of the wild-type allele is not complete and LOH remains an important event during tumorigenesis(237).

An alternative classification of p53 mutants that has been applied to SCCHN is the designation of mutants as either disruptive or non-disruptive. This classification specifically defines disruptive mutations as either nonsense mutations or missense mutations in the L2–L3 DNA-binding domain of p53 leading to an amino acid change that results in a residue with a different polarity or charge, with all other mutations classified as non-disruptive(56). On the basis of this classification, mice injected with SCCHN cells harbouring disruptive *TP53* mutations have been reported to exhibit faster tumour growth, greater incidence of cervical lymph node metastasis, and shorter survival than mice injected with cells harbouring either wild-type *TP53* or non-disruptive *TP53* mutations(238). Consistent with this, a study of *TP53* mutation status in 420 patients with surgically treated SCCHN demonstrated that *TP53* mutations were associated with decreased survival relative to patients with wild-type *TP53* tumours, and that disruptive *TP53* mutations were associated with the shortest survival(56). Furthermore, in a subsequent study of 74 SCCHN patients treated with surgery and post-operative RT although *TP53* mutation alone was not a clinical prognosticator, disruptive *TP53* mutation was a strong negative predictor of locoregional recurrence, which was shown to relate to increased radioresistance mediated via the inhibition of senescence(57).

More recently, a computational strategy for mutant p53 classification based on phylogenetic divergence and predicted functional impact has been proposed. This so-

called evolutionary action score or EAp53 classifies mutations as either high- or low-risk, with sequence variations giving rise to larger phylogenetic divergences ascribed higher scores than those resulting in conservative amino acid changes(58). Interestingly, high-risk *TP53* mutations, as determined using this classification system, have been associated with more invasive and tumorigenic characteristics than low-risk mutations in both *in vitro* and *in vivo* SCCHN models(58), with poorer survival outcomes and a higher rates of distant metastases in SCCHN patients(58), and with resistance to cisplatin-based chemotherapy(239).

A further important concept to consider when it comes to varying oncogenic potency of *TP53* mutants is that of oncogenic GOF. Dominant-negative effects on the wild-type protein notwithstanding, some p53 mutants have been suggested to acquire additional oncogenic properties contributing to accelerated cell growth and tumorigenic potential – so called oncogenic GOF(55). This concept that mutant p53 may be more than simply an inactivated tumour suppressor came from a study showing that point mutations in wild-type *TP53* activate it for cellular transformation in cooperation with the *RAS* oncogene(240), and the term GOF was first proposed in 1990 when different mutant forms of p53 were reported to gain transforming potential(241). More recently, further studies have provided more convincing evidence of mutant p53 GOF properties. In particular, studies of two mouse models of Li-Fraumeni syndrome, which focused on R175H and R273H p53 mutants, demonstrated that although the two *TP53* mutations did not distinguish on overall survival, mice heterozygous for the mutant p53 (p53M/+) developed different tumour spectra than mice hemizygous for wild-type p53 (p53+/-)(242, 243). Furthermore, mice hemizygous for the mutant *TP53* allele (p53M/-) developed novel tumours compared to p53-null (p53-/-) mice suggesting that these two p53 mutants play a role in stimulating tumorigenesis(242, 243). Additionally, each of the p53 mutants demonstrated distinct tumour spectra, importantly indicating that different mutants exhibit distinct profiles with respect to GOF activity(243). In support of this, the p53 mutant R248Q has a consistently strong GOF phenotype in contrast to the G245S mutant in mutant *TP53*–knock-in mice(244).

Despite the evidence suggestive of GOF properties, the mechanistic basis remains poorly understood. To date, three main mechanisms of action have been proposed to understand the possible role of mutant p53 GOF in regulation of novel gene transcription: firstly, direct DNA binding of mutant p53 to novel target gene promoters in a DNA structure-specific manner to activate them(55); secondly, binding and co-

operation of mutant p53 with other transcription factors such as p63, p73, NF-κB, NF-Y, E2F1, VDR, SP1, SREBP, and ETS to enhance or repress target gene expression(55); and lastly, through epigenetic regulation of chromatin remodelling(245).

1.3. Metabolism in cancer

The concept that metabolism in tumour cells is altered from that in normal tissues was first introduced over 80 years ago by Otto Warburg (reviewed in (246)). Only relatively recently, however, has it become clear that many key oncogenic signalling pathways are fundamentally involved in adapting tumour cell metabolism in order to support growth and survival, thus providing links between tumour metabolism and the causal changes determining the cancer phenotype(247). In light of this, Hanahan and Weinberg have recently added a state of "deregulated cellular energetics" to the original hallmarks of cancer described in their seminal paper from 2000(43, 44), reflecting the now widely held consensus that cellular metabolism is substantially altered during oncogenesis and tumour progression. Indeed, the fact that interfering with these altered metabolic programs in cancer mouse models profoundly limits tumour cell growth highlights the dependence of cancers on metabolic re-programming(248, 249). It is important to recognise, however, that the precise ways in which metabolism is re-programmed can vary widely between cancers, depending both on genotype and tissue of origin(250), highlighting the need for cancer-specific study of metabolic perturbations.

1.3.1. Principles of altered tumour metabolism

Since Warburg's seminal observation that cancer cells metabolise glucose in a manner distinct from that used by normal eukaryotic cells(246), it has become evident that rewiring of tumour cellular metabolism is highly complex and may differ in many ways from that in normal eukaryotic cells, including use of secondary metabolic pathways and increased anaplerotic and cataplerotic flux(251-254). Nonetheless, Warburg's observation that cancer cells have a propensity to "ferment" glucose using glycolysis under both anaerobic and aerobic conditions – often referred to as the Warburg effect – remains chief among the recognised metabolic perturbations of the cancer phenotype, is certainly the best characterised, and consequently will be the focus throughout this thesis. Indeed, microarray studies have shown that glycolytic genes comprise one of the most up-regulated gene sets in cancer(255, 256), and it is on the principle of the Warburg effect that ^{18}F-FDG PET imaging is based, which has come into widespread

clinical use in the diagnosis, staging, and assessment of treatment response of many cancers, SCCHN included(93).

Most cells in normal tissues first catabolise glucose to pyruvate through glycolysis and, provided there is sufficient oxygen tension, convert pyruvate into acetyl-CoA in the mitochondria by pyruvate decarboxylation before completely oxidising most of that acetyl-CoA to carbon dioxide and water in the mitochondrial tricarboxylic acid (TCA) cycle. This produces reduced nicotinamide adenine dinucleotide (NADH) and flavin adenine dinucleotide ($FADH_2$), which then fuel oxidative phosphorylation to maximise adenosine triphosphate (ATP) production(257). Only under anaerobic conditions is the pyruvate generated by glycolysis redirected away from mitochondrial oxidative phosphorylation to produce large amounts of lactate(257). In contrast, cancer cells often appear to have a predilection for the latter regardless of whether or not oxygen is present, which is also accompanied by an increase in glucose uptake and glycolytic flux, necessitated by the fact that aerobic glycolysis is far less efficient in terms of ATP generation than oxidative phosphorylation(257).

The fact that this switch in glucose metabolism is an energetically inefficient process, yielding only two molecules of ATP per molecule of glucose consumed as opposed to up to 36 with oxidative phosphorylation, invites scrutiny of the impetus driving proliferating cancer cells to engage in such a process. Whilst Warburg originally proposed that such reliance on glycolytic metabolism was compensatory for energy deficiency resulting from defective mitochondrial oxidative phosphorylation(246), more recent studies have demonstrated that mitochondrial function is frequently unimpaired in cancer cells and many tumours retain the capacity for oxidative phosphorylation and consume oxygen at rates similar to those observed in normal tissues(249, 258-261). Alternatively, it has been suggested that such a metabolic switch is an adaptive response to hypoxic conditions during the early avascular phase of tumour development, as it allows for ATP production in the absence of oxygen(257). However, considering that certain leukemic cells have been observed as highly glycolytic(262, 263) despite existing in the bloodstream at higher oxygen tensions than found in most normal tissues, and that bronchogenic tumours, which are exposed to a continuous supply of oxygen during tumorigenesis, also exhibit aerobic glycolysis(264, 265), it seems that hypoxia may not be a major factor in the switch to aerobic glycolysis by cancer cells. Accordingly, such traditional views of tumour metabolism as a self-correcting, homeostatic system have largely given way to more contemporary thinking that metabolic switching is a dynamic

process adopted by cancer cells to fit the requirements of rapid cell proliferation. Indeed, the ever-evolving intricate links between metabolism and critical oncogenic events, such as *TP53* mutation, Myc and Ras overexpression, persistent activation of PI3K–AKT growth signalling, and enhanced mammalian target of rapamycin (mTOR) activity, lend credence to this notion, suggesting metabolic switching is central to malignant transformation rather than a secondary consequence(247).

Evidently, cancer cells have important metabolic requirements that extend beyond ATP generation to support cell growth and proliferation, but the principal selective advantage that glycolytic metabolism may provide is not entirely clear. One possible rationale is that glycolysis, although inefficient in yield of ATP produced per molecule of glucose consumed, has the capacity to generate ATP at a higher rate compared with oxidative phosphorylation, which would be advantageous provided glucose supplies were not limited(266). Perhaps more tenable explanations, however, relate to the concepts of 1) anabolic biosynthesis to enhance production of proper intermediates to allow for cell growth and proliferation, and 2) regulation of cellular redox potential to minimise the damaging effects of ROS(247, 257, 267). In order to support growth and proliferation a cell must replicate all of its cellular contents to yield two daughter cells, which in the context of an incessantly proliferating cancer cell requires liberal generation of nucleotides, amino acids, and lipids, without which rapid cell proliferation will halt irrespective of how vast a supply of ATP is provided. This in turn demands production of intermediates such as carbon, nitrogen, nicotinamide adenine dinucleotide phosphate (NADPH), ribose, and acetyl-CoA, which are, for the most part, generated from high flux of substrate through glycolysis and utilisation of subsidiary metabolic pathways(247, 257). Such increased generation of intermediates, chiefly NADPH, may also be important for cancer cells to up-regulate their antioxidant systems to quench the increased ROS levels resulting from heightened oxidative substrate flux and deregulated cellular proliferation, giving rise to the enigmatic situation of high ROS production in the presence of high antioxidant levels (192, 247, 267, 268). Although conceivably advantageous to tumour cells at moderate levels – stimulating cell proliferation, anchorage-independent growth, survival pathways, and induction of genetic instability(269-271) – excessively high ROS levels result in DNA damage(271), activation of protein kinase Cδ prompting senescence (detailed in section 1.2.6.)(227), and permeabilisation of mitochondria leading to cytochrome c release and apoptosis (detailed in section 1.2.5.)(192). In line with the potential importance of ROS limitation in tumour growth, several oncogenes actively suppress ROS through increased

transcription of Nrf2 – a transcription factor that promotes ROS detoxification – while deletion of Nrf2 *in vivo* reduces the ability of the oncogenic K-Ras to induce proliferation and tumorigenesis(272). Importantly, pyruvate, oxaloacetate, and α-ketoglutarate can all act as ROS scavengers(273-275), while NADPH is centrally involved in redox control, providing the reducing power for the major cellular antioxidant systems, specifically the glutathione and thioredoxin systems, which scavenge ROS and protect against oxidative damage-induced cell death(276).

In support of these concepts, several independent lines of investigation have demonstrated, in addition to the Warburg effect, activation of alternative carbohydrate metabolic pathways in cancer cells that use glycolytic intermediates as precursors. Such pathways include the hexosamine pathway, uridine diphosphate−glucose synthesis, and the pentose phosphate pathway (PPP)(277-279), all of which generate the macromolecular precursors and/or reducing equivalents necessary to support cell proliferation and combat oxidative stress. Increased PPP shunting, which produces phosphopentoses and ribonucleotides and is also a major source of NADPH, may be particularly significant given the bipartite importance of NADPH in promoting both macromolecular biosynthesis and redox control(280). In further support of the selective advantage conferred by utilisation of such subsidiary carbohydrate metabolic pathways, cancer cells have a propensity to express the M2 isoform of pyruvate kinase (PKM2)(248, 281, 282) − a relatively inefficient isoform of the enzyme that catalyses the rate-limiting, ATP-generating step of glycolysis(281, 283, 284). Although on initial consideration this may seem counter-intuitive as glycolytic flux is slowed, this facilitates effective shunting of carbon into the aforementioned key subsidiary pathways. Similarly, TIGAR, an enzyme discovered relatively recently through microarray analysis of gene expression following p53 activation(205, 285), also promotes such advantageous shuttling and has been shown to be overexpressed in cancer cells(286-288). TIGAR acts principally as a fructose-2,6-bisphosphatase, thereby reducing the concentration of intracellular fructose-2,6-bisphosphate, a powerful allosteric activator of phosphofructokinase-1 (PFK-1)(205) − an essential glycolytic enzyme that catalyses conversion of fructose-6-phosphate to fructose-1,6-bisphosphate. Thus, by decreasing PFK-1 activity TIGAR limits glycolytic flux downstream of this point, redirecting the metabolites to subsidiary pathways(205) (figure 1.3.1.1.). Furthermore, the resulting accumulation of fructose-6-phosphate can also increase flux into the non-oxidative branch of the PPP (figure 1.3.1.1.), and under hypoxic conditions TIGAR has also been shown to translocate to the mitochondria and bind to hexokinase-II (an isoform of the

first enzyme of the glycolytic pathway), stimulating hexokinase-II activity independently of its bisphosphatase activity. This results in an increase in glycolytic flux and availability of glycolytic intermediates for use in subsidiary pathways, implying that TIGAR is a positive regulator of the PPP in both a phosphatase-dependent and independent manner(280, 289).

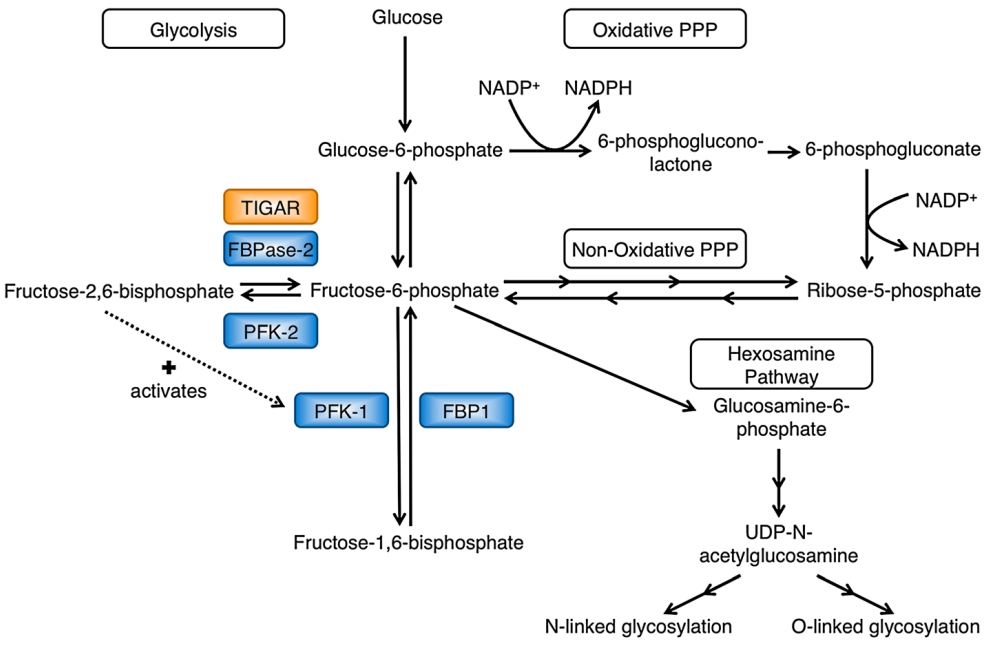

Figure 1.3.1.1: Relationship of TIGAR, glycolysis and subsidiary pathways of carbohydrate metabolism. TIGAR functions primarily as a fructose-2,6-bisphosphatase and therefore reduces the concentration of fructose-2,6-bisphosphate, which is an allosteric activator of PFK-1. TIGAR is predicted to promote both the PPP and hexosamine pathways by lowering the levels of fructose-2,6-bisphosphate and redirecting glycolytic intermediates. Figure reproduced from (290).

Accumulating evidence that some tumour cells metabolise substantial amounts of alternative oxidisable substrates such as glutamine(252, 253, 291) also lends support to the notions that biosynthetic and redox balance advantages underpin the rationale for metabolic re-programming in cancer cells. During glutaminolysis mitochondrial activity is diverted towards biomass production whereby TCA cycle intermediates are used to generate essential macromolecular building blocks. Following cellular uptake, glutamine is converted to glutamate by mitochondrial glutaminase enzymes, which is then converted to α−ketoglutarate, which supplies the carbon input required for the TCA cycle to engage in the production of other amino acids and fatty acids(252, 292). Moreover, initial conversion of glutamine to glutamate releases and facilitates potential capture of nitrogen from the amino group for nucleoside and amino acid synthesis(252,

292). In addition to fuelling biosynthesis, glutamate can be converted directly into reduced glutathione (GSH) by the enzyme glutathione cysteine ligase, and recent evidence also suggests that glutamine-derived carbon may exit the TCA cycle as malate, serving as a substrate for malic enzyme 1, which produces NADPH(252).

1.3.2. The role of p53 in altered tumour metabolism

Although the precise sequence of events and driving forces that converge to perturb core cellular metabolism in cancer cells remain unclear, it has become evident that multiple events critical in initiating oncogenesis are intricately linked with metabolic regulation, and as such are likely implicated this metabolic switch(247, 267). One such fundamental oncogenic event that may contribute to metabolic re-programming is loss of wild-type p53 function, which is particularly pertinent to SCCHN given its crucial importance in SCCHN tumorigenesis (discussed in sections 1.1.3. and 1.2.7.). Although p53, an extensively studied tumour suppressor, is best known for its complex and critical roles in the regulation of processes including cell proliferation, death, and responses to exogenous stress (detailed in sections 1.2.3 –1.2.6.), recent studies have revealed that p53 also plays a central role in metabolic homeostasis, balancing glycolytic activity and mitochondrial respiration(174). Indeed, recent studies have raised questions regarding the relative importance of the "classical" p53 functions in p53-mediated tumour suppression, suggesting the possibility that emerging p53-regulated processes, such as metabolic homeostasis, may be central in limiting tumorigenesis(293).

In keeping with its tumour suppressor properties, p53 appears to counteract metabolic alterations typically associated with cancer development, with loss of wild-type p53 function potentially leading to acquisition of a glycolytic phenotype at the expense of mitochondrial respiration(247, 267, 294). p53 can exert influence over both glycolysis and oxidative phosphorylation through multiple mechanisms, which may also modulate the activity of related subsidiary pathways (figure 1.3.2.1.). PFK-1 represents a key regulatory point in the glycolytic pathway and, as alluded to above, p53 plays a role in regulating glycolysis at this critical point. By inducing the transcription of TIGAR, which acts primarily as a bisphosphatase that reduces intracellular fructose-2,6-bisphosphate concentration, allosteric activation of PFK-1 is lost, resulting in a dampening of glycolytic flux. Additionally, activation of p53 typically decreases the activity of phosphoglycerate mutase (PGAM) − the catalyst for conversion of 3-phosphoglycerate to 2-phosphoglycerate − through increased ubiquitylation and subsequent proteosomal

degradation(295), mediated via direct binding to MDM2(296). p53 has also been shown to repress the expression of pyruvate dehydrogenase kinase (PDK), an enzyme which inactivates the pyruvate dehydrogenase complex (PDC), activity of which is crucial in determining the fate of pyruvate, with PDC acting to convert pyruvate to acetyl-CoA at the expense of lactate production(297). Thus, p53 activates PDC, promoting pyruvate decarboxylation and TCA cycle flux(297). In concert with negatively regulating glycolytic enzymatic activity, p53 may also curb glycolysis by down-regulating relevant transporter molecules: the expression of the glucose transporters GLUT1 and GLUT4, which are involved in cellular glucose uptake, is transcriptionally repressed by p53(298), while further downstream in glycolysis p53 suppresses monocarboxylate transporter-1 (MCT-1) expression, which prevents lactate efflux under hypoxic conditions, a necessity in sustaining elevated rates of glycolysis(299).

Complementary to its proposed actions to restrict glycolytic flux, p53 is also thought to be coupled to the maintenance of mitochondrial integrity and promotion of oxidative phosphorylation. p53 has been reported to regulate stability of mitochondrial DNA and mitochondrial biomass through induction of genes such as the ribonucleotide reductase subunit p53R2(300-302), and may play a role in repairing or removing compromised mitochondria via induction of mitochondria-eating protein (Mieap), thereby modulating mitochondrial quality control(303). Specific to oxidative phosphorylation, p53 can enhance transcription of Parkin, which promotes mitochondrial respiration by increasing the cellular level of acetyl-CoA through upregulation of pyruvate dehydrogenase(304). p53 can also transcriptionally activate the gene for subunit I of the cytochrome c oxidase (COX) complex (complex IV in the mitochondrial electron transport chain [ETC] and major site of cellular oxygen utilisation)(305), as well as the gene for synthesis of COX 2, which, in conjunction with synthesis of COX 1, is required for the assembly of the COX complex(286, 306, 307). Moreover, apoptosis inducing factor, which is crucial to the maintenance of ETC complex I, has been shown to be subject to positive transcriptional regulation by p53(308), while p53 localised to the mitochondria may promote assembly of the ATP synthase complex (the final complex in the ETC involved in generation of ATP) in a p53-transcription-independent manner(309).

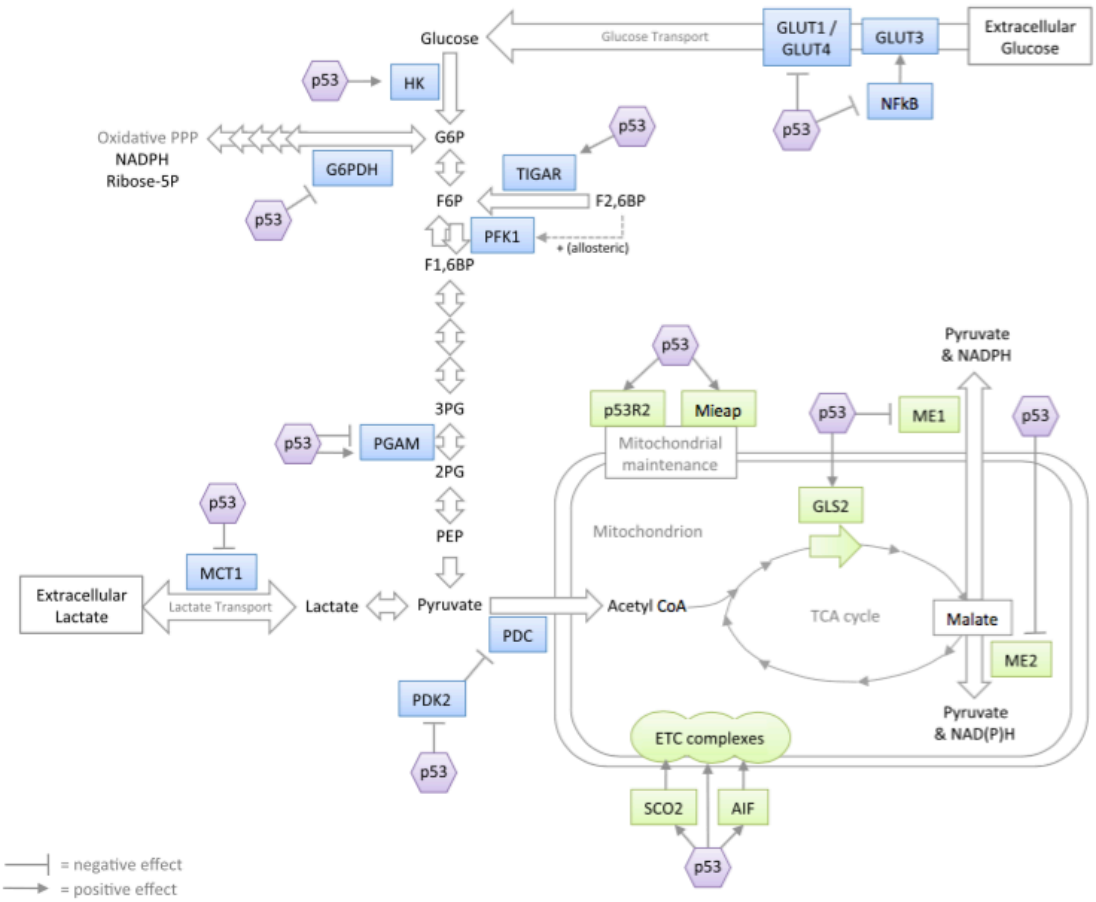

Figure 1.3.2.1: Proposed actions of p53 on glycolysis and mitochondrial respiration. p53 has been reported to exert influence over both glycolysis and oxidative phosphorylation through numerous mechanisms, all of which are depicted in this schematic. In general p53 acts to restrict glycolysis and promote mitochondrial respiration. Figure reproduced from (294).

Further to direct regulatory effects promoting a glycolytic phenotype, there is also a substantial degree of cross-talk between the p53 system and several other key metabolic mediating pathways, resulting in indirect p53 regulation. Perhaps of foremost importance, activation of p53 inhibits the activities of two master regulators of cellular metabolism, the PI3K/Akt and mTOR pathways, which ultimately results in suppression of glycolysis together with inhibition of cell growth, and possibly p53-directed apoptosis and autophagy. In general, p53 exercises such inhibition through upstream transcriptional regulation(310, 311): for instance, p53 promotes transcription of phosphatase and tensin homolog (PTEN), IGF-binding protein-3 (IGFBP3), tuberous sclerosis protein 2 (TSC2), and the β subunit of AMP-activated protein kinase (AMPK), all of which negatively regulate PI3K/Akt and mTOR pathways(310). Furthermore, p53 promotes the expression of SESN1 and SESN2, which also serves to stimulate AMPK

activity(311, 312). AMPK was also recently identified to inhibit the hypoxia-induced factor-1α (HIF-1α) pathway(313), which in turn negatively regulates aerobic glycolysis given that HIF-1α acts to enhance the transcription of numerous glycolytic transporters and enzymes(314), adding further to the web of indirect p53 effects impeding aerobic glycolysis. To this end, p53 has also been implicated in direct upregulation of HIF-1α ubiquitylation and degradation(315). Additionally, p53 can inhibit the NF-kβ pathway through inhibition of IKKβ, which also results in decreased glucose transporter expression, and by association a dampening of glycolytic flux(316).

Although for the most part p53 acts to repress the malignant metabolic phenotype, dampening glycolysis and promoting mitochondrial respiration, seemingly contradictory roles have also been described. For instance, the promoters for the glycolytic enzymes PGAM and hexokinase-II contain p53-REs(317, 318), and p53 has been shown to both promote and inhibit PPP flux(294). Whilst the precise reasons for these opposing p53 responses remain to be elucidated, it is well recognised that p53 does not act, nor is it regulated, in the same manner in the wide variety of tissues from which cancers develop(193). It is highly likely, therefore, that p53-mediated metabolic regulation is tissue-dependent(174, 294), emphasising the importance of cancer-specific study of metabolic perturbations. Consistent with this, in contrast to the p53-dependent destabilisation of PGAM in fibroblasts detailed above(295), a muscle-specific isoform of PGAM is transcriptionally activated by p53 in cardiocytes(317). It is also likely, as with many p53-induced responses, that there is environmental context dependency(166).

Notwithstanding a minority of ostensibly conflicting effects, in general p53 appears to play a role in metabolic homeostasis by balancing glycolytic activity and mitochondrial respiration, with loss of wild-type p53 function, therefore, potentially involved in the acquisition of the unbalanced malignant metabolic phenotype. Furthermore, as discussed in section 1.2.7, some mutated forms of p53 may acquire oncogenic GOF properties, further contributing to tumorigenesis(55). Although the underlying mechanisms involved remain relatively poorly characterised, interestingly a recent study revealed the first link between such GOF properties and metabolic regulation(319). In contrast to wild-type p53, which increases AMPK activity(310), GOF mutant p53 proteins were shown to inhibit specifically AMPK activation and AMPK signalling in SCCHN cells through a direct and distinct protein-protein interaction with the AMPKα subunit, leading to increased aerobic glycolytic capacity, lipid anabolism, and invasive cell growth(319).

1.3.3. Evidence for metabolic re-programming in SCCHN

Although metabolic reprogramming is now recognised as an emerging hallmark of cancer(44), the specific nature and extent of the metabolic perturbations can differ significantly between cancers, depending both on genotype and tissue of origin(250). For instance, aerobic glycolysis is the best-documented metabolic phenotype, yet it is not a universal feature of all cancers: glutaminolysis has been shown to predominate in cervical cancer and glioblastoma(252, 320), while enhanced rather than reduced oxidative phosphorylation is a feature of both breast cancer(321) and chronic lymphocytic leukaemia(322). In keeping with this, there is wide variability clinically in FDG-PET uptake between tumours, and up to 30% of tumours are considered FDG−PET-negative(323). Clearly, this further highlights the importance of detailed study of metabolism in cancer site-specific experimental systems.

Specific to SCCHN, metabolic studies had been somewhat lacking and for the most part have focused on isolated or limited transporter or enzyme expression and their prognostic significance, rather than characterising dynamic metabolic flux and presenting a clear picture of the metabolic phenotype. Several retrospective pathological studies have investigated GLUT-1 expression and have consistently shown overexpression relative to normal mucosa and/or benign squamous lesions(324-328), with one study also demonstrating overexpression in early pre-neoplastic lesions(324). Moreover, expression was associated with the extent of dysplasia, implying that GLUT-1 upregulation is a relatively early event during development of SCCHN. GLUT-1 expression may also have clinical utility in SCCHN: GLUT-1 staining is discernibly higher in recurrent disease compared to primary disease(329); correlates inversely with degree of tumour differentiation(329); and has been shown to be an independent marker of prognosis in both oral cavity and hypopharyngeal SCC, with a high staining index associated with a significant reduction in survival(330, 331). Furthermore, pre-treatment GLUT-1 overexpression has also been identified as a marker of radioresistance in oral cavity SCC(332). Whilst GLUT-1 is the glucose transporter typically associated with SCCHN, other members of the GLUT family have also been examined, albeit less extensively. In a study of 48 cases of laryngeal SCC, although GLUT-1 was universally expressed, GLUT-3−positive cases were associated with more poorly differentiated tumours and reduced overall survival, and in a more recent and large-scale study utilising a tissue microarray comprising 142 oral cavity SCCs both GLUT-1 and GLUT-3 expression was shown to negatively prognosticate(333). Similarly, in a gene

expression profile study GLUT-3 overexpression was identified as a prognosticator for increased depth of tumour invasion, larger tumour size, advanced pathologic stage, recurrence, and unfavourable survival(334).

Importantly, GLUT overexpression, unlike most other tumour markers, has a biochemical and clinically utilised correlate in ^{18}F-FDG-PET. The glucose analogue ^{18}F-FDG is taken up rapidly into tumour cells by the glucose transporters GLUT 1 and 3 whereupon phosphorylation by hexokinase prevents release from the cell, while the absence of the 2' hydroxyl group present in normal glucose prevents further glycolysis(93). Thus, ^{18}F-FDG is trapped in the cell allowing PET detection prior to radioactive decay, and the resulting ^{18}F-FDG signal primarily reflects the cells' capacity for glucose uptake(93). Despite some limitations, ^{18}F-FDG-PET with computed tomography is currently used successfully in the initial diagnosis, staging work-up, monitoring of response to therapy, and post-treatment surveillance for recurrence in SCCHN(93). Furthermore, a recent meta-analysis demonstrated both pre- and post-treatment ^{18}F-FDG signal, as measured by standard uptake value, as a reliable predictor of long-term survival in SCCHN(335). This, together with the above GLUT expression data, does suggest that protein levels are indeed linked to a functional tumour phenotype.

Aside from the GLUTs, only a handful of studies have characterised other metabolic markers in SCCHN. Using immunohistochemistry, Deron et al observed hexokinase overexpression, particularly hexokinase-I, in a panel of oropharyngeal and oral cavity SCCs(336), and similarly Chen et al reported significantly higher hexokinase-II expression in laryngeal SCC than in benign squamous laryngeal lesions(337). Furthermore, in the latter study stable knock-down of hexokinase-II expression in laryngeal SCC cells resulted in cell cycle arrest, increased apoptosis, and reduced viability, findings which were paralleled *in vivo* where xenograft tumours derived from such cells were smaller and exhibited reduced proliferation relative to those from untransfected or control-plasmid-transfected cells, suggesting that hexokinase-II, and by extension glycolytic flux, plays an important role in the development of laryngeal SCC(337). One study has also examined PDC activity and found that negative regulation of the PDC occurs as a consequence of enhanced expression of PDK-1, which in turn is partially attributable to the glycolytic phenotype observed in SCCHN cell lines(338). Furthermore, normoxic stabilisation of HIF-1α by glycolytic metabolites secondary to PDC inhibition was observed, which given that PDK-1 is a HIF-1α-regulated gene,

suggests a feed-forward effect is at play in contributing to malignant progression(338). Similarly, study of SCCHN cell lines harbouring mitochondrial mutations also suggests interplay between PDK-2 upregulation, and the resulting attenuation in PDC activity, pyruvate accumulation, and HIF-1α stabilisation(339). Consistent with these findings, a parallel study also demonstrated the importance of PDK-1 expression in maintaining glycolysis in SCCHN cells and additionally showed PDK-1 overexpression in SCCHN tissue, which was strongly related to poor survival outcome(340). Data regarding PKM2 – a relatively inefficient isoform of the enzyme that catalyses the rate-limiting, ATP-generating step of glycolysis(281, 283, 284) – are equivocal. Although one study found PKM2 expression to be an unsuitable tool for differentiating oral cavity SCC from normal tissues(341), Wong et al observed PKM2 overexpression in a small cohort of oral tongue specimens(342), and a more recent analysis of the cancer genome atlas RNA sequencing and exon array datasets demonstrated PKM2 overexpression, which correlated strongly with poor prognosis, despite an absence of PKM1 to PKM2 isoform switching in SCCHN(343).

Whilst these findings collectively provide evidence of increased glucose uptake and possibly increased expression of a number of glycolytic markers in SCCHN, particularly in poorly differentiated and more aggressive tumours, such findings in isolation do not necessarily demonstrate increased glycolytic flux, and are limited in their mechanistic insights into SCCHN metabolism and its role in tumorigenesis. For instance, an important caveat of many of these studies relates to the role of glucose uptake and catabolism in supporting rapid cell proliferation: overexpression of these glycolytic markers may simply be a surrogate for cell proliferation akin to other markers of proliferation such as Ki-67.

As the final by-product of glycolysis, lactate has also been examined as a proxy of glycolytic activity in several SCCHN studies. Brizel et al demonstrated high pre-treatment tumour lactate levels, which despite bearing no relationship to presenting T or N classification, did correlate with decreased overall and metastasis-free survival(344). A recent prospective study following SCCHN patients for up to 15 years also correlated high lactate levels with both reduced overall survival and tumour recurrence post-irradiation(345). Congruous with this, findings from the same research group from two *in vivo* studies, in which SCCHN cell lines were xenografted into nude mice, suggest that increased tumour lactate levels confer relative radioresistance, which was attributed to the antioxidative capacity of lactate(346, 347). Interestingly, although

similar results were observed in a comparative study of cryobiopsies of SCCHN and normal mucosa, expression of lactate dehydrogenase (LDH) (the catalyst for conversion of pyruvate to lactate) did not correlate with tumour lactate content(348). This arguably lends credence to the notion that the raised lactate content was indeed a by-product of increased glycolytic flux rather than a result of any dysregulation of LDH expression. At odds with this, however, are findings from two recent studies examining LDH isoenzyme expression in oral cavity SCC, which demonstrated LDH expression as an independent predictor of disease recurrence and poor survival outcomes, as well as specifically conferring resistance to the chemotherapeutic agent paclitaxel(349, 350).

Recent studies employing magic angle spinning nuclear magnetic resonance (MAS NMR)-spectroscopy to enable broad-spectrum metabolomic analyses, have also utilised lactate levels to infer glycolytic activity. Two MAS NMR-spectroscopy studies, which scrutinised SCCHN cell lines(351) and snap-frozen tumour specimens(352), demonstrated a diversity of metabolic derangements reliably distinct from normal tissue, with heightened lactate levels a consistent feature. In contrast, however, a further NMR-spectroscopy study reported no evidence of elevated lactate in the observed metabolomic profile in a cohort of oral cavity SCC specimens(353).

Findings from several therapeutic studies, which have explored the use of the hexokinase inhibitor 2-deoxy-D-glucose (2-DG), also lend some support to the notion of a glycolytic phenotype in SCCHN. These studies have demonstrated 2-DG to exhibit selective cytotoxicity in both *in vitro* and *in vivo* SCCHN models, and to potentiate the effects of conventional treatments when used in combination, suggestive of a survival dependence of these tumours on glycolysis(354-356). Nonetheless, findings have not been universal(357), and the observed effects of 2-DG may not be simply the result of a catabolic block(358).

A recent study, also utilising 2-DG, sought to compare dependence on different metabolic pathways in SCCHN cell lines(359). In this study, glycolytic inhibition was reported to suppress proliferation and anchorage-independent growth to a greater extent than inhibition of glutaminolysis, suggesting a predominant dependence on glucose catabolism(359). As with previous studies, however, significant heterogeneity in response among the SCCHN cell lines was observed. Interestingly though, further analysis revealed that a pair of isogenic cell lines derived from the same patient but divergent on *TP53* mutational status displayed differing degrees of sensitivity to glucose

deprivation, with the wild-type *TP53* cell line exhibiting relative resistance, suggesting for the first time in SCCHN a possible role for p53 in determining response to glucose starvation, and by extension the metabolic underpinnings(359). A follow-on study from the same research group examined this further, again using the same isogenic cell line pair divergent on *TP53* status(360). Using fluorescence-based, extracellular flux analysis the mutant *TP53* cell line was observed to exhibit a metabolic phenotype distinct from the wild-type *TP53* cell line, with a seemingly greater utilisation of glycolysis and reduced utilisation of oxidative phosphorylation in the mutant *TP53* cells(360). This was also associated with ionising radiation (IR) response following glycolytic inhibition, which potentiated IR effects in mutant *TP53* but not wild-type *TP53* cells, again suggestive of a role of *TP53* status in determining metabolic phenotype in SCCHN(360).

Considering this possible association between loss of wild-type p53 function and glycolytic dependence, together with the importance of the HPV E6 oncoprotein in targeting p53 for proteasomal degradation in HPV-positive SCCHN (see section 1.1.3.), invites scrutiny of metabolism in HPV-driven disease. Only one study has addressed this issue to date, examining both resected HPV-positive oropharyngeal SCC specimens and an *in vitro* HPV-positive cell line, albeit one derived from a hypopharyngeal tumour(361). Perhaps surprisingly, HPV-positive tumours exhibited increased levels of proteins indicative of oxidative phosphorylation and a relatively lower level of extracellular lactate accumulation(361). Again, however, this study represents an isolated and relatively limited analysis of biomarker expression, which has also utilised a cell line model from an unusual sub-site.

Interestingly, evidence from several of the aforementioned therapeutic studies implicates oxidative stress as the mechanism underlying the cytotoxic effects of glycolytic inhibition, which accords with the proposed impetus driving cancer cells to acquire a glycolytic phenotype, and is suggestive of involvement of subsidiary metabolic pathways critical to cellular reducing potential, such as the PPP. For instance, glycolytic inhibition has been shown to cause perturbations in surrogates of oxidative stress, including decreased intracellular total glutathione with a reduced proportion of GSH(354), lessened cellular reducing potential(359), and significantly elevated ROS levels(360). Consistent with this, simultaneous treatment with the thiol antioxidant N-acetyl cysteine (NAC) has been shown to reverse these surrogates as well as the cytotoxic effects of glycolytic inhibition(354, 359, 360). Moreover, under conditions of glucose deprivation, addition of excess pyruvate only partially rescued the cytotoxic

effects of inhibiting glycolysis, further suggesting the importance of upstream subsidiary pathways in limiting oxidative stress(359). In keeping with this, recent research that sought to examine the reprogramming of metabolism associated with the development of radioresistance, using a matched model of radio-resistant and -sensitive SCCHN cells, demonstrated that in addition to an increased dependence on overall glucose catabolism, radioresistant cells specifically exhibited increased PPP flux(277, 362). Specifically, radioresistant SCCHN cells displayed elevated expression of key PPP enzymes, increased production of NADPH, and higher levels of TIGAR expression(277, 362). Unfortunately, however, this study only included two cell lines and information on *TP53* status was conspicuously absent, thereby preventing any inferences on the relationship between *TP53* status, PPP flux, and TIGAR expression. Further evidence in support of heightened PPP flux in SCCHN generally, comes from three studies scrutinising transketolase-like protein (TKTL1, another PPP enzyme), which have shown the gene encoding TKTL1 to be hypomethylated and TKTL1 to be overexpressed in SCCHN cell lines and tissues. These studies also suggested that TKTL1 overexpression promotes SCCHN tumorigenicity *in vitro* and *in vivo* through a feed-forward effect on glycolysis(363-365).

Notwithstanding the evidence supporting a glycolytic phenotype in SCCHN, perhaps mediated by loss of wild-type p53 function, one research group has offered an alternative model of SCCHN metabolism. In a recent biomarker analysis of SCCHN resection specimens, three metabolically and morphologically distinct cell populations were identified: highly proliferative epithelial cancer cells utilising oxidative phosphorylation with high lactate and ketone body uptake; and non-proliferative epithelial tumour cells and stromal cancer-associated fibroblasts both deficient in mitochondria with elevated lactate and ketone body generation(366). Furthermore, in a subset of specimens both non-proliferative compartments were noted to be highly glycolytic and observed to represent a significant proportion of the tumour(366). Based on this analysis, the authors propose a model of metabolic symbiosis whereby the non-proliferative glycolytic stromal and cancer epithelial cells generate catabolites which are released into the tumour microenvironment and subsequently taken up and utilised by the mitochondrial rich cancer cells to drive energy production and proliferation through oxidative phosphorylation(366). Indeed, similar findings of metabolic coupling have been reported for other tumour types(367, 368), and clearly further and more robust exploration in SCCHN is required to reconcile these discrepancies and/or reveal underlying mechanistic explanations.

1.4. Aims

As outlined in section 1.1.5., there remains a common goal in the treatment of both HPV-negative and HPV-driven SCCHN: to identify means of sensitising these tumours to the effects of current treatment regimes. In the context of traditional HPV-negative SCCHN there is a need to improve treatment efficacy to enhance survival outcomes, while for HPV-related oropharyngeal SCC there is a drive to minimise the substantial treatment-associated toxicity. RT remains a mainstay of treatment for all SCCHN, with 74% of SCCHN patients recommended to receive RT at some point during their treatment pathway, either as stand-alone or as adjuvant therapy(27). Consequently, it is imperative to identify novel radiosensitising therapeutic approaches.

Alteration to cellular metabolism is now widely considered to be a crucial hallmark of the cancer phenotype and intrinsic to malignant transformation(44) (section 1.3.1.), and as such presents a potentially attractive therapeutic target. This is particularly the case in the context of identifying novel radiosensitising strategies given the proposed links between altered tumour metabolism and cellular redox status (section 1.3.1.), and the fact that the mechanism underlying the therapeutic effect of RT relies on free radical formation(369). Whilst a generalised disruption of normal metabolic homeostasis may occur to some degree in all tumours, there is undoubtedly heterogeneity between cancers, which may reflect both tissue-specific effects and differing oncogenic events driving tumorigenesis in different tumour types(250, 258, 267). As such, detailed study and consideration of the metabolic phenotype of individual cancers is paramount if effective therapeutic strategies targeting metabolism are to be developed and effectively deployed.

Primary studies of metabolism specific to SCCHN, however, have been limited, have at times produced conflicting results, and have failed present a clear picture of the SCCHN metabolic phenotype (section 1.3.3.). Interestingly though, recent findings from one research group have suggested that *TP53* status may play a key role in determining metabolic re-programming in SCCHN, with associated therapeutic implications(359, 360). Consequently, the aims of this project were primarily to explore in greater depth the metabolic phenotype in SCCHN, with a specific focus on elucidating any correlation with *TP53* status, and to determine whether anti-metabolic therapy might be employed to potentiate the effects of IR. Secondary aims of the project were to examine the

mechanistic basis of any observed metabolic re-programming and any observed therapeutic effects of anti-metabolic treatment.

2. Materials and Methods

2.1. List of reagents

2.1.1. General reagents

Reagent or product	Manufacturer
Acetic acid (glacial) 100% anhydrous	Merck, Feltham, UK
Acrylogel 40% solution	VWR, Lutterworth, UK
ADP disodium salt hydrate	Sigma-Aldrich, Gillingham, UK
Ammonium persulfate (APS)	Sigma-Aldrich
Albumin from bovine serum (BSA), 96%	Sigma-Aldrich
BSA solution, fatty acid free (10%)	Sigma-Aldrich
Aprotinin	Roche, Welwyn, UK
L-ascorbic acid	Sigma-Aldrich
Blotting grade blocker, non-fat dry milk	Bio-Rad, Hemel Hempstead, UK
5-Bromo-4-chloro-3-indolyl β-D-galactopyranoside (X-gal)	VMR
Bromophenol blue	Sigma-Aldrich
Calcium chloride	Sigma-Aldrich
Citric acid monohydrate	Merck
Chloroform	Sigma-Aldrich
Crystal Violet	Sigma-Aldrich
CyQUANT® cell proliferation assay kit	Invitrogen, Paisley, UK
Dichloroacetic acid (DCA), potassium salt	Sigma-Aldrich
2'-7'-Dichlorodihydrofluorescein diacetate (DCF-DA)	Life Technologies, Paisley, UK
Dimethyl Sulphoxide (DMSO)	Sigma-Aldrich
N,N-dimethylformamide	Sigma-Aldrich
3-(4,5-dimethylthiazol-2-yl)-2,5-diphenyl tetrasodium bromide (MTT)	Molekula, Newcastle, UK
DNA ladder (100bp)	New England Biolabs, Ipswich, UK
ECL Prime	GE Healthcare, Little Chalfont, UK
Ethanol, absolute	Sigma-Aldrich
Ethidium bromide	Roche
Ethylenediaminetetraacetic acid (EDTA)	Sigma-Aldrich
Ethylene glycol-bis(β-aminoethyl ether)-	

N,N,N',N'- tetracetic acid (EGTA)	Sigma-Aldrich
Fluorescein isothiocyanate (FITC)-conjugated annexin V solution	Cambridge Bioscience, Cambridge, UK
Formaldehyde solution 37%	Merck
GenSieve LE agarose	Flowgen, Nottingham, UK
D-glucose	Sigma-Aldrich
Glutamic acid	Sigma-Aldrich
Gluteraldehyde solution (25%)	VWR
Glycerol	Sigma-Aldrich
Glycerol-3-phosphate	Sigma-Aldrich
Glycine	Thermo Fisher Scientific, Paisley, UK
HEPES free acid, molecular biology grade	Calbiochem, Beeston, UK
Hi-Di™ formamide	Thermo Fisher Scientific
Hydrogen peroxide solution (30%)	Sigma-Aldrich
Isoamyl alcohol	Sigma-Aldrich
ISOTON® solution	Beckmann Coulter, High Wycombe, UK
Leupeptin	Roche
Magnesium chloride	Sigma-Aldrich
L-malic acid	Sigma-Aldrich
Malonic acid	Sigma-Aldrich
Mannitol	Sigma-Aldrich
β-mercaptoethanol	Sigma-Aldrich
Methanol, analytical grade	Thermo Fisher Scientific
NADP/NADPH quantification kit	Sigma-Aldrich
Pepstatin	Roche
Phenol	Thermo Fisher Scientific
Phenylmethylsulphonyl fluoride (PMSF)	Sigma-Aldrich
Ponceau S	Sigma-Aldrich
Potassium dihydrogen phosphate	Merck
Potassium hexacyano-ferrate (II) trihydrate	Merck
Potassium hexacyano-ferrate (III)	Merck
Pre-stained protein marker, broad range	New England Biolabs
Propidium iodide (PI)	Sigma-Aldrich
Protein assay dye reagent	Bio-Rad

Proteinase K	Sigma-Aldrich
RNase A	Qiagen, Manchester, UK
Sodium acetate	Sigma-Aldrich
Sodium chloride	VWR
Sodium dodecyl suphate (SDS)	Thermo Fisher Scientific
Sodium dihydrogen phosphate dihydrate	Sigma-Aldrich
Sodium phosphate dibasic dihydrate	Sigma-Aldrich
Sodium pyruvate solution (100mM)	Sigma-Aldrich
Succinic acid	Sigma-Aldrich
Sucrose	Sigma-Aldrich
N, N, N', N'-tetramethylenediamine (TEMED)	VWR
N,N,N′,N′-tetramethyl-*p*-phenylenediamine Dihydrochloride (TMPD)	Sigma-Aldrich
Tris base	Calbiochem
Tris EDTA buffer (20x)	Invitrogen
Triton X-100	GE Healthcare
Trypan blue solution (0.4%)	Invitrogen
Trypsin inhibitor from soybean (STI)	Roche
Tween-20	Sigma-Aldrich
XF plasma membrane permeabiliser (PMP)	Seahorse Bioscience, Copenhagen, Denmark
XF calibrant solution	Seahorse Bioscience

2.1.2 Tissue culture reagents

Dulbecco's modified Eagle's medium (DMEM), HEPES modification	Sigma-Aldrich
Dulbecco's phosphate buffered Saline (PBS)	Sigma-Aldrich
Eagle's Minimum essential medium	Sigma-Aldrich
Fetal bovine serum (FBS)	Sigma-Aldrich
L-glutamine solution 200mM	Sigma-Aldrich
MEM non-essential amino acid solution (100x)	Sigma-Aldrich
Penicillin-streptomycin	Sigma-Aldrich
Trypsin-EDTA solution (1×)	Sigma-Aldrich
XF base medium	Seahorse Bioscience

2.1.3 Drugs

2-deoxy-D-glucose (2-DG): stock solution prepared by dissolving to 1M in PBS. Supplied by Sigma-Aldrich. Stored at -20°C for six weeks.

3-bromopyruvate (3-BP): stock solution prepared by dissolving to 20mM in PBS. Supplied by Sigma-Aldrich. Stored at -20°C for six weeks.

6-aminonicotinamide (6-AN): stock solution prepared by dissolving to 2mM in PBS. Supplied by Sigma-Aldrich. Stored at -20°C for six weeks.

Antimycin A: stock solution prepared by dissolving to 2mM in 95% (w/v) ethanol. Supplied by Sigma-Aldrich. Long-term storage was at -20°C.

Carbonyl cyanide 4-(trifluoromethoxy)phenyl-hydrazone (FCCP): stock solution prepared by dissolving to 10mM in 95% (w/v) ethanol. Supplied by Sigma-Aldrich. Long-term storage was at -20°C.

Geneticin: various concentrations prepared in DMEM as described in section 2.5.2. Supplied by Calbiochem.

Metformin: stock solution prepared by dissolving to 1M in PBS. Supplied by Sigma-Aldrich. Stored at -20°C for six weeks.

N-acetylcysteine (NAC): a final working concentration of 25mM was used and prepared freshly on each occasion. Supplied by Sigma-Aldrich.

Oligomycin: stock solution prepared by dissolving to 5mM in 95% (w/v) ethanol. Supplied by Sigma-Aldrich. Long-term storage was at -20°C.

Plasmocin: a final working concentration of 25µg/ml was used and prepared freshly on each occasion. Supplied by Invivogen, Toulouse, France.

Rotenone: stock solution prepared by dissolving to 2mM in 95% (w/v) ethanol. Supplied by Sigma-Aldrich. Long-term storage was at -20°C

Staurosporine: stock solution prepared by dissolving to 1mM in DMSO. Supplied by LC Laboratories, Woburn, MA, USA. Long-term storage was at 4°C.

UK-5099: stock solution prepared by dissolving to 1mM in DMSO. Supplied by Sigma-Aldrich. Long-term storage was at 4°C.

2.1.4 Antibodies for Western blotting

The following primary antibodies were diluted from stock in 5% blotting grade milk-PBS-Tween solution at the indicated concentrations:

α-6PGD (G-2), mouse monoclonal antibody, final concentration of 2µg/ml, supplied by Santa Cruz Biotechnology, Heidelberg, Germany.

α-G6PD (D5D2), rabbit monoclonal antibody, final dilution of 1:1000, supplied by Cell Signaling Technology, Leiden, Netherlands.

α-actin (C-2), mouse monoclonal antibody, final concentration of 3µg/ml, supplied by Santa Cruz Biotechnology.

α-GLUT-1 (ab652), rabbit polyclonal antibody, final dilution of 1:500, supplied by Abcam, Cambridge, UK.

α-hexokinase-II (4C5), mouse monoclonal antibody, final dilution of 1:1000, supplied by Novus Biologicals, Abingdon, UK.

α-MCT-1 (AB3538P), rabbit polyclonal antibody, final concentration of 5µg/ml, supplied by Merck

α-MDM2 (IF-2), mouse monoclonal antibody, final concentration of 3µg/ml, supplied by Calbiochem.

α-p21 (F-5), mouse monoclonal antibody, final concentration of 3µg ml, supplied by Santa Cruz Biotechnology.

α-p53 (DO-1), mouse monoclonal antibody, final concentration of 3µg/ml, supplied by Calbiochem.

α-PDK-2 (NBP1-87307), rabbit polyclonal antibody, final concentration of 1μg/ml, supplied by Novus Biologicals.

α-PGAM (D3J9T), rabbit monoclonal antibody, final dilution of 1:1000, supplied by Cell Signaling Technology.

α-TIGAR (AB10545), rabbit polyclonal antibody, final concentration of 1μg/ml, supplied by Merck.

α-vinculin (V9131), mouse monoclonal antibody, final dilution of 1:100 000, supplied by Sigma-Aldrich.

The following secondary antibodies were also diluted from stock in 5% blotting grade milk-PBS-Tween solution at the indicated concentrations:
Sheep α-mouse antibody (RPN4201), used at a 1:2500 dilution, supplied by GE Healthcare.

Donkey α-rabbit antibody (NA934), used at a 1:5000 dilution, supplied by GE Healthcare.

2.2 Cell culture

2.2.1. Cell lines

The parental cell lines included in this work are summarised in table 2.2.1.1. accompanied by details of SCCHN subsite of origin, reported HPV status, and reported *TP53* status.

The majority of cell lines used were parental University of Michigan squamous cell carcinoma (UM-SCC) cell lines, which were kindly provided by Professor T. Carey (University of Michigan Medical School). UM-SCC-17A cells stably expressing short-hairpin RNA (shRNA) specific for p53 (shp53) or an empty vector control (lenti), and several derivative cell lines of UM-SCC-1, transduced with various *TP53* mutations (R282W, C176F, R175H), wild-type *TP53*, or an empty vector (pBABE) were also utilised and were obtained through collaboration with Professor J. Myers (University of Texas MD Anderson Cancer Center, TX, USA). These derivative cells lines had been produced

using standard cloning and transfection techniques. Briefly, after infection with green fluorescent protein (GFP)-tagged empty lentiviral vector or encoding an shRNA against p53, cells were cultured for several passages, and sorted using flow cytometry. *TP53* constructs (C176F, R282W, R175H, wild-type) were generated by extracting RNA from cell lines known to express these mutants. Reverse transcriptase PCR was then carried out using *TP53*-specific primers, and the resulting products purified and inserted into a pBABE retroviral vector containing a puromycin-resistance insert. After transfection and packaging in 293T cells, the viral supernatant was centrifuged to remove cellular debris and added to UM-SCC-1 cells in combination with polybrene. After one passage, the cells underwent selection with puromycin.

UPCI:SCC 154 was kindly provided by Professor S. Gollin (University of Pittsburgh School of Public Health, PA, USA), while 93-VU-147T was obtained from Dr. J. Risk, (University of Liverpool, Liverpool, UK).

Table 2.2.1.1: Parental cell lines used in this study.

Cell Line	Subsite of Origin	Type of Lesion	Reported *TP53* Status	Reported HPV Status	Primary References
UM-SCC-1	Floor of mouth	Primary	Splice site mutation	Negative	(238, 370, 371)
UM-SCC-5	Supraglottis	Primary	Mutant: V157F	Negative	(370-372)
UM-SCC-10A	True vocal cord	Primary	Mutant: G245C	Negative	(238, 370, 372, 373)
UM-SCC-11A	Supraglottis	Primary: pre-treatment biopsy	Wild-type		(374-376)
UM-SCC-11B	Supraglottis	Primary: post-chemotherapy surgery	Mutant: C242S	Negative	(238, 370-374)
UM-SCC-17A	Supraglottis	Primary	Wild-type	Negative	(370-373)
UM-SCC-17AS	Supraglottis	Primary	Wild-type	Negative	(370-373)
UM-SCC-81B	Tonsil	Metachronous primary	Mutant: H193R	Negative	(370-372, 374, 377)
UM-SCC-104	Floor of mouth	Primary	Wild-type	Positive	(378, 379)
UPCI:SCC154	Lateral tongue	Primary	Wild-type	Positive	(378, 380)
93VU147T	Floor of mouth	Primary	Wild-type	Positive	(378, 381)

2.2.2. Cell medium and growth environment

Cells were grown in Nunc™ cell culture treated flasks with filter caps (Thermo Fisher Scientific) of various sizes (T25, T75, T175) in a humidified cell incubator at 37°C with 5% CO_2. With the exception of UPCI:SCC154, all cell lines were maintained in DMEM supplemented with 10% FBS, 1% penicillin/streptomycin, 1% L-glutamine, and 1% Non-Essential Amino Acids. UPCI:SCC154 was maintained in Eagle's minimum essential medium supplemented with 15% FBS, with additional supplements as before.

2.2.3. Cell sub-culture technique

Aseptic technique was observed at all times in order to avoid contamination and tissue culture work was carried out in a class II laminar flow tissue culture cabinet.

All cell lines used in this study grew as adherent monolayers on cell culture treated surfaces. Regular sub-culture, or passage, of cells was performed to ensure cells were maintained at optimum health, as once cells reach maximum confluence in culture, death can result from overcrowding and the associated stress. Passaging was carried out when cell reached approximately 70-90% confluence and was performed as follows: media was aspirated and the cell monolayer was washed once in PBS, typically 10ml when using a T75 tissue culture flask. PBS was then aspirated before 3-5ml of trypsin-EDTA was added to the monolayer and the culture flask returned to the cell incubator at 37 °C. The flask was agitated as required to facilitate the detachment of cells, which was regularly assessed by examination under light microscopy. Once adequately detached, the trypsin-EDTA was neutralised by the addition of an excess of media, the precise volume of which was dependent on the ratio of the cell split, which, in turn, was dependent on the growth characteristics of the individual cell line. For instance, relatively slowly growing cell lines were typically split 1:10, and rapidly proliferating cell lines 1:20. The relevant volume of the re-suspended cells was then aspirated from the flask before fresh media was added – typically 25ml for a T75 flask.

2.2.4 Cryopreservation and recovery of cryopreserved cell stocks

For the cryopreservation of cells, cells were harvested by trypsinisation as described above (section 2.2.3.) and pelleted by centrifugation at 300 x *g* for five minutes at 4°C. The supernatant was aspirated and the resulting cell pellet re-suspended in 1-2ml of freezing media (10% DMSO in FBS), before transfer to Nunc™ cryovials (Thermo Fisher Scientific). The cryovials were then placed in a pre-cooled Styrofoam rack and stored at -

80°C, allowing gradual freezing of the cells. Subsequently, cryovials were transferred to liquid nitrogen for long-term storage after approximately 24–48 hours.

When recovering cells from stocks stored in liquid nitrogen, cryovials were thawed expediently in a 37°C water bath. Recognising that DMSO toxic to cells at concentrations above 0.5%, the cells were re-suspended in a tissue flask containing at least 25 ml of media that was pre-warmed to 37°C. Once the cells had adhered to the flask surface, typically the following day, the media was changed.

2.3. Verification and optimisation of cell lines

2.3.1. STR profiling

Prior to use in experiments, all cell lines were subjected to short tandem repeat (STR) profiling to verify their identity, as determined by comparison with published profiles for each individual cell line. Firstly, genomic DNA was isolated from cells. Cells were harvested by trypsinisation and pelleted by centrifugation as described in sections 2.2.3. and 2.2.4. The cell pellet was then re-suspended in 500µl of genomic DNA preparation lysis buffer (50mM Tris [pH 8.0], 100mM EDTA and 0.5% SDS) with 250µg proteinase K at a final concentration of 5µg/µl and incubated overnight in a heat block at 55°C. The following day, DNA was extracted using an organic solvent-based extraction method. The cell lysate was mixed with 500µl phenol and left for one hour with gentle shaking. Samples were then mixed thoroughly by hand for five minutes before undergoing centrifugation at 13,000 x *g* for five minutes. Next, the aqueous phase was transferred to a fresh Eppendorf® 1.5ml microcentrifuge tube (Sigma-Aldrich) and mixed with 500µl PCI (phenol, chloroform, isoamyl alcohol at the ratio 24:25:1) for five minutes each by hand and centrifugation as before. The aqueous phase was again transferred into a fresh Eppendorf® 1.5ml microcentrifuge tube, and the DNA then precipitated by adding 50µl of 3M sodium acetate solution (pH 6.0) and 500µl of 100% ethanol to each tube. Tubes were then mixed by hand for one minute and centrifuged for 10 minutes (13,000 x *g*) before the supernatant was removed and the pellet washed with 70% ethanol. The DNA pellet was re-suspended in 50µl of TE buffer (10mM Tris and 1mM EDTA [pH 8.0]) containing ribonuclease (RNase) A at a final concentration of 10µg/ml, and the concentration of DNA and its purity determined using a NanoDrop® UV spectrophotometer (Thermo Fisher Scientific). Samples were then serially diluted with ddH_2O to achieve a DNA concentration of 2ng/µl in preparation for subsequent PCR and

STR profiling, which were performed using the GenePrint® 10 System (Promega, Southampton, UK) as per the manufacturer's instructions. The appropriate volume of PCR amplification mix was first made up (7.5µl/reaction), which comprised 3.5µl ddH_2O, and 2µl each of master mix and primer pair mix from the pre-amplification box from the GenePrint® 10 System. Next, 7.5µl of PCR amplification mix was added to each well in a 96-well MicroAmp® plate (Thermo Fisher Scientific), along with 2.5µl sample template DNA, or in the case of positive and negative controls GenePrint® 10 control DNA or ddH_2O respectively. After thorough mixing by pipetting and sealing of the plate, a Px2 thermal cycler (Thermo Fisher Scientific) was used to perform the following thermal cycle:

- 96°C – 1 minute
- 94°C – 10 seconds
- 59°C – 1 minute
- 72°C – 30 seconds

  } 30 cycles

- 60°C – 20 minutes
- 4°C – soak

Following amplification, a loading cocktail was prepared by combining and mixing the GenePrint® 10 Internal Lane Standard 600 and Hi-Di™ formamide, with respective volumes of 0.5µl and 9.5µl required for each sample. 10µl of this was then added to each well in a fresh 96-well MicroAmp® plate before adding 1µl of amplified sample (or 1µl of GenePrint® 10 Allelic Ladder Mix for the positive control). Samples were then denatured at 95°C for three minutes using a heat block, and then immediately chilled on crushed ice for a further three minutes. Samples were subsequently transferred to the Applied Biosystems 3130 Genetic Analyser (Thermo Fisher Scientific) for processing, and data was analysed using GeneMapper® software (Thermo Fisher Scientific).

2.3.2. Mycoplasma testing

Following verification of cell line identity, all cell lines were screened for mycoplasma infection as mycoplasma contamination is characteristically unapparent macroscopically or microscopically and may alter any parameter measured in cell culture or in experimental investigations(371, 382). Screening for mycoplasma contamination was performed using the e-Myco™ mycoplasma PCR detection kit (ChemBio, Luton, UK) to detect mycoplasma-specific sequences. Cells were brought to confluence in T75 cell culture flasks and then harvested using trypsin-EDTA, as described in section 2.2.3, before 1ml of cell suspension was transferred to an

Eppendorf® 1.5ml microcentrifuge tube. Following centrifugation at 13,000 x *g* for 30 seconds, the supernatant was carefully removed and the cells resuspended in 1ml PBS. This process was then repeated for a second PBS wash before the cells were again resuspended in 100µl PBS, heated for 10 minutes at 100°C in a heat block, vortexed for 15 seconds, and centrifuged at 13,000 x *g* for two minutes. The supernatant was then removed and aliquoted into a fresh Eppendorf® 1.5ml microcentrifuge tube. Next, 10µl of this supernatant, which was used as the DNA template in the PCR, was added to a pre-prepared e-Myco™ reaction tube along with 10µl of ddH_2O. This was repeated for each sample. Negative and positive controls comprising 20µl ddH_2O and 1µl of e-Myco™ control DNA with 19µl ddH_2O respectively were also included in each reaction. A Px2 thermal cycler (Thermo Fisher Scientific) was used to perform the following PCR:

- 94°C – 1 minute
- 94°C – 30 seconds
- 60°C – 20 seconds
- 72°C – 1 minute

} 35 cycles

- 72°C – 5 minutes

A 2% agarose gel, comprising 2g GenSieve LE agarose in 100ml TAE buffer (40mM Tris-Base, 1mM EDTA [pH 8.0], and 1.142% glacial acetic acid) supplemented with 0.5µg/ml ethidium bromide, was then used to separate the DNA fragments by gel electrophoresis. Once fully dissolved, the agarose solution was allowed to cool and then poured into a sealed gel cast, with comb, to set. Once set, the comb and sealing tape were carefully removed and the assembled gel submerged in TAE buffer inside an electrophoresis tank. Amplified samples were then prepared for loading by mixing 2µl of each sample with 16µl ddH_2O and 2µl with 10% (v/v) orange G loading buffer in a fresh PCR reaction tube. Samples (10µl) were then loaded carefully into the wells along with a 100bp DNA ladder in the first well. Subsequently, electrophoresis was performed in horizontal gel units (Scie-Plas, Cambridge, UK) using a two-gel Mini-PROTEAN® Tetra cell (Bio-Rad) at 100V until the desired band separation had taken place (typically 35 minutes). Finally, DNA bands were visualised, enabled by the presence of ethidium bromide in the agarose gel, by placing the gel onto a High Performance UV-transilluminator, and a picture recorded digitally using a Kodak EDAS 290 (Kodak, Watford, UK). Further image processing was performed using CorelDRAW graphics suite X7 (Corel, Luton, UK). If cell lines were found to be positive for mycoplasma contamination (see appendix [section 5.1] for details) alternative stocks were sought and also tested for the presence of mycoplasma contamination. If no negative stocks were available eradication treatment

was instigated accordingly until subsequent testing was negative (see appendix [section 5.2] for details).

2.4. Metabolic profiling using microplate-based extracellular flux analysis

2.4.1. Principles of microplate-based extracellular flux analysis

Metabolic profiling was performed using microplate-based extracellular flux (XF) analysis, which is a high-throughput means of measuring the rate of change of dissolved oxygen and pH, resulting from the extrusion of protons, in the media immediately surrounding living cells cultured in a microplate(383). These measurements were performed using the XF24 instrument (Seahorse Bioscience), which utilises optical fluorescent biosensors embedded in disposable XF24 sensor cartridges (Seahorse Bioscience,) that are placed into a 24-well tissue culture microplate (Seahorse Bioscience) (figure 2.4.1.1.). This experimental system is able to make accurate and repeatable measurements over short periods of time during measurement cycles by isolating small volumes of media above the cell monolayer, which allows for detection of precise changes to analyte levels resulting from cellular metabolism(383). Experimental readouts are oxygen consumption rate (OCR) in pmol/min and extracellular acidification rate (ECAR) in mpH/min, surrogate measures of oxidative phosphorylation and glycolysis respectively. These measurements can be taken at baseline as well as following the administration of a variety metabolic substrates and/or inhibitors during specifically designed stress test, which will be detailed further in sections 2.4.6. and 2.4.7., giving this system quantitative and real-time capacity.

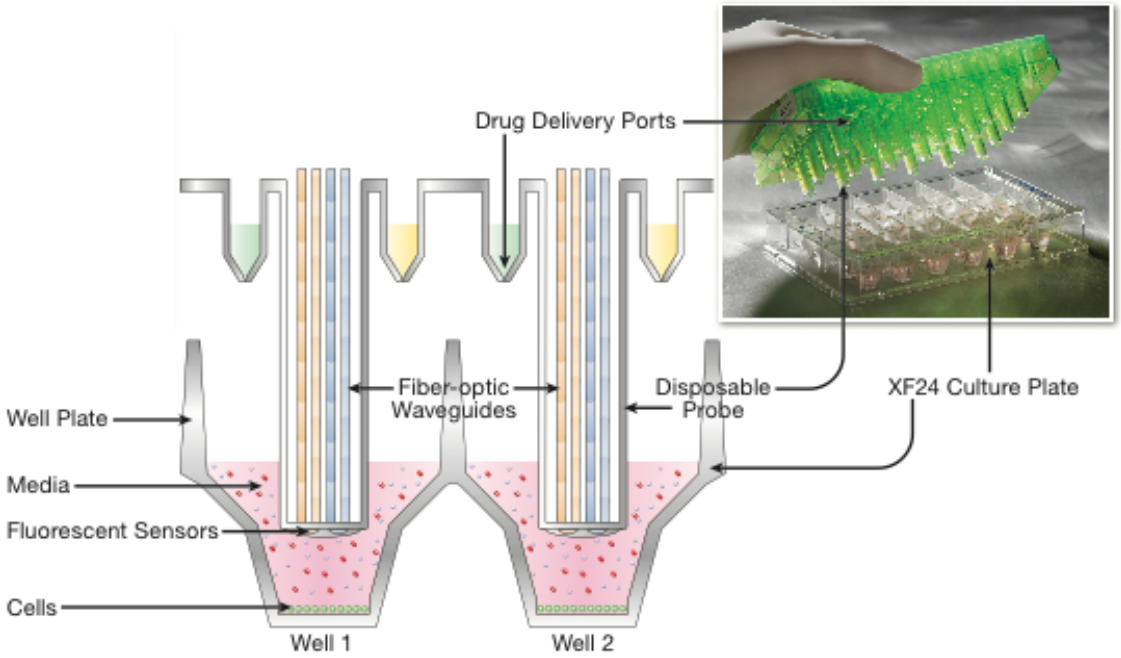

Figure 2.4.1.1: An illustration of how the XF24 experimental system works (adapted from reference(384). Optical fluorescent biosensors embedded in a disposable XF24 sensor cartridge that is placed over a 24-well tissue culture microplate, in which cells are seeded, enable the XF24 instrument to measure the oxygen consumption rate (OCR) and extracellular acidification rate (ECAR). There are also four drug delivery ports per well in the sensor cartridge, which allows for the administration of compounds during specifically designed stress tests.

2.4.2. Media preparation

When undertaking both mitochondrial and glycolytic stress tests (detailed in sections 2.4.6. and 2.4.7. respectively) unbuffered XF base medium was used. For glycolytic stress tests this was supplemented with 2mM L-glutamine only, while for mitochondrial stress tests 2mM of sodium pyruvate and 10mM D-glucose were also added. Media was then adjusted to pH 7.4 and sterile filtered. These media will be herein referred to as "Seahorse glycolytic assay medium" and "Seahorse mitochondrial assay medium".

For XF PMP assays (detailed in section 2.4.9.) a non-ionic medium was used as salt-based buffers can increase cell detachment from the monolayer. 3X mitochondrial assay solution (MAS) was made up as the base assay medium according to the follow recipe:

660mM mannitol

210mM sucrose

30mM KH_2PO_4

15mM $MgCl_2$

6mM HEPES

3mM EGTA
0.6% (w/v) fatty acid free BSA

On the day of the assay the required volume of 3x MAS was aliquoted and diluted to 1x using ddH_2O.

2.4.3 Preparation of the XF24 instrument

All assay designs and calibration steps described in the following sections were setup and executed using either XF or Wave software (Seahorse Bioscience). Subsequent data analysis was carried out using Wave software.

2.4.4. Preparation of the XF24 sensor cartridge

In order to hydrate the XF24 sensor cartridge in preparation for any Seahorse assay, 1mL of XF calibrant solution was added to each well in the XF24 calibration microplate before placing the sensor cartridge into the microplate. This was then incubated overnight in the XF24 Prep station (Seahorse Bioscience) at 37°C under ambient atmospheric conditions and used within 24 hours.

2.4.5 Cell seeding and preparation of the XF24 microplate

The day prior to any Seahorse assay, cells were harvested using trypsin-EDTA as described previously (section 2.2.3.) and cellular concentrations determined using the mean from three independent cell counts from a Coulter counter (Beckmann Coulter). Prior to counting the cells the Coulter counter was calibrated by flushing with ISOTON® solution. Flushing was repeated until a cell count of less than 3000 cells/ml for ISOTON® solution alone was achieved. For ease of subsequent seeding, cells were pelleted by centrifugation at 300 x *g* for five minutes at ambient temperature before being re-suspended in the appropriate volume of DMEM to obtain a concentration of $1x10^6$ cells/ml. Cells were then seeded in each well of the XF24 microplate at pre-determined densities (with the exception of the designated blank wells – A1, B4, C3, and D6 – that served as background temperature control wells), with each well then topped up with an excess of DMEM to give a total volume of 500µl per well. Following this, the microplate was incubated overnight at 37°C with 5% CO_2 to allow for cell attachment. Optimal cell seeding densities were determined for each individual cell line in the first instance by visual assessment using light microscopy, with the aim of achieving evenly distributed cells at 50-90% confluence within each well. Basal OCR and ECAR values obtained during subsequent cell titration assays, in which several cell seeding densities

were evaluated, were then used to confirm or refute whether optimal seeding density had been achieved, with respective target values of 50-400pmol/min and 20-120mpH/min as per manufacturer's guidelines. Seeding densities used for each cell line are shown in table 2.4.5.1.

Table 2.4.5.1: **Seeding densities used for each cell line in XF assays.**

Cell Line	Number of Cells/Well
UM-SCC-1 (and derivative lines)	25 000
UM-SCC-5	50 000
UM-SCC-10A	100 000
UM-SCC-11A	75 000
UM-SCC-11B	75 000
UM-SCC-17A (and derivative lines)	375 000
UM-SCC-17AS	500 000
UM-SCC-81B	50 000
UM-SCC-104	100 000
UPCI:SCC154	150 000
93VU147T	75 000

On the day of the assay, relevant compounds were prepared and added in appropriate volumes to the designated stress test injection ports in the previously hydrated XF sensor cartridge, dependent on the assay type being performed (see sections 2.4.6. and 2.4.7.). This sensor cartridge, with the XF24 calibration plate prepared previously, was then used to calibrate the XF24 instrument.

Simultaneously, cell attachment to the XF24 microplate was confirmed using light microscopy. The DMEM was then aspirated from each well and cells were carefully washed with 1ml of pre-warmed relevant assay media to ensure all FBS containing media was completely removed. Subsequently, in the case of mitochondrial and glycolytic stress tests, 500µl of relevant assay media was slowly added per well without disrupting the monolayer, the integrity of the monolayer re-checked, and the plate left to equilibrate for one hour in the XF24 Prep station at 37°C under ambient atmospheric conditions before being loaded into the pre-calibrated XF24 instrument. For XF PMP assays, 1x MAS media was supplemented with the desired substrates, ADP, and XF PMP reagent (see section 2.4.9. for details), 500µl of which was then carefully added per well. The microplate was then transferred immediately to the calibrated XF24 instrument to minimise cell exposure time to the MAS and to avoid cell lifting from the microplate.

2.4.6. Mitochondrial stress test

During mitochondrial stress tests cells were metabolically perturbed by the sequential addition of three different mitochondrial stressor compounds as follows: oligomycin, FCCP, and a combination of antimycin-A and rotenone. 10x stock concentrations of each of these compounds were first prepared in Seahorse mitochondrial assay media and added to injection ports A (oligomycin), B (FCCP), and C (antimycin-A/rotenone) in the designated stress test wells so that upon injection of respective volumes of 55µl, 61µl, and 68µl the desired working concentrations in the microplate wells were achieved. Equal volumes of Seahorse mitochondrial assay media were added to the injection ports in the allocated control wells. Desired working concentrations of both antimycin-A and rotenone were 1µM, while concentrations of oligomycin and FCCP required careful titration because the effects of these compounds can vary between different cell types, and relatively small changes in concentration can affect final measurement(383, 384). Data generated during the course of such optimisation is presented later in this thesis (section 3.1.2.).

Following instrument calibration and loading of the cell microplate as described above, a baseline was established to start the assay. This was achieved by programming the instrument as follows: initial measurement, mixing the plate for two minutes, allowing a delay of two minutes, and then taking a further measurement (mix two minutes, wait two minutes, measure two minutes). This cycle was repeated five times to establish a robust baseline OCR. Following this, the oligomycin was delivered into the stress test wells through port A. Oligomycin inhibits ATP synthase (ETC complex V) and causes a drop in OCR, which can be used to distinguish the amount of oxygen consumption devoted to ATP synthesis from that required to overcome the natural proton leak across the inner mitochondrial membrane(383, 384) (figure 2.4.6.1). At this point the instrument was programmed to undertake three measurement cycles as before. Next, FCCP was delivered into the stress test wells via port B, after which three further instrument measurement cycles were performed. FCCP is an ionophore, which disrupts ATP synthesis by transporting hydrogen ions across the inner mitochondrial membrane instead of through the proton channel of ATP synthase, and as such uncouples the mitochondria from the ETC(383). This leads to collapse of the mitochondrial membrane potential that results in a rapid and uncontrolled consumption of energy and oxygen without the generation of ATP, which manifests in a maximal increase in OCR that can be used to calculate the spare respiratory capacity of cells(383, 384) (figure 2.4.6.1).

Finally, antimycin-A and rotenone were added through port C, after which two measurement cycles were taken. These compounds are ETC complex III and I inhibitors respectively, the combination of which shuts down mitochondrial respiration completely, enabling identification of residual respiration that is non-mitochondrial, which then needs to be subtracted from the previous measurements(383, 384) (figure 2.4.6.1).

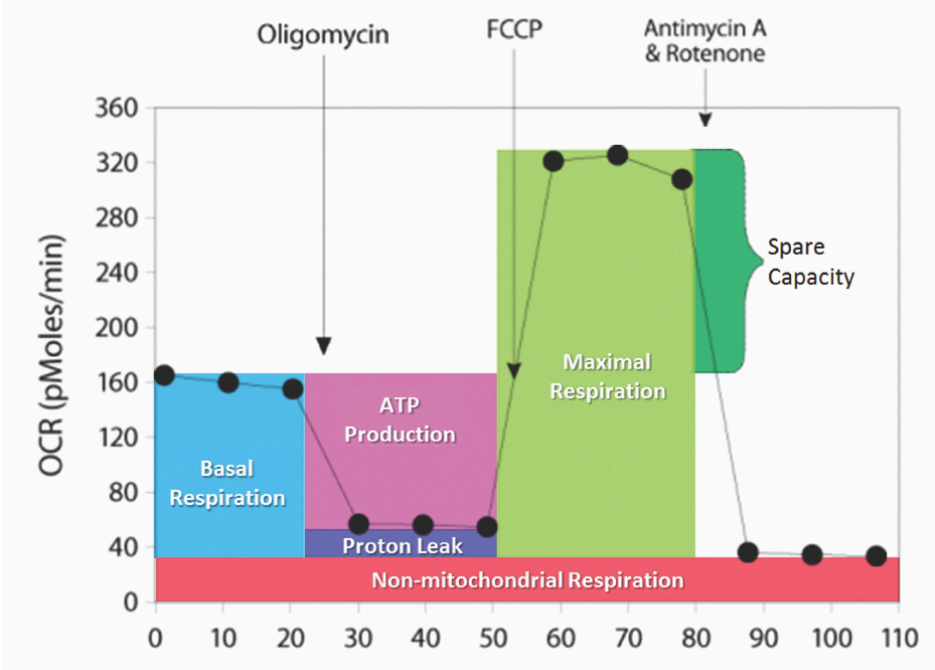

Figure 2.4.6.1: Experimental read-out from the mitochondrial stress test. This depicts how the sequential delivery of the three compounds (oligomycin, FCCP, and a combination of antimycin A and rotenone) allows derivation of several metabolic parameters (basal respiration, ATP-linked respiration, proton leak-linked respiration, maximal respiration, spare respiratory capacity, an non-mitochondrial respiration). The underlying mechanisms are as described in the text.

2.4.7. Glycolytic stress test

Akin to the mitochondrial stress test described above, the glycolytic stress test involves the sequential injection of three compounds that manipulate cellular metabolism to facilitate derivation of several key glycolytic parameters. In this instance the injected compounds comprise D-glucose, oligomycin, and 2-DG(383, 384). Again, 10x stock concentrations of each of these compounds were first prepared in Seahorse glycolytic assay media, such that upon injection of respective volumes of 55µl, 61µl, and 68µ, final working concentrations of 10mM D-glucose and 50mM 2-DG were achieved in the designated stress test microplate wells. As described previously the desired

concentration of oligomycin was titrated and the relevant data is presented later in this thesis (section 3.1.2.). Equal volumes of Seahorse glycolytic assay media were added to the injection ports in the allocated control wells.

Again similar to the mitochondrial stress test, the assay commenced with initial ECAR measurement, mixing the plate for two minutes, allowing a delay of two minutes, and then taking a further ECAR measurement (mix two minutes, wait two minutes, measure two minutes), and this cycle was repeated five times. Next, the first injection of a saturating concentration of glucose was delivered through port A to the stress test wells. The cells catabolise this through the glycolytic pathway and the resulting extrusion of protons into the surrounding medium causes an increase in ECAR, which gives the rate of glycolysis under basal conditions (383, 384)(figure 2.4.7.1.). Following three measurement cycles as before, oligomycin was then injected through port B, before a further three measurement cycles. As detailed previously, oligomycin inhibits mitochondrial ATP production, which also results in cells shifting to a more glycolytic state to maintain energy requirements, with a consequent increase in ECAR reflecting the cellular maximal glycolytic capacity(383, 384) (figure 2.4.7.1.). Finally, 2-DG was delivered through port C and two final measurement cycles performed. 2-DG is a stable glucose analogue, which inhibits glycolysis through competitive binding to hexokinase – the first enzyme in the glycolytic pathway – and results in a significant decrease in ECAR(383, 384). The residual ECAR is attributable to cellular processes other than glycolysis and is subtracted from previous measurements.

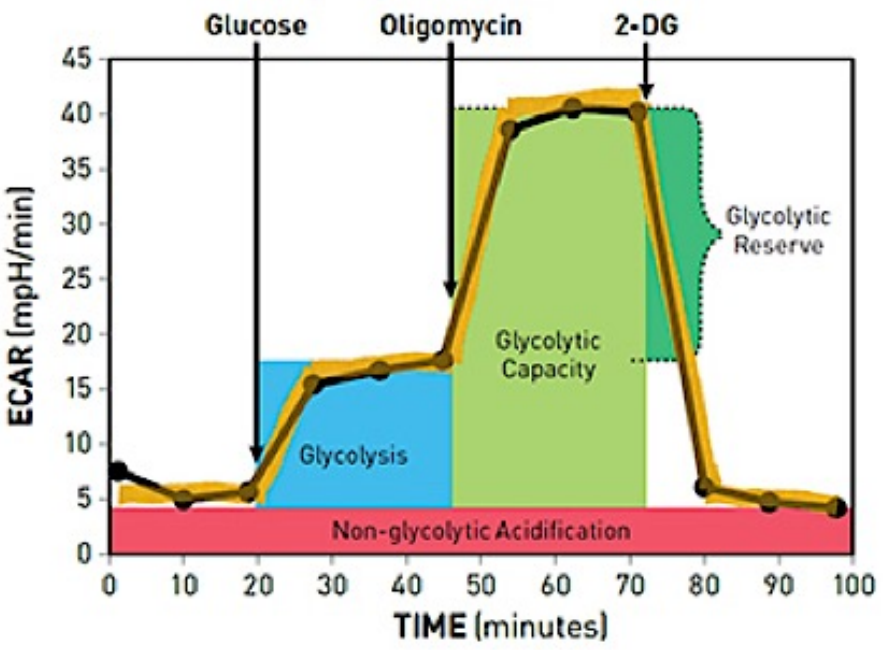

Figure 2.4.7.1: Experimental read-out from the glycolytic stress test. This depicts how the sequential delivery of the three compounds (glucose, oligomycin, and 2-DG) allows derivation of several metabolic parameters (basal glycolysis, maximal glycolysis, spare glycolytic capacity, an non-glycolytic acidification). The underlying mechanisms are as described in the text.

2.4.8. Normalisation to cellular DNA content

To enable comparison of metabolic measurements between cell lines, normalisation of the OCR and ECAR data was necessary. Consequently, following completion of all mitochondrial and glycolytic stress tests, the XF microplate was removed from the instrument and the media removed from each of the wells, before the microplate was stored at -80°C for future normalisation.

At a later date, typically within one month, DNA content in each of the microplate wells was determined to facilitate normalisation of data to DNA content. Measurement of total DNA content was performed using the CyQUANT® cell proliferation assay kit as per the manufacturer's instructions. Experiments were carried out in Corning® 96-well black-bottom plates (Sigma-Aldrich), which allowed for normalisation of three XF microplates simultaneously during each experiment. Lysis buffer was prepared using 38ml of solution containing 180mM NaCl in 1mM of EDTA and 2ml of stock cell lysis buffer from the CyQUANT® kit. Next, 150µl of RNase A was added to 7.5ml of this lysis buffer, and 100µl of this final solution was then added to each well of the XF24 microplates, with the exception of the designated blank wells (A1, B4, C3, and D6). The microplates were then placed on an orbital shaker for one hour at room temperature to extract cellular

DNA. In the interim, in order to generate a standard curve for DNA content, DNA standards were prepared using the stock DNA standard from the CyQUANT® kit diluted in lysis buffer without RNase A to the following concentrations: 0, 10, 50, 100, 200, 400, 800, and 1000ng/ml. 50µl of each of the standards was then added in duplicate to the designated wells in the 96-well plate. Following the aforementioned lysis step, the lysed cells were diluted 1:5 with lysis buffer without RNase A, and 50µl also transferred to the pre-designated wells of the 96-well plate. Subsequently, dye solution was prepared (20µl of dye from the CyQUANT® kit and 200µl of 2x TE buffer made up to a final volume of 4ml using dH_2O) and added to each well in a 1:1 dilution. This was then left for two minutes prior to measurement using a POLARstar Omega plate reader (BMG LABTECH, Ortenberg, Germany), on which fluorescence measurements were taken using excitation and emission wavelengths of 508nm 520nm respectively. The values obtained were then multiplied by the sample dilution factor of five and converted from ng/ml to ng of DNA by accounting for the original sample volume of 50µl.

2.4.9. Measurement of electron transport chain complex activity in permeabilised cells

To further investigate the possible contribution of altered mitochondrial substrate oxidation in any observed differences in the metabolic phenotypes of the cell lines, cells were permeabilised using XF PMP, supplied with varying substrates and inhibitors, and subjected to mitochondrial stress tests (section 2.4.6.) to assess the activity of individual ETC complexes. Many oxidisable substrates are unable to cross the plasma membrane freely, which prevents control over which substrates the mitochondria are oxidising(385, 386). Permeabilising cells using XF PMP, which contains a mutant cholesterol-dependent recombinant perfringolysin that selectively permeabilises the plasma membranes of adherent cell monolayers, affords this experimental control, and by exploiting the fact that specific substrates feed differentially into mitochondrial pathways (figure 2.4.9.1.) any defects in function of ETC complexes responsible for the altered OCR originally observed in intact cells can be isolated(385, 386). Accordingly, substrates bypassing potentially defective ETC complexes were sequentially added, along with relevant ETC complex inhibitors, in each new experiment to determine whether any OCR defects could be rescued. Given that this experimental design did not allow for the bypassing of complex IV (see figure 2.4.9.1.), and thus the detection of any contributing defective complex IV function, direct measurement of complex IV-linked respiration was determined by supplying permeabilised cells with TMPD and ascorbate

along with the complex III inhibitor antimycin A, and comparing normalised OCR values between cell lines.

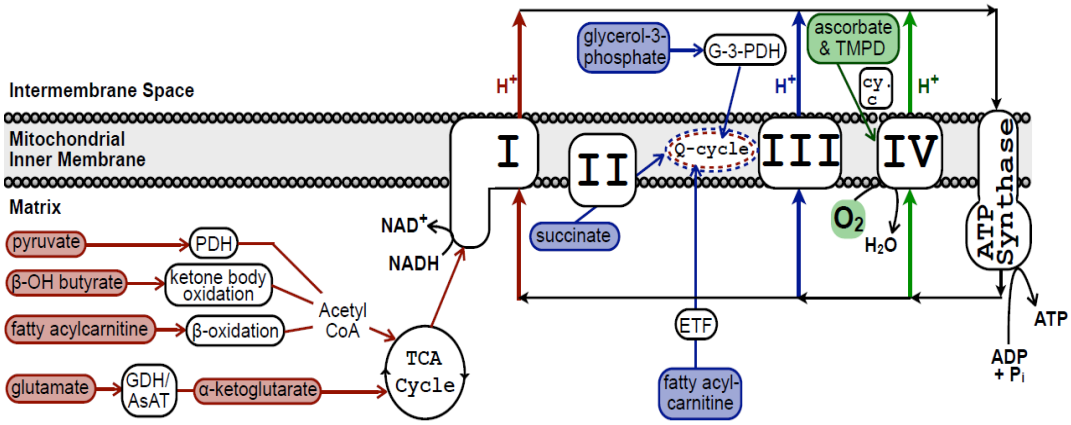

Figure 2.4.9.1: Oxidisable substrates feed into different parts of the respiratory chain (adapted from reference (387))**.** Plasma membrane permeabilisation allows for controlled delivery of endogenous substrates into mitochondria**.** Complex I-linked substrates are labeled in red. Oxidation of pyruvate in the TCA cycle in the mitochondrial matrix promotes the reduction of NAD+ to NADH. Electrons from NADH enter complex I, and are transferred through to complexes III and IV. The oxidation of succinate to fumarate causes the reduction of FAD+ to FADH, the electrons of which enter complex II, thereby bypassing complex I. Glycerol-3-phosphate, an FADH-linked substrate, donates electrons to complex III via the Q-cycle. TMPD, in the presence of ascorbate, can donate electrons to cytochrome *c* to reduce complex IV, which then reduces oxygen to water. The overall proton gradient across the inner mitochondrial membrane created by these redox reactions drives the phosphorylation of ADP to ATP by the ATP synthase (complex V).

Prior to XF PMP assays, stock solutions of the substrates were prepared using 1x MAS and are detailed in table 2.4.9.1. On the day of the assay, the required volume of 1x MAS was aliquoted (typically 6ml of one condition per microplate) and the desired substrates and inhibitors added, the final concentrations of which are also listed in table 2.4.9.1. In initial experiments, the NADH-linked complex I substrates pyruvate and glutamate were added. Subsequently, in order to bypass ETC complexes and analyse OCRs attributable to the remaining ETC complexes, the following substrates and inhibitors were supplied: succinate with rotenone to bypass and inhibit complex I; glycerol-3-phosphate with malonate to bypass and inhibit complex II; and ascorbate and TMPD with antimycin A to bypass and inhibit complex III. Additionally, a volume of 3x MAS equivalent to half the volume of substrate supplemented was also added to maintain solution osmotic strength (e.g. 500µl of 3x MAS for every 1ml of substrate). ADP and XF PMP reagent

were also added at final concentrations of 4mM and 1nM respectively. Subsequently, it was ensured that the pH of any assay medium was 7.2

Subsequent to addition of the relevant supplemented MAS media and insertion of the microplate into the XF24 instrument as described previously, a mitochondrial stress test (section 2.4.6.) was performed with the following modifications: compounds for injection were prepared in the relevant supplemented MAS rather than mitochondrial assay media, with injections into designated control wells comprising supplemented MAS alone; measurement cycles were reduced in duration to mix 30 seconds, wait 30 seconds, measure two minutes; measurement cycles were only repeated twice at baseline and following each compound injection. These time deviations from the standard XF assay with intact cells were designed to minimise time-dependent cell detachment and safeguard against time-dependent loss of mitochondrial function(385, 386).

Table 2.4.9.1: **Oxidisable substrates added during XF PMP assays.**

Substrate	Stock Concentration	Final Concentration	Additives
Pyruvate	1M	10mM	10mM malate, 2mM DCA[a]
Glutamate	1M	10mM	10mM malate[b]
Succinate	1M	10mM	2μM rotenone
Glycerol-3-phosphate	250mM	10mM	20mM malonate
Ascorbate	2M	10mM	2μM antimycin A, 100μM TMPD[c]

a – DCA is used to relieve potential kinase inhibition of the pyruvate dehydrogenase (PDH) complex.

b – An equimolar concentration of malate is added to ensure maximal aminotransferase activity.

c – TMPD is stored with 10mM ascorbate to ensure its reduction.

2.5. Cell proliferation and viability assays

2.5.1. Trypan blue exclusion assay

This assay is based on the principle that in viable cells cell membranes remain intact and exclude the dye, while in non-viable cells membranes are compromised and absorb the dye(388). Thus, under microscopic examination viable cells remain colourless and non-viable cells appear blue(388).

Cells were harvested using trypsin-EDTA and cellular concentrations determined as described previously. Cells were then seeded at a density of 7.5 x 10^5 in Nunc™ 6cm culture dishes (Thermo Fisher Scientific), 4ml of DMEM added, and incubated overnight at 37°C with 5% CO_2 to allow for cell attachment. The following day, cells were either left untreated or treated with 25mM 2-DG and/or 2μM UK5099 (an inhibitor of the mitochondrial pyruvate carrier) as indicated. Cells were then re-incubated at 37°C with 5% CO_2 for 8, 16 or 24 hours before being harvested with trypsin-EDTA and suspended in 10ml of DMEM. 10μl of cell suspension was then transferred in duplicate to each enclosed chamber within a disposable Countess™ cell counting chamber slide (Invitrogen), to which 10μl of 0.4% Trypan blue stain was also loaded. Next, the slide was inserted into the Countess™ automated cell counter (Invitrogen) to determine total cell count/ml, live cell count/ml, and cell viability. The Countess™ automated cell counter was calibrated and cell mode parameters setup as per the manufacturer's instructions to avoid falsely low or falsely high counts.

2.5.2. MTT assay

The MTT assay is a rapid colorimetric assay that relies on mitochondrial function as a surrogate indicator of cell viability. Mitochondrial dehyrodgenase enzymes in living cells are capable of cleaving the tetrazolium ring in MTT, reducing yellow MTT into a purple formazan precipitate, which can be dissolved with DMSO(389). Therefore, absorbance at 570nm can be used as a surrogate indicator of the viability of cells treated with MTT.

Cells were brought to 80-90% confluence in T75 cell culture flasks and then harvested using trypsin-EDTA as described in section 2.2.3. Cellular concentrations were then determined using the mean from three independent cell counts from a Coulter counter (Beckmann Coulter) as described previously (section 2.4.5.). Serial dilutions were performed on the cells in culture medium, ensuring cells were thoroughly mixed before each dilution, to give desired concentrations of cells/ml. Cells were then seeded in Nunc™ 96-well plates (Thermo Fisher Scientific) using a Costar® multi-channel pipette (Corning Life Sciences, Kings Norton, UK) with a total volume of 200μl added to each well and incubated overnight at 37°C with 5% CO_2 to allow for cell attachment. The following day desired concentrations of geneticin were prepared in 200μl of DMEM. The media from each well was then carefully suctioned and replaced with the appropriate geneticin solution (except in control wells where DMEM alone was added). Subsequently, 20μl of 5 mg/mL MTT was added to each well using a Costar® multi-

channel pipette (Corning Life Sciences) on day 0, 2, 4, 6, or 10 as indicated. Following addition on MTT on the relevant day the 96-well plate was incubated at 37 °C with 5% CO_2 for three hours. Following incubation, all of the liquid in was aspirated from each well and 100µl of DMSO added to lyse the cells and dissolve the purple formazan precipitate. After further incubation at 37 °C with 5% CO_2 for 15 minutes and agitation on a shaker at room temperature for one minute, plates were sealed and optical absorbance at 570nm was measured using a GENios plate reader (TECAN, Reading, UK).

2.6. Clonogenic survival assay

The clonogenic or colony-formation assay aims to determine the ability of cells to continue to proliferate and form colonies following exposure to a certain insult such as IR. A colony is defined as a collection of ≥50 cells, which represents more than five cell divisions(390).

Cells were harvested, counted, seeded at a density of 7.5 x 10^5 in Nunc™ 6cm culture dishes, and incubated overnight at 37°C with 5% CO_2 to allow for cell attachment as described above. The following day, cells were irradiated in the Nunc™ 6cm culture dishes at doses of 0Gy (untreated), 2Gy, 4Gy, or 6Gy at room temperature using a CellRad cabinet X-ray cell irradiator (Faxitron Bioptics LLC, Tucson, AZ, USA) calibrated to deliver 2Gy/min of X-ray radiation. Prior to irradiation cells were either left untreated or treated for one hour with varying combinations of the following drugs: 25mM 2-DG; 25mM NAC; 20mM metformin; 5µM 3-BP; 5µM 6-AN. Subsequent to irradiation the cell culture media was aspirated and replaced with 4ml of fresh DMEM before cells were returned to a humidified cell incubator (37°C with 5% CO_2) for between two and three hours. Next, cells were harvested by trypsinisation and cell suspension concentrations determined as described previously. Cells were then seeded in triplicates into Nunc™ six-well plates (Thermo Fisher Scientific) at pre-determined seeding densities optimised to generate a feasibly countable number of colonies out with the margin of error (30-100 colonies) at the end of the experiment. Optimal seeding densities were dependent on cell line, dose of IR, and presence or absence of drug, and were determined through trial and error by seeding initially at a wide range of densities before tailoring this for each cell line. Typically cell seeding densities ranged from 100/well to 102 400/well. Each well was then topped up with DMEM to give a final volume of 5ml/well and plates were gently agitated to distribute the cells evenly, before

plates were placed in the incubator (37°C, 5% CO2) and incubated for 14 days until sufficiently large colonies had formed.

Following 14 days of incubation, a fixing and staining solution of crystal (methyl) violet 0.5% w/v in 6% glutaraldehyde v/v was prepared. Media was then aspirated from the wells of all 6-well plates and each well washed with an excess of PBS (≈2ml). Next, 2ml of the crystal violet solution was added to each well and left to fix and stain for at least 30 minutes at room temperature. Subsequently, the crystal violet solution was removed and plates were washed by immersion in cold H_2O. After air drying overnight, a marker was used to divide the wells into quadrants and colonies were counted manually under the light microscope.

The plating efficiency (PE) was calculated from the 0Gy conditions by dividing the number of colonies formed by the number of cells seeded. The number of colonies formed after treatment was then used to calculate the surviving fraction (SF) for each treatment condition, accounting for the plating efficiency: SF = (number of colonies formed/number of cells seeded) × PE. Survival parameters to generate treatment-dose survival curves for treatment conditions were then derived from fitting the data by weighted, stratified, linear regression according to the linear–quadratic formula $S(D)=\exp(\alpha D+\beta D^2)$, where S is survival following a given dose (D) of IR, using IBM SPSS version 21 (Armonk, NY, USA)(390). Such modelling also enabled statistical testing of the difference between two survival curves, where the null hypothesis states that the data scatter was described best with one curve. Thus, p values of <0.05 state that the data scatter is best described with two curves, i.e. a statistical difference in survival parameters between the two curves(390).

2.7. Cytochemical detection of cellular senescence

2.7.1. General principles of Senescence-associated β-galactosidase staining

SA-βgal staining was used to investigate whether different treatment conditions induced cellular senescence in SCCHN cell lines. This cytochemical assay is based upon the chromogenic substrate 5-bromo-4-chloro-3-indoyl β-D-galactopyranoside (X-gal), which yields an insoluble blue compound that can be visualized when cleaved by the enzyme β-galactosidase(219). Whilst acidic β-galactosidase activity, detectable at pH 4.0, is present in all cells, SA-βgal activity is detectable at pH 6.0 and can therefore be

distinguished by using a citric acid/sodium phosphate buffer at pH 6.0(219). This enzymatic activity at suboptimal pH is due to an increase in the abundance of the lysosomal enzyme, secondary to the increased lysosomal biogenesis observed in senescent cells(219).

2.7.2. Reagents prepared for cytochemical detection of cellular senescence

Fixation solution:

2% (v/v) formaldehyde

0.2% (v/v) glutaraldehyde

Solution made up in PBS.

Staining solution:

40 mM citric acid/sodium phosphate buffer (pH 6.0)

5 mM potassium hexacyano-ferrate (II) trihydrate

5 mM potassium hexacyano-ferrate (III)

150 mM sodium chloride

2 mM magnesium chloride

1 mg/ml X-gal

2.7.3. Using senescence-associated β-galactosidase for detection of cellular senescence

Cells were harvested, counted, seeded at a density of 2.5 x 10^5 in Nunc™ 6cm culture dishes, and incubated overnight at 37°C with 5% CO_2 to allow for cell attachment as described previously. Cells were seeded at a lower density in this assay because of the requirement for subconfluent cell populations, as higher confluence may induce SA-βgal activity(219). The following day, cells were irradiated as described above, either in the absence of drug or following a one hour pre-treatment with 25mM 2-DG. Following twenty-four hours of incubation (37°C with 5% CO_2), cells were washed twice with an excess of PBS (≈2ml), before 2ml of fixation solution was added to each dish and incubated for five minutes at room temperature. The fixation solution was then removed and the fixed cells were washed twice with ≈2ml PBS, before 2ml of staining solution was added per dish. Cells were then incubated overnight for 16 hours at 37 °C without CO_2. After the incubation, cells were again washed twice with ≈2ml PBS, and once with 1ml methanol. Dishes were then allowed to air dry before being viewed by

bright field microscopy to count the proportion of blue cells in the total cell population, thus determining the proportion of senescent cells.

2.8. Detection of apoptosis by flow cytometry

2.8.1. General principles of flow cytometry

Flow cytometry is a high-throughput means of obtaining detailed quantitative information on every single cell in a larger population of cells. A flow cytometer aligns cells in single file in an annular fluid stream before propelling these cells from the sample tube through a cuvette by air pressure. The machine then focuses a laser beam on the cuvette, where the cell perturbs the beam direction, which is dependent on the difference in refractive index between the cell contents and the surrounding fluid, the size of the cell, and particulate elements within the cell. The resulting deflected light is measured by suitably positioned detectors, which collect information on light emitted out of the cell in the forward direction (forward scatter channel)) and light emitted at 90° (side scatter channel). The extent of forward scatter (FS) is generally related to cell size and can be used to distinguish between cell debris and live cells, while side scatter (SS) is characteristically associated with cellular granularity. Individual cells from the same cell line display similar degrees of FS and SS to each other, and as such this data can be used to isolate this group of cells from analysis, excluding data from either cell debris or clumps of cells. Generating FS versus SS dot plots and "gating" the central population of cells achieves this.

Using specific markers (usually antibodies) conjugated with fluorochromes, a flow cytometer can be used to detect cell surface or intracellular components. A fluorochrome is a compound that absorbs light energy from the laser beam and then emits this energy in the form of light energy (fluorescence), which is of a relatively longer wavelength, and thus a different colour. The difference between the energy absorbed from the laser and that emitted, in the form of fluorescence, is known as shift. Numerous fluorochromes are available, which all share this property, but differ in the wavelength, and therefore colour, of light they emit. The different colours of emitted light are separated from each other by a system of optical filters and mirrors, at which point appropriately placed photomultiplier tubes can register the shift and quantify this in terms of intensity.

During this project, initial flow cytometry studies were conducted on a FACSCalibur™ instrument (BD Biosciences, Oxford, UK) and data analysed with CellQuest Pro Software (BD Biosciences), but following mechanical failure of this machine subsequent studies were conducted using an Attune® acoustic focusing cytometer (Life Technologies) and data analysed with Attune® Cytometric Software (Life Technologies).

2.8.2. Reagents prepared for detection of apoptosis

10x annexin binding buffer:

0.1M HEPES/NaOH (pH 7.4)

1.4M NaCl

25mM $CaCl_2$

PI solution:

100µg/ml PI

10mM potassium phosphate (pH 7.4)

150mM NaCl

2.8.3. Using annexin V and propidium iodide to detect apoptosis

Phosphatidylserine (PS) is a phospholipid membrane component that is actively held facing the cytosolic side of the cell membrane, completely sequestered away from the outer membrane in healthy mammalian cells(391). During the early stages of apoptosis, however, there is a loss of this phospholipid membrane asymmetry, with PS no longer restricted to the cytosolic side of the membrane(391). This exposure of PS on the extracellular surface acts as a signal for macrophages to engulf the cells in vivo(391). Annexin V is a protein that can bind to PS in a calcium-dependent manner(392). Thus, annexin V conjugated to the fluorochrome FITC allows for identification of cells in the early stages of apoptosis(392). During late apoptosis, there is loss of normal cell membrane integrity, which permits the influx of the fluorescent DNA intercalating agent PI(393). Exploiting these facts, a population of unfixed cells can be stained simultaneously with FITC-conjugated annexin V (green fluorescence) and PI (red fluorescence) and the emitted fluorescence measured by flow cytometry to identify four distinct populations of cells, distinguished, or gated, based on the fluorescence emitted. Cells that remain unstained are healthy cells, cells that stain with just annexin V are undergoing early apoptosis, cells that stain with just PI are necrotic cells, and cells that stain with both annexin V and PI are cells which have entered late apoptosis. These four

populations can be clearly depicted on a dot plot graph of annexin V versus PI using quadrants (figure 2.7.3.1).

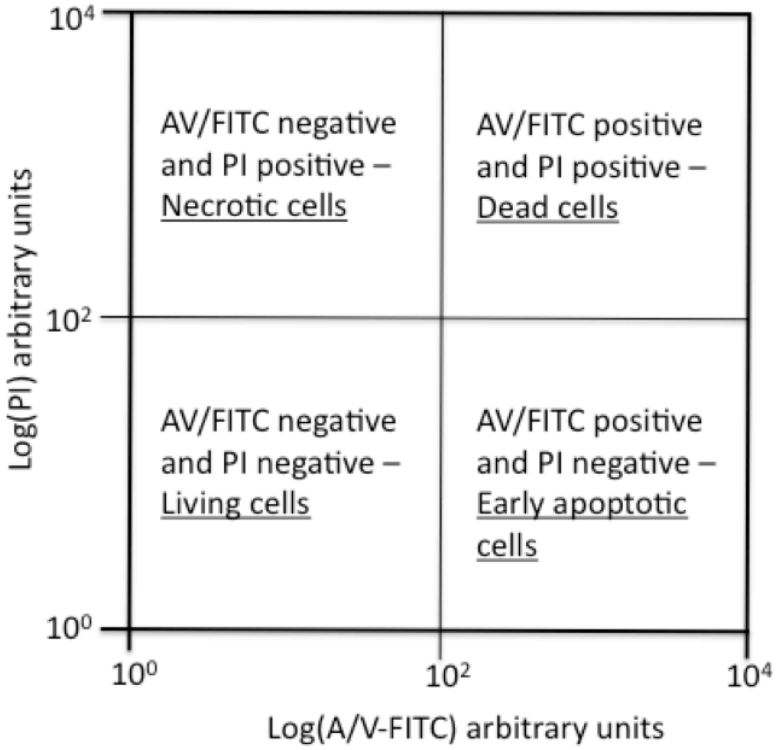

Figure 2.8.3.1: Populations of cells after annexin V/PI staining. Dot-plot output summarising positions of distinct cell populations determined by differential staining with FITC-conjugated Annexin V (A/V-FITC) and propidium iodide (PI), and analysis by flow cytometry.

Cells were harvested, counted, seeded at a density of 7.5 x 10^5 in Nunc™ 6cm culture dishes, and incubated overnight at 37°C with 5% CO_2 to allow for cell attachment as described above. The following day, the designated negative control cells were left untreated and the positive control cells treated with 1μM staurosporine. Staurosporine is tyrosine kinase inhibitor, which is a known potent inducer of apoptosis. The negative and positive control cells, known healthy and apoptotic populations of cells respectively, were required for calibration of the positioning of the four quadrants for each of the cell lines during subsequent analysis. Otherwise, cells were treated as indicated with combinations of 6Gy IR, 25mM 2-DG, 25mM NAC, all delivered as described previously. Cells were then transferred back to a humidified cell incubator at 37°C with 5% CO_2 for either 24 or 48 hours. Cells were then trypsinised as described previously – modified such that the media in which the cells were cultured was also collected in order to obtain dead cells that may have detached from the surface – and pelleted by

centrifugation at 300 x *g* for 5 minutes in a pre-cooled centrifuge at 4°C. Supernatant was removed and cells were re-suspended and washed twice in 5ml of ice cold PBS. Samples were kept on ice hereafter. Following this, cells were counted as described previously and density was adjusted to $1x10^6$ cells per sample. Following a final centrifugation at 300 x *g* for 5 minutes, cell pellets were re-suspended in 385µl of 1x annexin binding. FITC-conjugated annexin V (5µl) was then added to 385µl of cell suspension and incubated in the dark on ice for 10 minutes. PI solution (10µl) was then added to each sample before being passed into the flow cytometer for analysis.

2.9. Detection of reactive oxygen species by flow cytometry

DCFH-DA, a chemically reduced and acetylated form of reduced fluorescein and calcein, was utilised for the detection of ROS by flow cytometry. Although non-fluorescent, DCF-DA is cell permeable, and on entering the cell is cleaved at the two ester bonds by intra-cellular esterases, which yields a charged form of the dye that is much better retained by cells than is the parent compound(394). As such, this compound accumulates intracellularly and subsequent oxidation by ROS generates the highly fluorescent product 2′,7′-di-chlorofluorescein (DCF), which can be detected and quantified by flow cytometry(394) by the principles described in section 2.8.1.

Cells were harvested, counted, seeded at a density of 7.5 x 10^5 in Nunc™ 6cm culture dishes, and incubated overnight at 37°C with 5% CO_2 to allow for cell attachment as described above. The following day, the designated negative and positive control cells were left untreated. Otherwise, cells were treated as indicated with combinations of 6Gy IR, 25mM 2-DG, 25mM NAC, all delivered as described previously. Cells were then transferred back to a humidified cell incubator at 37°C with 5% CO_2 for a designated amount of time (1, 2, 4, 8, 16, or 24 hours) before being harvested by trypsinisation as described previously, modified such that the media in which the cells were cultured was also collected in order to obtain dead cells that may have detached from the surface. On the day of the assay, a fresh vial of DCFH-DA (50µg) was reconstituted using 85µl of DMSO and was then diluted in an appropriate volume of PBS, dependent on the number of samples, to give a final working concentration of 10µM. Following harvesting, cells were pelleted by centrifugation at 300 x *g* for 5 minutes in a pre-cooled centrifuge at 4°C. Supernatant was removed and cells were re-suspended and washed twice in 2ml of PBS. Subsequently, cells were counted as described previously and density was adjusted

to $1x10^6$ cells per sample. After a final centrifugation at 300 x *g* for 5 minutes, cell pellets were re-suspended in 500µl of the 10µM DCFH-DA solution. At this point, H_2O_2 was added to the positive control sample to a final concentration of 100µM. Samples were then incubated at 37°C for 15 minutes before being transferred to the flow cytometer for analysis. Positive and negative controls were first used to calibrate instrument settings, after which treatment samples were analysed. The fluorescence output histogram for the negative control was used to tailor the position of a marker, which included approximately 90% of cells in the population. This marker was then used to quantitatively assess the shift in fluorescence in the other samples tested.

2.10. Measurement of NADP/NADPH

2.10.1. Reagents prepared for NADP/NADPH measurement

Master reaction mix (100µl):

98µl NADP cycling buffer

2µl NADP cycling enzyme mix

2.10.2. Protocol for Measurement of NADP/NADPH

Measurement of relative levels of intracellular NADP and NAPH was performed using the NADP/NADPH quantification kit as per the manufacturer's instructions. Cells were harvested, counted, seeded at a density of 7.5 x 10^5 in Nunc™ 6cm culture dishes, and incubated overnight at 37°C with 5% CO_2 to allow for cell attachment as described above. The following day, cells were either left untreated or treated as indicated with 5µM 6-AN, all administered as described previously. Cells were then transferred back to a humidified cell incubator at 37°C with 5% CO_2 for 24 hours before being harvested by trypsinisation as before. Cells were then pelleted by centrifugation 300 x *g* for 5 minutes in a pre-cooled centrifuge at 4°C and washed with ice cold PBS. Subsequently, cells were counted as described previously and density was adjusted to $1x10^5$ cells per sample. Each sample was then transferred to an Eppendorf® 1.5ml microcentrifuge tube and cells pelleted by centrifugation at 300 x *g* for five minutes. Next, cells were extracted in 200µl of NADP/NADPH extraction buffer by two cycles of freeze/thawing using liquid nitrogen. Samples were then vortexed for 10 seconds and centrifuged at 13,000 x *g* for 10 minutes, before being deproteinised by filtering through a 10kDa cutoff spin filter to prevent consumption of NADPH by lysate enzymes. To detect NADPH, NADP was decomposed by aliquoting 100µl of each extracted sample into a new microcentrifuge

tube and heating to 60°C for 30 minutes in a dry block heater (Anachem, Luton, UK), followed by cooling on ice. During this time, in order to generate a standard curve for NADPH content, NADPH standards were prepared using the stock NADPH standard from the kit diluted in NADP/NADPH extraction buffer to a final volume of 50µl in designated wells of Corning® 96-well clear-bottom plates (Sigma-Aldrich) at the following concentrations: 0, 20, 40, 60, 80, and 100pmol/well. Each standard was represented in duplicate. Subsequently, 50µl each of both the NADPH (NADP decomposed) samples and the original extracted total NADP samples were transferred into the designated wells of the 96-well plate in duplicate. Next, 100µl of the master reaction mix was added to each of the standard and sample wells, mixed well on a horizontal shaker, and incubated for five minutes at room temperature to convert NADP to NADPH. Subsequently, 10µl of NADPH developer was also added to each well and incubated at room temperature for two hours, before the absorbance measurements were taken at 450nm using SpectraMax® Plus 384 microplate reader (Molecular Devices, Wokingham, UK). Results were obtained by comparison with the generated standard curve. The values obtained in all samples wells were then normalised to the number cells added to each well to give values expressed in pmol/1 x 10^6 cells. Values for the NADPH only samples were then subtracted from the values for the corresponding total NADP samples (all NADP had been converted to NADPH by the NADP Cycling Enzyme Mix in these samples) to determine the amount of NADP. NADP/NADPH ratios were also then calculated.

2.11. Western blotting

2.11.1. General principle of western blotting

Western blotting is a technique, which is used for detection of specific proteins in a studied sample. Proteins are first separated by size using gel electrophoresis and then transferred to a membrane, which is probed with antibodies raised specifically to the proteins of interest.

2.11.2. Reagents prepared for western blotting

SLIP (Stuart Linn Immunoprecipitation) buffer:

50mM HEPES (pH 7.5)

10% glycerol

0.1% Triton X-100

150mM NaCl
0.5mg/ml BSA

PBS/tween:
65mM $Na_2HPO_4 \cdot 2H_2O$
15mM $NaH_2PO_4 \cdot 2H_2O$
75mM NaCl
0.1% (v/v) Tween-20

Tris-glycine electrophoresis running buffer:
25mM Tris
250mM glycine
0.1% (w/v) SDS

Tris-glycine transfer buffer:
25mM Tris
192mM glycine
20% (v/v) methanol

4x protein sample loading buffer:
250mM Tris (pH 6.8)
8% (w/v) SDS
40% (v/v) glycerol
4mg/ml bromophenol blue
1% (v/v) β-mercaptoethanol
Diluted with dH_2O to make 2x and 1x sample buffer.

Ponceau S solution:
0.2% (w/v) Ponceau S
5% (v/v) acetic acid

2.11.3. Bradford assay

Proteins for analysis were extracted from either untreated cells or following treatment with 6Gy IR at various time points. Cells were harvested by trypsinisation and pelleted by centrifugation at 300 x *g* for five minutes at 4°C as described previously. The pellets were washed with 1ml of PBS, transferred to Eppendorf® 1.5ml microcentrifuge tubes,

and the cells were again pelleted by centrifugation and the supernatant aspirated as before. The pellets were then frozen at -80°C prior to further processing. On the day of sample processing, cell pellets were lysed by re-suspension in SLIP buffer supplemented with the following protease inhibitors (hereafter referred to as lysis buffer): aprotinin (2µg/ml), leupeptin (0.5µg/ml), pepstatin A (1µg/ml), trypsin inhibitor from soybean (100µg/ml) and PMSF (1mM in 100% ethanol). Samples were then incubated on ice for 10 minutes, centrifuged for 10 minutes at 13,000 x *g* at 4°C, before the supernatant from this centrifugation was transferred to a clean microcentrifuge tube. In the interim, protein standards were prepared for the Bradford assay. Firstly, a solution of 20mg/ml BSA in lysis buffer was prepared and a serial dilution performed to produce six further standards of the following BSA concentrations: 10mg/ml, 5mg/ml, 2.5mg/ml, 1.25mg/ml, 0.625mg/ml, and 0.3125mg/ml. 2µl of each of the standards was then added to 1ml of protein assay dye reagent (diluted 1:5 with dH_2O) and vortexed for 10 seconds. 2µl of the SLIP buffer was also added to 1 ml of protein assay dye reagent and assigned as the blank. A standard curve was prepared on a BioPhotometer (Eppendorf AG, Hamburg, Germany) using the Bradford program, which measures absorbance at 595nm. A coefficient of variable of less than 5% was deemed an acceptable level of calibration. Following generation of the standard curve, 2µl of each of the protein samples was added to 1ml of protein assay dye reagent in pre-chilled microcentrifuge tubes, and the protein concentrations determined based on the prepared standard curve using the BioPhotometer. Samples were then adjusted such that 50µg of total protein was made up in sample loading buffer using indicated volumes of 1X, 2X and 4X (final concentration of the buffer 1X) to a total volume of 20µl. These samples were then frozen at -80°C prior to gel electrophoresis.

2.11.4. Polyacrylamide gel electrophoresis

A SDS polyacrylamide gel was used to separate proteins by gel electrophoresis. The percentage of acrylamide used in the separating gel was dependent on the size of proteins to be resolved, with a higher percentage acrylamide gel suited to the resolution of low molecular weight proteins and vice versa. The separating gels were prepared as detailed in table 2.11.4.1. Glass slides for making 0.75mm thick gels were assembled, the separating gel poured into the gap, overlaid with dH_2O, and allowed to polymerise. Once the gel had set (typically after one hour) the water was poured off and the stacking gel table 2.11.4.1 poured, a 10-well comb inserted, and the gel left to polymerise (typically 20 minutes).

Table 2.11.4.1: **Composition of SDS-PAGE gels** (volumes required to make 10ml).

Reagent	Separating Gel		Stacking Gel
	10%	12%	
40% acrylamide mix	2.5ml	3ml	1.275ml
1.5M Tris (pH 8.8)	2.5ml	2.5ml	
1M Tris (pH 6.8)			1.25ml
10% SDS	100µl	100µl	100µl
10% APS	100µl	100µl	100µl
TEMED	8µl	8µl	10µl
dH_2O	4.8ml	4.3ml	7.225ml

Following polymerisation, the comb was removed and the gels, with the assembled glass slides, were placed in an electrophoresis tank filled with tris-glycine electrophoresis running buffer. The previously prepared protein samples were retrieved from the -80°C freezer and were denatured by heating in a heat block at 100°C for five minutes, vortexed, and centrifuged at 13,000 x *g* at 4°C for two minutes. 20µl of each sample (containing 50 µg of total protein) was then loaded into the designated wells of the gel, alongside a blue broad-range pre-stained protein marker. SDS-polyacrylamide gel electrophoresis (PAGE) was performed using a two-gel Mini-PROTEAN® Tetra cell (Bio-Rad) at 200V for one hour.

2.11.5. Protein detection

Following SDS-PAGE, proteins were transferred onto a Hybond ECL nitrocellulose membrane (GE Healthcare) using a Mini Trans-Blot® Electrophoretic Transfer Cell (Bio-Rad). Firstly, Hybond ECL nitrocellulose membrane, two pieces of Whatman® chromatography paper (Sigma-Aldrich), and two sponges where pre-soaked in transfer buffer, and the running apparatus dismantled. Next, the gel was removed from between the glass slides, the stacking gel discarded, and the separating gel placed in between the nitrocellulose membrane and chromatography paper. Another piece of chromatography paper was placed on the opposing side of the nitrocellulose membrane and two sponges were added on the outside to complete the assembly. This was then placed in a transfer cassette, which was then placed in a tank in such a way that the membrane faced the positive electrode whilst the gel faced the negative electrode, thereby enabling the negatively charged proteins on the gel to run in the direction of the nitrocellulose membrane towards the cathode. The tank was filled with transfer along with an ice pack

in order to ensure cooling during transfer. The transfer was performed at 100 V for one hour using a two-gel Mini-PROTEAN® Tetra cell.

Subsequently, the transfer apparatus was dismantled and the membrane stained briefly with Ponceau S and rinsed with H_2O to ensure the transfer of proteins had been successful. At this point, the membrane was cut horizontally into strips based on the size of proteins to be probed. The membrane was then washed briefly in PBS/Tween to remove the Ponceau S stain and blocked in 5% (w/v) non-fat dry milk in PBS/Tween solution at 4°C overnight (to prevent non- specific binding of antibodies to the membrane).

The following day, the membranes were agitated on a shaker at room temperature for one hour before blocking milk was removed and the membrane strips incubated with appropriate primary antibodies (section 2.1.4.) for one hour at room temperature on a shaker. The membranes were then washed for 15 minutes in PBS/Tween three times, after which horseradish peroxidase (HRP)-conjugated secondary antibodies (section 2.1.4.) raised to the relevant species were applied and the membranes incubated for a further hour at room temperature. Next, the membranes were washed three times as previously, before being transferred into dry trays. Amersham ECL Prime detection reagent (GE Healthcare Life Sciences) was then applied (typically 1-2ml per membrane) for five minutes, and the signal detected by chemiluminescence and recorded on a Kodak IM4000 image station using Carestream molecular imaging software (Carestream Health UK, Hemel Hempstead, UK). Further image processing was performed using CorelDRAW graphics suite X7.

3. Results

3.1. Investigating the metabolic phenotype in SCCHN

3.1.1. Introduction

As discussed in sections 1.3.1. and 1.3.3., although altered metabolism is now generally considered to constitute an emerging hallmark of the cancer phenotype(44) and has received renewed attention in the field of cancer research(257, 267, 395), primary studies of metabolism specific to SCCHN have been somewhat lacking. Several SCCHN studies have examined glucose transporter or glycolytic enzyme expression in isolation, often focusing on their prognostic significance(324-334, 336-343, 348), and a handful of studies have explored the effects of the glycolytic inhibitor 2-DG(354-357). Nonetheless, these studies have neglected to characterise dynamic metabolic flux, have at times produced conflicting results, and have failed present a clear picture of the SCCHN metabolic phenotype. Interestingly, two relatively recent studies from the same research group have implicated *TP53* status as a determinant of metabolic phenotype in SCCHN, with associated therapeutic implications(359, 360), while another recent study has proposed an alternative three-compartment model of metabolism in SCCHN based on Paget's "seed and soil" hypothesis(366).

Given the variation in metabolic perturbations between cancers(250) and the resulting importance of cancer type specific study of metabolism, the aim of this chapter is to further explore the metabolic phenotype in SCCHN. This was achieved taking advantage of the relatively recent development of highly sensitive, fluorescence and microplate-based XF analysis, which allows quantitative metabolic analysis that provides real-time information about metabolic phenotype during specifically designed mitochondrial and glycolytic stress tests(383, 384). As detailed in sections 2.4.6. and 2.4.7., by examining changes in OCR and ECAR during sequential injections of substrates and inhibitors that form the basis of these stress tests, the following parameters can be calculated: basal respiration and glycolysis; ATP-linked respiration, proton leak, maximal respiration and glycolysis, and spare respiratory and glycolytic capacity(383, 384).

3.1.2. Optimising the concentration of compounds for injection during XF24 metabolic assays

Prior to conducting XF assays, it was necessary to optimise the measurement conditions for the analysis of SCCHN cell lines. Firstly, cell seeding titrations were performed for each of the cell lines to determine optimal seeding densities, as previously described in section 2.4.5. The aim was to achieve evenly distributed cells at 50-90% confluence within each well, and obtain basal OCR and ECAR values of 50-400pmol/min and 20-120mpH/min respectively, as per manufacturer's guidelines. The resulting cell seeding densities were previously summarised in table 2.4.5.1.

The next step in optimisation involved titrating the concentrations of oligomycin and FCCP. This is because the effects of these compounds can vary between different cell types, and relatively small changes in concentration can significantly affect final measurements – particularly the case for FCCP(383, 384). Optimisation assays were first performed for oligomycin, in which OCR measurements were taken at baseline and following the addition of oligomycin at the following concentrations: 0.625, 1.25, 2.5, 5, and 10μM. These concentrations were chosen based on manufacturer's guidelines and were also consistent with concentrations used in other SCHNN cell lines published elsewhere(360). Figure 3.1.2.1. shows the resulting OCR responses in three selected SCCHN cell lines. Given that 1.25μM was the lowest concentration to consistently induce a maximal decline in OCR, and therefore in mitochondrial uncoupling, together with the fact that dose-dependent responses appeared highly conserved between SCCHN cell lines, this concentration of oligomycin was selected for use in all subsequent XF assays.

A

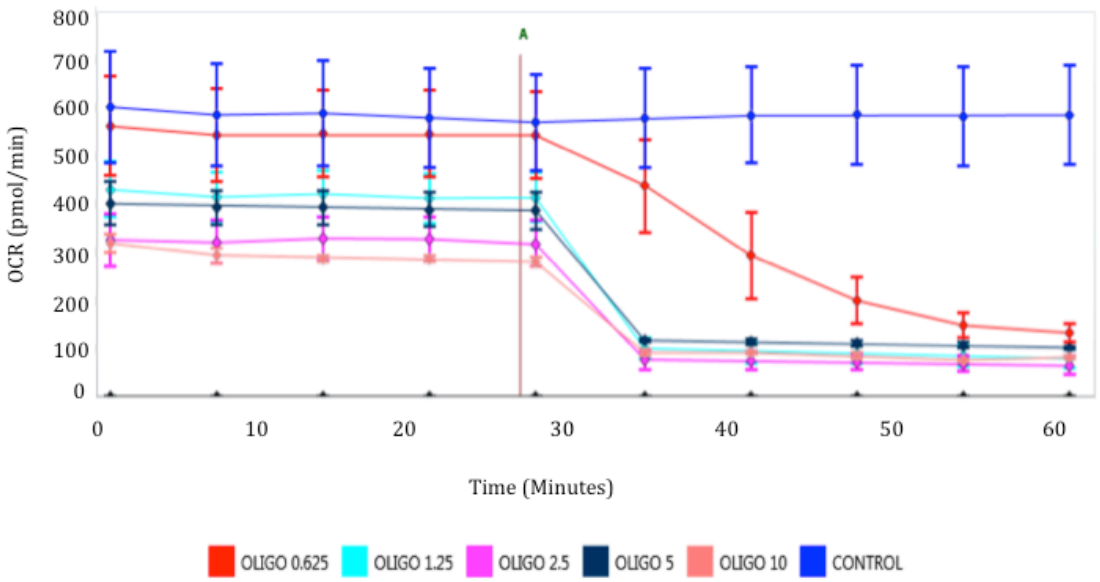
800
700
600
500
400
300
200
100
0
OCR (pmol/min)
A
0
10
20
30
40
50
60
Time (Minutes)
OLIGO 0.625
OLIGO 1.25
OLIGO 2.5
OLIGO 5
OLIGO 10
CONTROL

B

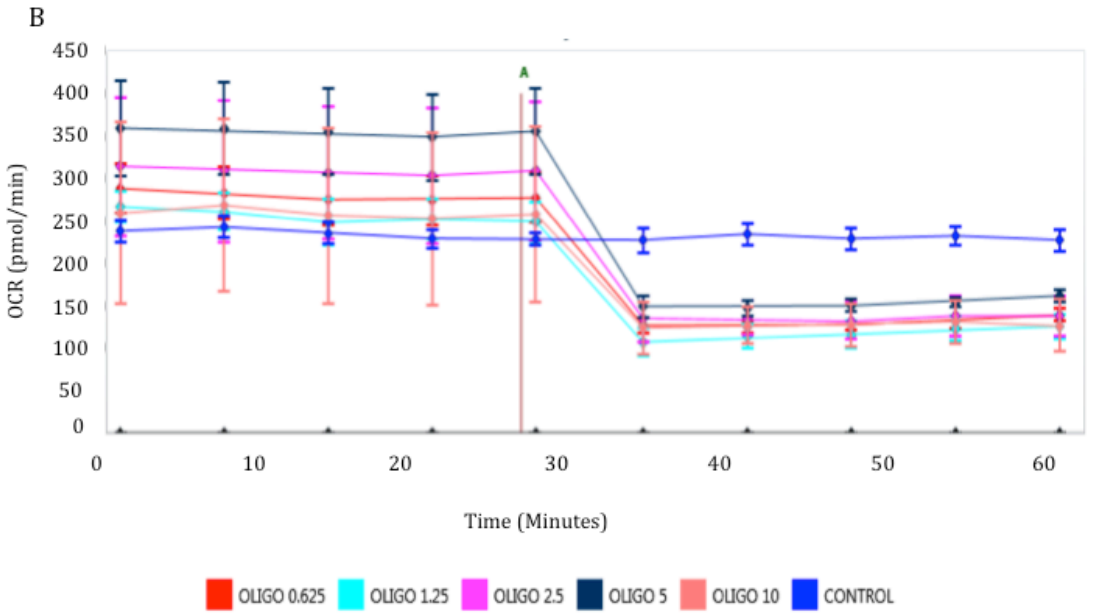
450
400
350
300
250
200
150
100
50
0
OCR (pmol/min)
A
0
10
20
30
40
50
60
Time (Minutes)
OLIGO 0.625
OLIGO 1.25
OLIGO 2.5
OLIGO 5
OLIGO 10
CONTROL

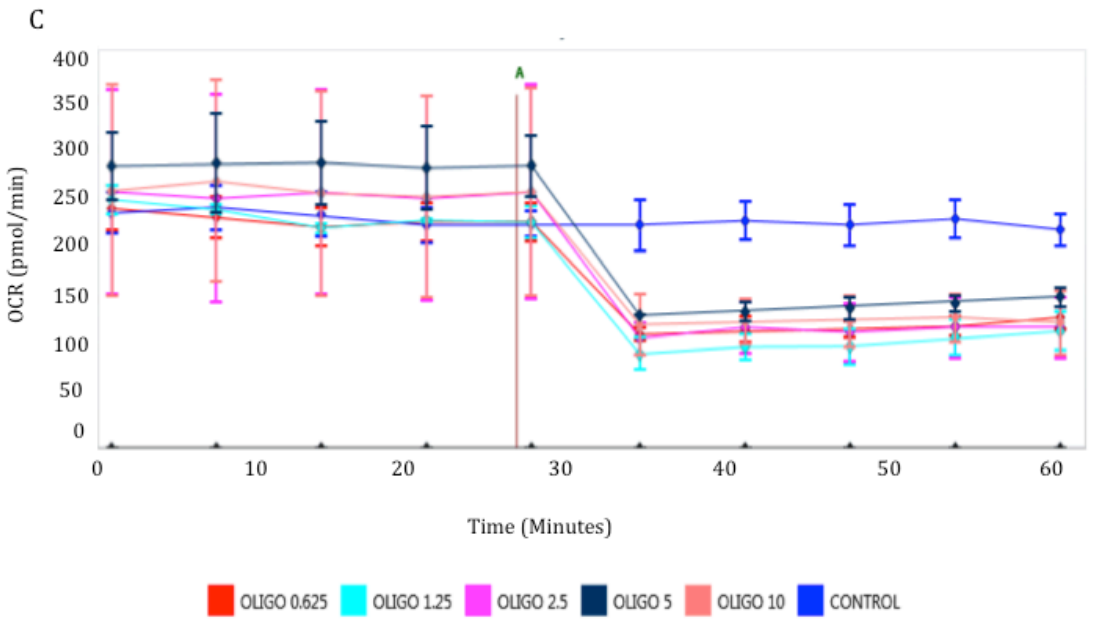

Figure 3.1.2.1: Oligomycin titration. OCR responses following administration of 0 (control), 0.625, 1.25, 2.5, 5, and 10μM oligomycin (point A on each graph). Each condition was performed in triplicate for each cell line and error bars represent the standard error of the mean (SEM). Three SCCHN cell lines were selected for optimisation to ensure consistency of responses across cell lines. Panels A, B, and C depict results for UM-SCC-5, UM-SCC-11A, and UM-SCC-11B respectively.

Following titration of oligomycin, optimisation assays were then performed for FCCP, in which OCR measurements were taken at baseline and following the addition of FCCP at the following concentrations: 0.5, 0.75, 1.0, 1.5 and 3μM. Again, these concentrations were selected on the basis of manufacturer's guidelines and published data(360). Figure 3.1.2.2. shows the resulting OCR responses in three selected SCCHN cell lines. Given that 1.5μM was the lowest concentration to consistently induce a maximal increase in OCR, and thus in ETC acceleration, together with the fact that dose-dependent responses appeared similar between SCCHN cell lines, this concentration of FCCP was selected for use in all subsequent XF assays.

A

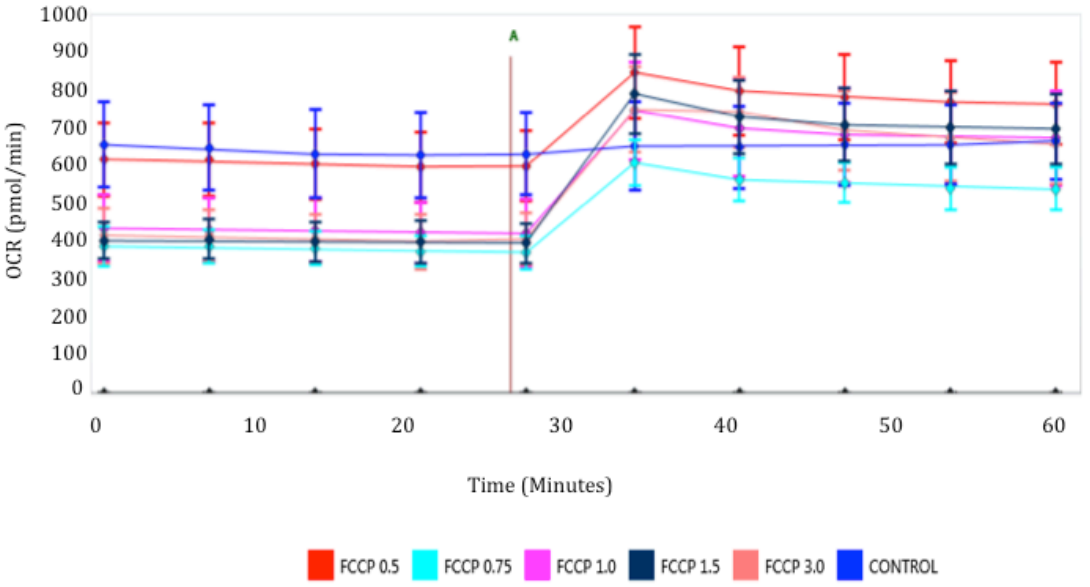
1000
900
800
700
600
500
400
300
200
100
0
OCR (pmol/min)
A
0
10
20
30
40
50
60
Time (Minutes)
FCCP 0.5
FCCP 0.75
FCCP 1.0
FCCP 1.5
FCCP 3.0
CONTROL

B

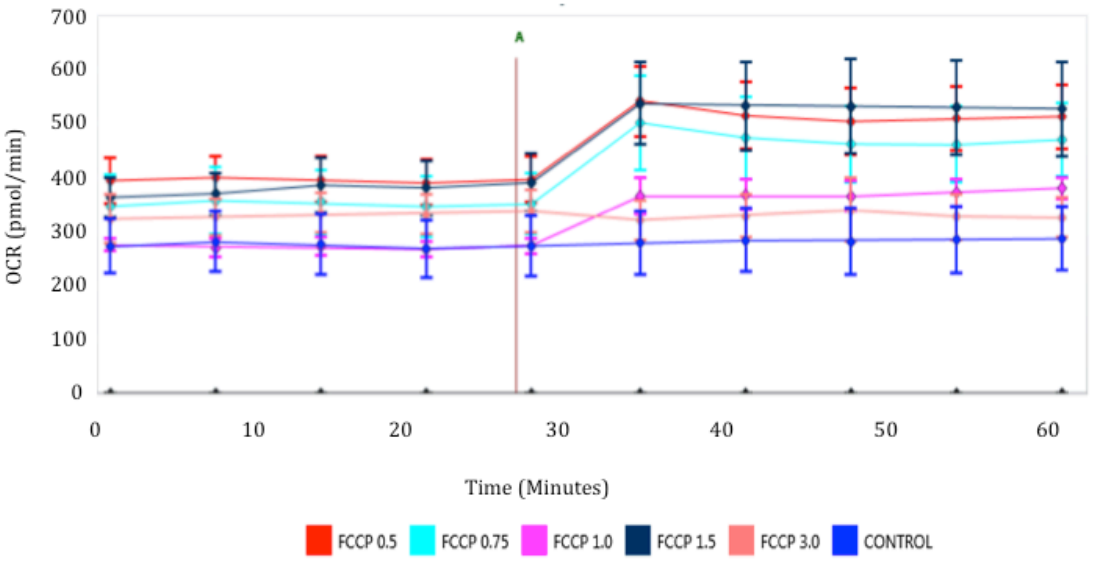
700
600
500
400
300
200
100
0
OCR (pmol/min)
A
0
10
20
30
40
50
60
Time (Minutes)
FCCP 0.5
FCCP 0.75
FCCP 1.0
FCCP 1.5
FCCP 3.0
CONTROL

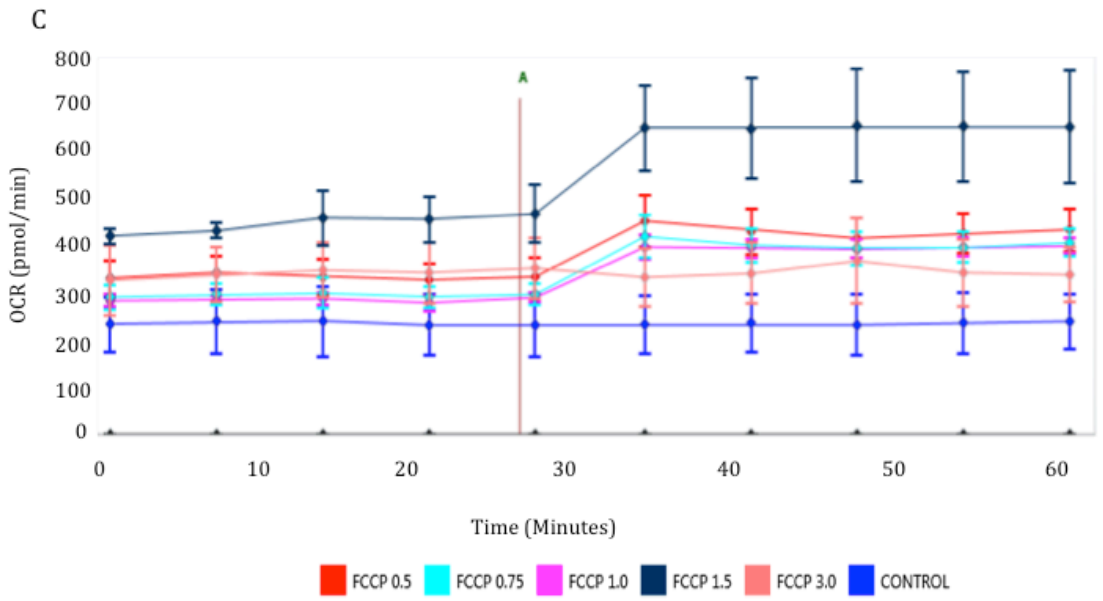

Figure 3.1.2.2: FCCP titration. OCR responses following administration of 0 (control), 0.5, 0.75, 1.0, 1.5 and 3μM FCCP (point A on each graph). Each condition was performed in triplicate for each cell line and error bars represent SEM. Three SCCHN cell lines were selected for optimisation to ensure consistency of responses across cell lines. Panels A, B, and C depict results for UM-SCC-5, UM-SCC-11A, and UM-SCC-11B respectively.

3.1.3. The metabolic phenotype of SCCHN cells is dependent on TP53 status

To determine the metabolic phenotype of our panel of SCCHN cell lines and to examine any potential relationship between metabolic profile and *TP53* status we next performed XF24 mitochondrial and glycolytic stress tests on our panel of SCCHN cell lines, as described in sections 2.4.6. and 2.4.7. Outputs from the mitochondrial and glycolytic stress tests for each of the cell lines are shown in figures 3.1.3.1. and 3.1.3.2. respectively, with data scaled to the fractional change relative to baseline OCR and ECAR, and thus presented as percentage increases or decreases from the assigned baseline following injection of the relevant substrates and/or inhibitors. The mutant *TP53* SCCHN cell lines (UM-SCC-5, UM-SCC-10A, UM-SCC-11B, and UM-SCC-81B) exhibited a distinct metabolic phenotype to that of wild-type *TP53* cell lines (UM-SCC-11A, and UM-SCC-17AS): wild-type *TP53* cells maintained metabolic diversity, displaying robust mitochondrial and glycolytic reserves, while mutant *TP53* cells exhibited markedly reduced mitochondrial and glycolytic reserves, functioning near or at capacity under basal conditions.

A

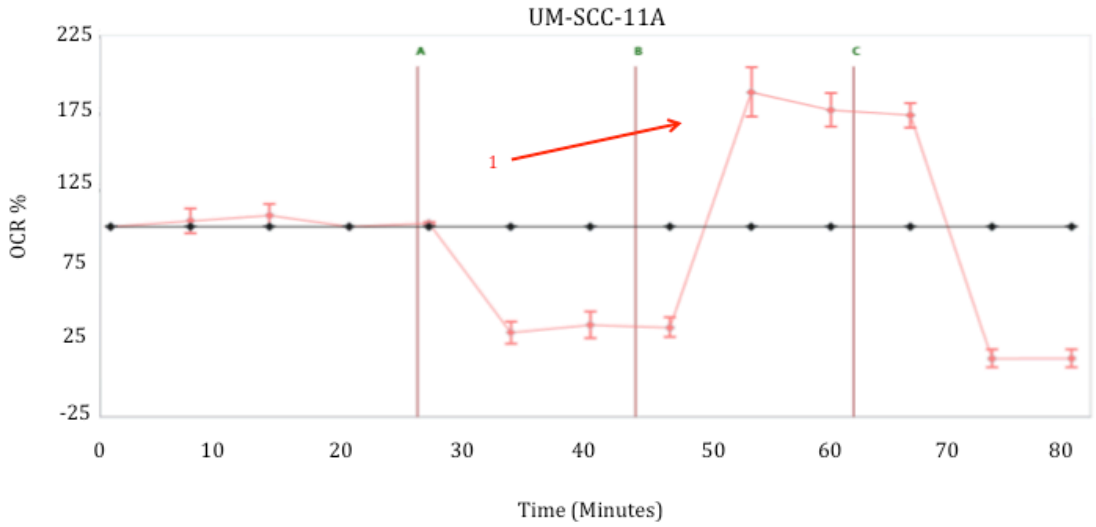
UM-SCC-11A
OCR %
225
175
125
75
25
-25
0
10
20
30
40
50
60
70
80
A
B
C
1
Time (Minutes)

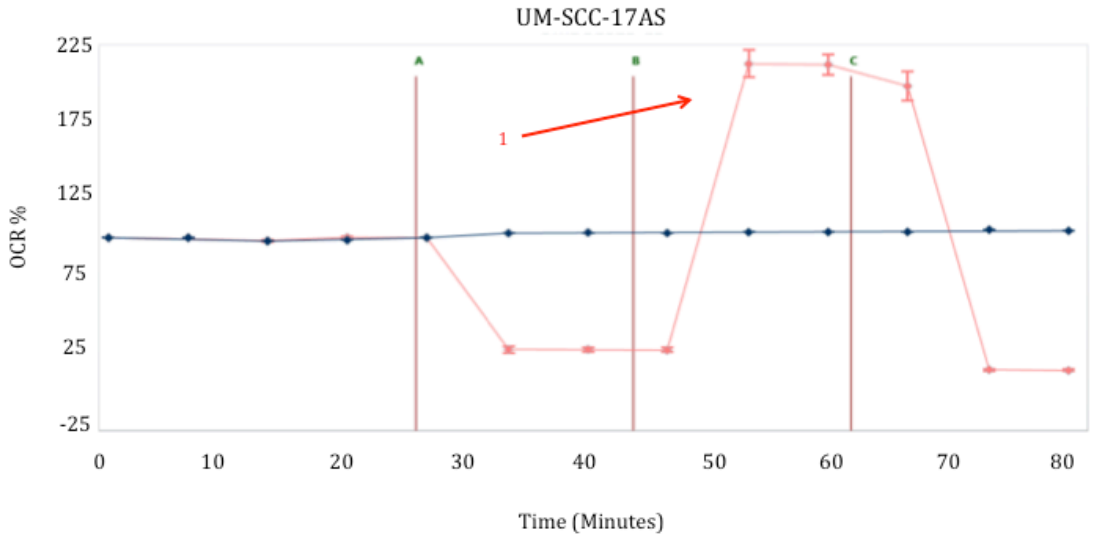
UM-SCC-17AS
OCR %
225
175
125
75
25
-25
0
10
20
30
40
50
60
70
80
A
B
C
1
Time (Minutes)

B

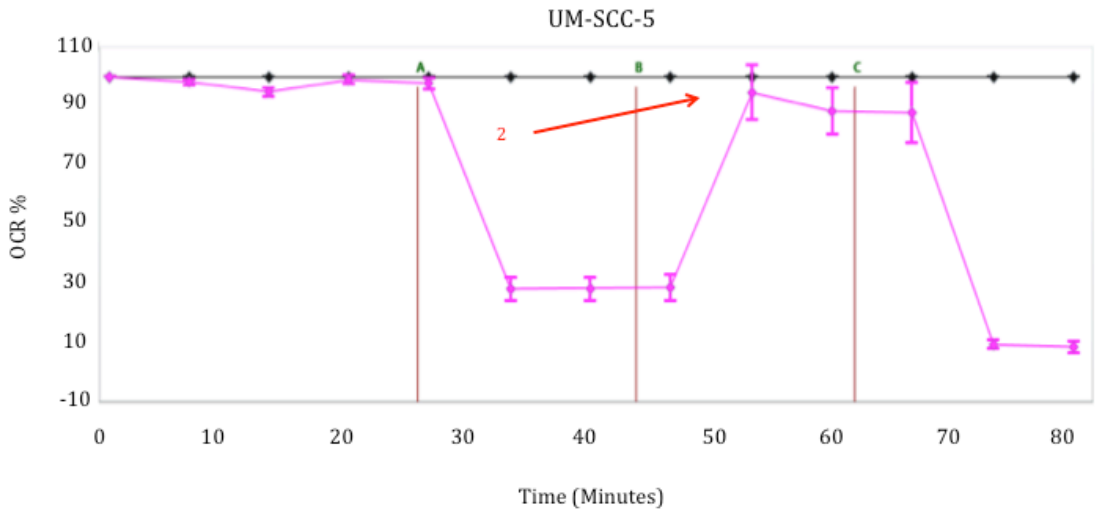
UM-SCC-5
OCR %
Time (Minutes)
A
B
C
2

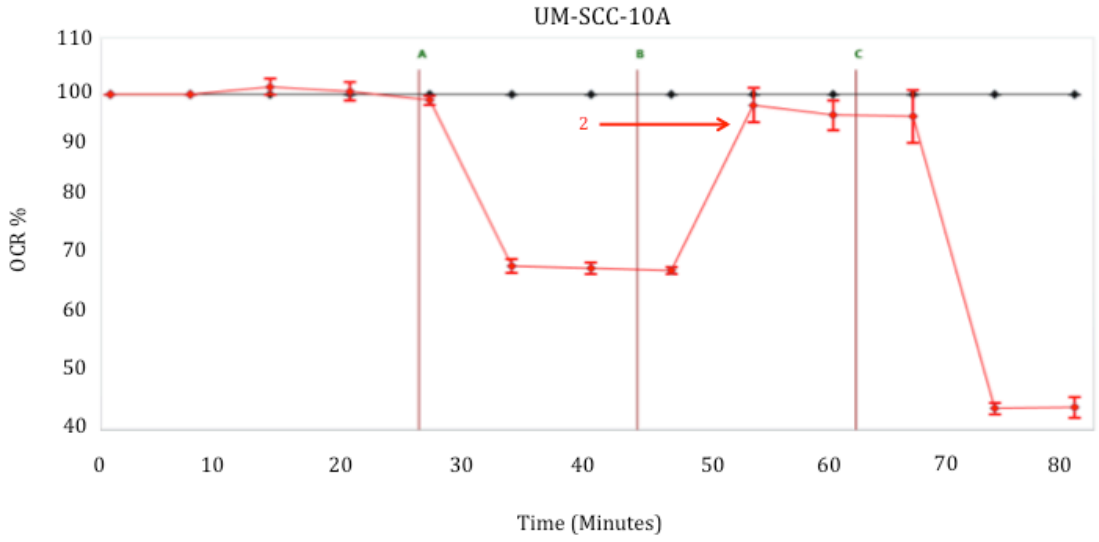
UM-SCC-10A
OCR %
Time (Minutes)
A
B
C
2

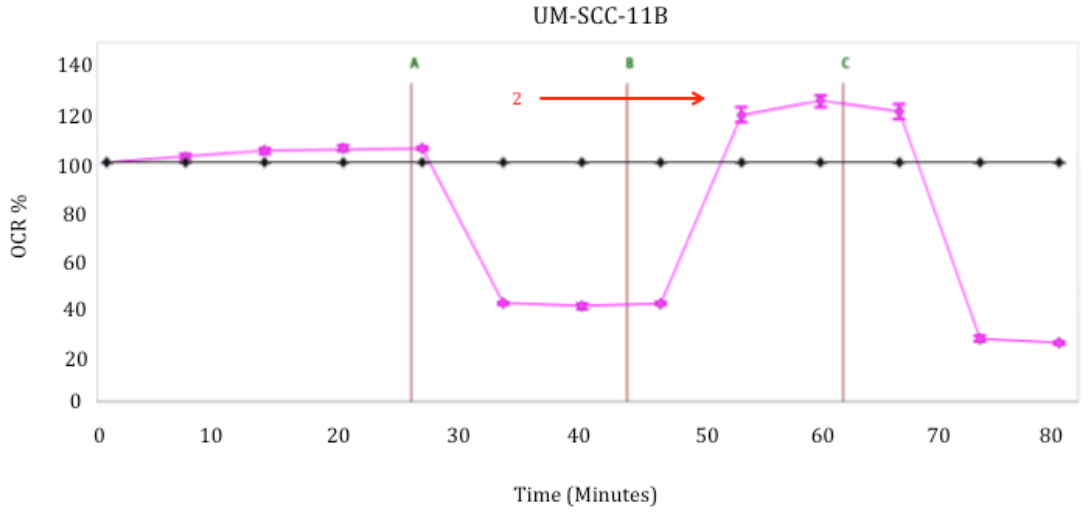
UM-SCC-11B
OCR %
Time (Minutes)
A
B
C
2

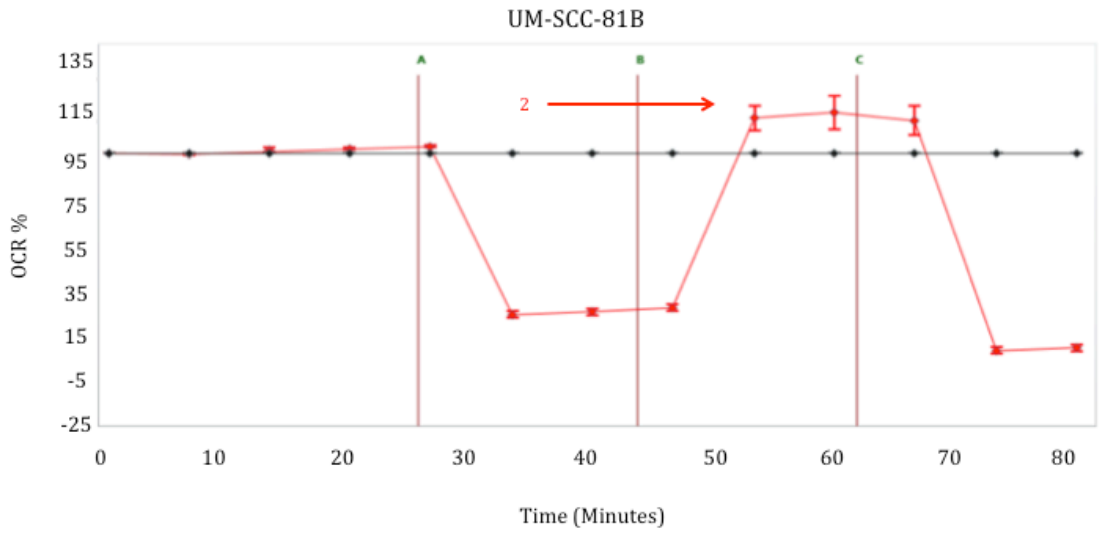

Figure 3.1.3.1: Changes in oxidative phosphorylation indicated by OCR in response to mitochondrial stressors in a panel of SCCHN cell lines. SCCHN cells were subjected to mitochondrial stress tests, in which oligomycin 1.25μM (point A), FCCP 1.5μM (point B), and rotenone and antimycin-A 1μM (point C) were sequentially injected, and OCR (pmol/min) measured. Data is presented as percentage increases or decreases in OCR relative to baseline measurements. The baseline is shown as the black line on the graphs. (A) *TP53* wild-type SCCHN cell lines, which maintained robust spare respiratory capacities (see red arrows labelled 1) and (B) mutant *TP53* cell lines, which exhibited reduced spare respiratory capacities (see red arrows labelled 2). Error bars represent SEM.

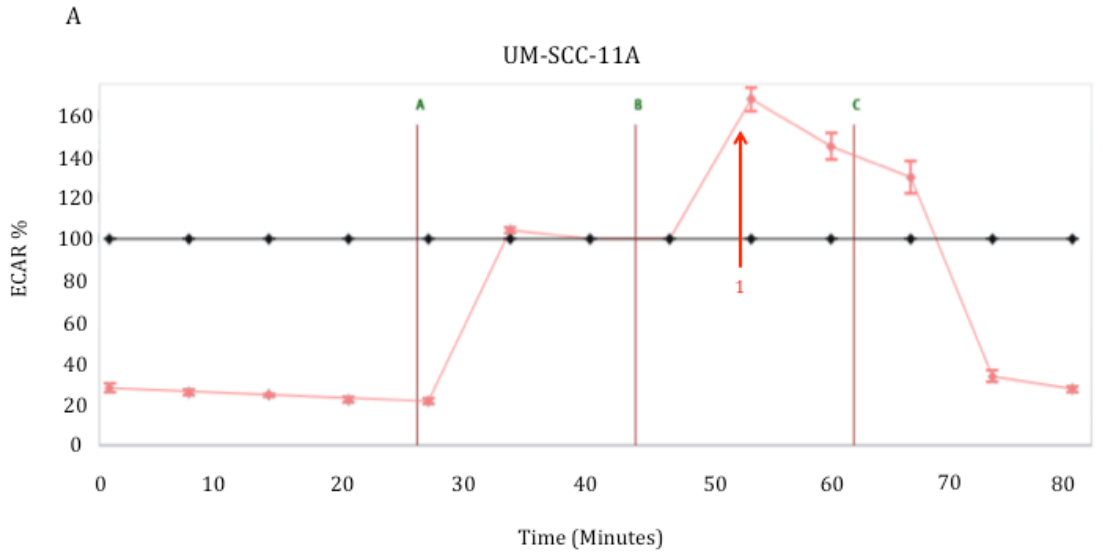

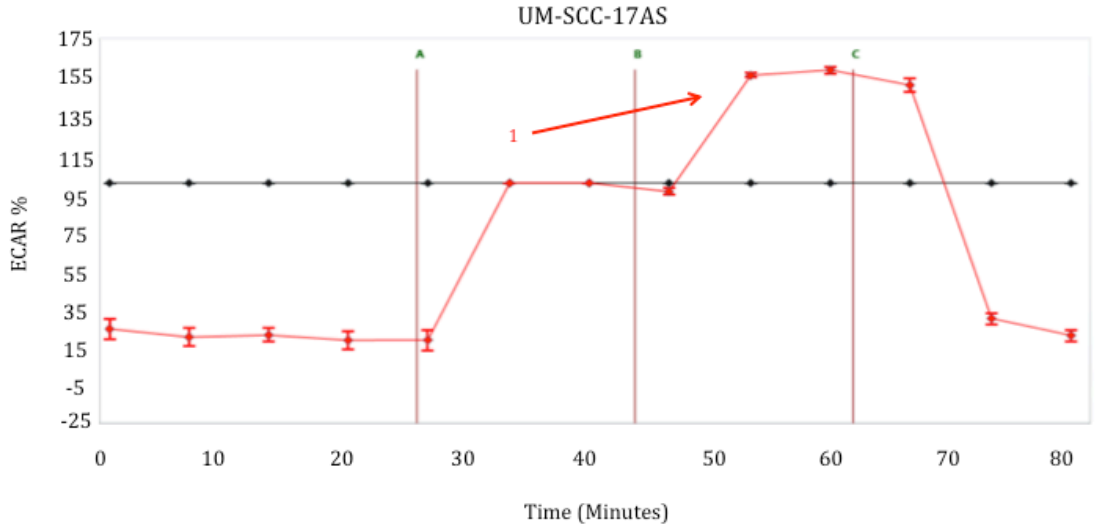
UM-SCC-17AS
ECAR %
175
155
135
115
95
75
55
35
15
-5
-25
A
B
C
1
0
10
20
30
40
50
60
70
80
Time (Minutes)

B

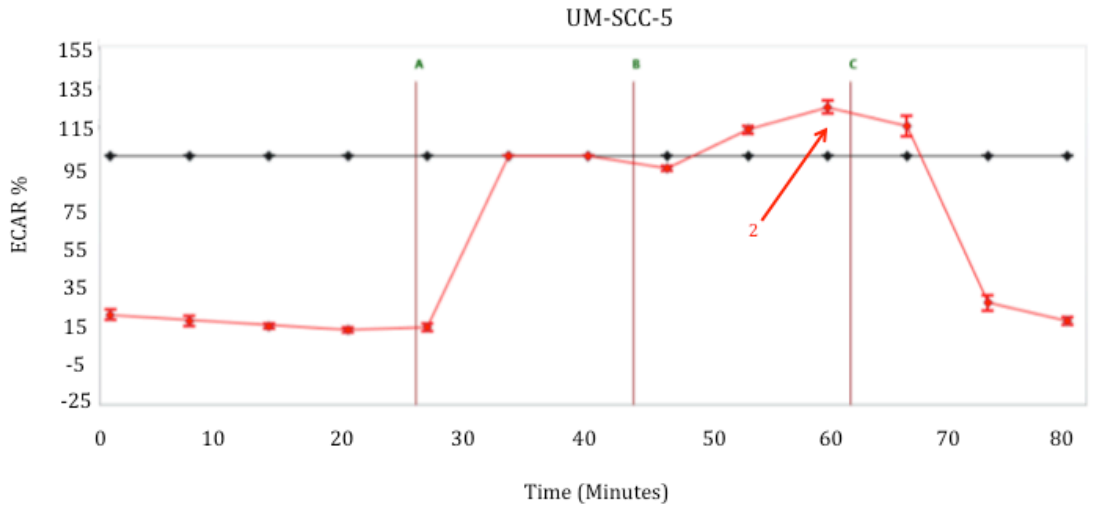
UM-SCC-5
ECAR %
155
135
115
95
75
55
35
15
-5
-25
A
B
C
2
0
10
20
30
40
50
60
70
80
Time (Minutes)

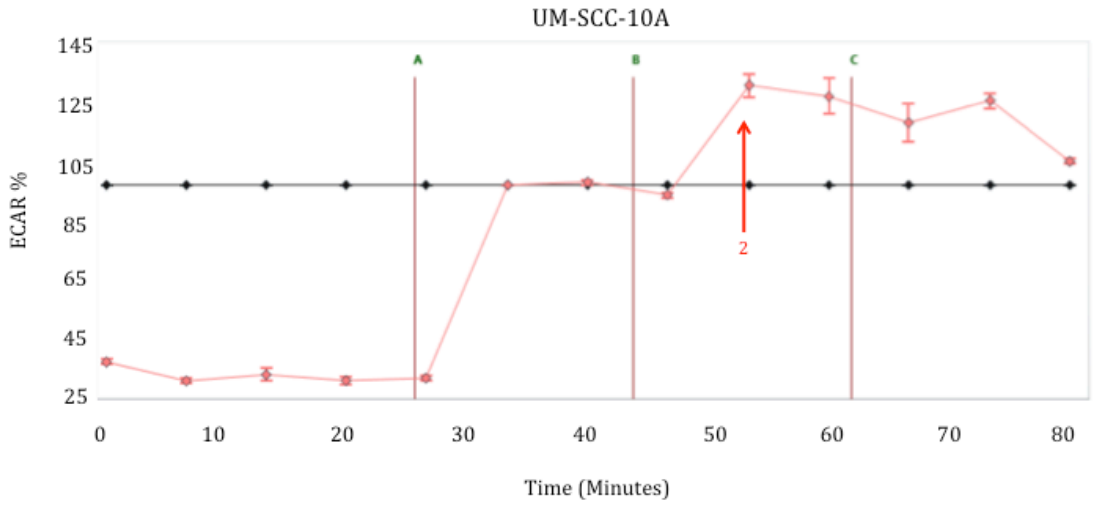
UM-SCC-10A
ECAR %
145
125
105
85
65
45
25
A
B
C
2
0
10
20
30
40
50
60
70
80
Time (Minutes)

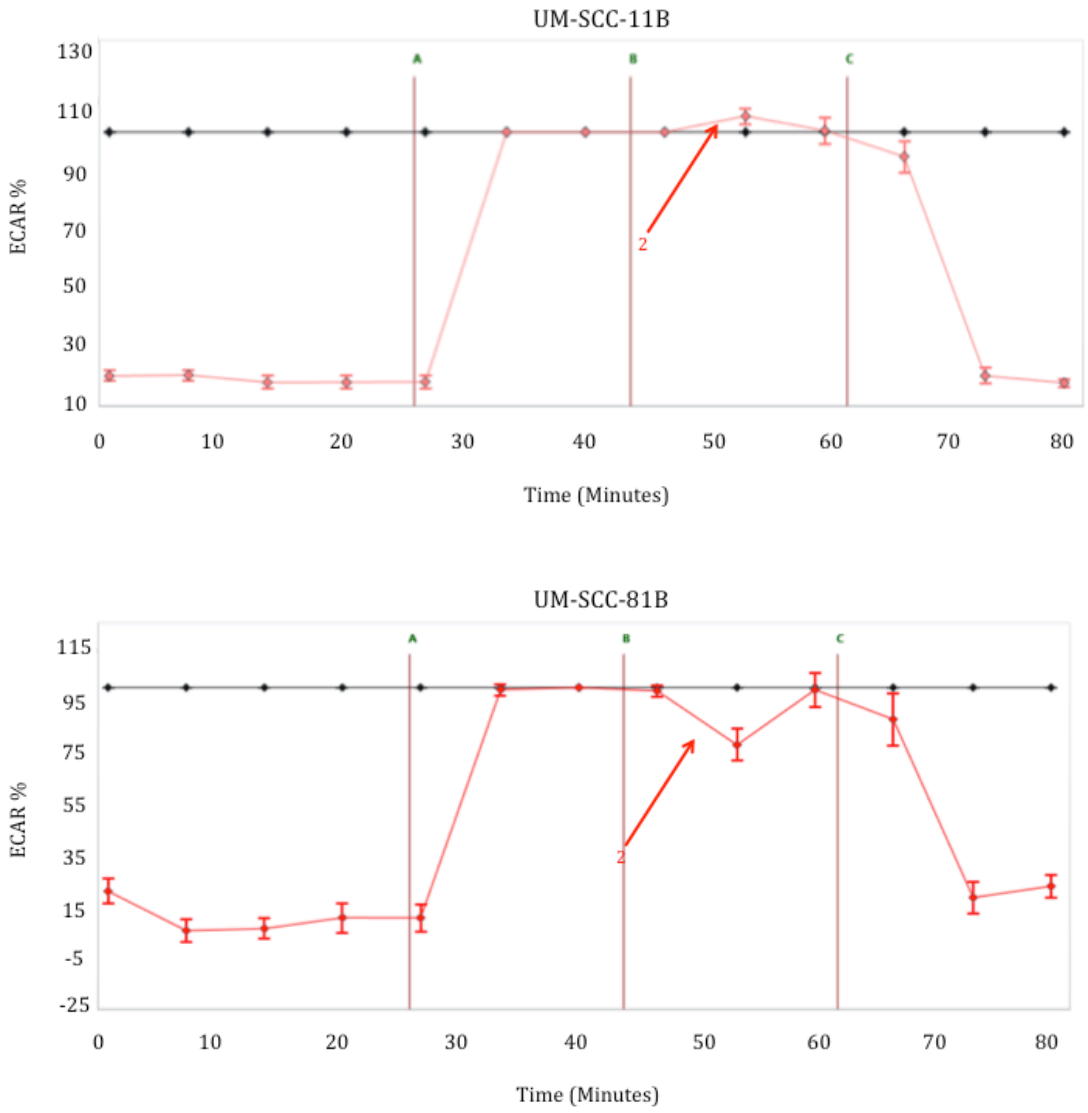

Figure 3.1.3.2: Glycolytic changes indicated by ECAR monitored in response to glycolytic substrates and stressors in a panel of SCCHN cell lines. SCCHN cells were subjected to glycolytic stress tests, in which glucose 10mM (point A), oligomycin 1.25μM (point B), and 2-DG 50mM (point C) were sequentially injected, and ECAR (mpH/min) measured. Data is presented as percentage increases or decreases in ECAR relative to baseline measurements. The baseline is shown as the black line on the graphs. (A) *TP53* wild-type SCCHN cell lines, which maintained robust glycolytic reserves (see red arrows labelled 1) and (B) mutant *TP53* cell lines, which exhibited reduced glycolytic reserves (see red arrows labelled 2). Error bars represent SEM.

In light of the consistent pattern of observed metabolic phenotypes in the panel of SCCHN cell lines, ostensibly distinguished by *TP53* status, isogenic cell lines divergent on *TP53* status were next interrogated to further explore the possibility of a cause-effect relationship between metabolic phenotype and *TP53* status in SCCHN cells. These groups of isogenic cell lines comprised the following: the wild-type *TP53* cell line UM-

SCC-17A and its derivative lines, UM-SCC-17A shp53 (cells stably expressing shRNA specific for p53) and UM-SCC-17A lenti (cells stably expressing the empty vector control); and the endogenously p53 null cell line UM-SCC-1 and its derivative lines transduced with wild-type *TP53* (UM-SCC-1 wtp53), empty vector control (UM-SCC-1 pBABE), or several clinically relevant *TP53* mutations (UM-SCC-1 R175H, UM-SCC-1 C176F, UM-SCC-1 R282W). Outputs from the mitochondrial and glycolytic stress tests for UM-SCC-1 and derivative lines are shown in figure 3.1.3.3., and in figure 3.1.3.4. for UM-SCC-17A and derivative lines. Importantly, the metabolic phenotypes observed in these groups of isogenic cell lines followed a similar pattern to those observed in the aforementioned panel of SCCHN cell lines. Specifically, forced expression of wild-type p53 in UM-SCC-1 resulted in a switch in metabolic profile from limited respiratory and glycolytic reserves, functioning near capacity at baseline, to a discernible increase in these parameters, while metabolic profiles in the derivative lines expressing *TP53* mutations did not differ from that of the parental line. In keeping with this, the opposite effect was observed in the context of stable knock-down of wild-type p53 in UM-SCC-17A. Such findings corroborate a functional dependence on p53, and further demonstrate that the observed switch in metabolic profile is the result of loss of wild-type p53 function rather than any oncogenic GOF properties harboured by a particular *TP53* mutation.

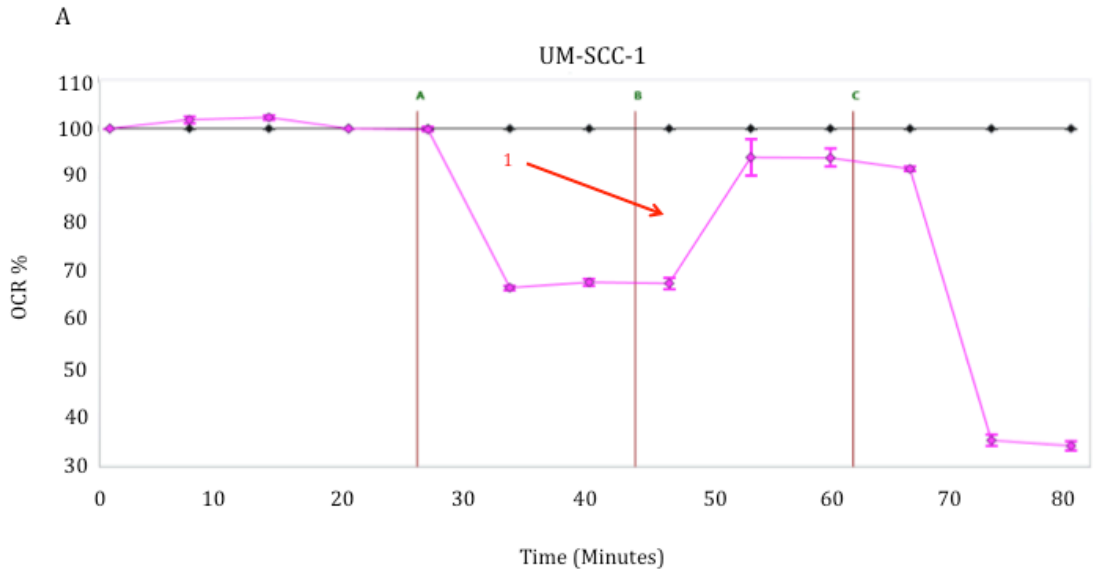

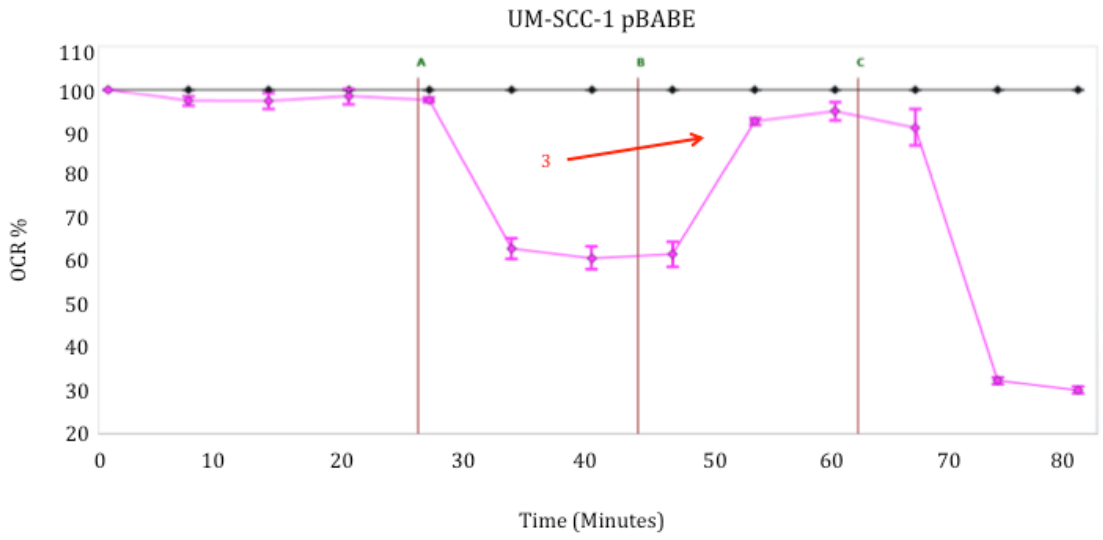
UM-SCC-1 pBABE
OCR %
Time (Minutes)
A
B
C
3

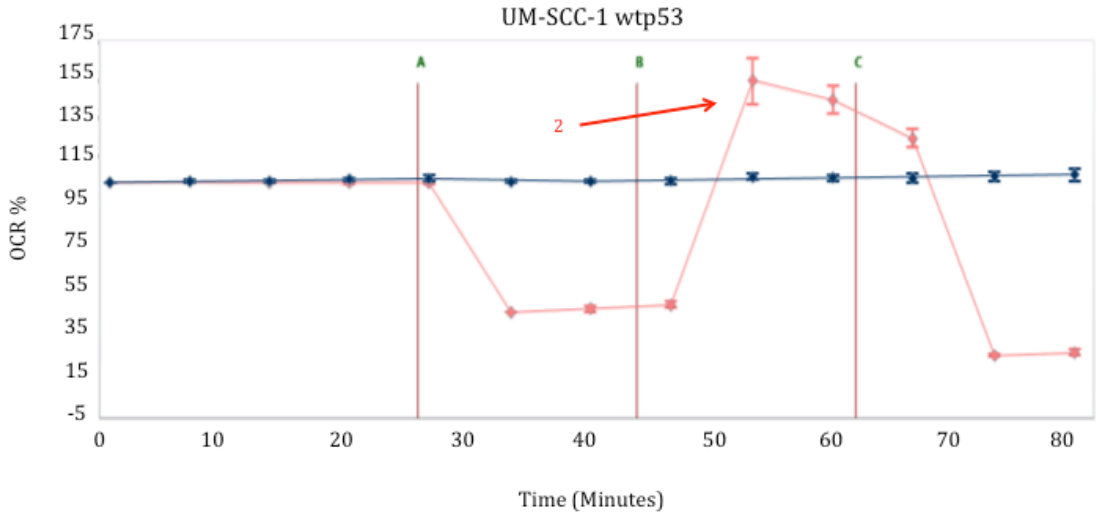
UM-SCC-1 wtp53
OCR %
Time (Minutes)
A
B
C
2

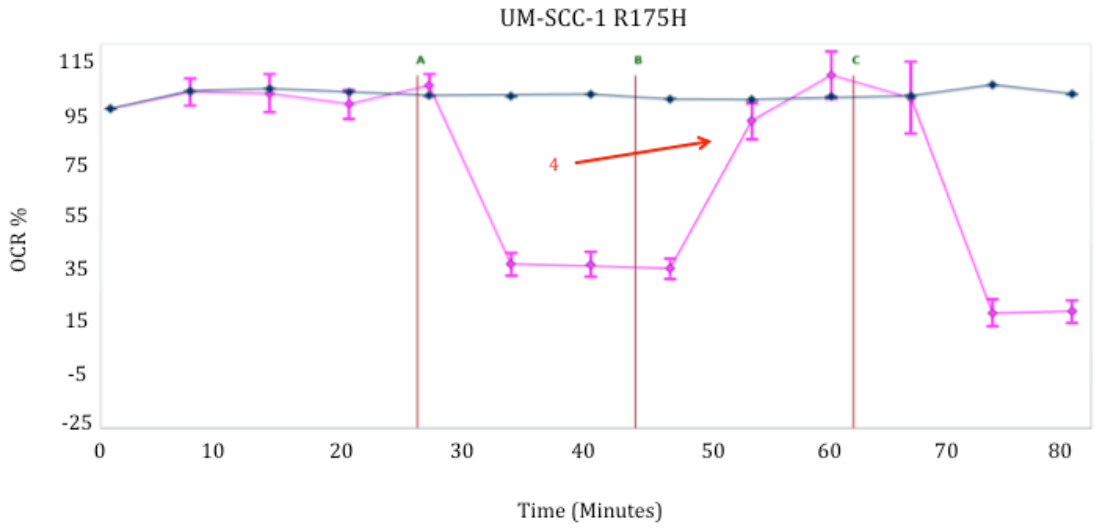
UM-SCC-1 R175H
OCR %
Time (Minutes)
A
B
C
4

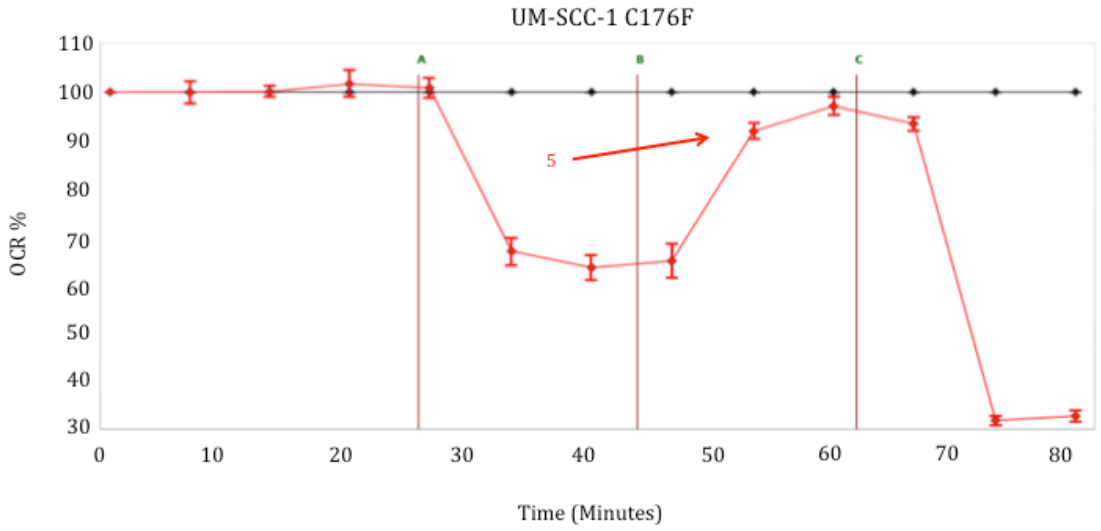
UM-SCC-1 C176F
OCR %
Time (Minutes)
A
B
C
5

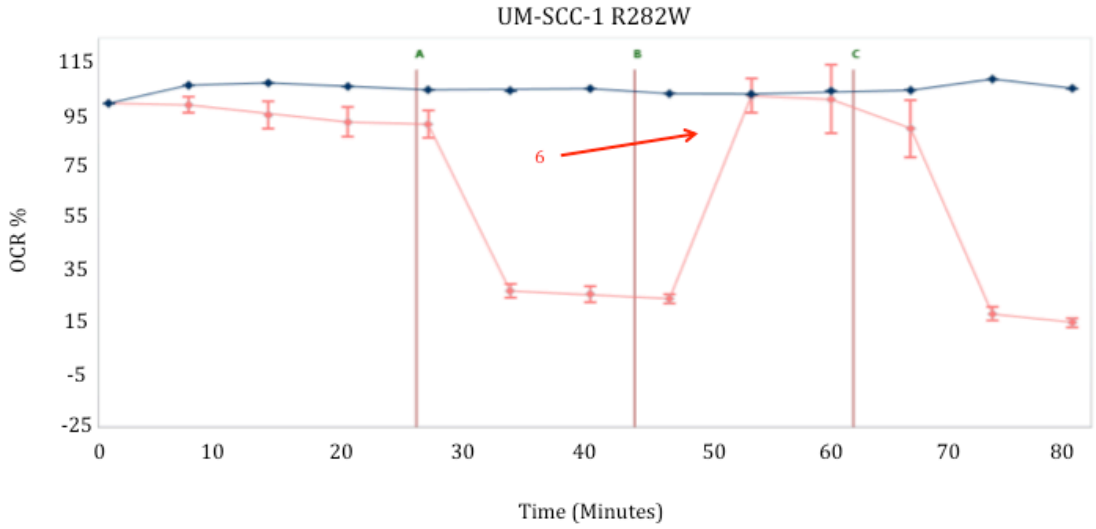
UM-SCC-1 R282W
OCR %
Time (Minutes)
A
B
C
6

B

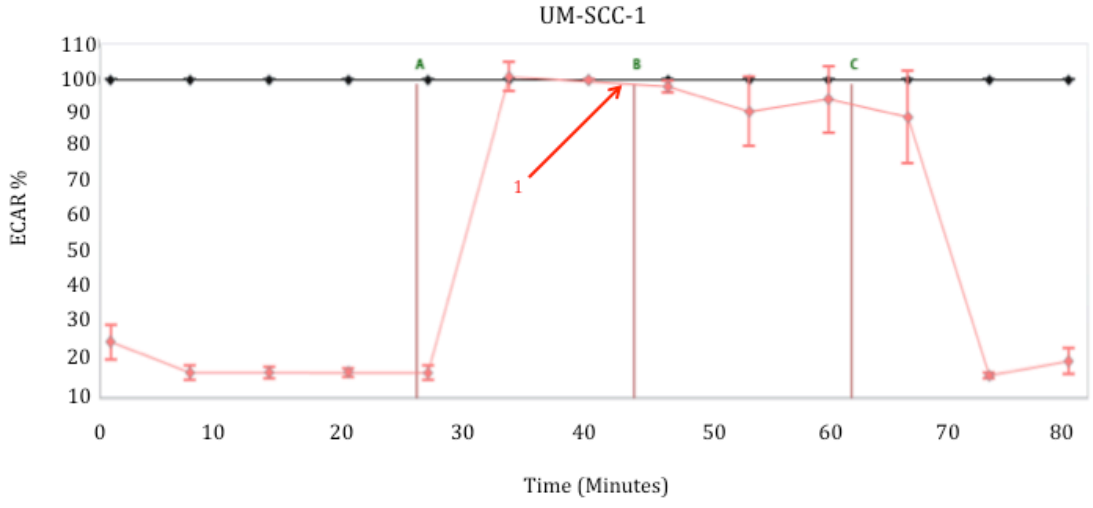
UM-SCC-1
ECAR %
Time (Minutes)
A
B
C
1

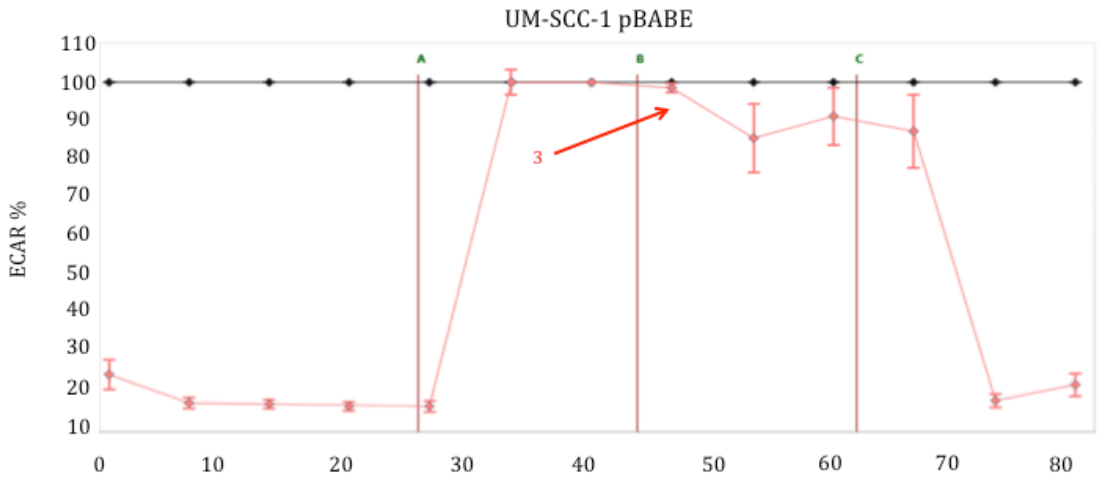
UM-SCC-1 pBABE
ECAR %
A
B
C
3

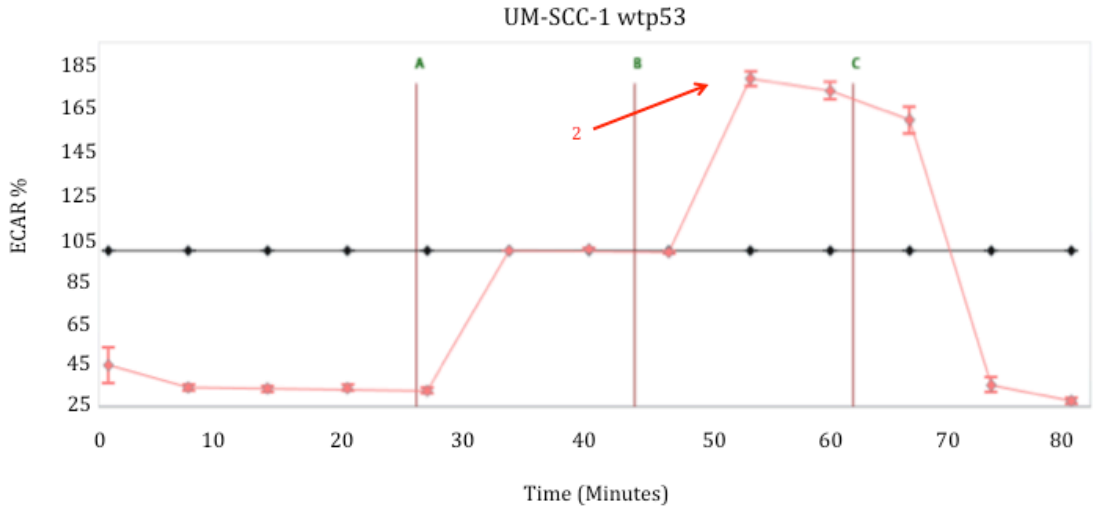
UM-SCC-1 wtp53
ECAR %
A
B
C
2
Time (Minutes)

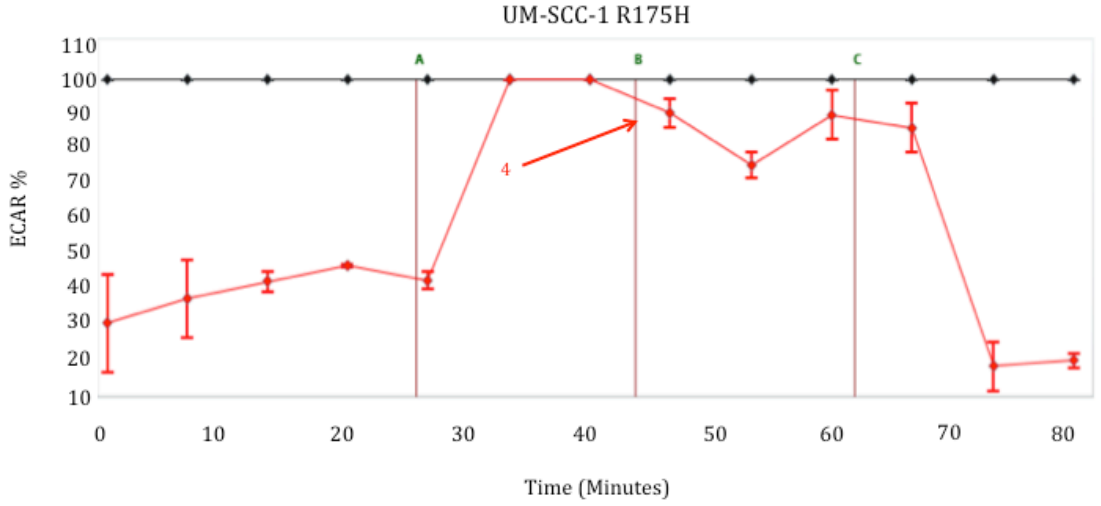
UM-SCC-1 R175H
ECAR %
A
B
C
4
Time (Minutes)

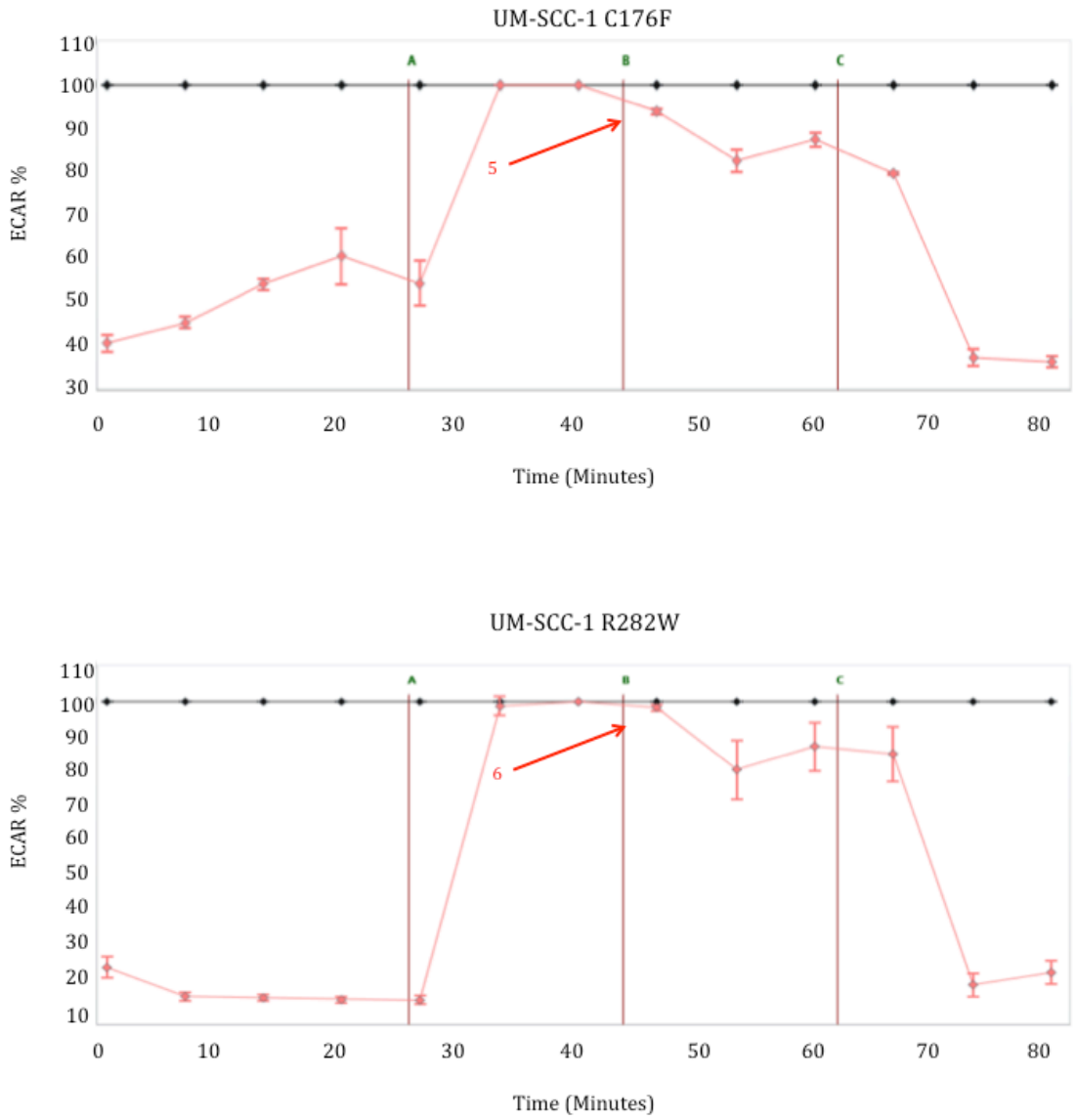

Figure 3.1.3.3: Metabolic profiles of UM-SCC-1 and derivative cell lines in mitochondrial and glycolytic stress tests. UM-SCC-1, UM-SCC-1 pBABE, UM-SCC-1 wtp53, UM-SCC-1 R175H, UM-SCC-1 C176F, and UM-SCC-1 R282W cell lines were subjected to mitochondrial (A) and glycolytic stress tests (B). As before, for mitochondrial stress tests points A, B, and C on the graphs refer to the injections of oligomycin 1.25μM, FCCP 1.5μM, and rotenone and antimycin-A 1μM respectively. For glycolytic stress tests, points A, B, and C on the graphs refer to the injections of glucose 10mM, oligomycin 1.25μM, and 2-DG 50mM respectively. Data is presented as percentage increases or decreases in OCR or ECAR relative to baseline measurements. The baseline is shown as the black line on the graphs. Forced expression of wild-type p53 in UM-SCC-1, an endogenously p53-null cell line, resulted in a marked increase in respiratory and glycolytic reserves (compare red arrows labelled 1 and 2), while metabolic profiles in the empty vector control cell line (pBABE) and the derivative lines expressing *TP53* mutations did not differ from that of the parental line (compare red arrows labelled 1 with those labelled 3-6). Error bars represent SEM.

A

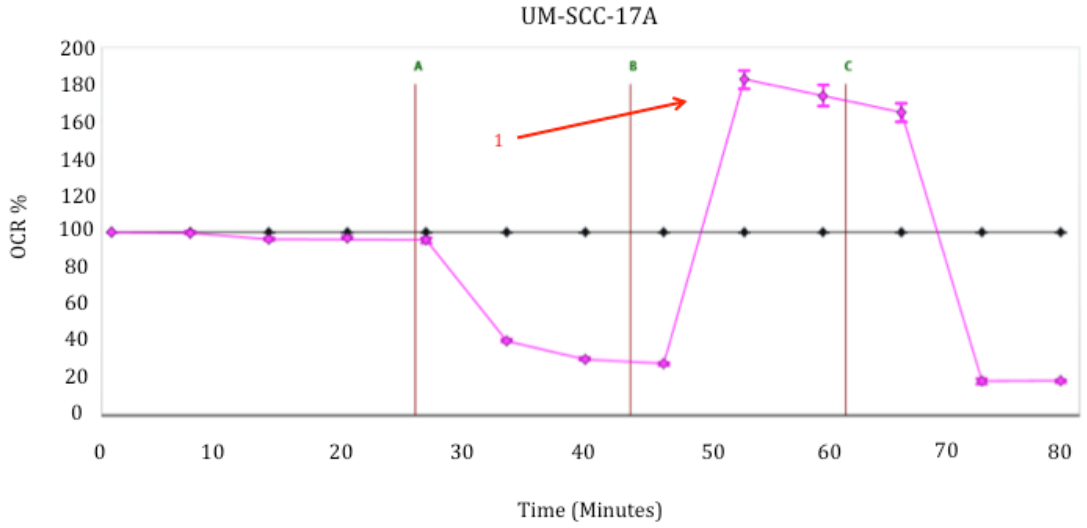
UM-SCC-17A
OCR %
Time (Minutes)
A
B
C
1

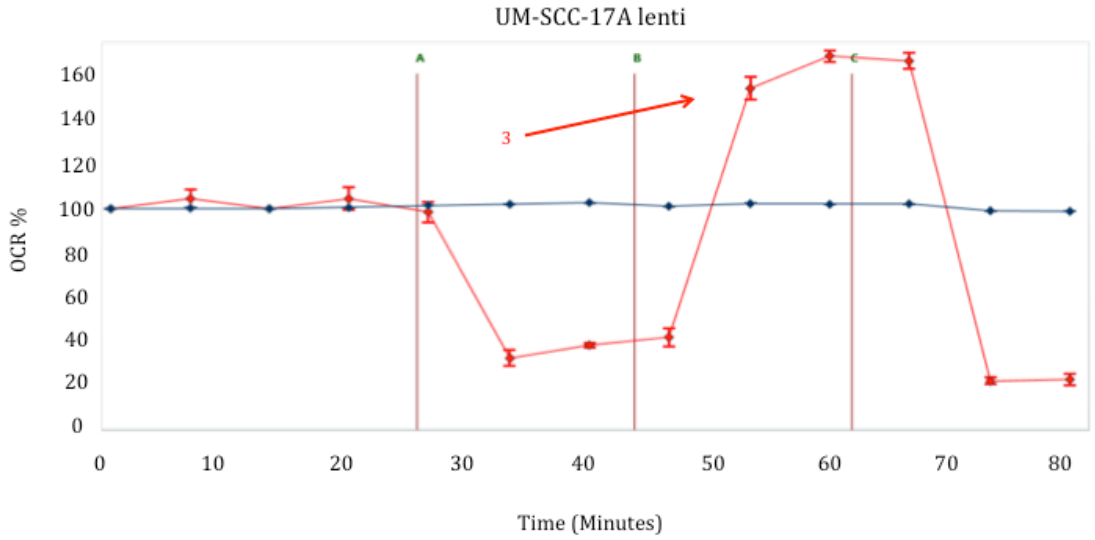
UM-SCC-17A lenti
OCR %
Time (Minutes)
A
B
C
3

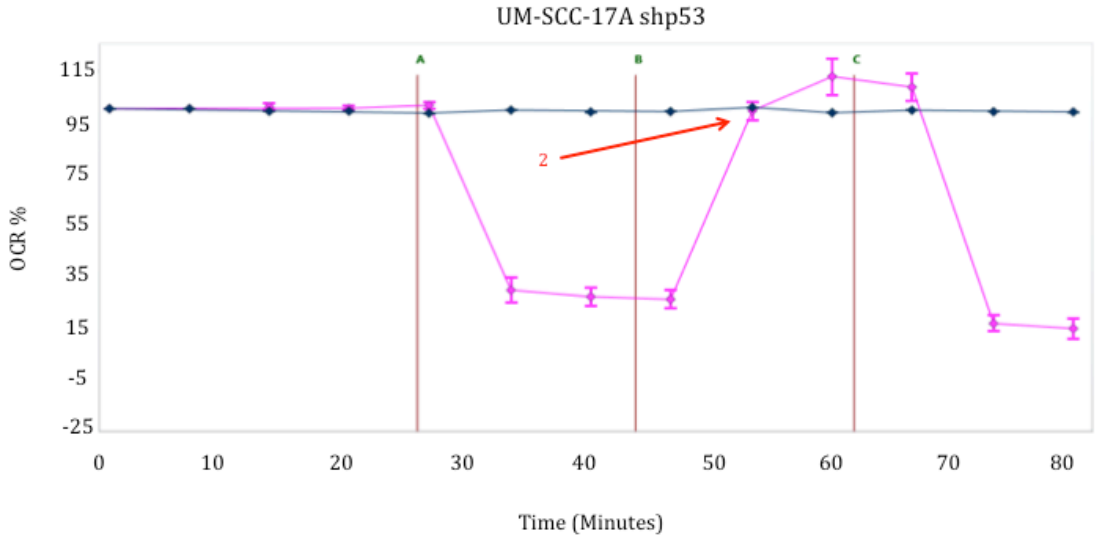
UM-SCC-17A shp53
OCR %
Time (Minutes)
A
B
C
2

B

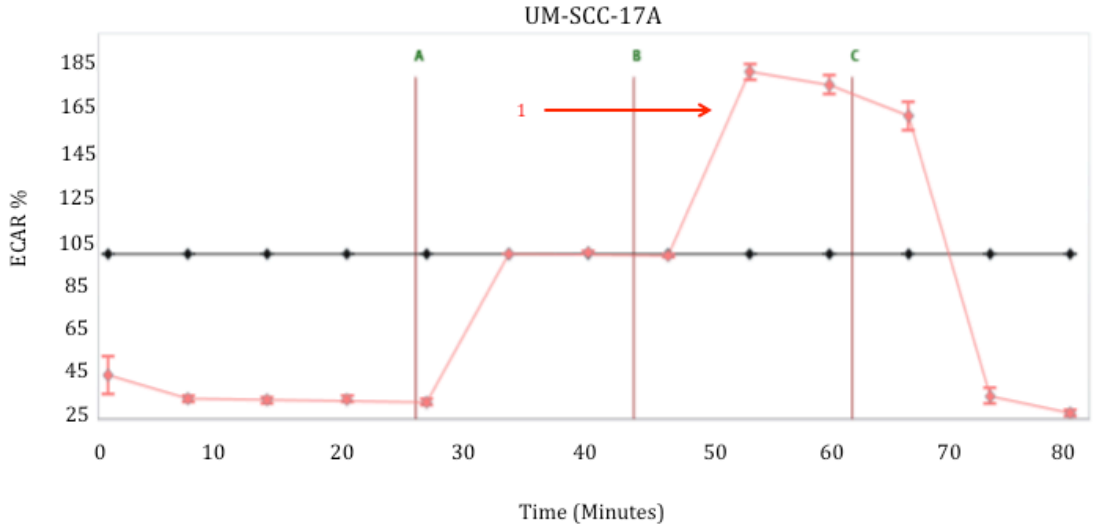
UM-SCC-17A
ECAR %
185
165
145
125
105
85
65
45
25
A
B
C
1
0
10
20
30
40
50
60
70
80
Time (Minutes)

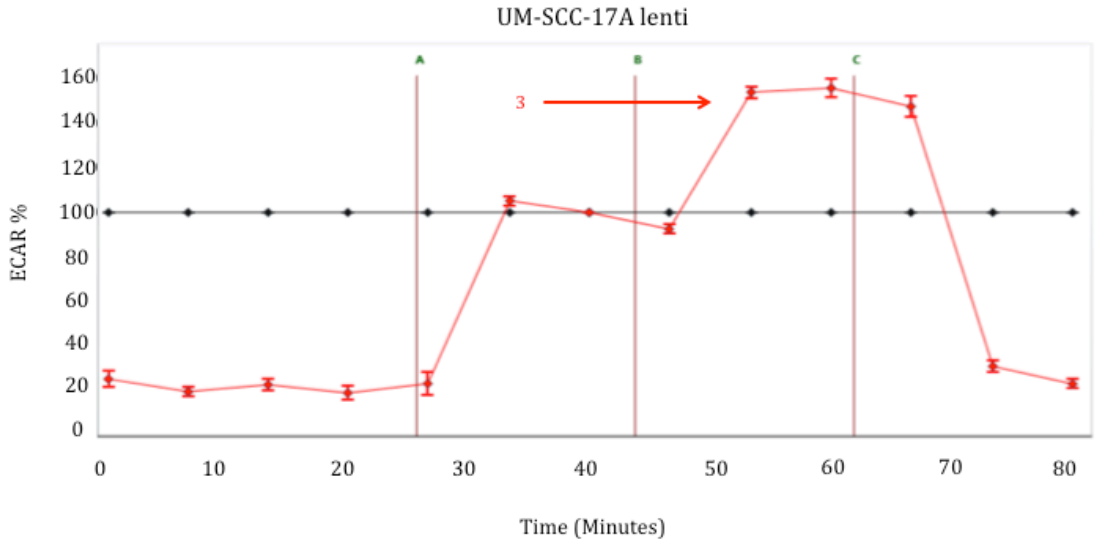
UM-SCC-17A lenti
ECAR %
160
140
120
100
80
60
40
20
0
A
B
C
3
0
10
20
30
40
50
60
70
80
Time (Minutes)

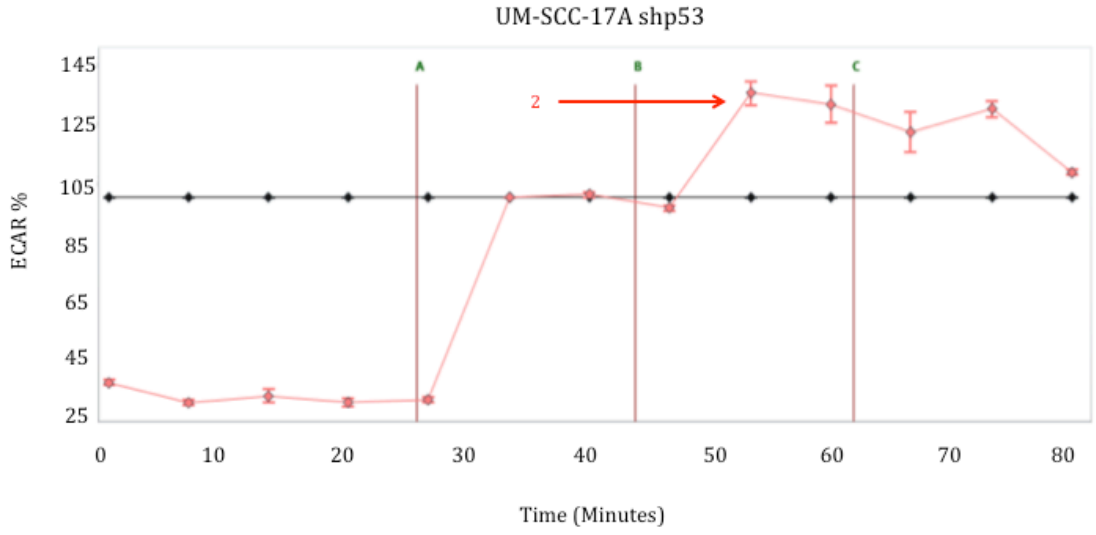
UM-SCC-17A shp53
ECAR %
145
125
105
85
65
45
25
A
B
C
2
0
10
20
30
40
50
60
70
80
Time (Minutes)

Figure 3.1.3.4: Metabolic profiles of UM-SCC-17A and derivative cell lines in mitochondrial and glycolytic stress tests. UM-SCC-17A, UM-SCC-17A lenti, and UM-SCC-17A shp53 cell lines were subjected to mitochondrial (A) and glycolytic stress tests (B). As before, for mitochondrial stress tests points A, B, and C on the graphs refer to the injections of oligomycin 1.25μM, FCCP 1.5μM, and rotenone and antimycin-A 1μM respectively. For glycolytic stress tests, points A, B, and C on the graphs refer to the injections of glucose 10mM, oligomycin 1.25μM, and 2-DG 50mM respectively. Data is presented as percentage increases or decreases in OCR or ECAR relative to baseline measurements. The baseline is shown as the black line on the graphs. Stable knockdown of wild-type p53 in UM-SCC-17A resulted in a loss of mitochondrial and glycolytic reserves (compare red arrows labelled 1 and 2), while there was no change in the empty vector control cell line (lenti) (compare red arrows labelled 1 and 3). Error bars represent SEM.

This observed relationship between *TP53* mutation and loss of metabolic diversity is consistent with the limited metabolic data in SCCHN relatively recently published elsewhere. In an initial study examining the metabolic pathways on which SCCHN cells predominantly depend, although a general dependence on glucose catabolism over glutaminolysis was observed, significant heterogeneity was noted among the panel of cell lines evaluated(359). Further analysis revealed that a pair of cell lines derived from the same patient but divergent with respect to *TP53* mutational status displayed differing degrees of sensitivity to glucose deprivation, with the wild-type *TP53* cell line exhibiting relative resistance, suggesting a possible role for wild-type p53 in determining response to glucose starvation, and by extension the metabolic underpinnings(359). A follow-on study from the same research group examined this further, again using the same isogenic cell line pair divergent with respect to *TP53* status, utilising a similar experimental system of microplate-based XF analysis as used in the present study(360). Mutant *TP53* cell lines were observed to exhibit markedly reduced spare respiratory capacity relative to wild-type *TP53* cell lines, functioning near capacity under basal conditions, findings which were reproduced in a wild-type *TP53* cell line and a derivative cell line with stable wild-type p53 knockdown(360). Interestingly, another recent metabolic study in SCCHN employing microplate-based measurement of cellular oxygen consumption and proton efflux, which sought to investigate the reprogramming of metabolism associated with the development of radioresistance using a matched model of radio-resistant and -sensitive SCCHN cells, demonstrated that relatively radio-resistant cells displayed reduced respiratory spare capacity(277). Whilst unfortunately information of *TP53* status of the cell lines was lacking, sequential treatment of the parental radiation-sensitive cell line with several

fractions of IR to generate the radio-resistant cell line may have resulted in acquisition of a *TP53* mutation. Clearly, however, this is highly speculative.

It is perhaps unsurprising to consider that *TP53* status would strongly influence metabolic phenotype in SCCHN, recognising the critical importance of loss of wild-type p53 function in SCCHN oncogenesis and the intricate links between p53 and maintenance of metabolic homeostasis. *TP53* mutation, which in the majority of cases results in loss of wild-type function (see section 1.2.7.), is the most commonly mutated gene in SCCHN, harboured in upwards of 60% of SCCHNs(52). Furthermore, *TP53* mutation, in particular disruptive mutation, is characteristically associated with a more aggressive and treatment resistant disease phenotype(56, 57). In keeping with this, in terms of our metabolic findings, p53 has been reported to exert influence over several aspects of glucose catabolism both directly and indirectly, in general restricting glycolytic flux, maintaining mitochondrial integrity and function, and promoting oxidative phosphorylation(247, 267, 294) (discussed in section 1.3.2.).

Contrary to the reporting by Sandulache et al in the above study(360), XF data demonstrating that *TP53* mutation confers reduced respiratory and glycolytic reserves in SCCHN cells, with cells functioning near capacity under basal conditions, can be interpreted in one of two ways. Firstly, in mutant *TP53* cells functioning of mitochondrial oxidative phosphorylation and/or glycolysis is compromised in some way, preventing cells from mounting a compensatory response to metabolic stressors; or secondly, that mutant *TP53* cells have significantly elevated rates of oxidative phosphorylation and/or glycolysis at baseline that represent maximal cellular rates. In order to reconcile these differing accounts, we normalised our XF stress test data to DNA content to capture absolute values of each of the metabolic parameters derived during the assays (detailed in section 2.4.8.) and to facilitate comparison of these measurements between cell lines, which were seeded at varying densities. Results of such analyses are summarised in figures 3.1.3.5 and 3.1.3.6. In keeping with the clear patterns shown in the stress test graphs presented above, the absolute values for maximal respiration, spare respiratory capacity, maximal glycolysis, and glycolytic reserve were significantly greater in wild-type *TP53* cell lines compared with mutant *TP53* cell lines. Interestingly, however, capturing absolute OCR and ECAR values revealed that wild-type *TP53* cells exhibited discernibly higher rates of mitochondrial respiration and lower rates of glycolysis under basal conditions compared with mutant *TP53* cells, findings which were borne out more definitively when analysing the relative

basal utilisation of mitochondrial respiration and glycolysis (figure 3.1.3.7.). Importantly, these findings again held true in the isogenic cell lines divergent with respect to *TP53* mutational status. Taken together, these findings allow for a clearer interpretation of the overall metabolic picture, which suggests that SCCHN cells harbouring wild-type p53 predominantly catabolise glucose through oxidative phosphorylation under basal conditions and maintain robust mitochondrial function, enabling these cells to mount a maximal increase in ETC activity when exposed to mitochondrial stressors. In contrast, in the context of loss of wild-type p53 function mitochondrial function appears to be compromised as cells display reduced oxidative phosphorylation under basal conditions and are unable to mount an increase in activity in response to mitochondrial stressors. Glycolysis seemingly predominates with significantly heightened basal levels, which are elevated to maximal cellular capacity leaving little or no glycolytic reserve. As would be expected the observed difference in rates of basal glycolysis between the cell lines is more marked than that of mitochondrial respiration. This reflects the fact that glycolysis is a relatively energetically inefficient process, yielding only two molecules of ATP per molecule of glucose consumed as opposed to up to 36 with oxidative phosphorylation, and thus mutant *TP53* cells would have to increase rates of glycolysis at an order of magnitude greater than the corresponding reduction in mitochondrial respiration to maintain sufficient ATP production. The fact that ATP-linked respiration is consistently reduced in mutant *TP53* cells compared with wild-type *TP53* cells lends further credence to the notion that mutant *TP53* cells have compromised ETC function, something which will be explored in more detail later in this thesis (section 3.4.2). It is also interesting to note that in addition to displaying higher basal levels of glycolysis and thus having lower glycolytic reserves, mutant *TP53* cells also exhibited higher overall glycolytic capacities. This likely reflects the probable upregulation of glucose transporters and glycolytic enzymes needed to sustain elevated rates of basal glycolysis. Again, this will be explored in more depth later in this thesis (section 3.4.3).

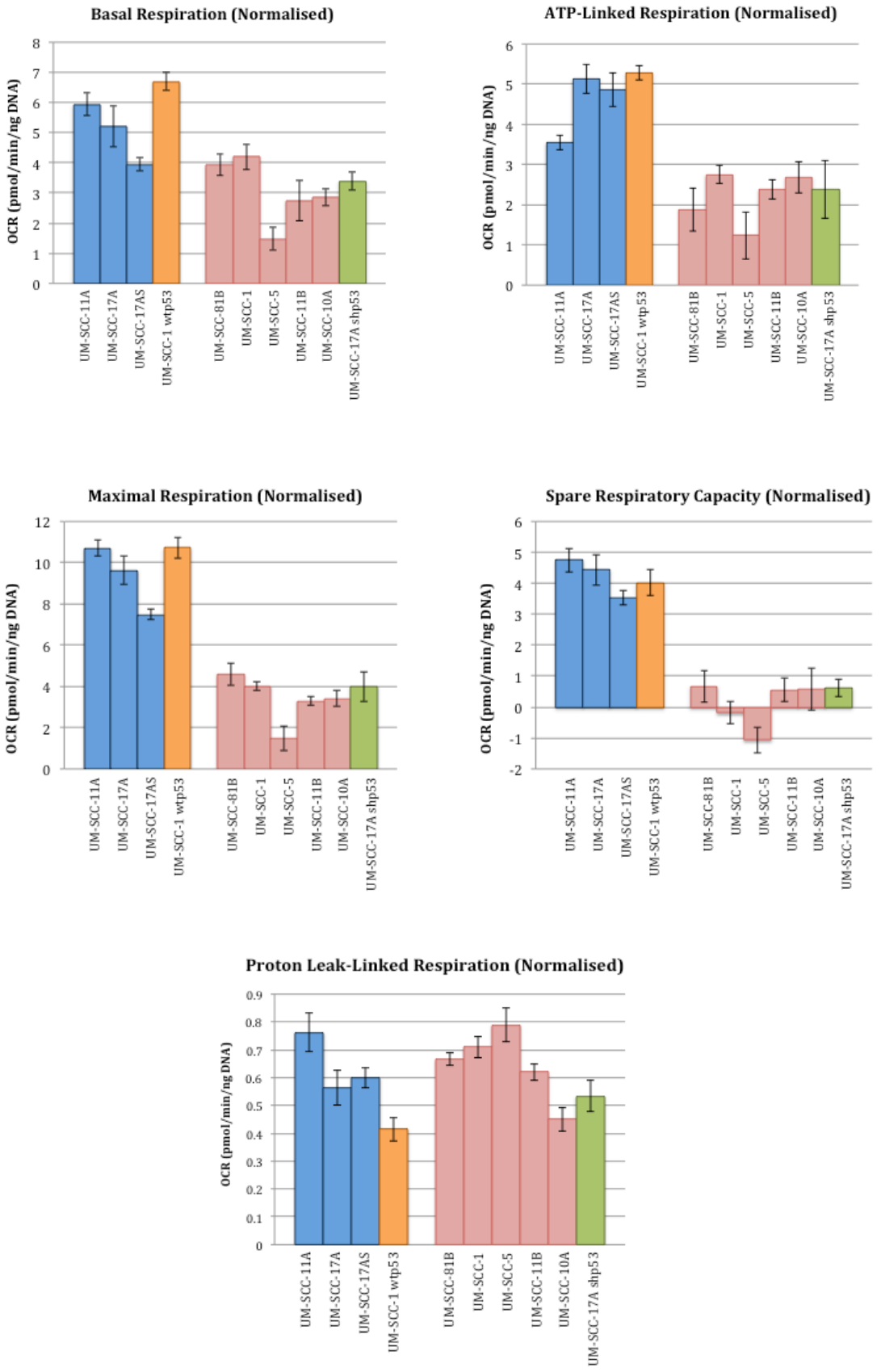

Figure 3.1.3.5: Absolute normalised data derived from mitochondrial stress tests. XF mitochondrial stress test data was normalised to DNA content for all cell lines to capture

absolute values for basal respiration, ATP-linked respiration, proton leak, maximal respiration, and spare respiratory capacity that could be compared between cell lines. Values for basal respiration, ATP-linked respiration, maximal respiration, and spare respiratory capacity were all greater in the wild-type *TP53* cell lines, while values for proton leak-linked respiration were broadly similar. Error bars represent SEM for each measurement. Blue bars represent wild-type *TP53* cell lines, red bars represent mutant *TP53* cell lines, orange bars represent UM-SCC-1 wtp53, and green bars represent UM-SCC-17A shp53.

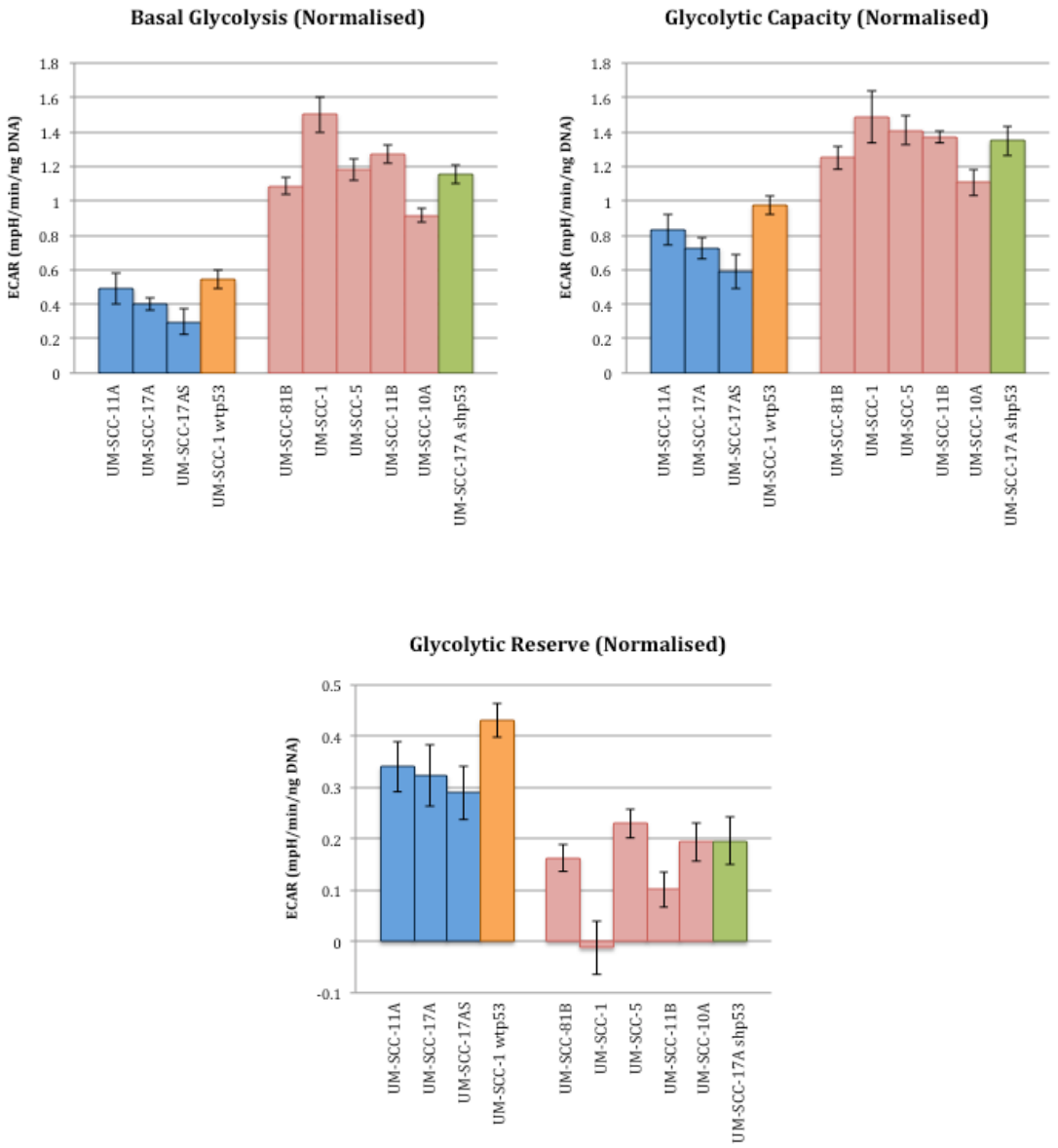

Figure 3.1.3.6: Absolute normalised data derived from glycolytic stress tests. XF glycolytic stress test data was normalised to DNA content for all cell lines to capture absolute values for basal glycolysis, glycolytic capacity, and glycolytic reserve that could be compared between cell lines. Values for glycolytic reserve were greater in in the wild-type *TP53* cell lines, while in the

mutant *TP53* cell lines basal glycolytic values were considerably greater and glycolytic capacity slightly elevated. Error bars represent SEM for each measurement. Blue bars represent wild-type *TP53* cell lines, red bars represent mutant *TP53* cell lines, orange bars represent UM-SCC-1 wtp53, and green bars represent UM-SCC-17A shp53.

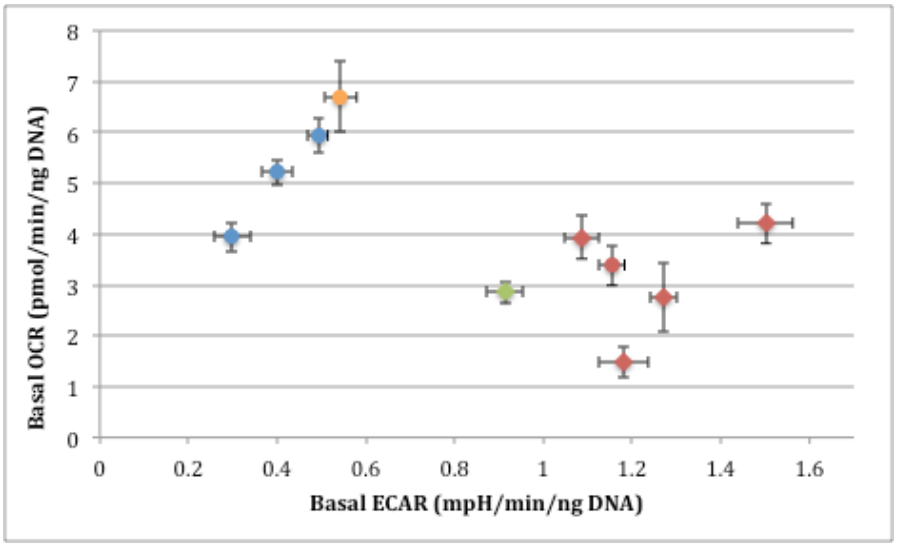

Figure 3.1.3.7: Relative basal utilisation of mitochondrial respiration and glycolysis. Normalised basal values from XF glycolytic and mitochondrial stress tests for all cell lines plotted against each other. There is clear grouping of wild-type *TP53* and mutant *TP53* cell lines, with the former displaying high levels of mitochondrial respiration relative to glycolysis and the latter the opposite. Error bars represent SEM for each measurement. Blue diamonds represent wild-type *TP53* cell lines, red diamonds represent mutant *TP53* cell lines, the orange circle represents UM-SCC-1 wtp53, and the green circle represents UM-SCC-17A shp53.

3.1.4. Metabolic switching associated with loss of wild-type p53 function confers increased dependence on glycolysis for survival

Results presented in the previous section demonstrated that mutational loss of wild-type p53 function results in a metabolic switch, resulting in increased utilisation of glycolysis accompanied by compromised oxidative phosphorylation. The proposed impetus driving cancer cells to undergo what is an energetically inefficient metabolic shift most likely relates to underlying proliferation and survival requirements of such cells: rapid ATP generation, combined with generation of intermediates for anabolic biosynthesis and reducing equivalents to regulate cellular redox potential to minimise the damaging effects of ROS(257, 267) (see section 1.3.1.). Consequently, our next aim was to determine whether mutant TP53 cells undergoing such metabolic

reprogramming were indeed dependent on this for survival, something which would also have potential therapeutic implications. In order to do so, assessment of cell proliferation and viability was performed using trypan blue exclusion assays following inhibition of glycolysis and oxidative phosphorylation using 2-DG and UK5099 respectively (section 2.5), with analysis performed at 16, 24, and 48 hours following treatment. Figures 3.1.4.1 and 3.1.4.2. show viability data for the panel of SCCHN cell lines and the isogenic cell lines respectively. Mutant *TP53* cells were highly sensitive to the effects of 2-DG in terms of viability from 24 hours post-treatment, while wild-type *TP53* cells required the addition of UK5099 for a significant reduction in viability. These findings also held true in the isogenic cell lines. UM-SCC-1 and derivative lines transduced with *TP53* mutations displayed sensitivity to 2-DG treatment alone, while with forced expression of wild-type p53 the addition of UK5099 was required for a reduction in viability. Similarly, in UM-SCC-17A combination treatment was required to reduce viability but stable p53 knockdown (shp53) rendered cells sensitive to 2-DG alone. Collectively, these findings indicate that in SCCHN cells with loss of wild-type p53 function there is a globalised loss of metabolic flexibility, which manifests as a survival dependence on glycolysis, whereas in wild-type *TP53* SCCHN cells metabolic plasticity is maintained and survival does not depend so heavily on one isolated metabolic pathway.

A

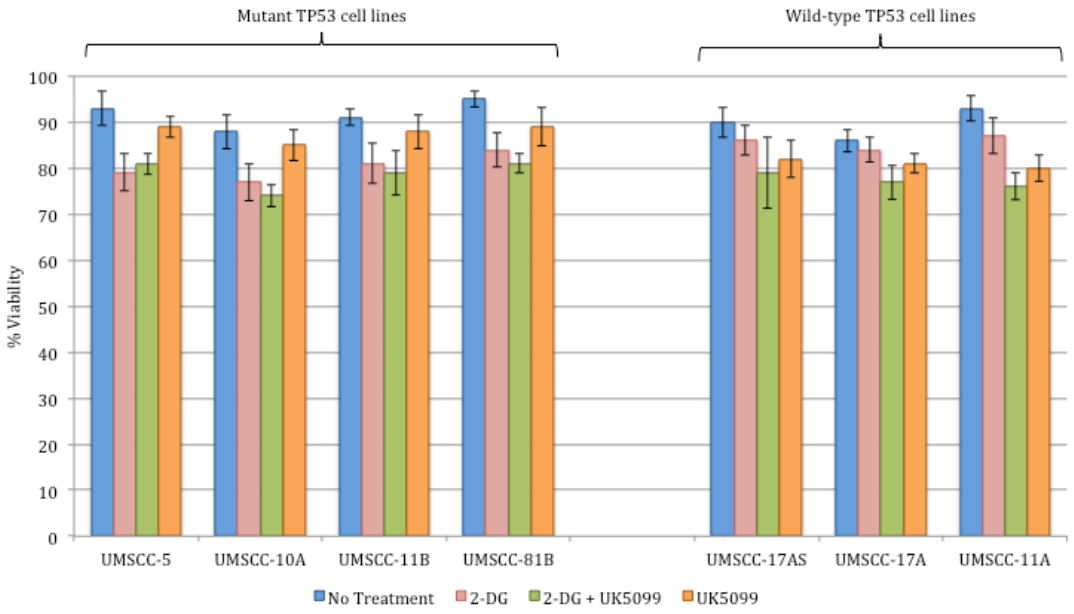

B

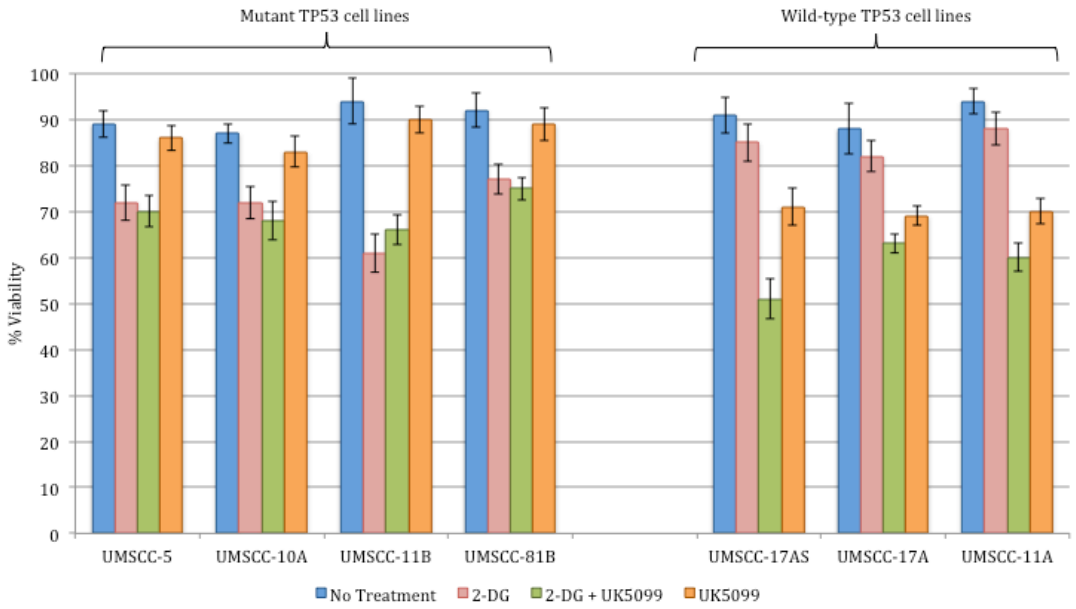

C

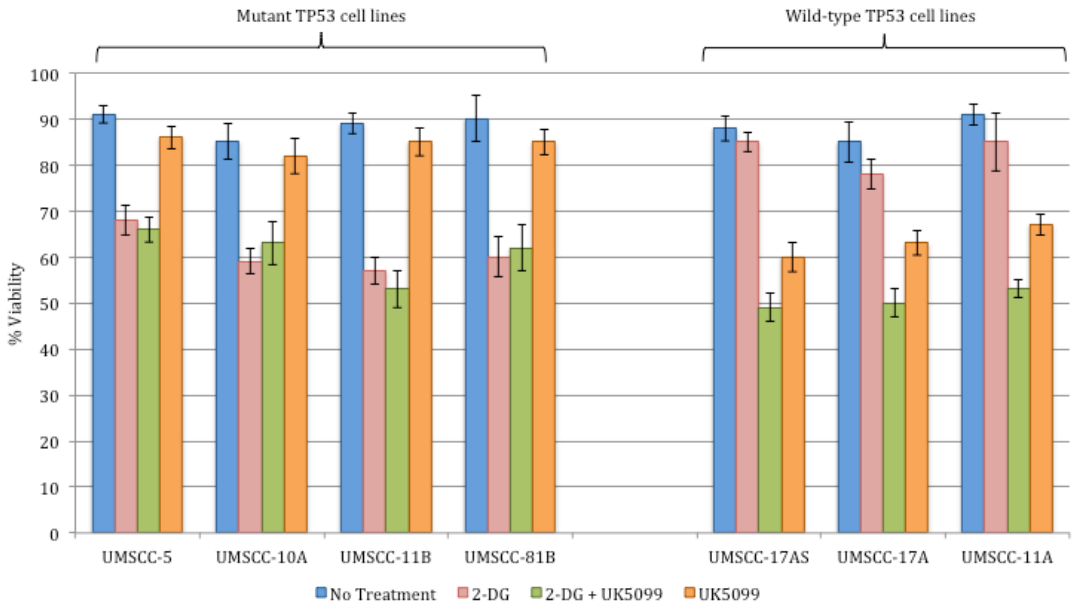

Figure 3.1.4.1: Cell viability as measured by trypan blue exclusions assays. Viability was assessed in a panel of SCCHN cell lines following no treatment, treatment with 25mM 2-DG (glycolytic inhibitor) alone, treatment with 2μM UK5099 (inhibitor of the mitochondrial pyruvate carrier), or combined treatment at 16 (A), 24 (B), and 48 hours (C). In mutant *TP53* cells there is a significant reduction in viability with 2-DG treatment alone from 24 hours but not in wild-type *TP53* cells. The addition of UK5099 was required in wild-type TP53 cells for a discernible reduction in viability, which again was observed from 24 hours. Values represent the mean from three separate experiments and error bars represent SEMs.

A

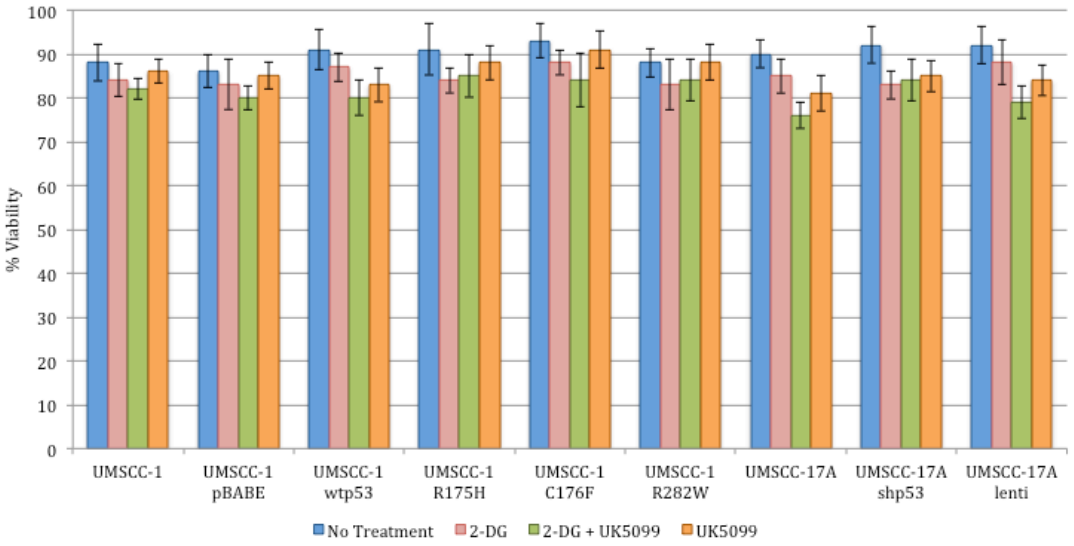
100
90
80
70
60
50
40
30
20
10
0
% Viability
UMSCC-1
UMSCC-1 pBABE
UMSCC-1 wtp53
UMSCC-1 R175H
UMSCC-1 C176F
UMSCC-1 R282W
UMSCC-17A
UMSCC-17A shp53
UMSCC-17A lenti
No Treatment
2-DG
2-DG + UK5099
UK5099

B

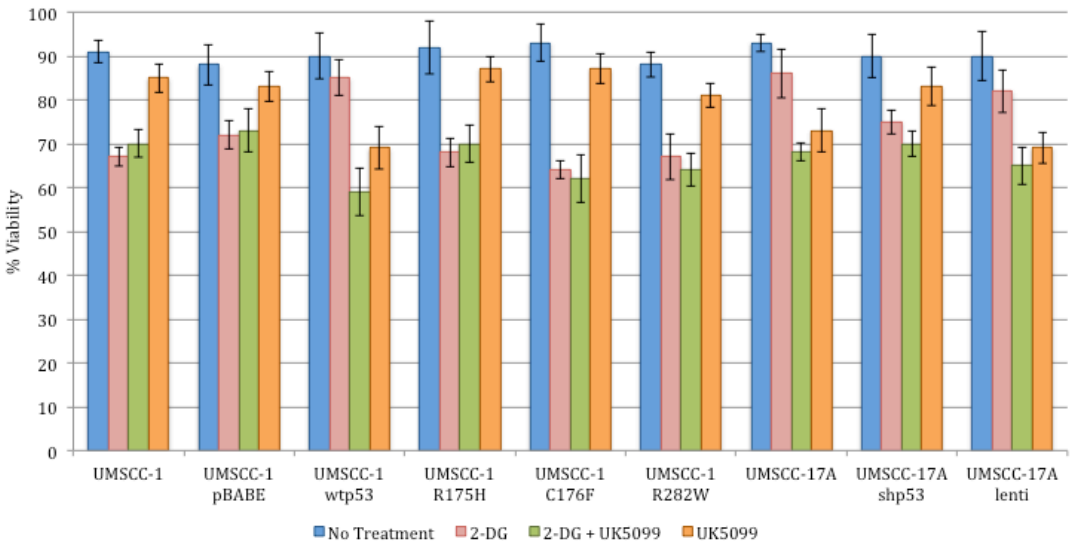
100
90
80
70
60
50
40
30
20
10
0
% Viability
UMSCC-1
UMSCC-1 pBABE
UMSCC-1 wtp53
UMSCC-1 R175H
UMSCC-1 C176F
UMSCC-1 R282W
UMSCC-17A
UMSCC-17A shp53
UMSCC-17A lenti
No Treatment
2-DG
2-DG + UK5099
UK5099

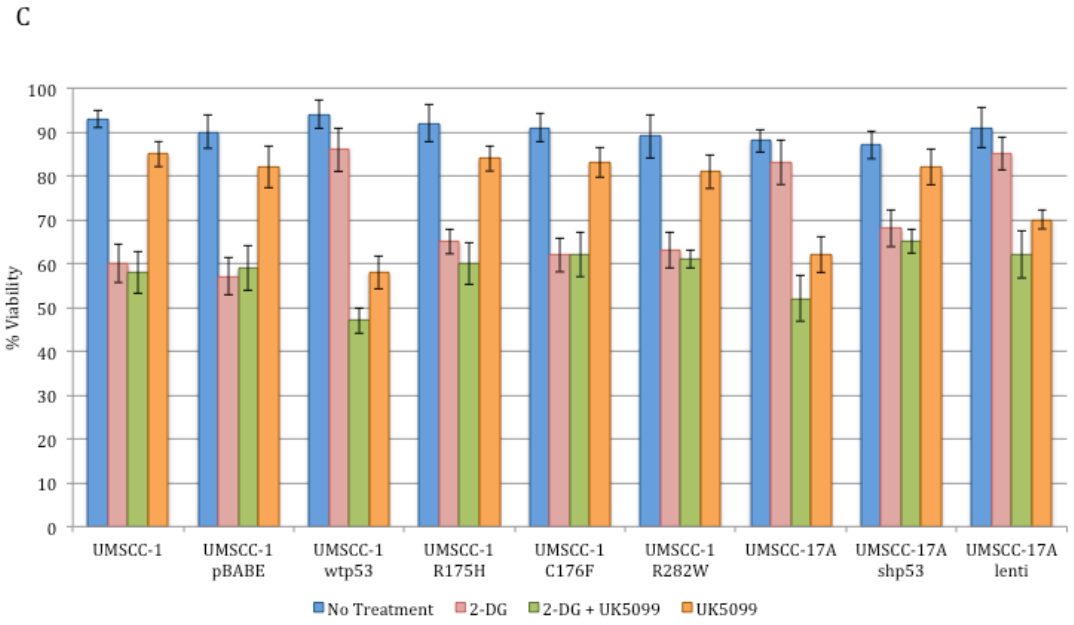

Figure 3.1.4.2: Cell viability as measured by trypan blue exclusion assays in isogenic cell lines. Viability was assessed the isogenic SCCHN cell lines following no treatment, treatment with 25mM 2-DG (glycolytic inhibitor) alone, treatment with 2μM UK5099 (inhibitor of the mitochondrial pyruvate carrier), or combined treatment at 16 (A), 24 (B), and 48 hours (C). In UM-SCC-1 and derivatives transduced with *TP53* mutations or the empty vector control there is a significant reduction in viability with 2-DG treatment alone from 24 hours, while with forced expression of wild-type p53 the addition of UK5099 was required for a discernible reduction in viability, which again was observed from 24 hours. Similarly, in UM-SCC-17A and the empty vector control (lenti) combination treatment was required to reduced viability but stable p53 knockdown (shp53) rendered cells sensitive to 2-DG alone. Values represent the mean from three separate experiments and error bars represent SEMs.

Similar results were also reported in the aforementioned study examining the role of *TP53* mutational status in determining metabolic phenotype in SCCHN(360). In that study, using microplate-based XF analysis, ECARs for mutant and wild-type SCCHN cells were compared when exposed to 2-DG(360). Mutant *TP53* cells were observed to display a greater and more sustained reduction in ECAR compared with wild-type cells, and on the basis of this the authors insinuated glycolytic dependence(360). However, a greater absolute reduction in ECAR following administration of 2-DG would be expected in mutant *TP53* cells simply as a result of their higher basal glycolytic levels, and does not alone demonstrate glycolytic dependence *per se*. Moreover, these findings may be explained by the fact that mutant *TP53* cells would likely express glucose transporters at higher levels than wild-type cells and thus there would be a greater influx of 2-DG.

Nonetheless, previous findings from proliferation assays conducted by the same research group do lend support to the idea of glycolytic dependence in mutant *TP53* cells(359) (as discussed in sections 1.3.3. and 3.1.3.).

Such dependence on glycolysis potentially presents a promising therapeutic window to preferentially target mutant *TP53* SCCHN, which is particularly attractive given the frequency of *TP53* mutation in SCCHN (upwards of 60%)(52) and the typically aggressive and treatment-resistant phenotype it confers(56, 57). This is explored in greater detail later in this thesis (section 3.2.).

3.1.5. The metabolic phenotype of HPV-positive SCCHN suggests functional wild-type p53

Considering this association between mutational loss of wild-type p53 function and glycolytic dependence, together with the importance of the HPV E6 oncoprotein in targeting p53 for proteasomal degradation in the molecular pathogenesis of HPV-related SCCHN(63, 396), invites scrutiny of metabolism in HPV-driven disease. In order to examine this, established SCCHN cell lines reported to be HPV-positive (UM-SCC-104, UPCI:SCC154, and 93VU147T) were metabolically profiled as before using microplate-based XF analysis. Figures 3.1.5.1. and 3.1.5.2. depict respective outputs from the mitochondrial and glycolytic stress tests for each of the cell lines, with data scaled to the fractional change relative to baseline OCR and ECAR, and thus presented as percentage increases or decreases from the assigned baseline following injection of the relevant substrates and/or inhibitors. Akin to results observed in wild-type *TP53* cells previously, the HPV-positive SCCHN cell lines maintained metabolic diversity, displaying robust mitochondrial and glycolytic reserves.

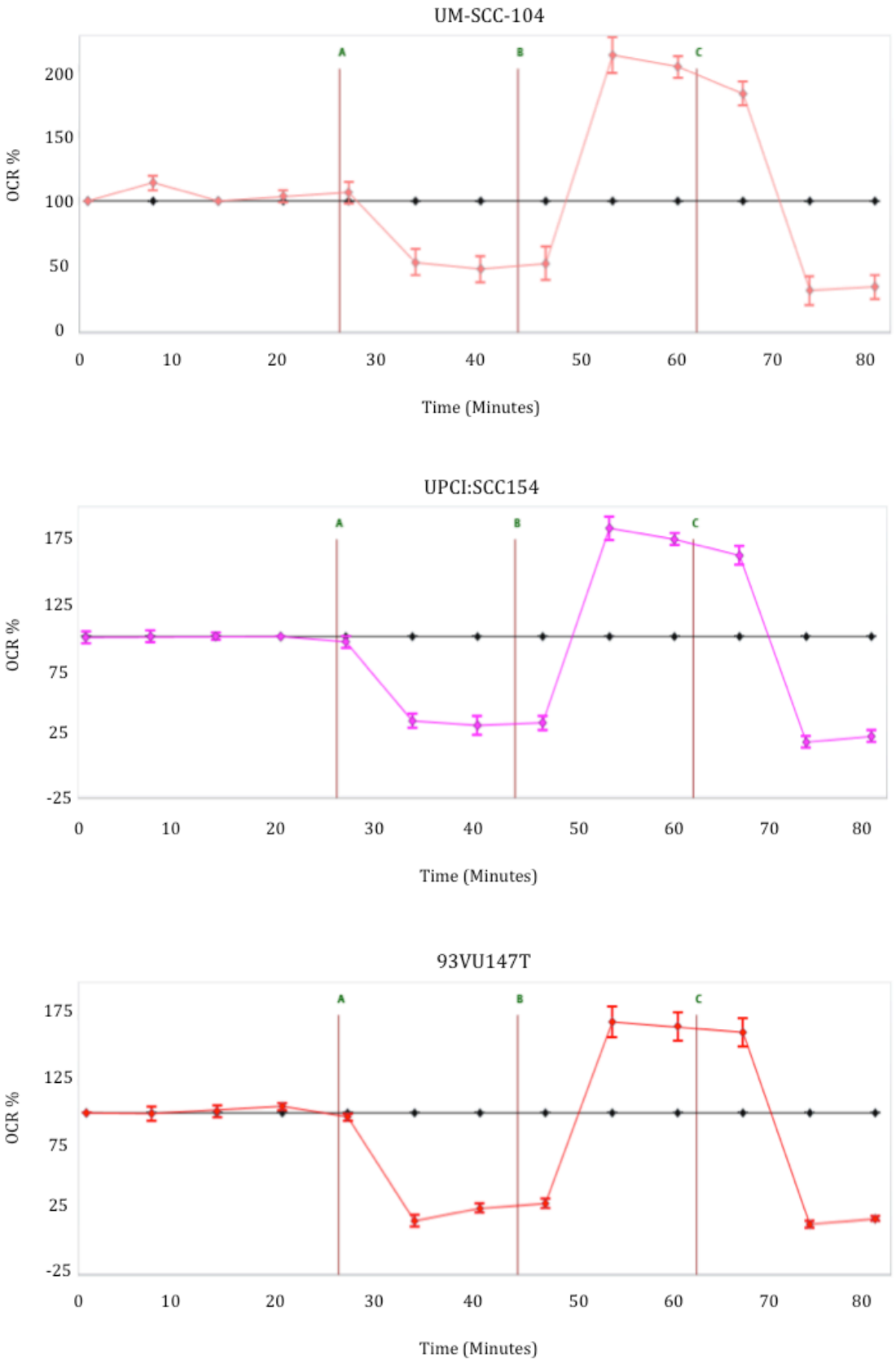

Figure 3.1.5.1: Chronological changes in OCR in response to mitochondrial stressors in HPV-positive SCCHN cell lines. Cells were subjected to mitochondrial stress tests, in which

oligomycin 1.25µM (point A), FCCP 1.5µM (point B), and rotenone and antimycin-A 1µM (point C) were sequentially injected, and OCR (pmol/min) measured. Data is presented as percentage increases or decreases in OCR relative to baseline measurements. The baseline is shown as the black line on the graphs. HPV-positive SCCHN cell lines maintained marked spare respiratory capacities. Error bars represent SEM.

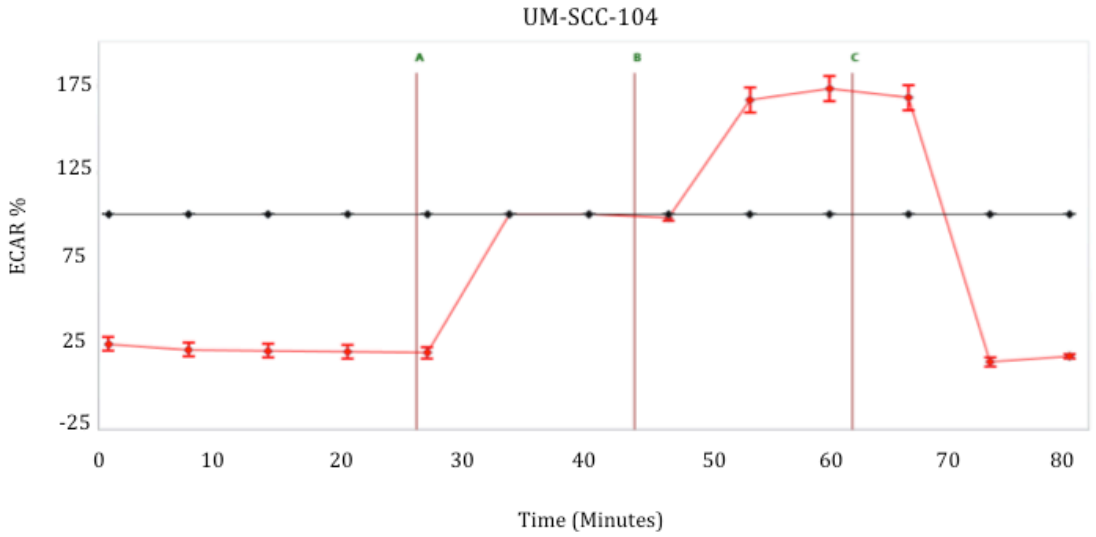

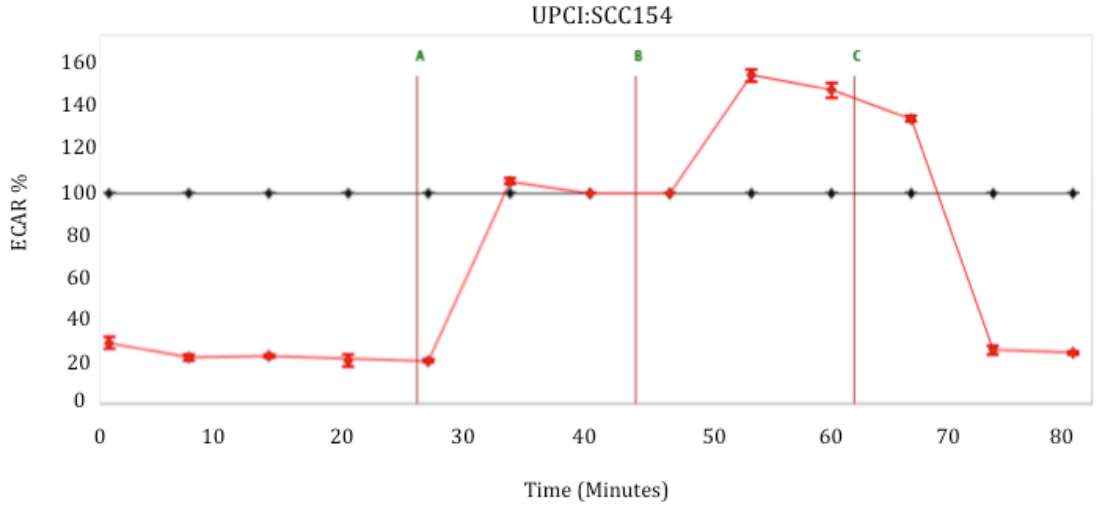

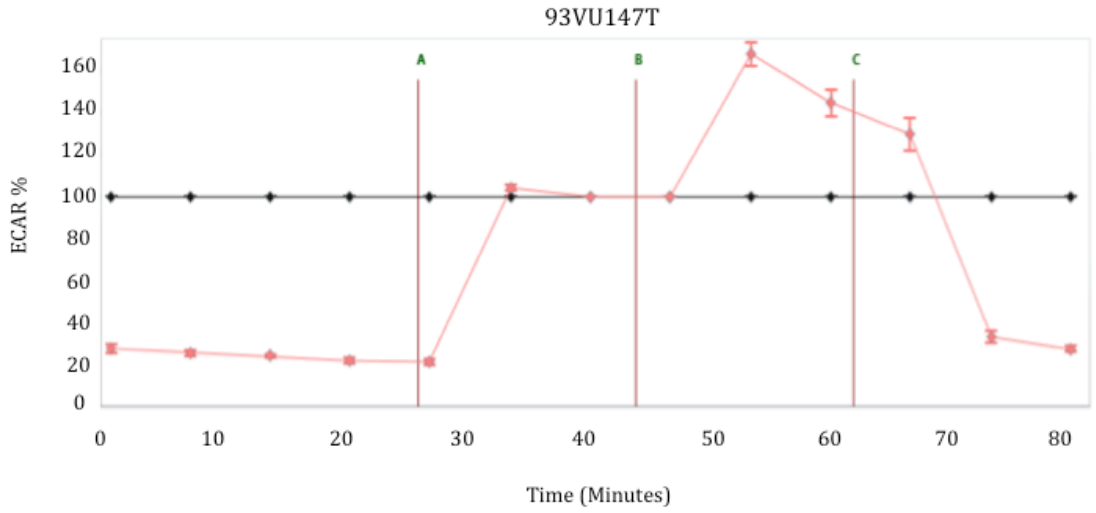

Figure 3.1.5.2: Chronological changes in ECAR in response to glycolytic substrates and stressors in HPV-positive SCCHN cell lines. Cells were subjected to glycolytic stress tests, in which glucose 10mM (point A), oligomycin 1.25μM (point B), and 2-DG 50mM (point C) were sequentially injected, and ECAR (mpH/min) measured. Data is presented as percentage increases or decreases in ECAR relative to baseline measurements. The baseline is shown as the black line on the graphs. HPV-positive SCCHN cell lines maintained considerable glycolytic reserves. Error bars represent SEM.

These cell lines may be criticised as model systems for HPV-related SCCHN, in that they were derived from patients with traditional SCCHN risk factors, specifically excessive tobacco and alcohol use, and from primary tumour sites outside of the oropharynx, which arguably may not represent the same disease phenotype as HPV-related oropharyngeal SCC. However, whilst there are now thousands of patients with HPV-positive SCCHN and biopsy specimens available, there are only a handful of documented HPV-related SCCHN cell lines available worldwide and there is currently an absence of established cell lines with such characteristics. Indeed, the scarcity of established HPV-positive SCCHN cell lines raises an important question as to why it has been so challenging to isolate and propagate SCCHN cell lines from patients with HPV-related tumours.

Moreover, the established cell lines utilised in this study have undergone recent characterisation, which revealed integrated and/or episomal viral DNA that is transcriptionally active in all cell lines, suggesting that these may indeed represent suitable model systems(378).

It is perhaps surprising that these HPV-positive cell lines displayed a metabolic profile similar to that observed in wild-type *TP53* cells rather than that seen in cells with mutational loss of wild-type p53 function given the role of the HPV E6 oncoprotein in targeting p53 for proteasomal degradation. It may be the case, however, that E6-mediated inactivation of p53 is incomplete, leaving sufficient functional wild-type p53 to maintain a balanced and diversified metabolic phenotype. In support of this, genome-wide microarray data from a recent study examining radiation response in HPV-positive and HPV-negative SCCHN cell lines suggested that low levels of wild-type p53 remain in HPV-positive cell lines, that this p53 can be activated by therapeutic stress such as radiation, and that this effect can be overcome by more complete knockdown of p53 using shRNA(381).

Interestingly, these results are in keeping with the only other study to date investigating metabolism specifically in HPV-related SCCHN, which examined both resected HPV-positive oropharyngeal SCC specimens and an in-vitro HPV-positive cell line(361). HPV-positive tumours were observed to express increased levels of proteins indicative of oxidative phosphorylation and a relatively lower level of extracellular lactate accumulation(361).

3.2. Evaluating anti-metabolic therapeutic strategies in SCCHN

3.2.1. Introduction

As outlined in section 1.1.5., there remains a common goal in the treatment of both HPV-negative and HPV-driven SCCHN from a translational research perspective: to identify means of sensitising these tumours to the effects of current treatments, not only to improve efficacy, but also to minimise the substantial toxic effects. In the context of traditional HPV-negative SCCHN there is a need to improve treatment efficacy to enhance survival outcomes, while for HPV-related oropharyngeal SCC the fact that clinical reports provide clear evidence of improved outcomes(80, 94, 95, 397), has led many to propose treatment de-intensification for these patients in order to minimise associated treatment toxicity. RT remains a cornerstone of treatment for SCCHN, with 74% of all SCCHN patients recommended to receive RT at some point during their treatment pathway, either as stand-alone or as adjuvant therapy, if current treatment guidelines are followed(107). As such, it is imperative to identify novel radiosensitising therapeutic approaches.

Therapeutic strategies are generally predicated on a discernible therapeutic index of the chosen agent. Considering this, in contrast to traditional cytotoxic agents, which largely rely on the inherently more incessant proliferative rate of cancer cells rather than true tumour specificity, metabolic targeting could potentially exploit the fact that tumour cells may become predominantly reliant on a particular metabolic pathway providing a selective therapeutic gain while sparing most normal cells. In keeping with this, the limited numbers of anti-metabolic therapeutic studies in SCCHN have, in general, demonstrated cytotoxicity and potentiation of the effects of conventional treatments with glycolytic inhibition(354-357, 359, 360). Findings, however, have not been universal(355, 357), and recent therapeutic studies have suggested a role for *TP53* status in determining such effects(355, 359, 360). The data presented in chapter 3.1. demonstrate that mutational loss of wild-type p53 function confers a switch in metabolic phenotype towards reduced oxidative phosphorylation and glycolytic dependence. Consequently, we hypothesised that such SCCHN cells may display increased susceptibility to glycolytic targeting with appropriate agents to potentiate the effects of IR, while those harbouring wild-type p53, and thus maintaining metabolic diversity, may be relatively resistant to such an approach. This aim of this chapter is to examine this hypothesis.

3.2.2. Glycolytic inhibition with 2-DG potentiates IR effects in mutant TP53 SCCHN cells only

Following optimisation of cell seeding densities for each cell line (described in section 2.6.), clonogenic survival assays were undertaken on our panel of SCCHN cell lines to explore whether glycolytic inhibition could potentiate the effects of IR, and to define the role of *TP53* mutational status in determining this. Clonogenic assays were performed and survival parameters calculated as described in section 2.6. in the absence and presence of the glycolytic inhibitor 2-DG, which was administered one hour prior to irradiation. A dose of 25mM was selected because this reflects doses used in previously published studies utilising 2-DG in SCCHN cell lines(354, 360), and also because this is equivalent to the concentration of glucose present in the cell culture media, with which 2-DG competes for cellular uptake. Clonogenic survival curves for the panel of SCCHN cell lines are shown in figure 3.2.2.1. Radiation response following glycolytic inhibition was observed to correlate with our earlier findings from the metabolic profiling studies, in that 2-DG consistently potentiated radiation effects in cells harbouring *TP53* mutations but not in those harbouring wild-type *TP53.*

A

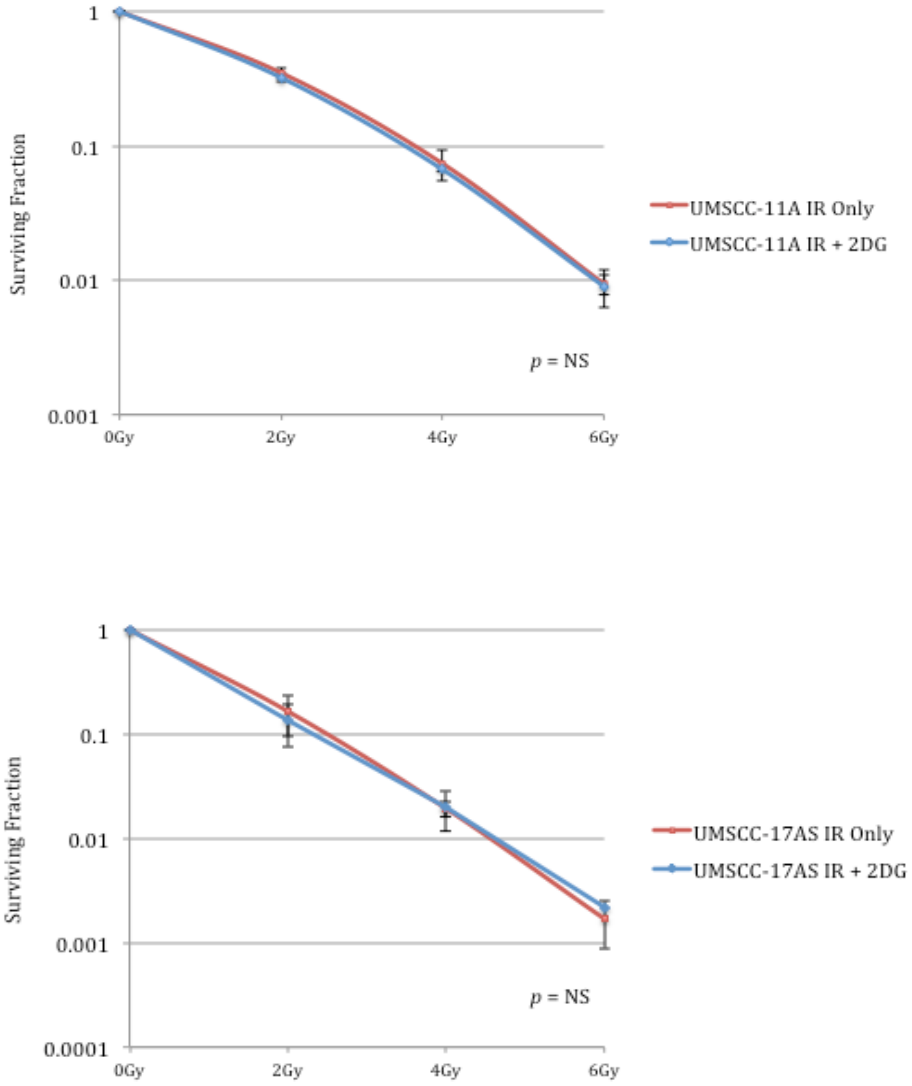
1
0.1
0.01
0.001
Surviving Fraction
0Gy
2Gy
4Gy
6Gy
p = NS
UMSCC-11A IR Only
UMSCC-11A IR + 2DG

1
0.1
0.01
0.001
0.0001
Surviving Fraction
0Gy
2Gy
4Gy
6Gy
p = NS
UMSCC-17AS IR Only
UMSCC-17AS IR + 2DG

B

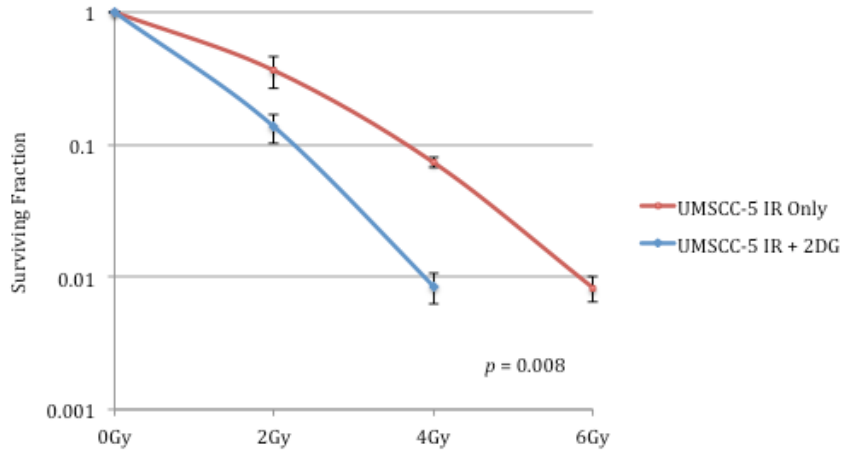
1
0.1
0.01
0.001
Surviving Fraction
0Gy
2Gy
4Gy
6Gy
p = 0.008
UMSCC-5 IR Only
UMSCC-5 IR + 2DG

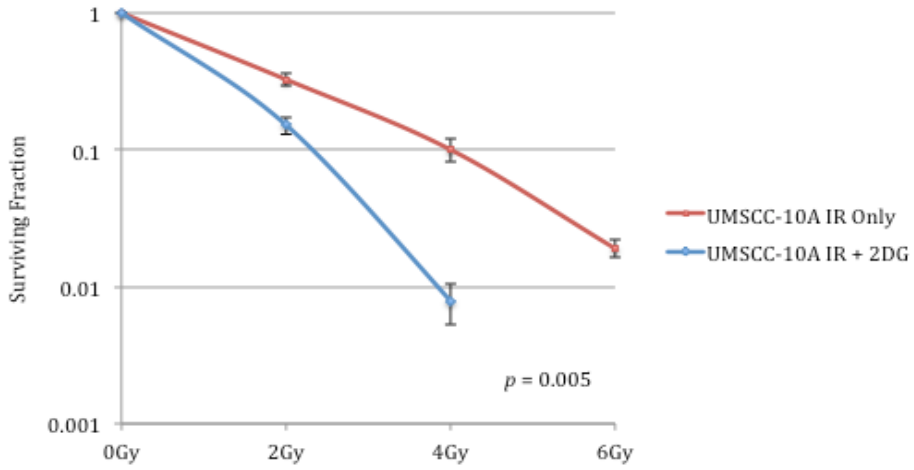
1
0.1
0.01
0.001
Surviving Fraction
0Gy
2Gy
4Gy
6Gy
p = 0.005
UMSCC-10A IR Only
UMSCC-10A IR + 2DG

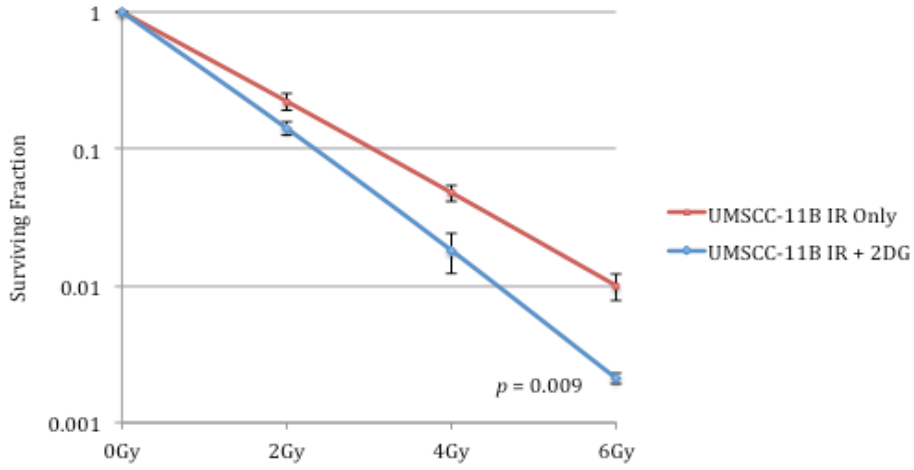
1
0.1
0.01
0.001
Surviving Fraction
0Gy
2Gy
4Gy
6Gy
p = 0.009
UMSCC-11B IR Only
UMSCC-11B IR + 2DG

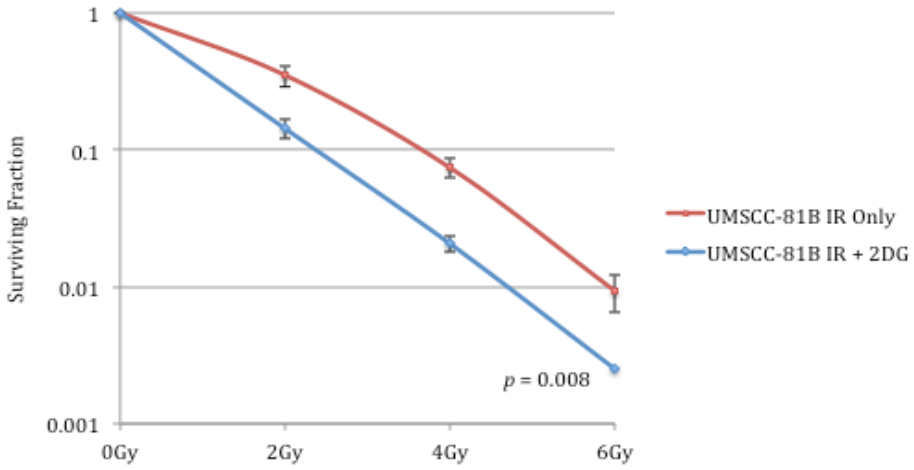
1
0.1
0.01
0.001
Surviving Fraction
0Gy
2Gy
4Gy
6Gy
p = 0.008
UMSCC-81B IR Only
UMSCC-81B IR + 2DG

Figure 3.2.2.1: Clonogenic survival curves for the panel of SCCHN cell lines with and without administration of 2-DG. Clonogenic assays were performed on SCCHN cell lines exposed to the indicated doses of IR. Cells were either left untreated or pre-treated with 25mM 2-DG for one hour prior to irradiation. Results for mutant *TP53* cells are shown first (A) and for wild-type *TP53* cell lines subsequently (B). 2-DG consistently potentiated the effects of IR in mutant *TP53* cells but not in wild-type TP53 cells. Survival parameters were calculated according to the linear quadratic formula $S(D)=\exp(\alpha D+\beta D^2)$, as described in section 2.6. The results shown represent the mean values obtained from at least three separate experiments and error bars represent SEMs. *p*-values are shown where there was a statistically significant difference between the clonogenic survival curves (<0.05), and are labelled as NS (not significant) where there was no statistically significant difference (≥0.05).

Although the consistent relationship between radiation responses following glycolytic inhibition with 2-DG and *TP53* status appears compelling, in line with findings from our previous metabolic studies, relative resistance or sensitivity can be driven by alterations in the functionality of a single transporter or enzyme. Thus, we next set out to investigate whether this association is deterministically related to *TP53* by examining the groups of cell lines with an isogenic background using the same experimental platform. Clonogenic survival curves for these cell lines are shown in figure 3.2.2.2.

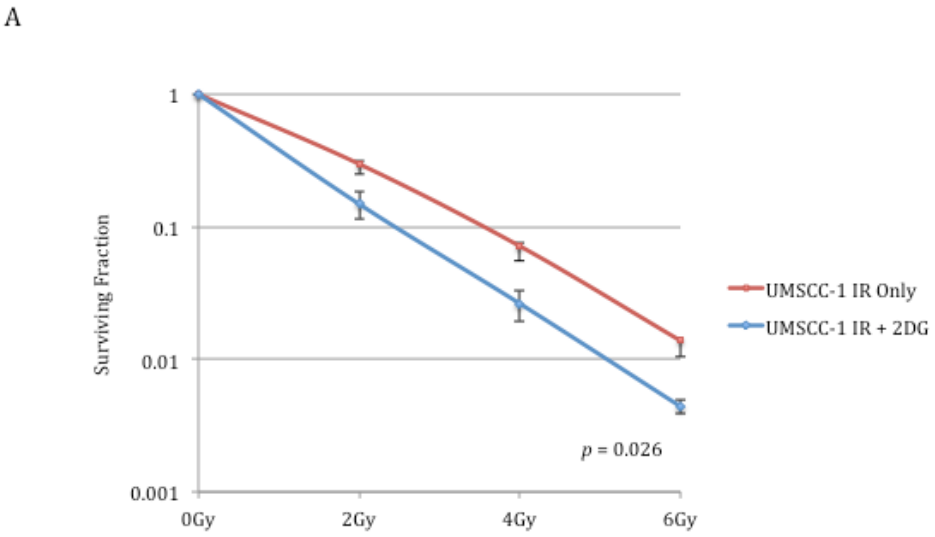

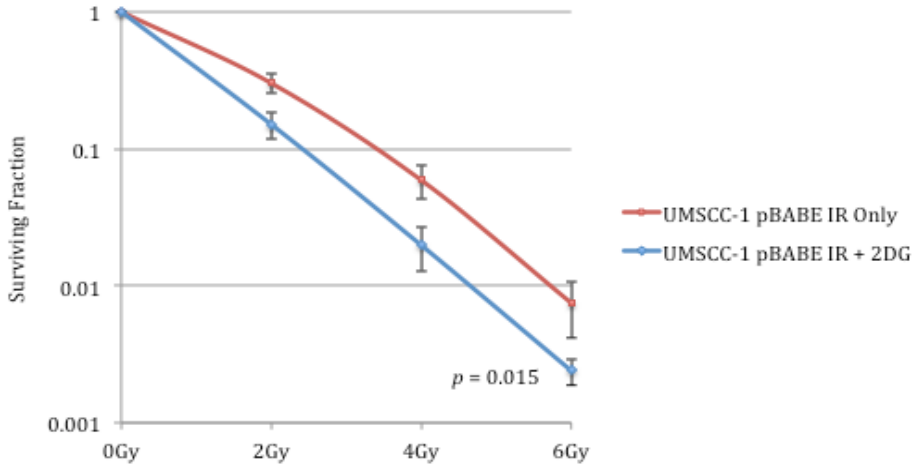
1
0.1
0.01
0.001
Surviving Fraction
0Gy
2Gy
4Gy
6Gy
p = 0.015
UMSCC-1 pBABE IR Only
UMSCC-1 pBABE IR + 2DG

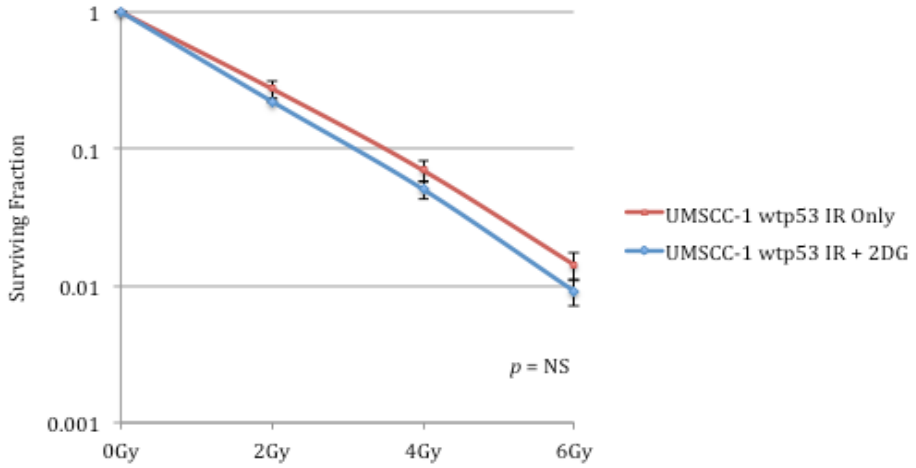
1
0.1
0.01
0.001
Surviving Fraction
0Gy
2Gy
4Gy
6Gy
p = NS
UMSCC-1 wtp53 IR Only
UMSCC-1 wtp53 IR + 2DG

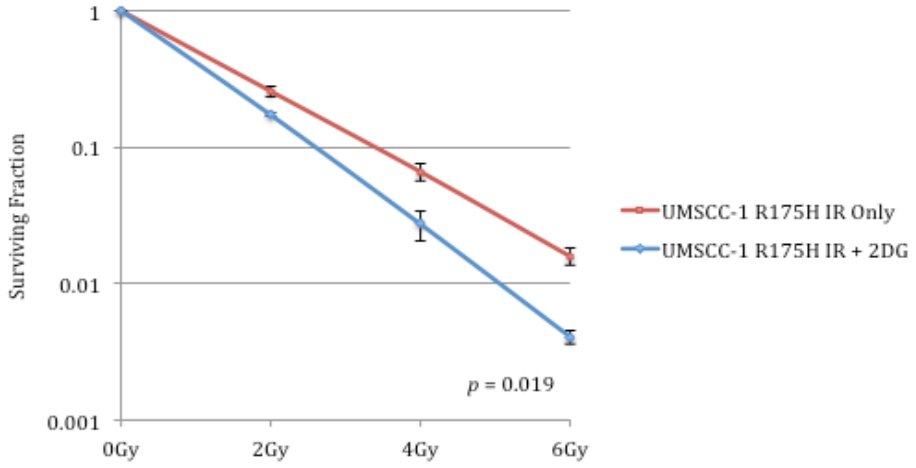
1
0.1
0.01
0.001
Surviving Fraction
0Gy
2Gy
4Gy
6Gy
p = 0.019
UMSCC-1 R175H IR Only
UMSCC-1 R175H IR + 2DG

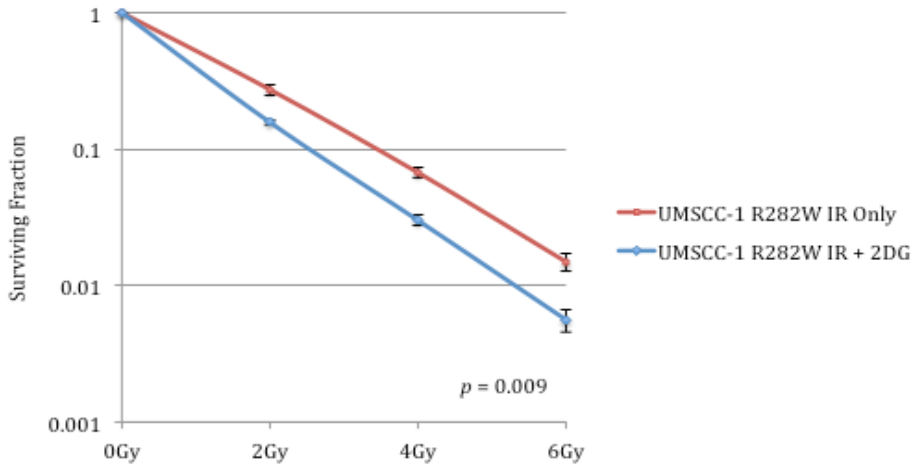
1
0.1
0.01
0.001
Surviving Fraction
0Gy
2Gy
4Gy
6Gy
p = 0.009
UMSCC-1 R282W IR Only
UMSCC-1 R282W IR + 2DG

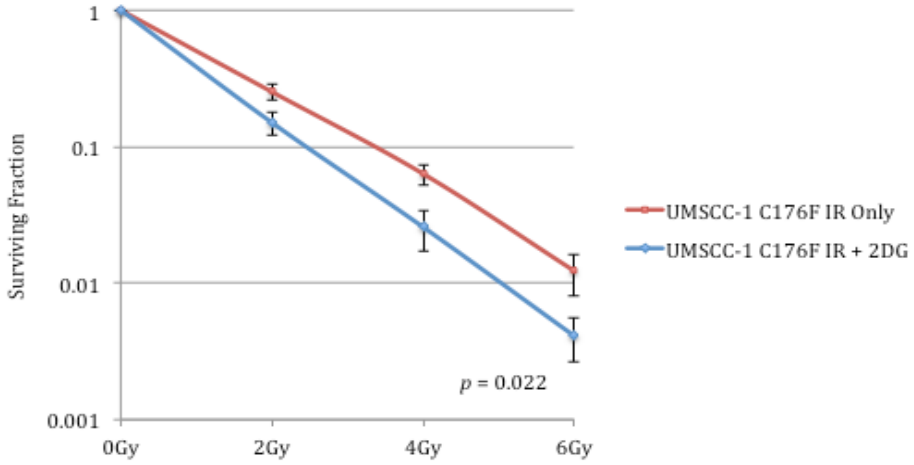
1
0.1
0.01
0.001
Surviving Fraction
0Gy
2Gy
4Gy
6Gy
p = 0.022
UMSCC-1 C176F IR Only
UMSCC-1 C176F IR + 2DG

B

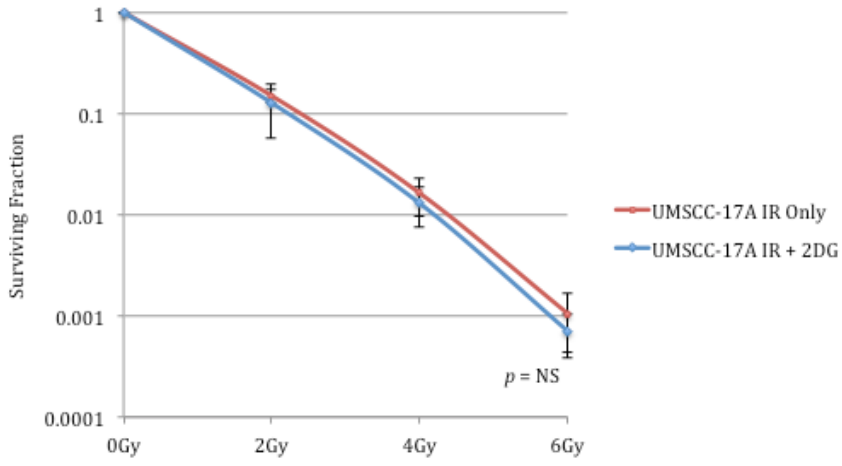
1
0.1
0.01
0.001
0.0001
Surviving Fraction
0Gy
2Gy
4Gy
6Gy
p = NS
UMSCC-17A IR Only
UMSCC-17A IR + 2DG

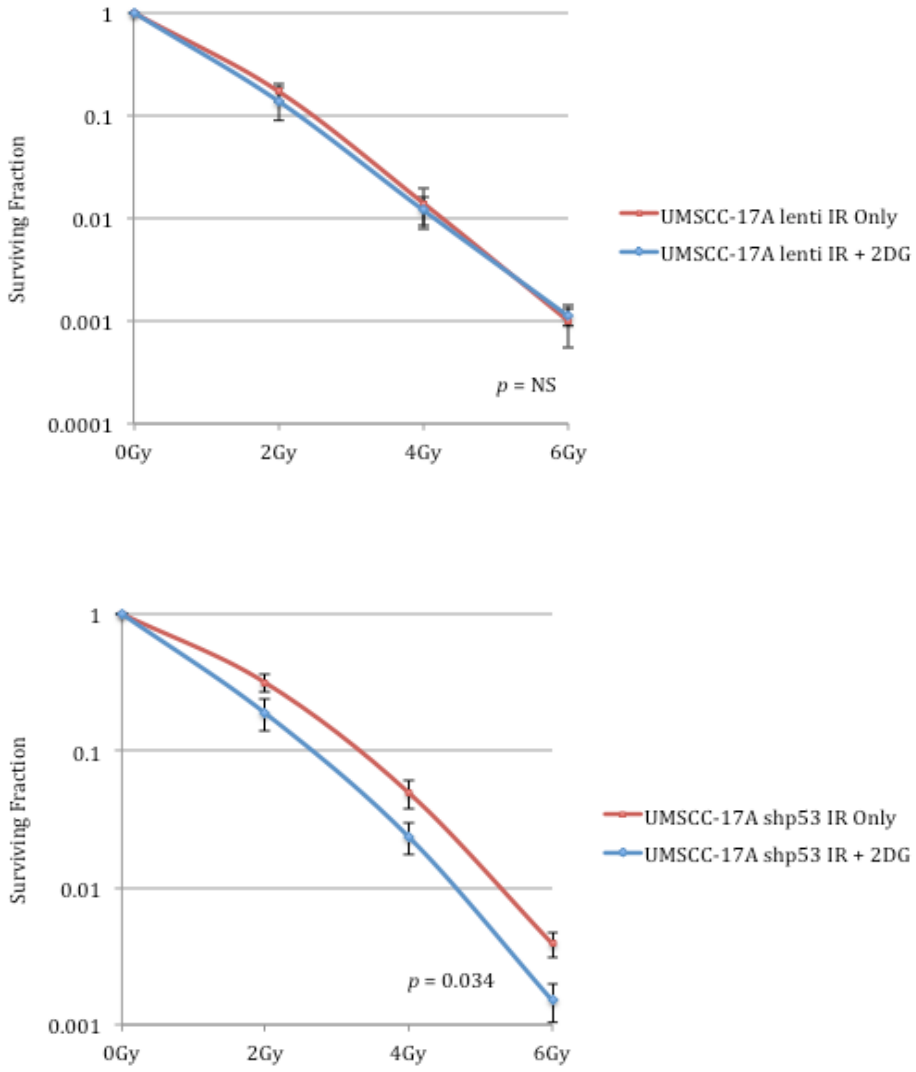

Figure 3.2.2.2: Clonogenic survival curves for isogenic SCCHN cell lines with and without administration of 2-DG. Clonogenic assays were performed on SCCHN cell lines with an isogenic background exposed to the indicated doses of IR. Cells were either left untreated or pre-treated with 25mM 2-DG for one hour prior to irradiation. Results for UM-SCC-1 and derivative cells are shown first (A) and for UM-SCC-17A and derivative cell lines subsequently (B). UM-SCC-17A and the empty vector control (lenti) displayed no sensitivity to 2-DG, stable knockdown of wild-type p53 resulted in sensitivity to the potentiating effects of 2-DG. 2-DG significantly potentiated the effects of IR in UM-SCC-1, the empty vector control (pBABE), and derivative cell lines transduced with *TP53* mutations. Forced expression of wild-type p53 in this cell line resulted in a loss of sensitivity to the potentiating effects of 2-DG. Survival parameters were calculated according to the linear quadratic formula $S(D)=\exp(\alpha D+\beta D^2)$, as described in section 2.6. The results shown represent the mean values obtained from at least three separate experiments and error bars represent the SEMs. *p*-values are shown where there was a statistically significant difference

between the clonogenic survival curves (<0.05), and are labelled as NS (not significant) where there was no statistically significant difference (≥0.05).

Importantly, the effects of 2-DG on radiation response observed in these groups of isogenic cell lines followed a pattern consistent with that observed in the panel of SCCHN cell lines. Specifically, while in UM-SCC-1, an endogenously p53-null cell line, 2-DG significantly potentiated the effects of IR, forced expression of wild-type p53 in this cell line resulted in a loss of sensitivity to the potentiating effects of 2-DG. Notably, there was no change in 2-DG effects from the parental line in the empty vector control or in the derivative cell lines transduced with *TP53* mutations. Similarly, in UM-SCC-17A and the empty vector control 2-DG had no effect on the efficacy of IR, while stable knockdown of wild-type p53 resulted in susceptibility to the potentiating effects of 2-DG. Again, such findings corroborate a functional dependence on p53. These findings accord with those from the aforementioned studies examining effects of *TP53* status on metabolism and response to 2-DG in SCCHN(355, 360), presaging an opportunity for a novel tailored anti-metabolic approach to the treatment of SCCHN that takes into account *TP53* mutational status, which would be preferentially effective in overcoming cellular resistance to radiation treatment in patients with treatment-resistant disease typically associated with T*P53* mutation. Clearly, however, such an approach will require extensive testing in pre-clinical *in vivo* models to further validate these *in vitro* results. Interestingly, these findings may also offer an explanation for the variable results observed in therapeutic studies of 2-DG and other glycolytic inhibitors in SCCHN, as well as other tumour types. Akin to our findings in SCCHN, it is conceivable that in tumours harbouring *TP53* mutations, concurrent glycolytic inhibition could result in significant chemo- and/or radiosensitisation, while those expressing wild-type p53 may be resistant to such an approach.

Having shown in the previous section that HPV-positive SCCHN cell lines exhibited a metabolic profile in keeping with functional wild-type p53, and given that in HPV-negative SCCHN cells this correlated with a resistance to the potentiating effects of 2-DG on IR, the effects of 2-DG were explored in HPV-positive SCCHN cell lines. The clonogenic survival curves are shown in figure 3.2.2.3.

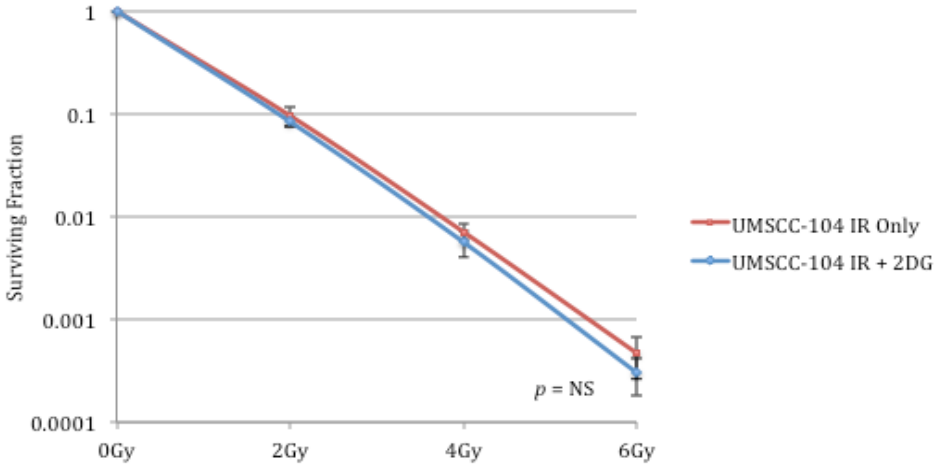
1
0.1
0.01
0.001
0.0001
Surviving Fraction
p = NS
0Gy
2Gy
4Gy
6Gy
UMSCC-104 IR Only
UMSCC-104 IR + 2DG

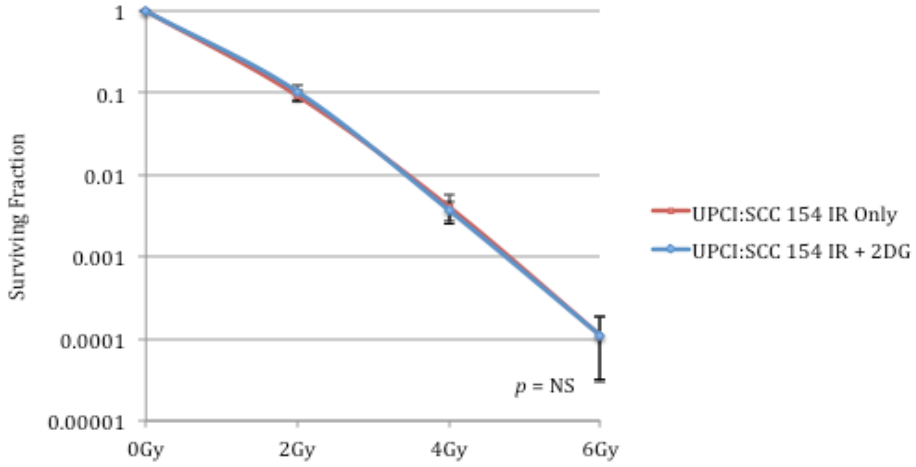
1
0.1
0.01
0.001
0.0001
0.00001
Surviving Fraction
p = NS
0Gy
2Gy
4Gy
6Gy
UPCI:SCC 154 IR Only
UPCI:SCC 154 IR + 2DG

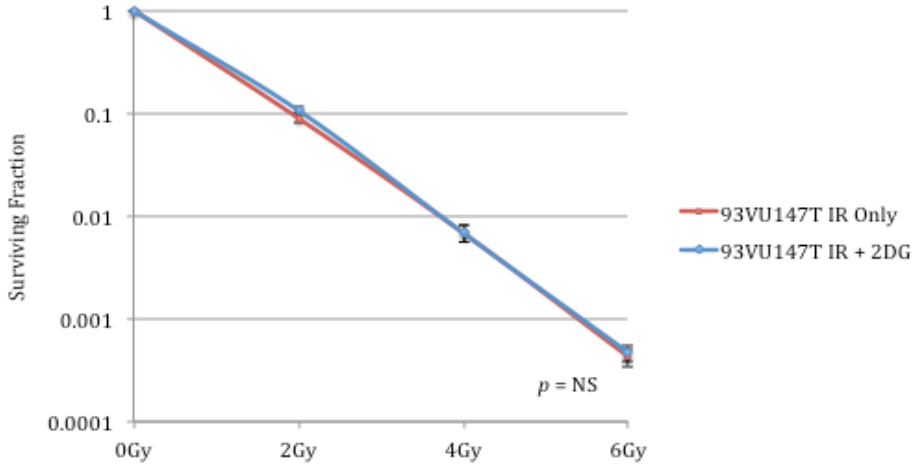
1
0.1
0.01
0.001
0.0001
Surviving Fraction
p = NS
0Gy
2Gy
4Gy
6Gy
93VU147T IR Only
93VU147T IR + 2DG

Figure 3.2.2.3: Clonogenic survival curves for HPV-related SCCHN cell lines with and without administration of 2-DG. Clonogenic assays were performed on HPV-related SCCHN cell lines exposed to the indicated doses of IR. Cells were either left untreated or pre-treated with 25mM 2-DG for one hour prior to irradiation. 2-DG failed to have any effect on radiation response in any of these cell lines. Survival parameters were calculated according to the linear quadratic formula $S(D)=\exp(\alpha D+\beta D^2)$, as described in section 2.6. The results shown represent the mean values obtained from at least three separate experiments and error bars represent the SEMs. *p*-values are shown where there was a statistically significant difference between the clonogenic survival curves (<0.05), and are labelled as NS (not significant) where there was no statistically significant difference (≥0.05).

Again in keeping with findings from our earlier metabolic profiling studies, in which these HPV-positive SCCHN cell lines were seen to display metabolic diversity, administration of 2-DG had no effect on IR effects in these cell lines. As mentioned in section 3.1.5., only one previous study has examined metabolism in HPV-related SCCHN(361), and although these findings accord with our metabolic profiling studies, there is no comparative data on anti-metabolic therapeutics in these tumour types. On the basis of the present data, it appears that in order to potentiate the effects of conventional treatments in HPV-driven SCCHN a broader anti-metabolic approach will be required, and this is explored further later in this chapter (section 3.2.5.).

Whilst it was not the aim of the present study to examine radiation sensitivity between HPV-negative and HPV-positive SCCHN cell lines, and as such no formal analysis has been carried out in this regard, it is interesting to note the clear differences in the clonogenic survival curves. Although there is considerable variation in radiation sensitivity in both HPV-negative and HPV-positive cells, there is a clear pattern of increased radiosensitivity in the HPV-positive cells, with reduced survival fractions (compare figures 3.2.2.1. and 3.2.2.2. with figure 3.2.2.3.). This finding certainly accords with clinical reports, which have shown favourable survival outcomes for HPV-driven oropharyngeal SCC irrespective of treatment modality employed(80, 94, 95, 397), and adds weight to the notion that these cell lines represent suitable, albeit potentially limited model systems. Curiously, the paucity of previous experimental data in HPV-positive SCCHN cell lines is conflicting, with some reports suggesting enhanced sensitivity to radiation and others suggesting reduced sensitivity or no effect(381, 398-400). Consistent with our findings, however, a relatively recent study, in which cell line HPV status was rigorously validated, demonstrated HPV-positive SCCHN cells to be

consistently more sensitive to radiation than HPV-negative SCCHN cells both *in vitro* and *in vivo*(381).

3.2.3. The potentiating effects of 2-DG on IR in mutant TP53 SCCHN cells are on-target

2-DG is a stable glucose analogue that is taken up by glucose transporters and phosphorylated. 2-DG, however, cannot be fully metabolised and 2-DG-6-phosphate accumulates in the cell and interferes with glycolysis by inhibiting the glycolytic enzymes phosphoglucose isomerase and hexokinase. The general presumption, therefore, is that the biological effects of 2-DG are the consequence of this block in carbohydrate catabolism. This presumption, however, has been challenged and any observed effects of 2-DG may not be simply the result of a catabolic block(358). The specificity of 2-DG anti-glycolytic effects in suppressing cellular proliferation and anchorage-independent growth in SCCHN cell lines has been demonstrated previously, with effects were reproduced under conditions of glucose deprivation(359). Furthermore, differential sensitivity to halogenated 2-DG analogues consistent with their underlying chemical structure has been reported, and quantitative, broad-based analysis of changes in intracellular metabolite levels in response to 2-DG revealed time-dependent reductions in lactate production and levels of upstream glycolytic and TCA cycle intermediates(359). Nonetheless, we sought to investigate whether the observed potentiating effects of 2-DG on IR in mutant *TP53* SCCHN cells were indeed a result of glycolytic inhibition by investigating whether these effects were reproduced using 3-BP, a distinct glycolytic inhibitor also acting on hexokinase, in the SCCHN cells with an isogenic background. Clonogenic assays were performed and survival parameters calculated as before, but in the absence and presence of 5μM 3-BP, which was administered one hour prior to irradiation. Clonogenic survival curves are shown in figure 3.2.3.1. Results were consistent with those obtained for 2-DG, whereby 3-BP potentiated radiation effects in cells with abrogated wild-type p53 function but failed to do so in cells harbouring wild-type p53. Although 3-BP also has effects beyond those of glycolytic inhibition(401), the fact that two distinct glycolytic inhibiting agents both acting on hexokinase have induced the same pattern of potentiating effects on IR lends support to the notion that antiglycolytic effects are the likely mechanism driving toxicity.

A

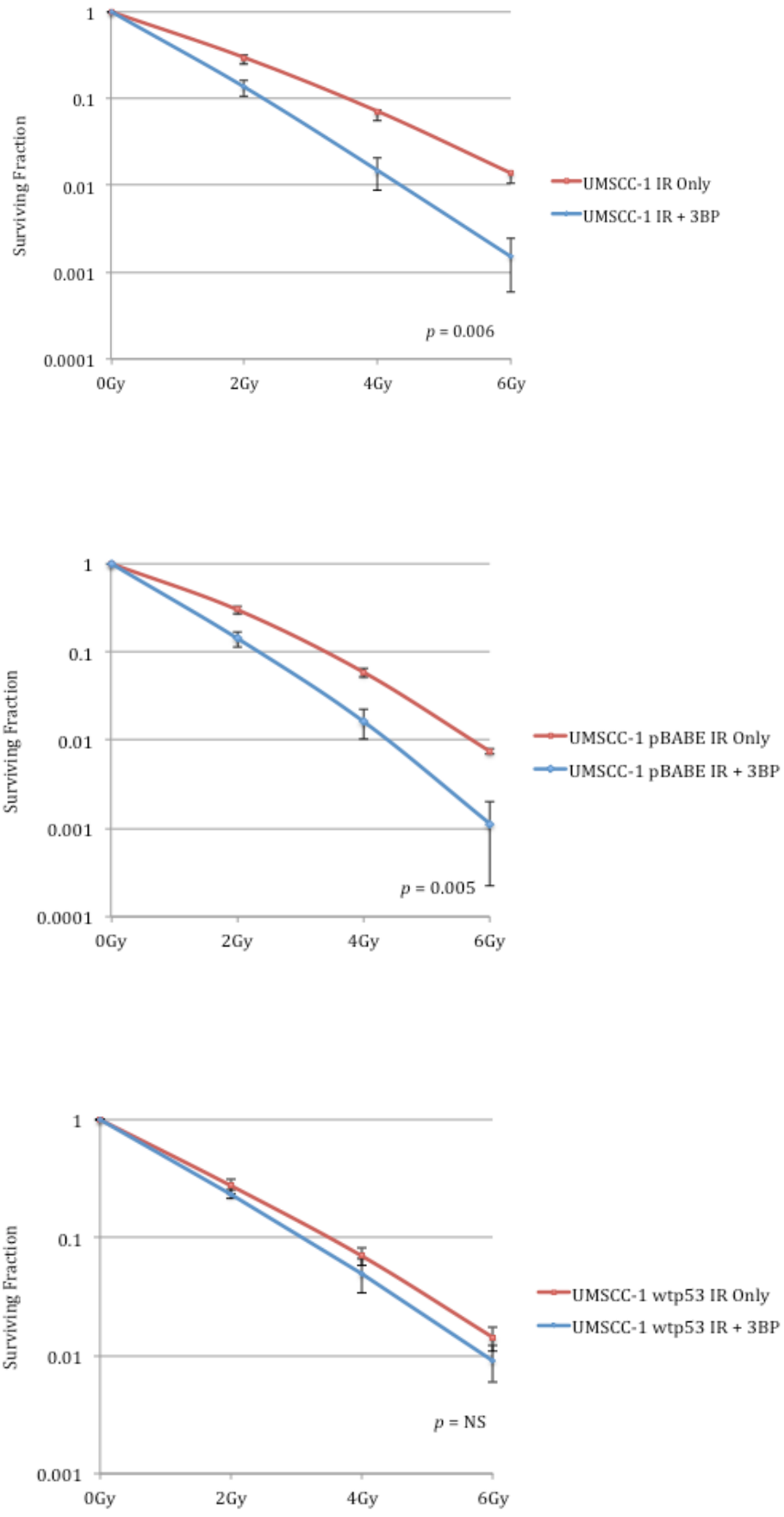
1
0.1
0.01
0.001
0.0001
Surviving Fraction
0Gy
2Gy
4Gy
6Gy
p = 0.006
UMSCC-1 IR Only
UMSCC-1 IR + 3BP
p = 0.005
UMSCC-1 pBABE IR Only
UMSCC-1 pBABE IR + 3BP
p = NS
UMSCC-1 wtp53 IR Only
UMSCC-1 wtp53 IR + 3BP

B

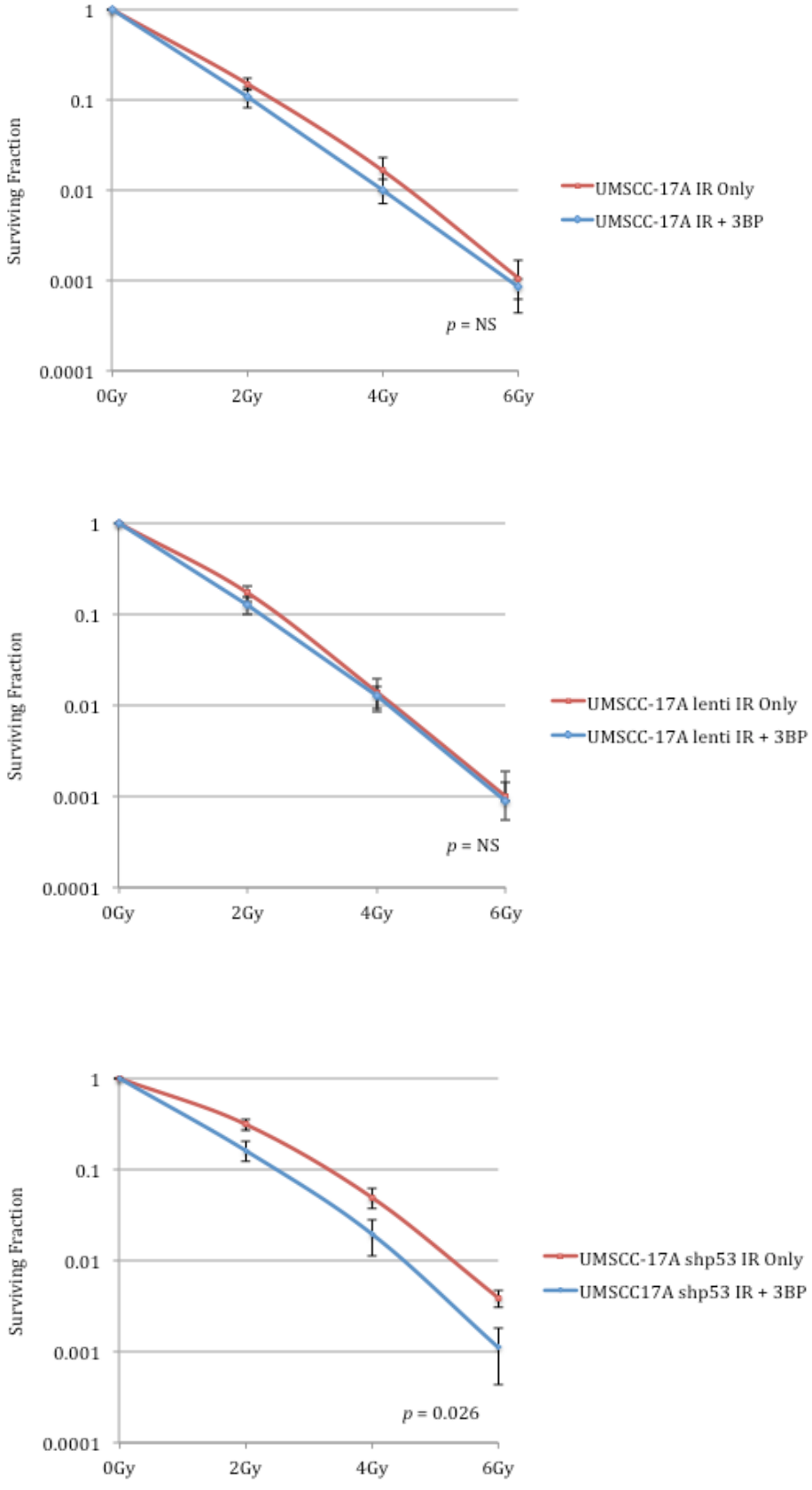
1
0.1
0.01
0.001
0.0001
Surviving Fraction
0Gy
2Gy
4Gy
6Gy
p = NS
UMSCC-17A IR Only
UMSCC-17A IR + 3BP
p = NS
UMSCC-17A lenti IR Only
UMSCC-17A lenti IR + 3BP
p = 0.026
UMSCC-17A shp53 IR Only
UMSCC17A shp53 IR + 3BP

Figure 3.2.3.1: Clonogenic survival curves for isogenic SCCHN cell lines with and without administration of 3-BP. Clonogenic assays were performed on SCCHN cell lines with an isogenic background exposed to the indicated doses of IR. Cells were either left untreated or pre-treated with 5μM 3-BP for one hour prior to irradiation. Results for UM-SCC-1 and derivative cells are shown first (A) and for UM-SCC-17A and derivative cell lines subsequently (B). UM-SCC-17A and the empty vector control (lenti) displayed no sensitivity to 3-BP, while stable knockdown of wild-type p53 resulted in sensitivity to the potentiating effects of 3-BP. 3-BP significantly potentiated the effects of IR in UM-SCC-1 and the empty vector control (pBABE). Forced expression of wild-type p53 in this cell line resulted in a loss of susceptibility to the potentiating effects of 3-BP. Survival parameters were calculated according to the linear quadratic formula $S(D)=\exp(\alpha D+\beta D^2)$, as described in section 2.6. The results shown represent the mean values obtained from at least three separate experiments and error bars represent the SEMs. *p*-values are shown where there was a statistically significant difference between the clonogenic survival curves (<0.05), and are labelled as NS (not significant) where there was no statistically significant difference (≥0.05).

3.2.4. Pentose phosphate pathway inhibition further potentiates IR effects in SCCHN cells with loss of functional wild-type p53

As discussed previously (section 1.3.1.), a major impetus for metabolic re-programming in cancer cells is thought to relate to regulation of cellular redox potential, whereby switching the balance away from oxidative phosphorylation towards glycolysis enables up-regulation of cellular antioxidant systems to quench the increased ROS levels resulting from heightened oxidative substrate flux and de-regulated cellular proliferation(257, 267). This up-regulation of anti-oxidant systems largely depends on the generation of the reducing equivalent NADPH, the principal source of which is PPP flux(280). Considering this, together with the fact that disruption of thiol metabolism and consequent oxidative stress has been implicated as the mechanism underlying the cytotoxic effects of glycolytic inhibitors(354, 359, 360, 402), prompted us to investigate whether inhibition of PPP flux, and by extension detoxifying antioxidant systems, has potential therapeutic gain over and above the potentiating effects of glycolytic inhibition on IR in mutant *TP53* SCCHN cells. Clonogenic assays were performed on isogenic SCCHN cell lines treated at the indicated doses of IR and survival parameters calculated as before. One hour prior to irradiation cells were pre-treated as follows: no treatment, 25mM 2-DG, 5μM 6-AN (an inhibitor of the key PPP enzyme 6-phosphogluconate dehydrogenase [6-PGD], which drives the second NADPH producing step in the oxidative phase of PPP), or 25mM 2-DG in combination with 5μM 6-AN. Clonogenic survival curves are shown in figure 3.2.4.1.

A

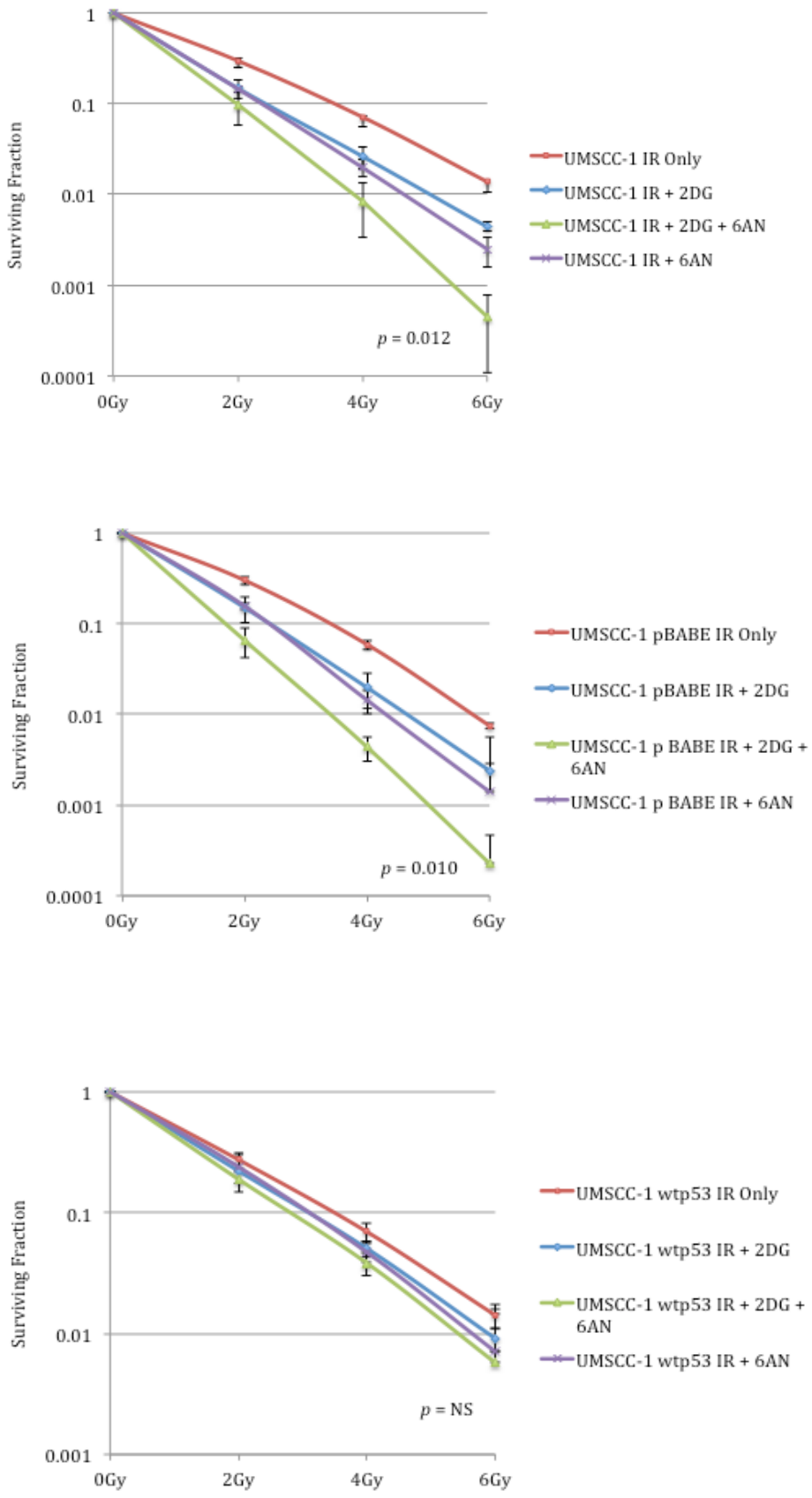
Surviving Fraction
1
0.1
0.01
0.001
0.0001
0Gy
2Gy
4Gy
6Gy
p = 0.012
UMSCC-1 IR Only
UMSCC-1 IR + 2DG
UMSCC-1 IR + 2DG + 6AN
UMSCC-1 IR + 6AN
Surviving Fraction
1
0.1
0.01
0.001
0.0001
0Gy
2Gy
4Gy
6Gy
p = 0.010
UMSCC-1 pBABE IR Only
UMSCC-1 pBABE IR + 2DG
UMSCC-1 p BABE IR + 2DG + 6AN
UMSCC-1 p BABE IR + 6AN
Surviving Fraction
1
0.1
0.01
0.001
0Gy
2Gy
4Gy
6Gy
p = NS
UMSCC-1 wtp53 IR Only
UMSCC-1 wtp53 IR + 2DG
UMSCC-1 wtp53 IR + 2DG + 6AN
UMSCC-1 wtp53 IR + 6AN

B

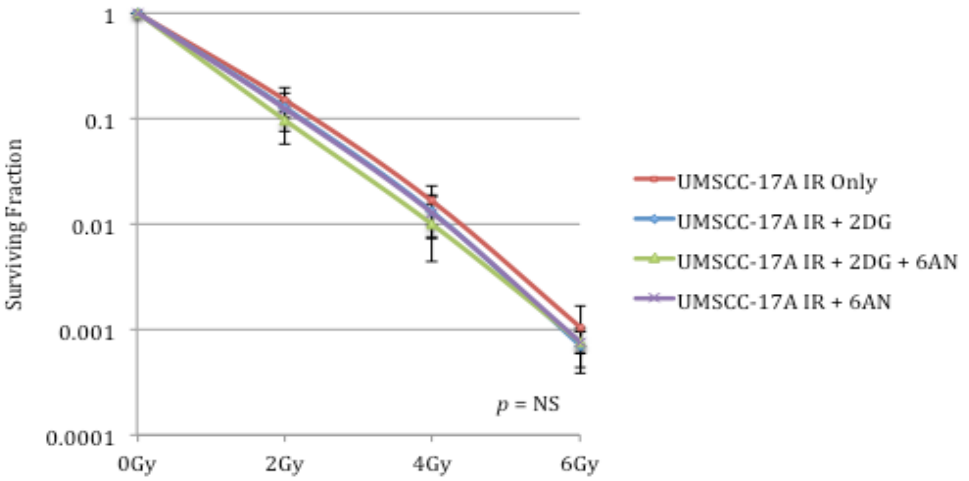
Surviving Fraction
1
0.1
0.01
0.001
0.0001
0Gy
2Gy
4Gy
6Gy
p = NS
UMSCC-17A IR Only
UMSCC-17A IR + 2DG
UMSCC-17A IR + 2DG + 6AN
UMSCC-17A IR + 6AN

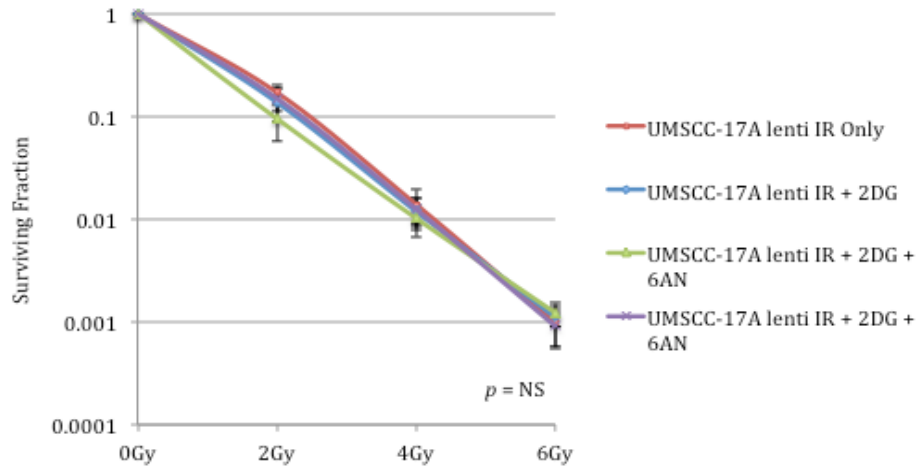
Surviving Fraction
1
0.1
0.01
0.001
0.0001
0Gy
2Gy
4Gy
6Gy
p = NS
UMSCC-17A lenti IR Only
UMSCC-17A lenti IR + 2DG
UMSCC-17A lenti IR + 2DG + 6AN
UMSCC-17A lenti IR + 2DG + 6AN

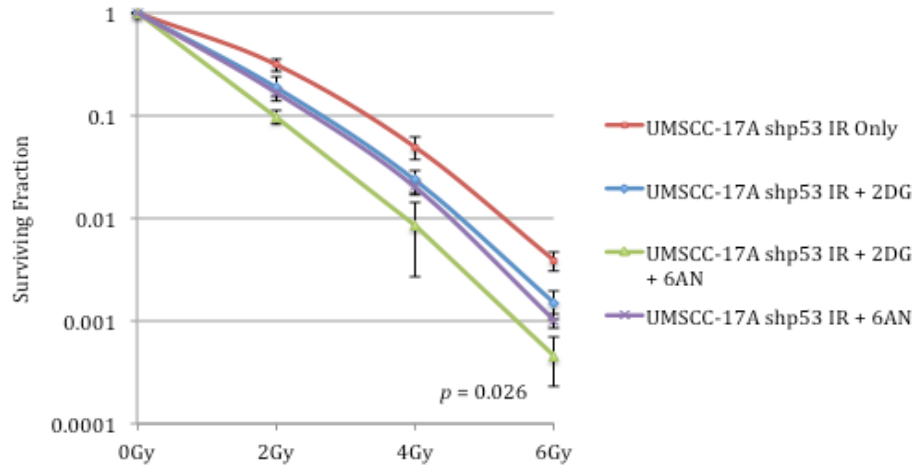
Surviving Fraction
1
0.1
0.01
0.001
0.0001
0Gy
2Gy
4Gy
6Gy
p = 0.026
UMSCC-17A shp53 IR Only
UMSCC-17A shp53 IR + 2DG
UMSCC-17A shp53 IR + 2DG + 6AN
UMSCC-17A shp53 IR + 6AN

Figure 3.2.4.1: Clonogenic survival curves for isogenic SCCHN cell lines with and without administration of 2-DG and 6-AN. Clonogenic assays were performed on SCCHN cell lines with an isogenic background exposed to the indicated doses of IR. Cells were either left untreated or pre-treated with 25mM 2-DG alone, 5μM 6-AN alone, or the combination of 25mM 2-DG and 5μM 6-AN for one hour prior to irradiation. Results for UM-SCC-1 and derivative cells are shown first (A) and for UM-SCC-17A and derivative cell lines subsequently (B). UM-SCC-17A and the empty vector control (lenti) displayed limited sensitivity to the addition of 6-AN, while stable knockdown of wild-type p53 resulted in sensitivity to the addition of 6-AN. 6-AN significantly augmented the potentiating effects 2-DG on IR in UM-SCC-1 and the empty vector control (pBABE). Forced expression of wild-type p53 in this cell line resulted in a loss of susceptibility to the addition of 6-AN. Survival parameters were calculated according to the linear quadratic formula $S(D)=\exp(\alpha D+\beta D^2)$, as described in section 2.6. The results shown represent the mean values obtained from at least two separate experiments and error bars represent the SEMs. *p*-values are shown where there was a statistically significant difference between the clonogenic survival curves (<0.05), and are labelled as NS (not significant) where there was no statistically significant difference (≥0.05). *p*-values represent comparison between the survival curves for IR + 2-DG and IR + 2-DG + 6-AN.

Interestingly, the addition of 6-AN significantly augmented the potentiating effects of 2-DG on IR in SCCHN cells with loss of functional wild-type p53, suggesting the PPP is critical to maintaining cellular reducing potential and an important subsidiary pathway in SCCHN oncogenesis in this context, something which is explored in greater detail later in this thesis (section 3.4.). This accords with findings from two previous studies examining 6-AN use in SCCHN, which also demonstrated that combining 2-DG with 6-AN results in an enhanced cytotoxic effect over 2-DG alone(277, 403). No previous studies have stratified this effect on the basis of *TP53* status but in the study discussed previously aiming to investigate the reprogramming of metabolism associated with the development of radioresistance using a matched model of radio-resistant and -sensitive SCCHN cells, treatment with 6-AN had a greater inhibitory effect on cell proliferation in radioresistant cells(277), which may have acquired *TP53* mutation during the course of their generation. That 6-AN further potentiated the effects of IR in SCCHN cells dependent on glycolysis, and by extension related subsidiary pathways such as the PPP, for survival was perhaps to be expected. Although 2-DG, as an analogue of glucose competes for uptake and entry into glycolysis, thereby creating a drug-induced state of glucose deprivation, it does not completely inhibit the generation of NADPH through the PPP as 2-DG is itself, a substrate for glucose-6-phosphate dehydrogenase (G6PD) – the enzyme catalysing the first step in the PPP(404).

3.2.5. SCCHN cells harbouring functional wild-type p53 require a broader anti-metabolic therapeutic approach

Having shown that SCCHN cells harbouring wild-type p53, including HPV-positive SCCHN cells, display metabolic diversity with robust mitochondrial respiratory and glycolytic reserves, and consequently are resistant to therapeutic targeting of glycolysis, we next investigated whether a broader anti-metabolic approach could be employed to sensitise these cells to the effects of IR. Metformin is a biguanide commonly used in clinical practice as a first line of treatment for type II diabetes with minimal toxicity, and has demonstrated activity against mitochondrial respiration, specifically against ETC complex I(405). Thus, metformin was an appropriate choice to combine with 2-DG to enable targeting of both glycolysis and mitochondrial respiration. Although more specific mitochondrial inhibitors, such as rotenone and cyanide, are available, their associated toxicity makes them unlikely therapeutic options. Indeed, there has been an ever-increasing interest in re-purposing metformin as a therapeutic agent in the context of cancer treatment(406), an interest which stems from several epidemiological studies demonstrating a lower cancer incidence in diabetic patients taking metformin than in the general diabetic population(407), and retrospective data indicating that metformin users have higher rates of disease control when treated with neoadjuvant chemotherapy for breast cancer(408).

HPV-negative wild-type *TP53* SCCHN cells and HPV-positive SCCHN cells were subjected to clonogenic assays, in which cells were treated at the indicated doses of IR and survival parameters calculated as before. One hour prior to irradiation cells were pre-treated as follows: no treatment, 25mM 2-DG, or 25mM 2-DG in combination with 20mM metformin. Clonogenic survival curves are shown in figures 3.2.5.1. and 3.2.5.2.

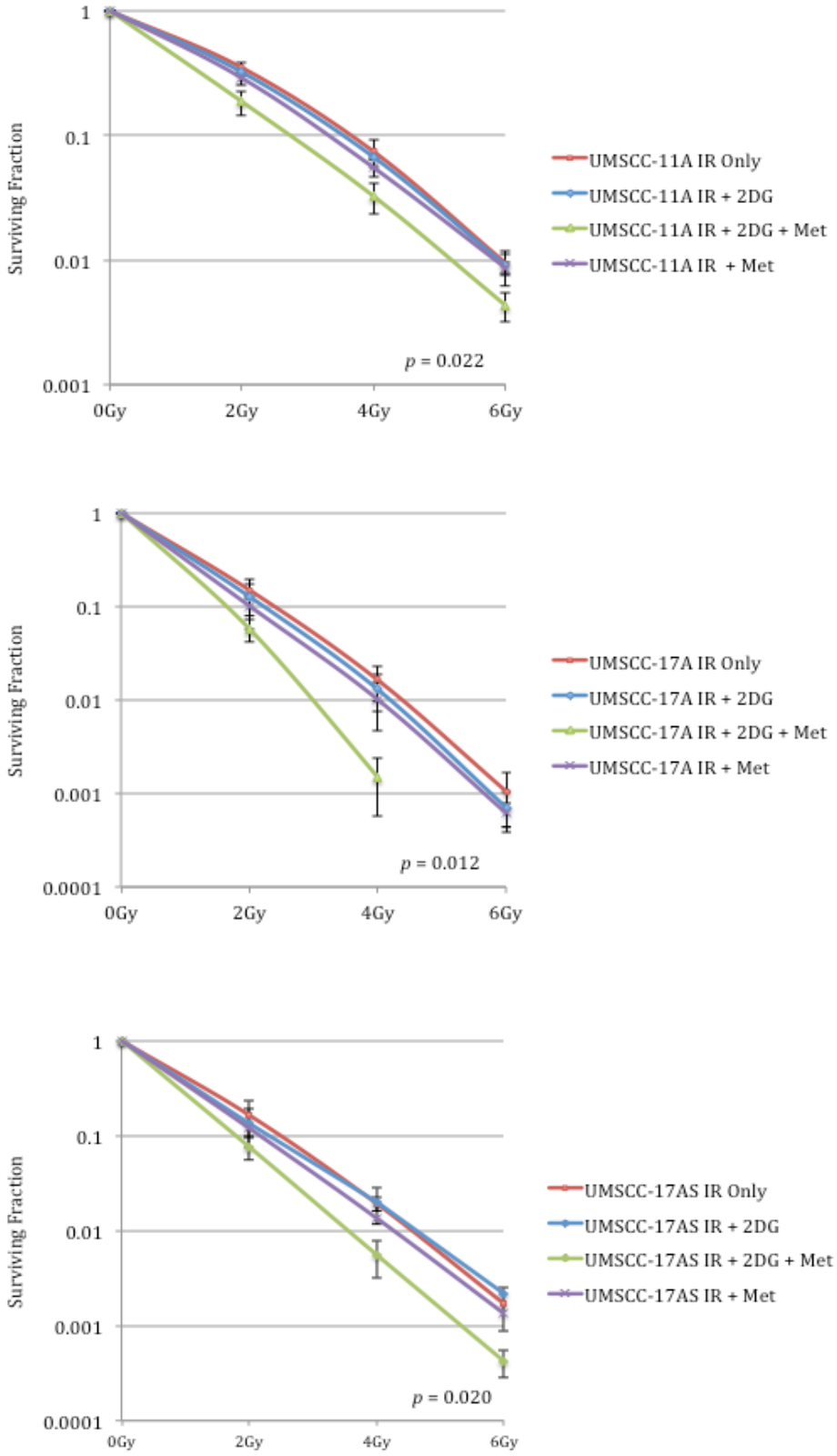

Figure 3.2.5.1: Clonogenic survival curves for wild-type *TP53* HPV-negative SCCHN cell lines with and without administration of 2-DG and metformin. Clonogenic assays were performed on HPV-negative wild-type *TP53* SCCHN cell lines exposed to the indicated doses of

IR. Cells were either left untreated or pre-treated with 25mM 2-DG, 20mM metformin, or combined treatment for one hour prior to irradiation. Whilst 2-DG alone failed to have any effect on radiation response in any of these cell lines, the addition of metformin resulted in a significant reduction in clonogenic survival (p values are shown where statistically significant differences were observed and represent the difference between the survival curves for the untreated condition and when combined pre-treatment with 2-DG and metformin was administered. Survival parameters were calculated according to the linear quadratic formula $S(D)=\exp(\alpha D+\beta D^2)$, as described in section 2.6. The results shown represent the mean values obtained from at least three separate experiments and error bars represent the SEMs. *p*-values are shown where there was a statistically significant difference between the clonogenic survival curves (<0.05), and are labelled as NS (not significant) where there was no statistically significant difference (≥0.05). *p*-values represent comparison between the survival curves for IR + 2-DG and IR + 2-DG + metformin.

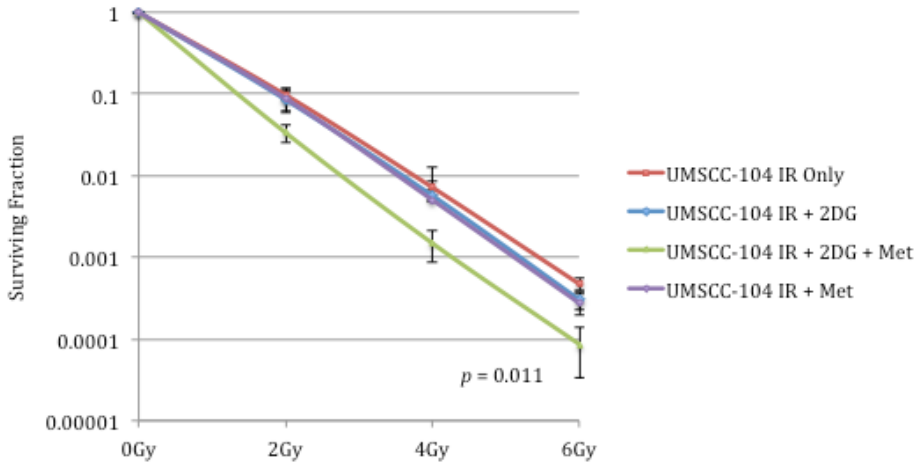

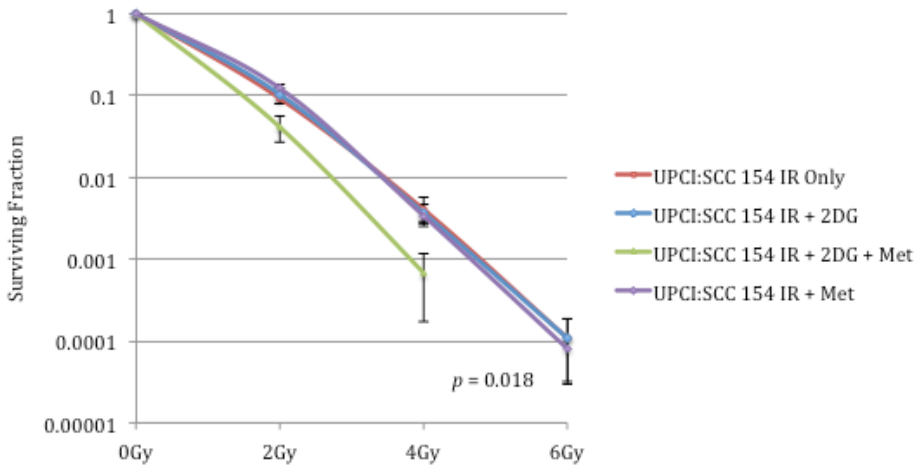

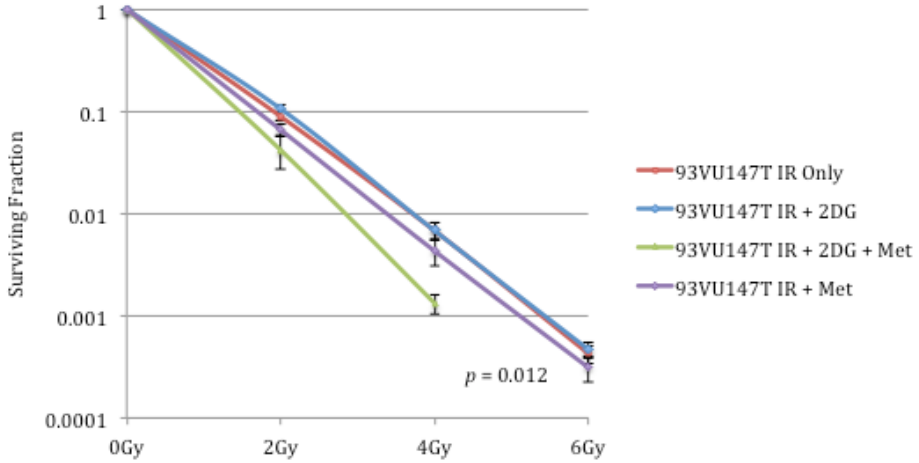

Figure 3.2.5.2: Clonogenic survival curves for HPV-positive SCCHN cell lines with and without administration of 2-DG and metformin. Clonogenic assays were performed on HPV-related SCCHN cell lines exposed to the indicated doses of IR. Cells were either left untreated or pre-treated with 25mM 2-DG, 20mM metformin, or combined treatment for one hour prior to irradiation. Whilst 2-DG alone failed to have any effect on radiation response in any of these cell lines, the addition of metformin resulted in a significant reduction in clonogenic survival (p values are shown where statistically significant differences were observed and represent the difference between the survival curves for the untreated condition and when combined pre-treatment with 2-DG and metformin was administered. Survival parameters were calculated according to the linear quadratic formula $S(D)=\exp(\alpha D+\beta D^2)$, as described in section 2.6. The results shown represent the mean values obtained from at least three separate experiments and error bars represent the SEMs. *p*-values are shown where there was a statistically significant difference between the clonogenic survival curves (<0.05), and are labelled as NS (not significant) where there was no statistically significant difference (≥0.05). *p*-values represent comparison between the survival curves for IR + 2-DG and IR + 2-DG + metformin.

We hypothesised that the addition of metformin to 2-DG would sensitise these cells, which maintain a diversified metabolic profile, to the effects of IR, given that this dual-targeted anti-metabolic strategy would target both glycolysis and mitochondrial respiration. Accordingly, this is what was observed. This fits with the proposed tailored anti-metabolic therapeutic paradigm discussed previously, with this approach enabling potentiation of radiation toxicity in those tumours resistant to the anti-glycolytic approach for *TP53* mutant disease.

Our findings are at odds with one previous study of SCCHN cell lines, which presented evidence that metformin selectively radiosensitises cells with disruptive *TP53* mutations, with little effect seen in cells expressing wild-type p53(57). Curiously,

however, in another study from the same research group p53 proficient SCCHN cell lines were reported to be radiosensitised by metformin(360), consistent with our findings. As mentioned previously, no previous studies have examined anti-metabolic therapeutic strategies in HPV-positive SCCHN. Our findings demonstrating that such cells can be radiosensitised with a combination of 2-DG and metformin, reflecting their metabolic profile, may, therefore, be particularly promising insofar as they potentially present a novel platform to facilitate the proposed treatment de-intensification in carefully selected HPV-positive cases. Again, however, such an approach will require extensive testing in pre-clinical *in vivo* models to further validate these *in vitro* results.

The mechanism underlying the effects of metformin appears to relate to induction of oxidative stress, as demonstrated by several studies(360, 409), which would fit with the reported potentiation of radiation toxicity given that IR induces DNA damage through a mechanism that relies to a large extent on free radical formation(369). However, the mechanistic basis for this oxidative stress remains unclear. From a metabolic perspective metformin dampens ETC activity, which intuitively would not lead to an increase in ROS. In addition to this effect on mitochondrial respiration, however, metformin has also been reported to activate AMPK(410). Through this mechanism metformin may act to dampen glycolytic flux, and by extension flux through subsidiary pathways such as the PPP, which may result in reduced production of the reducing equivalents necessary to upregulate cellular anti-oxidant systems and combat oxidative stress.

3.3. Examining the mechanistic basis underlying the potentiating effects of glycolytic inhibition on IR in mutant *TP53* SCCHN

3.3.1. Introduction

Having shown that glycolytic inhibition potentiates the effects of IR in mutant but not wild-type *TP53* SCCHN cells in accordance with the cellular metabolic profile, this chapter is devoted to the investigation of the mechanisms underlying this effect.

As discussed previously (see section 1.3.1.), an important aspect of the selective advantage that glycolytic metabolism may provide is regulation of cellular redox potential to minimise the damaging effects of excessive ROS resulting from heightened oxidative substrate flux and de-regulated cellular proliferation(257, 267). Accordingly,

there is accumulating evidence implicating inhibition of detoxifying antioxidant systems and associated oxidative stress as the mechanism underlying the therapeutic effects of glycolytic inhibition, with profound disruptions in thiol metabolism demonstrated in several solid tumour types, SCCHN included(354, 360, 402, 411, 412). This is particularly pertinent in the context of potentiation of IR effects given that IR induces DNA damage through a mechanism that relies predominantly on free radical formation(369).

Despite evidence implicating the involvement of oxidative stress in the mechanism underlying 2-DG effects on cell viability in SCCHN, until now no studies have characterised this further in terms of cell fate. Excessively high ROS levels can result in DNA damage(271), activation of protein kinase Cδ prompting senescence(227), and permeabilisation of mitochondria leading to cytochrome c release and apoptosis(192), and both apoptosis and more recently cellular senescence have been shown to play important roles in radiation response(186, 413, 414). In keeping with this, studies from other cancer types have demonstrated not only a slowing of cell cycle progression but also varying degrees of apoptosis following glycolytic inhibition, mediated through both intrinsic and extrinsic pathways(357, 415, 416). In addition, the combination of metformin and 2-DG has been shown to induce G2-M cell cycle arrest, typically characteristic of the induction of senescence(218), as well as apoptosis in prostate cancer cell lines(417).

3.3.2. The potentiating effects of 2-DG on IR in SCCHN cells with loss of functional wild-type p53 are driven by oxidative stress

Given the general consensus that regulation of cellular redox potential provides a major impetus for cancer cells to undergo metabolic switching to a glycolytic phenotype, the body of evidence implicating a loss of this regulation as a mechanism underlying the effects of targeted glycolytic inhibition, and our previous findings that PPP inhibition further augments the effects of 2-DG in potentiating IR effects (section 3.2.4.), we first set out to determine whether oxidative stress was involved in the potentiating effects of 2-DG on IR in SCCHN cells with loss of functional wild-type p53. SCCHN cell lines with loss of functional wild-type p53 that were sensitive to the potentiating effects of 2-DG on IR (mutant *TP53* cell lines and UM-SCC-17A shp53) were first subjected to clonogenic assays as described previously, and one hour prior to irradiation were either left untreated or pre-treated with 25mM 2-DG alone, 25mM of the free radical scavenging

agent NAC, or 25mM 2-DG and 25mM NAC in combination. Clonogenic survival curves are shown in figure 3.3.2.1.

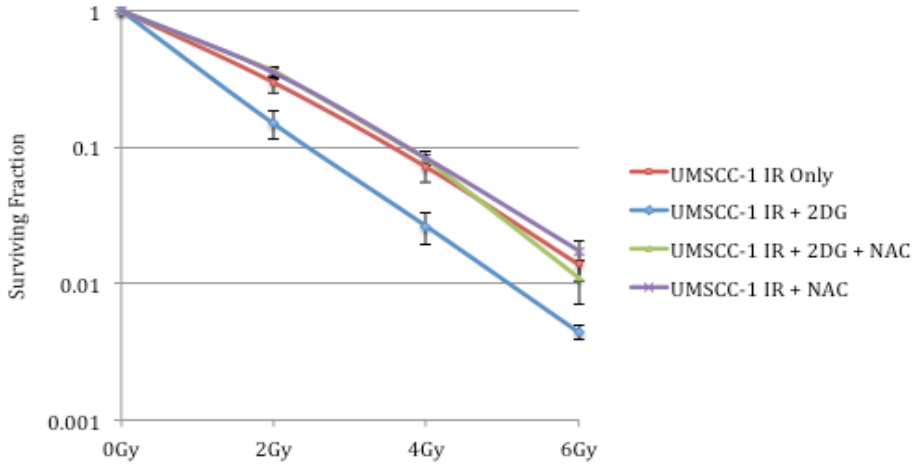

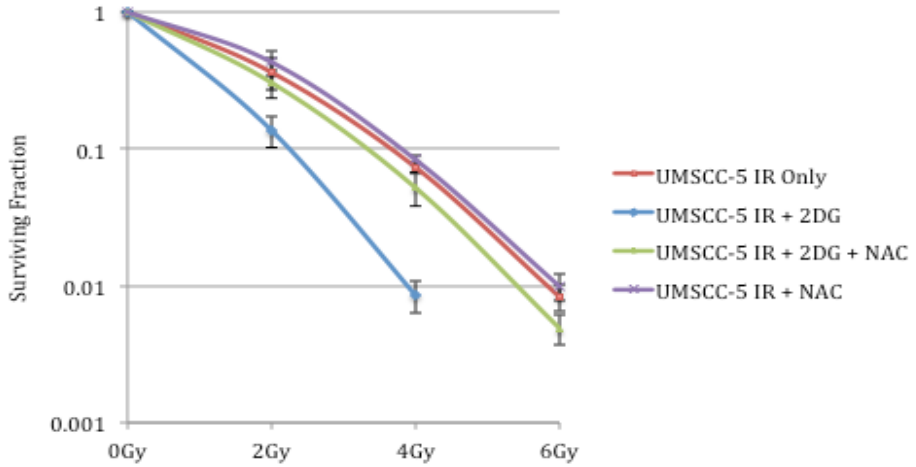

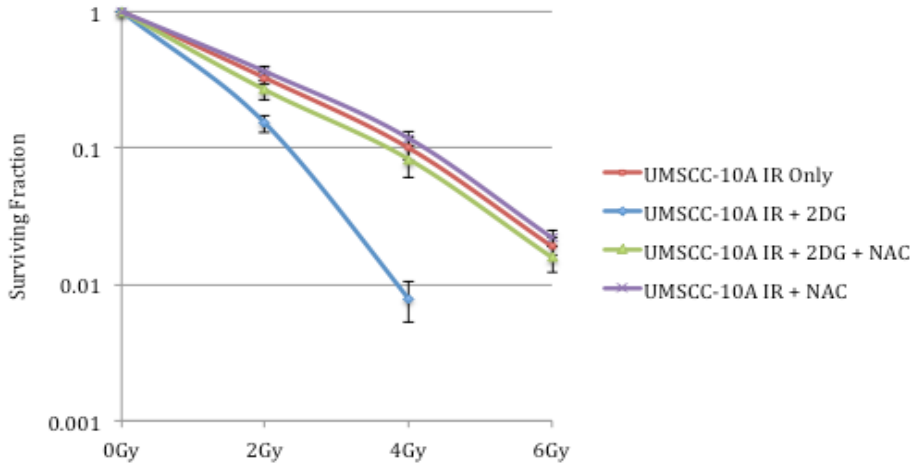

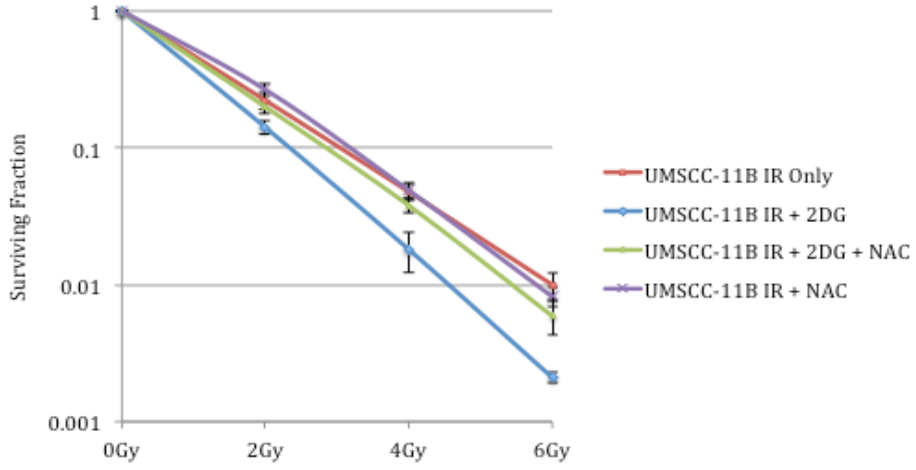
1
0.1
0.01
0.001
Surviving Fraction
0Gy
2Gy
4Gy
6Gy
UMSCC-11B IR Only
UMSCC-11B IR + 2DG
UMSCC-11B IR + 2DG + NAC
UMSCC-11B IR + NAC

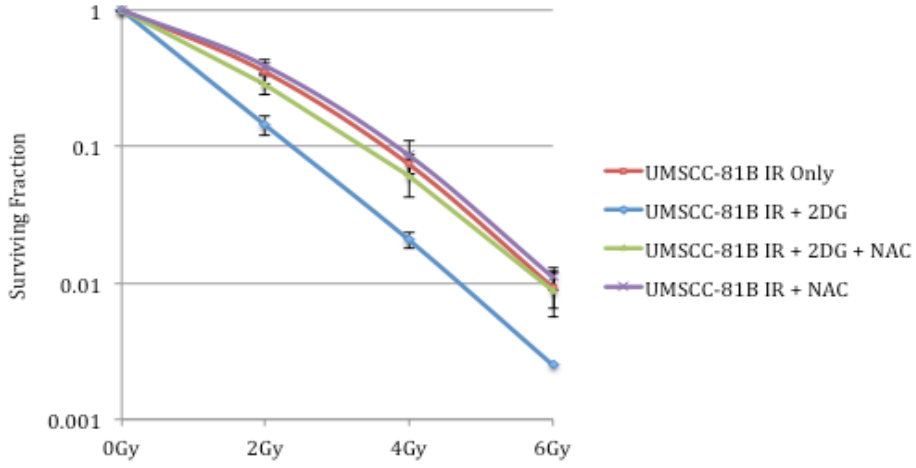
1
0.1
0.01
0.001
Surviving Fraction
0Gy
2Gy
4Gy
6Gy
UMSCC-81B IR Only
UMSCC-81B IR + 2DG
UMSCC-81B IR + 2DG + NAC
UMSCC-81B IR + NAC

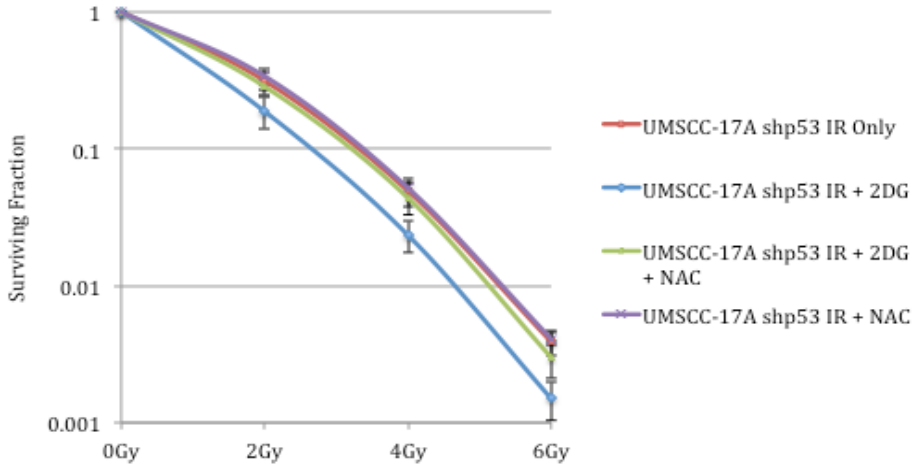
1
0.1
0.01
0.001
Surviving Fraction
0Gy
2Gy
4Gy
6Gy
UMSCC-17A shp53 IR Only
UMSCC-17A shp53 IR + 2DG
UMSCC-17A shp53 IR + 2DG + NAC
UMSCC-17A shp53 IR + NAC

Figure 3.3.2.1: Clonogenic survival curves for SCCHN cell lines with loss of functional wild-type p53 with and without administration of 2-DG and NAC. Clonogenic assays were performed on SCCHN cell lines exposed to the indicated doses of IR. Cells were either left untreated or pre-treated with 25mM 2-DG, 25mM NAC, or a combination of both agents for one hour prior to irradiation. NAC consistently reversed the potentiating the effects of 2-DG on IR, while treatment with NAC alone had no discernible effect on clonogenic survival. Survival parameters were calculated according to the linear quadratic formula $S(D)=\exp(\alpha D+\beta D^2)$, as described in section 2.6. The results shown represent the mean values obtained from at least three separate experiments and error bars represent the SEMs.

The addition of NAC consistently reversed the potentiating effects of 2-DG on IR in all *TP53* mutant cell lines and also in the stable p53 knock-down UM-SCC-17A derivative cell line, suggestive of involvement of oxidative stress in the mechanism attributable to the effects of 2-DG in SCCHN with loss of wild-type p53 function. To examine this further direct measurement of intracellular free radical production, and by association the function of cellular antioxidant defences, was performed using the molecular probe DCFH-DA and fluorescence measured by flow cytometry (described in section 2.9.). Cells were treated with 6Gy IR alone, or 6Gy IR following pre-treatment with 25mM 2-DG or a combination of 25mM 2-DG and 25mM NAC, with positive and negative controls for each experiment comprising 100μM H_2O_2 and no treatment respectively. In the first instance a time course experiment for UM-SCC-1 was performed to determine the optimal time point at which to assess ROS levels following treatment, so as to allow sufficient time for ROS generation following treatment but prior to significant cell death. Results are shown in figure 3.3.2.2. with the following post-treatment time points evaluated: 1, 2, 4, 8, 16, and 24 hours.

1 Hour

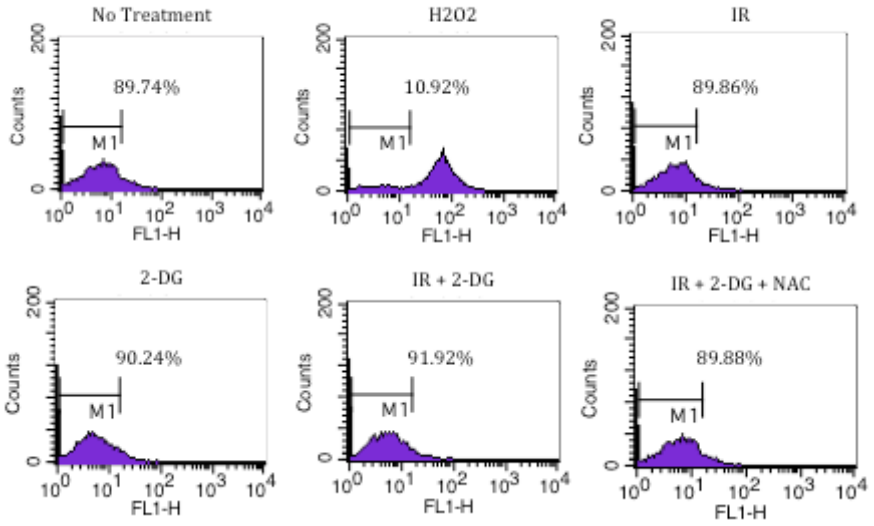

2 Hours

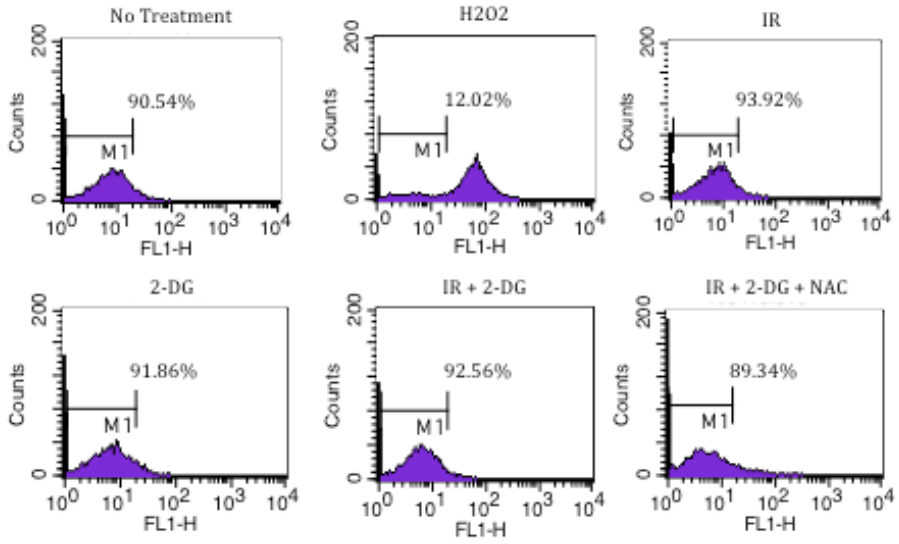

4 Hours

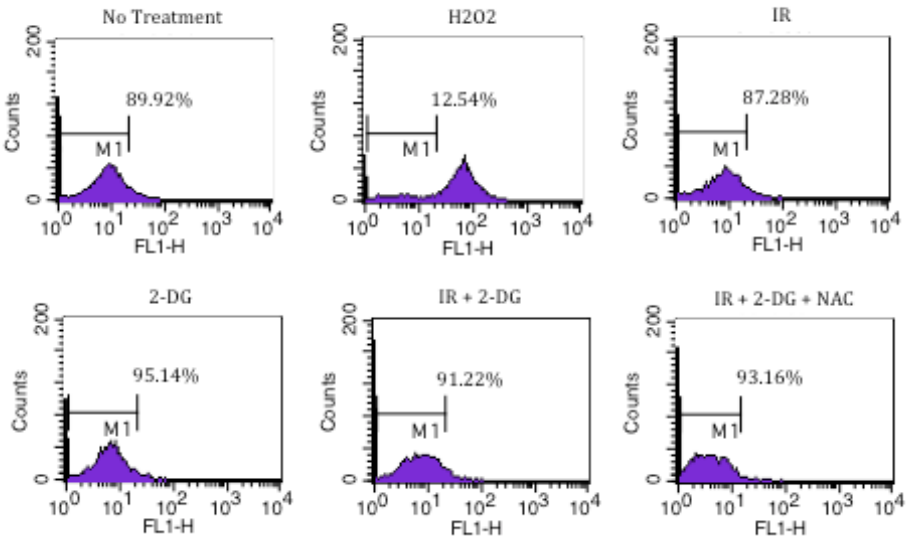

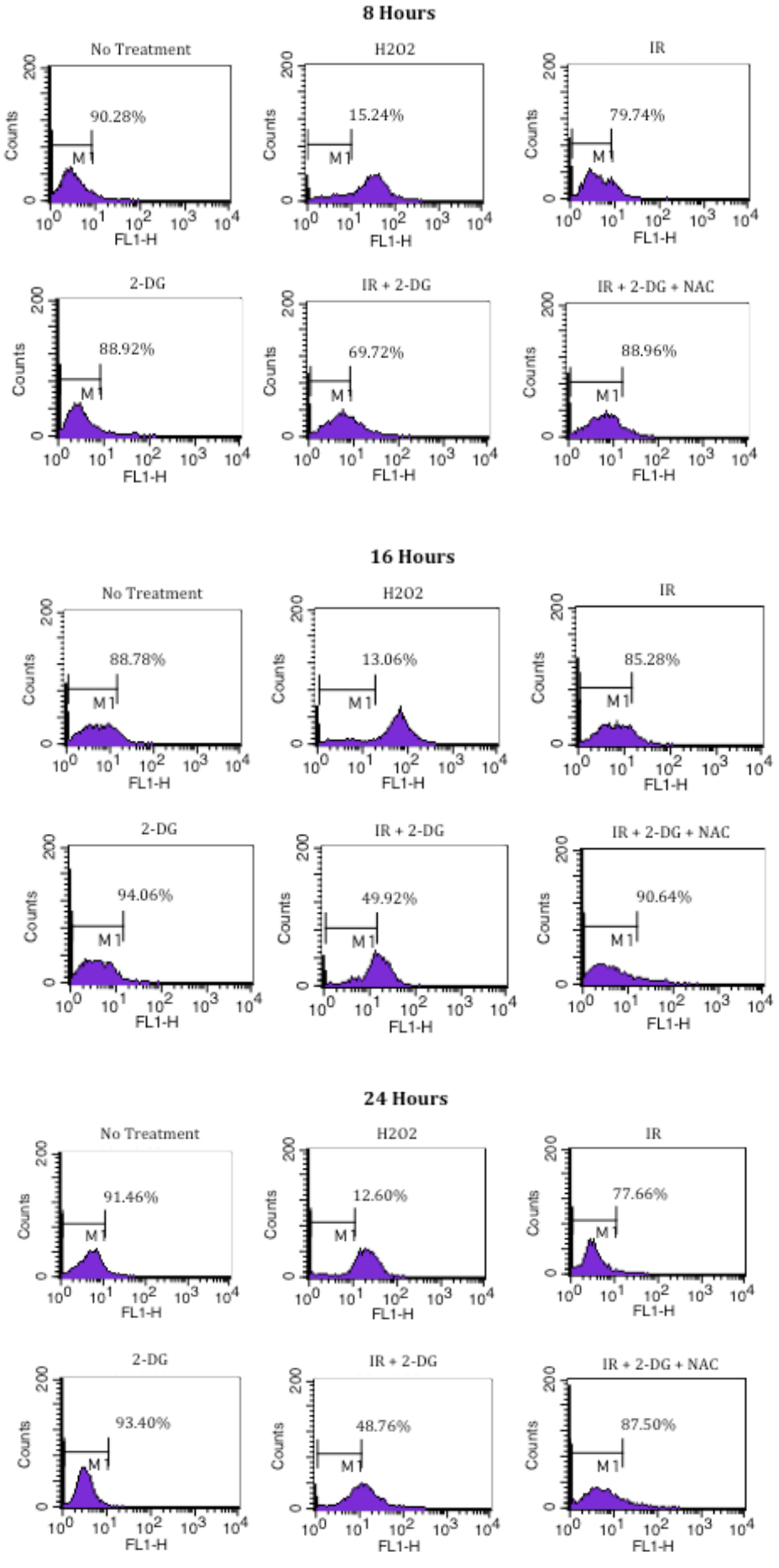
8 Hours
No Treatment
90.28%
H2O2
15.24%
IR
79.74%
2-DG
88.92%
IR + 2-DG
69.72%
IR + 2-DG + NAC
88.96%
16 Hours
No Treatment
88.78%
H2O2
13.06%
IR
85.28%
2-DG
94.06%
IR + 2-DG
49.92%
IR + 2-DG + NAC
90.64%
24 Hours
No Treatment
91.46%
H2O2
12.60%
IR
77.66%
2-DG
93.40%
IR + 2-DG
48.76%
IR + 2-DG + NAC
87.50%
Counts
FL1-H
M1

Figure 3.3.2.2: Time course analysis of intracellular ROS levels in UM-SCC-1 cells following treatment with IR with and without 2-DG. UM-SCC-1 cells were either left untreated or treated as follows: 100μM H_2O_2 alone, 6Gy IR alone, 6Gy IR following pre-treatment with 25mM 2-DG, 25mM 2-DG alone, or 6Gy IR following pre-treatment with 25mM 2-DG and 25mM NAC. Cells were then harvested at the indicated time points following treatment and stained with DCFH-DA and subjected to analysis by flow cytometry as described in Section 2.9. Results shown are representative of a typical experiment, all of which were performed at least in duplicate. The horizontal bars labelled M1 represent the gating, which was based on including approximately 90% of the cell population in the no treatment experiment to facilitate comparison of the shift in fluorescence under treatment conditions. The percentages depicted on each graph represent the proportion of cells falling within the gated parameter. A shift in fluorescence indicative of increased ROS was evident under IR and IR + 2-DG conditions from 8 hours and was maximal at 24 hours. It is also evident that in UM-SCC-1 there is a marked increase in ROS levels with the addition of 2-DG over IR alone and that this is then reversed by the addition of NAC.

Following treatment with IR alone and IR in combination with 2-DG, ROS levels increased from 8 hours post-treatment and were maximal at 24 hours. Consequently, 24 hours was the chosen time point for subsequent experiments with other SCCHN cell lines.

As detailed in section 2.8.1., during this project flow cytometry studies were conducted using two separate instruments owing to mechanical failure of the initial FACSCalibur™ instrument. Consequently, there are differing appearances of experimental output in the remainder of this section. In order to ensure that results were consistent between the two instruments, and thus experiments between cell lines comparable, an experiment with one cell line was repeated on both instruments to determine whether results were reproducible. Results are depicted in figure 3.3.2.3. and show broadly consistent results obtained between the two instruments.

A

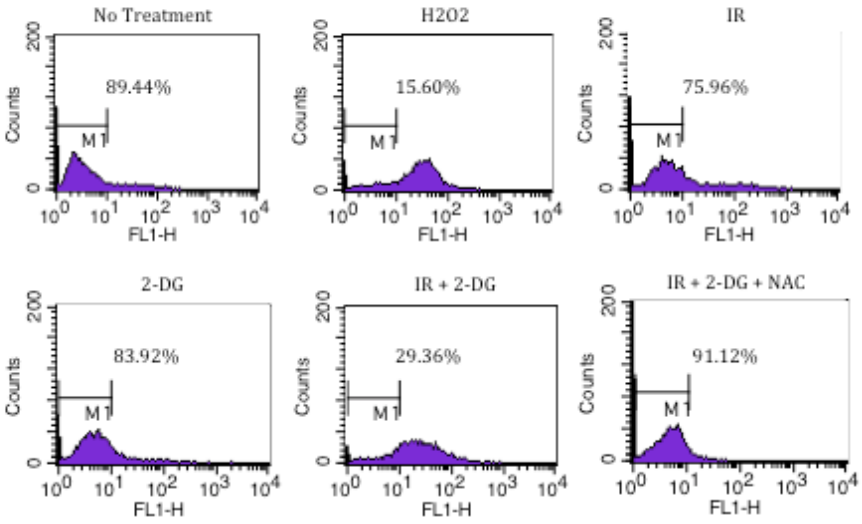

B

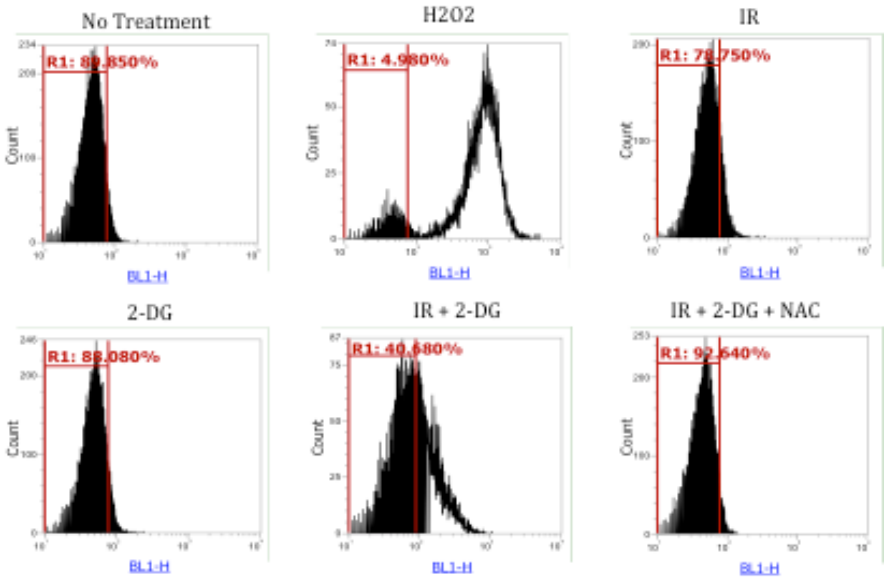

Figure 3.3.2.3: Analysis of intracellular ROS levels in a selected SCCHN cell line using two different flow cytometers. Cells were either left untreated or treated as follows: 100μM H_2O_2 alone, 6Gy IR alone, 6Gy IR following pre-treatment with 25mM 2-DG, 25mM 2-DG alone, or 6Gy IR following pre-treatment with 25mM 2-DG and 25mM NAC. Cells were then harvested 24 hours following treatment and stained with DCFH-DA and subjected to analysis by flow cytometry using the FACSCalibur™ instrument (A) or the Attune® acoustic focusing cytometer (B). Results shown are representative of a typical experiment, which was performed in duplicate. The horizontal bars labelled M1 in the case of the FACSCalibur™ instrument and R1 in the case the Attune® acoustic focusing cytometer represent the gating, which was based on including approximately 90% of the cell population in the no treatment experiment to facilitate

comparison of the shift in fluorescence under treatment conditions. The percentages depicted on each graph represent the proportion of cells falling within the gated parameter. Results are broadly consistent between the two instruments.

The results of subsequent experiments for other SCCHN cell lines with analysis performed 24 hours post-treatment are shown in figures 3.3.2.4 and 3.3.2.5.

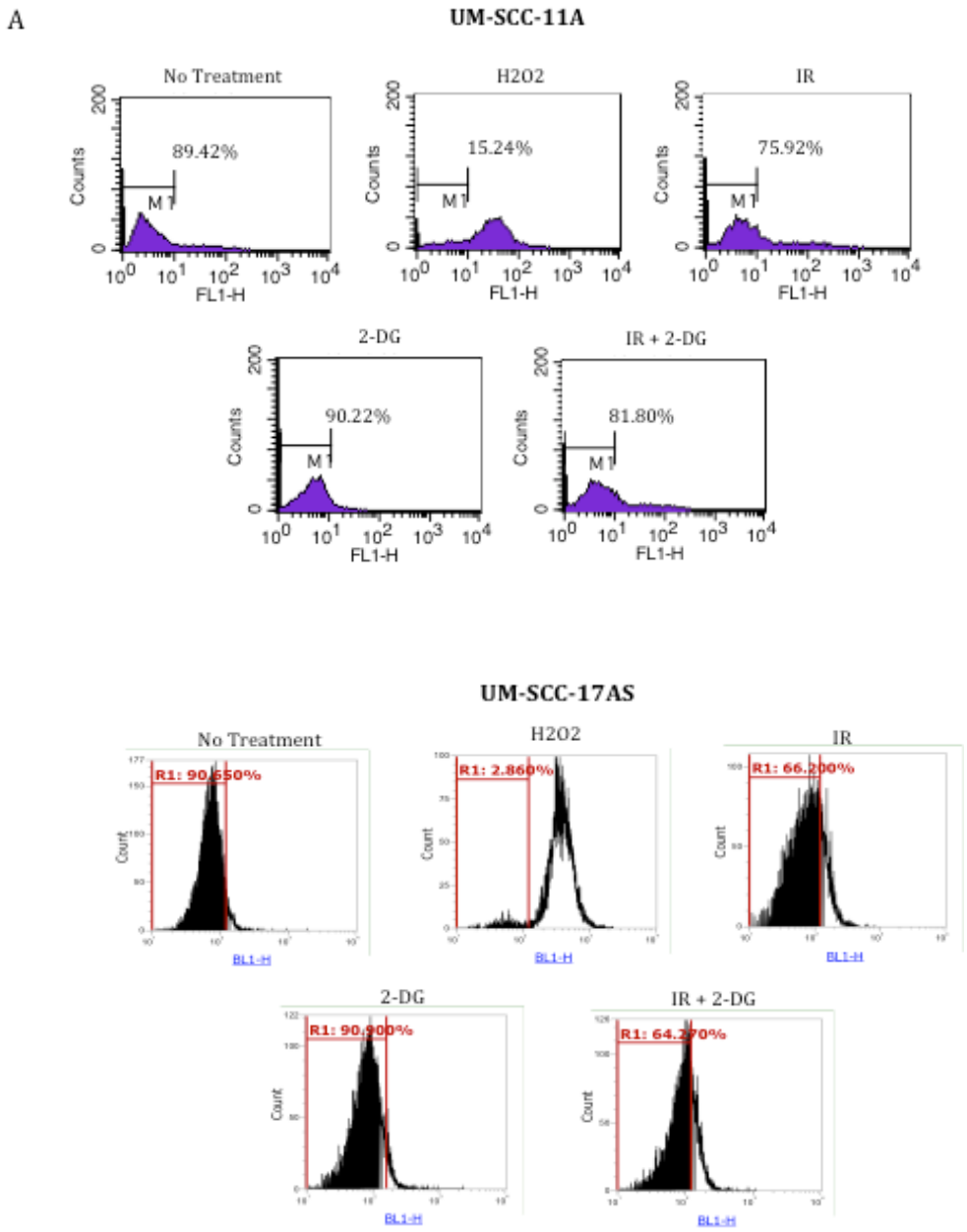

B

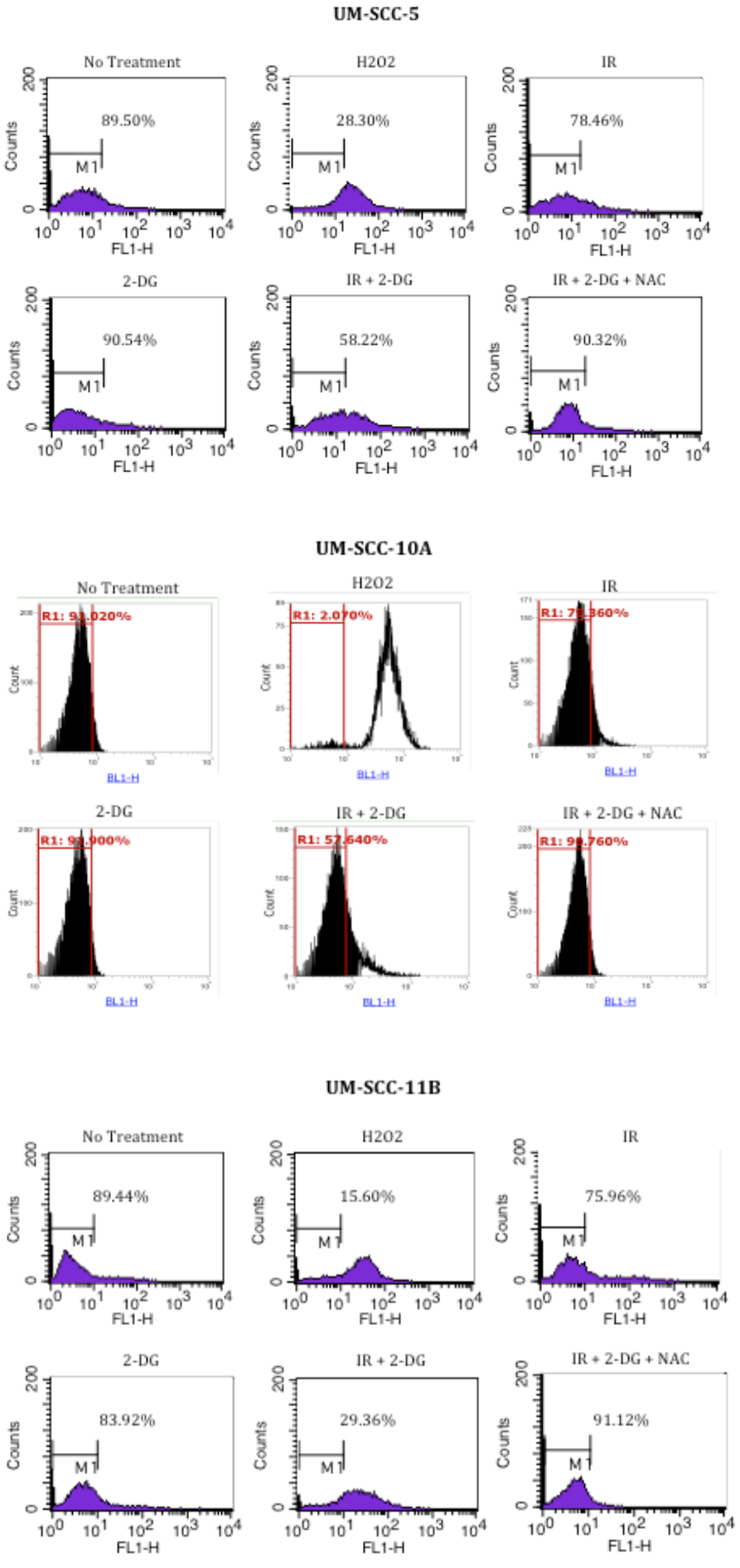
UM-SCC-5
No Treatment
89.50%
H2O2
28.30%
IR
78.46%
2-DG
90.54%
IR + 2-DG
58.22%
IR + 2-DG + NAC
90.32%
UM-SCC-10A
No Treatment
H2O2
IR
2-DG
IR + 2-DG
IR + 2-DG + NAC
UM-SCC-11B
No Treatment
89.44%
H2O2
15.60%
IR
75.96%
2-DG
83.92%
IR + 2-DG
29.36%
IR + 2-DG + NAC
91.12%
Counts
FL1-H
M1

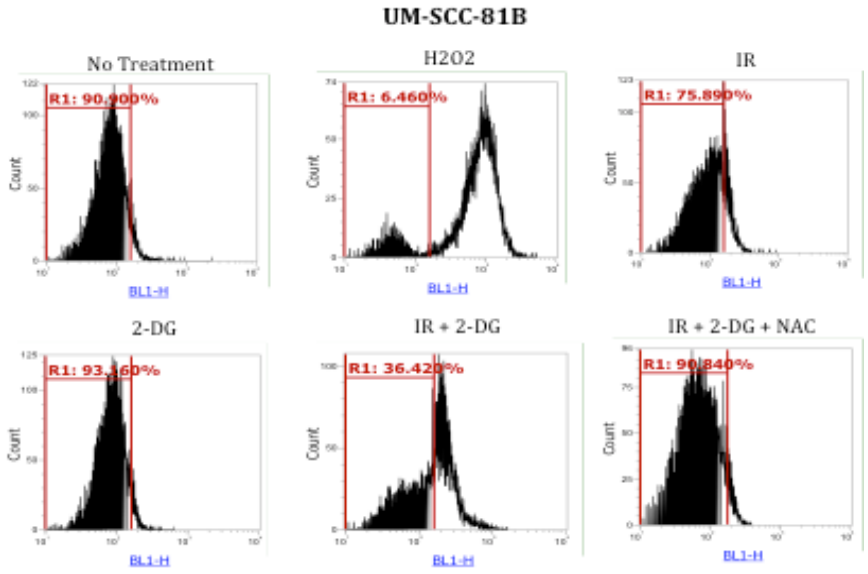

Figure 3.3.2.4: Analysis of intracellular ROS levels in the panel of SCCHN cells 24 hours following treatment with IR with and without 2-DG. Cells were either left untreated or treated as follows: 100μM H_2O_2 alone, 6Gy IR alone, 6Gy IR following pre-treatment with 25mM 2-DG, 25mM 2-DG alone, or 6Gy IR following pre-treatment with 25mM 2-DG and 25mM NAC. Cells were then harvested 24 hours following treatment and stained with DCFH-DA and subjected to analysis by flow cytometry as described in Section 2.9. Analysis following the addition of NAC was only undertaken if there was an observed effect to attempt to reverse with 2-DG. Results are shown for wild-type *TP53* SCCHN cell first (A) and mutant *TP53* cells subsequently (B). Results shown are representative of a typical experiment, all of which were performed at least in duplicate. The horizontal bars labelled M1 represent the gating, which was based on including approximately 90% of the cell population in the no treatment experiment to facilitate comparison of the shift in fluorescence under treatment conditions. The percentages depicted on each graph represent the proportion of cells falling within the gated parameter. A marked shift in fluorescence indicative of increased ROS was evident following treatment with IR + 2-DG compared with IR alone in mutant *TP53* cells but not in wild-type *TP53* cells, an effect that was reversed by the addition of NAC.

A

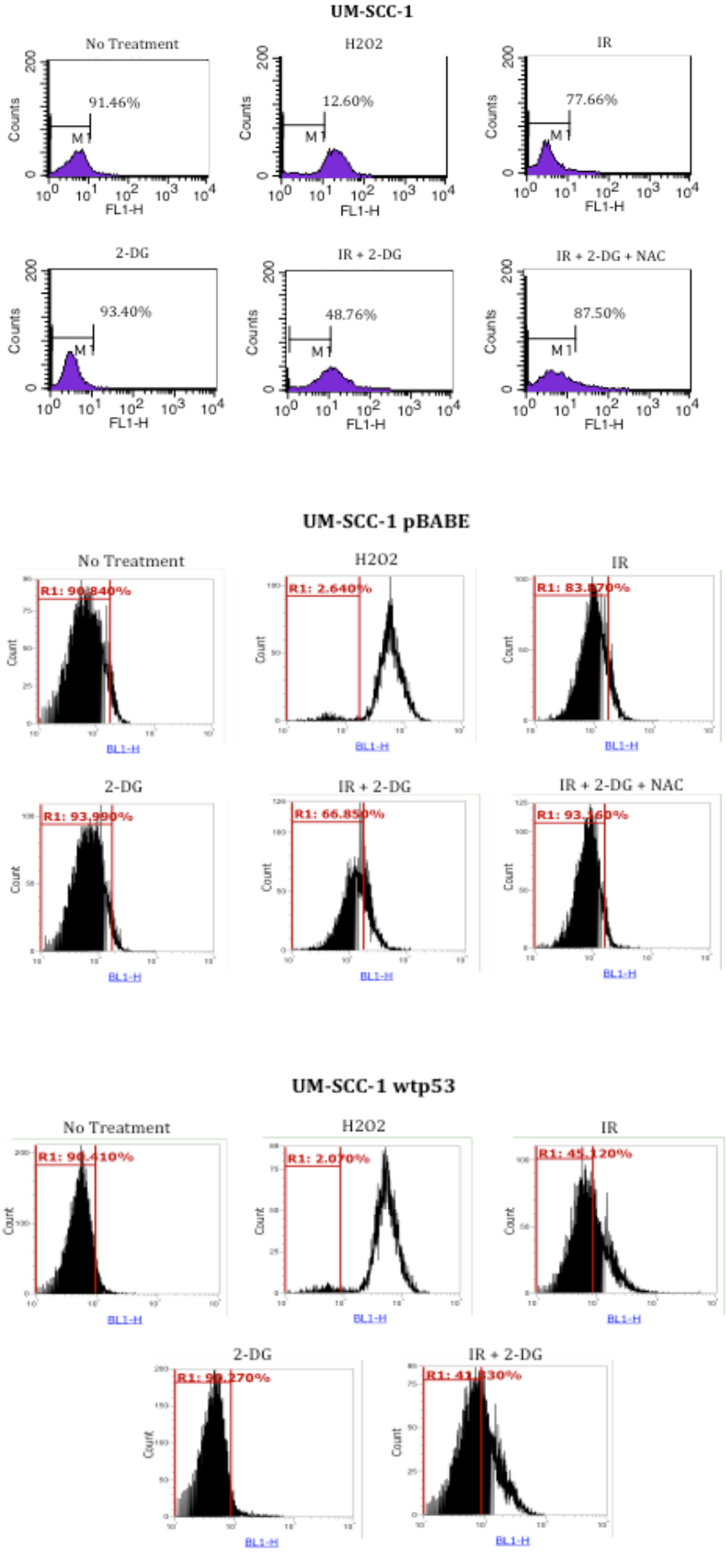
UM-SCC-1
No Treatment
91.46%
H2O2
12.60%
IR
77.66%
2-DG
93.40%
IR + 2-DG
48.76%
IR + 2-DG + NAC
87.50%
Counts
FL1-H
M1
UM-SCC-1 pBABE
No Treatment
R1: 90.840%
H2O2
R1: 2.640%
IR
R1: 83.870%
2-DG
R1: 93.990%
IR + 2-DG
R1: 66.850%
IR + 2-DG + NAC
R1: 93.160%
Count
BL1-H
UM-SCC-1 wtp53
No Treatment
R1: 90.410%
H2O2
R1: 2.070%
IR
R1: 45.120%
2-DG
R1: 90.270%
IR + 2-DG
R1: 41.830%

B

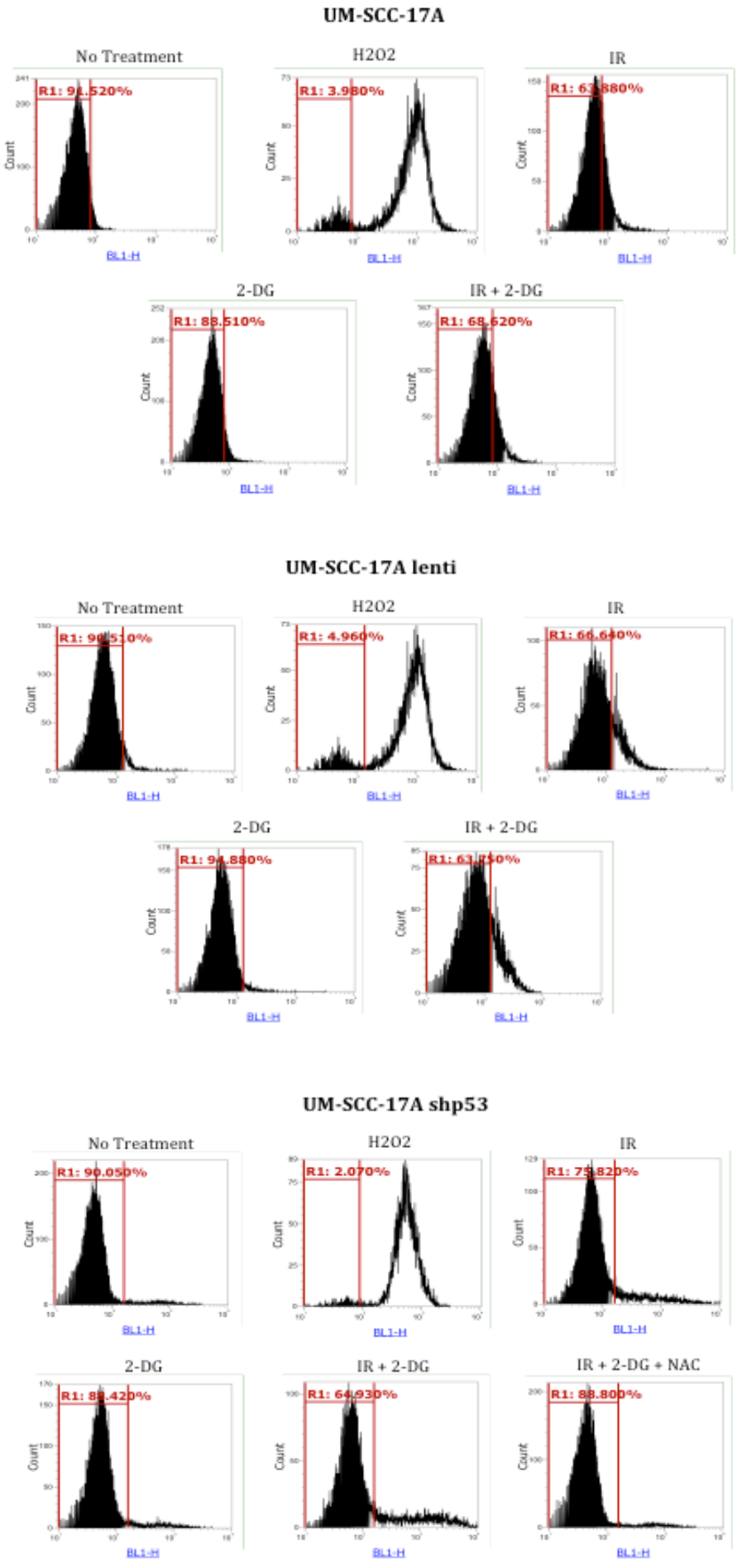
UM-SCC-17A
No Treatment
R1: 91.520%
H2O2
R1: 3.980%
IR
2-DG
R1: 88.510%
IR + 2-DG
R1: 68.620%
UM-SCC-17A lenti
No Treatment
H2O2
R1: 4.960%
IR
2-DG
IR + 2-DG
UM-SCC-17A shp53
No Treatment
R1: 90.050%
H2O2
R1: 2.070%
IR
R1: 75.820%
2-DG
IR + 2-DG
R1: 64.930%
IR + 2-DG + NAC
R1: 88.800%
Count
BL1-H

Figure 3.3.2.5: Analysis of intracellular ROS levels in isogenic SCCHN cells 24 hours following treatment with IR with and without 2-DG. Cells were either left untreated or treated as follows: 100μM H_2O_2 alone, 6Gy IR alone, 6Gy IR following pre-treatment with 25mM 2-DG, 25mM 2-DG alone, or 6Gy IR following pre-treatment with 25mM 2-DG and 25mM NAC. Cells were then harvested 24 hours following treatment and stained with DCFH-DA and subjected to analysis by flow cytometry as described in Section 2.9. Analysis following the addition of NAC was only undertaken if there was an observed effect to attempt to reverse with 2-DG. Results for UM-SCC-1 and derivative cells are shown first (A) and for UM-SCC-17A and derivative cell lines subsequently (B). Results shown are representative of a typical experiment, all of which were performed at least in duplicate. The horizontal bars labelled M1 represent the gating, which was based on including approximately 90% of the cell population in the no treatment experiment to facilitate comparison of the shift in fluorescence under treatment conditions. The percentages depicted on each graph represent the proportion of cells falling within the gated parameter. A marked shift in fluorescence indicative of increased ROS was evident following treatment with IR + 2-DG compared with IR alone in UM-SCC-1 and the empty vector control (pBABE), while forced expression of wild-type p53 in UM-SCC-1 resulted in a loss of this effect. Similarly, UM-SCC-17A and the empty vector control (lenti) displayed no difference in ROS levels between IR and IR + 2-DG conditions, while stable knockdown of wild-type p53 resulted in a discernible increase in ROS following treatment with IR + 2-DG compared with IR alone.

In keeping with our previous clonogenic assay results, where the addition of NAC reversed the potentiating effects of 2-DG on IR in SCCHN cells with loss of wild-type p53 function, the addition of 2-DG to IR resulted in a marked increase in ROS compared to IR alone in such cells, an effect which was reversed by the further addition of NAC. These findings are consistent with the hypothesis that the mechanism underlying the potential therapeutic effects of glycolytic inhibition involves inhibition of detoxifying antioxidant systems (since these cells have no capacity for increasing ETC), and supports the notion that the rationale behind metabolic re-programming towards glycolysis in cancer cells is at least partly to regulate cellular redox status. These findings are also in keeping with those of numerous studies of drug-induced glycolytic inhibition in cancer cells generally(402, 411, 412), and also with those of the limited number of studies in SCCHN(354, 359, 360). For instance, in studies specific to SCCHN glycolytic inhibition has been shown to cause perturbations in parameters indicative of oxidative stress, including decreased intracellular total glutathione with a reduced proportion of GSH(354), lessened cellular reducing potential(359), and significantly elevated ROS levels(360). Furthermore, simultaneous treatment with NAC has been shown to inhibit such parameters and reverse the cytotoxic effects of glycolytic inhibition(354, 359, 360).

Given that generation of the reducing equivalent NADPH is crucial for the up-regulation of major cellular antioxidant systems, specifically glutathione and thioredoxin systems, and that the PPP is the principal source of NADPH(280), it seems likely that glycolytic inhibition with 2-DG is dampening PPP flux and thus NADPH generation, leading to a loss of ROS quenching capacity. Indeed, our previous observations that the PPP inhibitor 6-AN further potentiated the effects of 2-DG on IR supports this suggestion and the involvement of the PPP will be examined in greater detail later in this thesis (section 3.4.5.).

3.3.3. The potentiating effects of 2-DG on IR in SCCHN cells with loss of functional wild-type p53 are not a consequence of increased cellular senescence

Having shown that inhibition of cellular detoxifying antioxidant systems and associated oxidative stress is involved in the mechanism underlying the potentiating effects of glycolytic inhibition on IR in SCCHN cells with loss of wild-type p53 function, we next examined this mechanism further in terms of cell fate. Cellular senescence was first investigated as a possible mechanism as high levels of ROS can result in activation of protein kinase Cδ, prompting senescence(227), and ROS are thought to be necessary for maintenance of the senescent phenotype(225, 226). Furthermore, although the exact role of senescence in the response to radiation remains to be elucidated, senescence is becoming increasingly recognised as an important contributor to radiation response(413, 418), and has been shown to be crucial in determining radio-sensitivity or radio-resistance in SCCHN cell lines(57).

As described in section 2.7. cellular senescence was assessed using cytochemical SA-βgal staining. Cells were either left untreated or treated with 6Gy IR alone, or 6Gy IR following pre-treatment with 25mM 2-DG, and after 24 hours were fixed and stained at pH 6.0. Results are depicted in figure 3.3.3.1. Interestingly, in all SCCHN cells there was a significant increase in the proportion of senescent cells following treatment with IR and 2-DG relative to IR alone, irrespective of *TP53* status. As such, although cellular senescence is increased under conditions of IR and 2-DG it is unlikely to underlie the potentiating effects of 2-DG on IR as these effects were specific to those SCCHN cells with abrogated wild-type p53 function. Although higher levels of cellular senescence were observed in SCCHN cells maintaining wild-type p53 function, it is perhaps surprising that there are such high levels of cellular senescence in the mutant *TP53* SCCHN cell lines considering that cellular senescence is thought to be significantly

dependent upon wild-type p53 function(418). SA-βgal activity is distinguished from the acidic β-galactosidase activity, present in all cells, by using a citric acid/sodium phosphate buffer at suboptimal pH, and it is possible that failure of this buffer to maintain the pH at 6.0 resulted in detection of acidic β-galactosidase activity. However, acidic β-galactosidase activity is a surrogate of lysosomal content, and the fact that signal did vary with treatment makes this an improbable explanation. Induction of p21, a transcriptional target of p53, is a critical mediator of cellular senescence and is proposed to be involved in a feedback loop with ROS, which is required for DNA damage-induced senescence(57, 225). The senescence observed in mutant *TP53* SCCHN cells here may, therefore, be the result of p53-independent induction of p21, as has been described elsewhere(419, 420), or may be attributable to residual p53 transcriptional activity. Indeed, recent findings have suggested that only a minority of p53 transcriptional targets are required to prompt senescence(421), with a small remnant of transcriptional function conceivably sufficient to induce senescence.

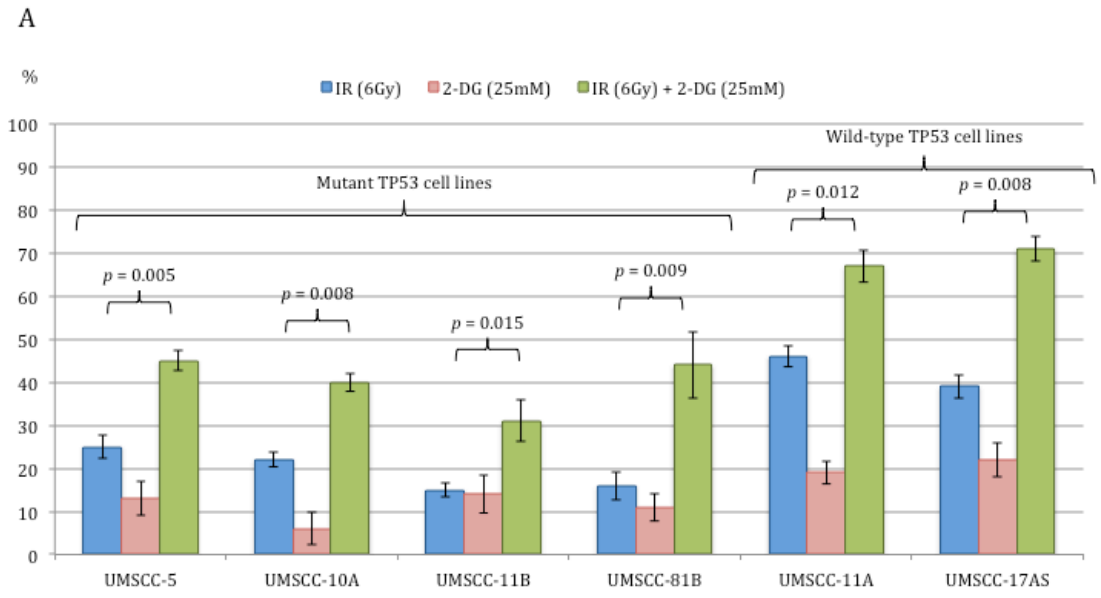

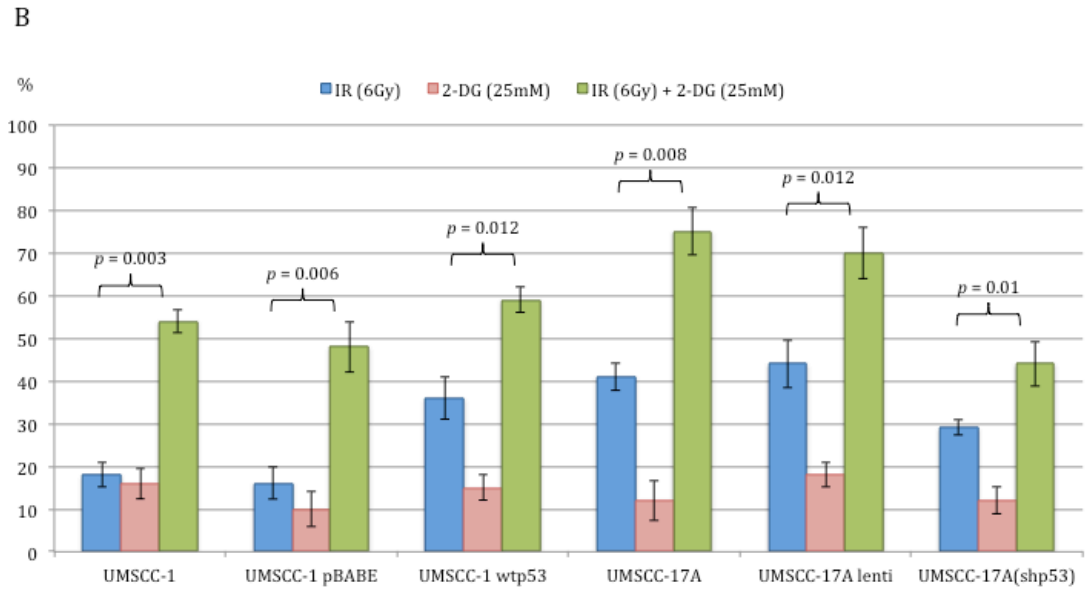

Figure 3.3.3.1: Levels of cellular senescence in SCCHN cells following treatment with IR with and without 2-DG. Following either no treatment or treatment with 6Gy IR alone or in the presence of 25mM 2-DG, cells were fixed and then incubated for 16 hours in staining solution as described in section 2.7. The proportion of senescent cells in the population was then determined by manual counting under bright field microscopy. Results are first shown for the panel of SCCHN cell lines (A) and subsequently for the isogenic SCCHN cell lines (B). Experiments were performed in triplicate with mean values depicted in the histograms and SEMs represented by error bars. Statistical significance was tested for any differences using the Mann–Whitney *U* test with a significance level of $p \leq 0.05$. All results shown are normalised to the proportion of senescent cells identified following no treatment for that particular cell line. Significant increases in the proportion of senescent cells were observed following treatment with IR + 2-DG compared with IR alone in both mutant and wild-type *TP53* SCCHN cells (A). This was also the case for isogenic cell lines, where all cell lines exhibited a significant increase in senescence following treatment with IR + 2-DG over and above IR alone (B).

3.3.4. Apoptosis underlies the potentiating effects of 2-DG on IR in SCCHN cells with loss of functional wild-type p53

Following the demonstration that the effects of 2-DG on IR in SCCHN cells with abrogated wild-type p53 function is not attributable to cellular senescence, we next investigated apoptosis as a possible mechanism. High levels of ROS can result in permeabilisation of mitochondria leading to cytochrome c release and apoptosis(192), and induction of apoptosis is an important factor in determining therapeutic response to anti-cancer treatments(186, 414). In order to measure levels of apoptosis, differential staining with FITC-conjugated annexin V and PI, analysed by flow cytometry was used as described in section 2.8. Cells were treated with 6Gy IR alone, 25mM 2-DG alone, or

6Gy IR following pre-treatment with 25mM 2-DG, with positive and negative controls for each experiment comprising 1μM staurosporine and no treatment respectively. Again, as detailed in section 2.8.1., during this project flow cytometry studies were conducted using two separate instruments owing to mechanical failure of the initial FACSCalibur™ instrument, and is the reason for the differing appearance of experimental output in this section. In section 3.3.2. it was demonstrated that output for ROS detection and quantification was broadly consistent between the two instruments, allowing comparison between experiments performed on the two instruments. Similarly, in order to ensure that results pertaining to the detection of apoptosis were also consistent between the instruments, detection of annexin V and PI staining with one cell line was repeated on both instruments. Results are depicted in figure 3.3.4.1 and show congruous results between the two instruments.

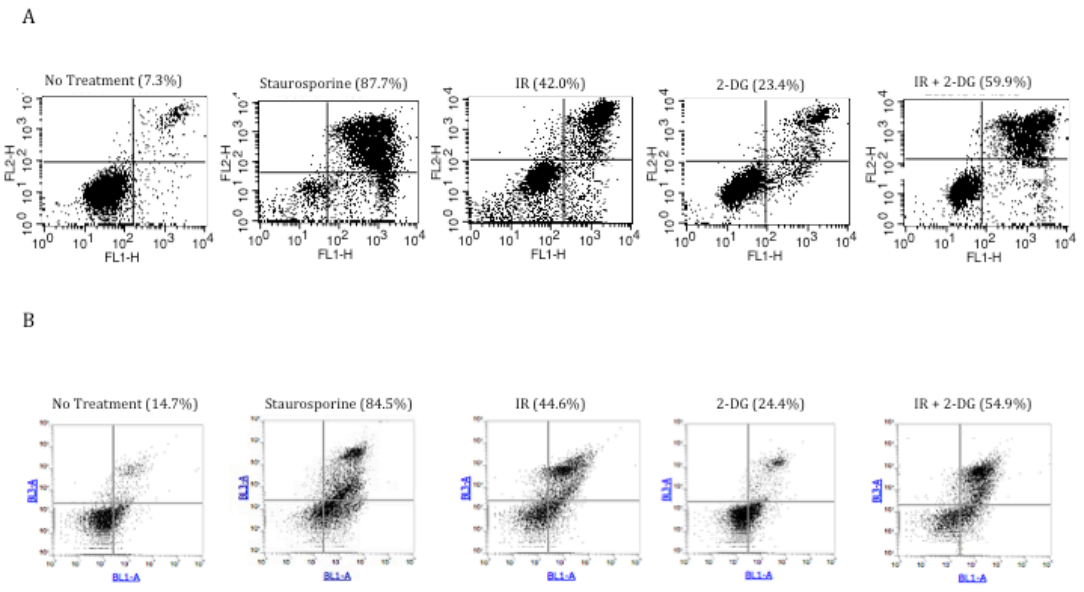

Figure 3.3.4.1: Analysis of levels of apoptosis in a selected SCCHN cell line using two different flow cytometers. 48 hours following treatment with 6Gy IR alone, 25mM 2-DG alone or combined treatment, cells were stained with annexin V and PI and subjected to analysis by flow cytometry using the FACSCalibur™ instrument (A) or the Attune® acoustic focusing cytometer (B). Results shown are representative of a typical experiment, which was performed in duplicate. Percentages shown represent the proportion of apoptotic cells (early and late combined), which is the proportion of cells in the upper and lower right quadrants combined. Results are broadly consistent between the two instruments.

All SCCHN cell lines were harvested and subjected to annexin V and PI staining and flow cytometric analysis at both 24 and 48 hour time points. Results are shown in figures 3.3.4.2. and 3.3.4.3.

A

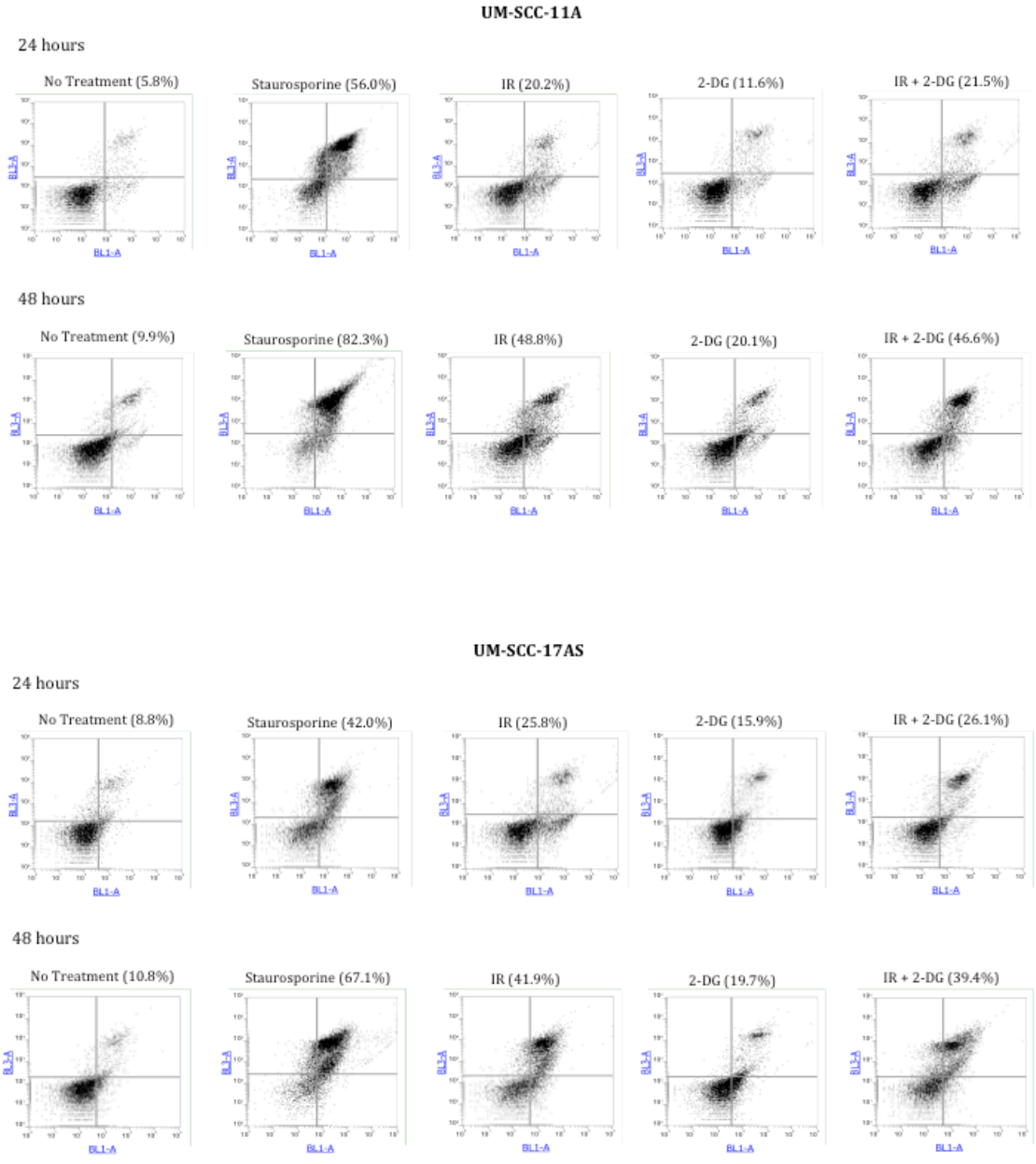

B

UM-SCC-5

24 hours

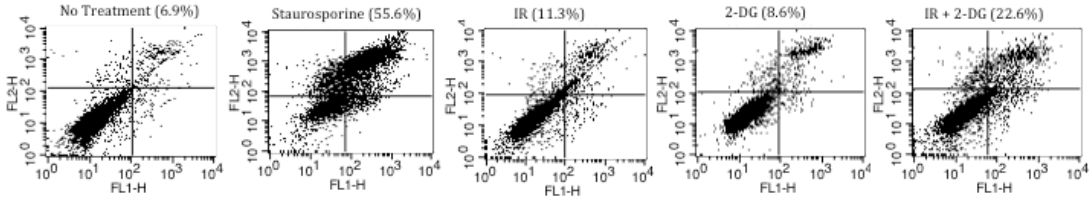

48 hours

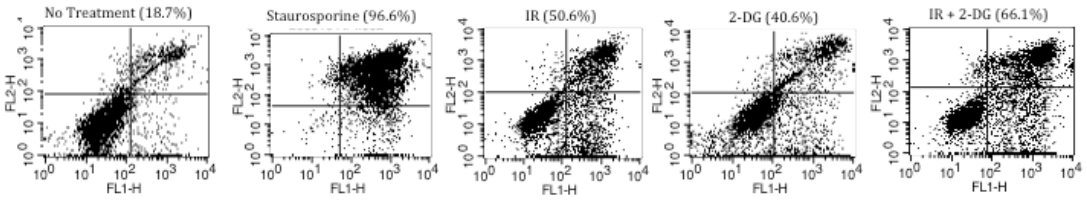

UM-SCC-10A

24 hours

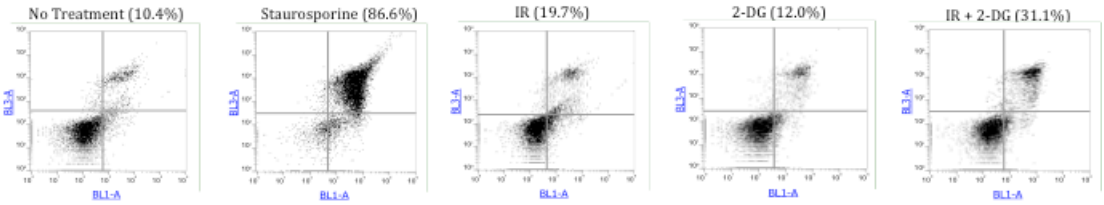

48 hours

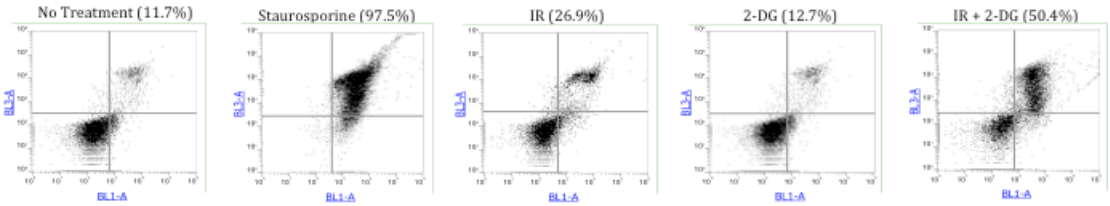

UM-SCC-11B

24 hours

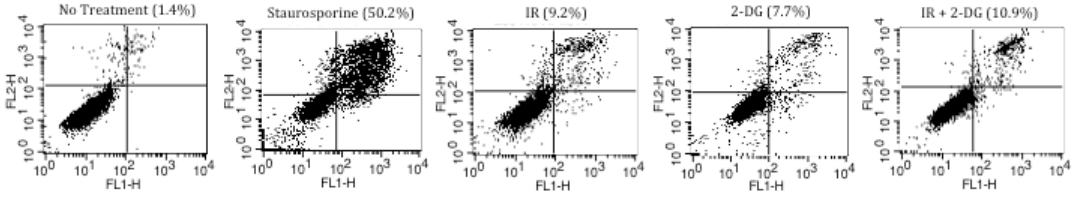

48 hours

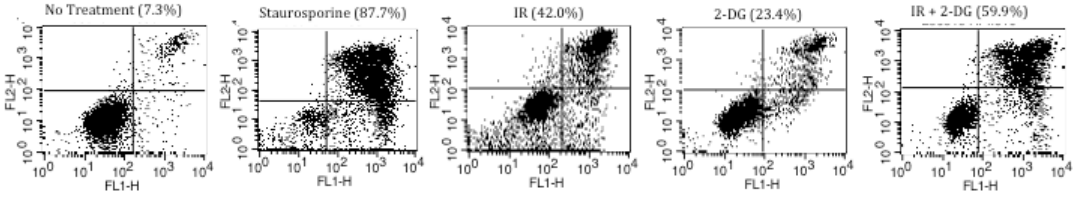

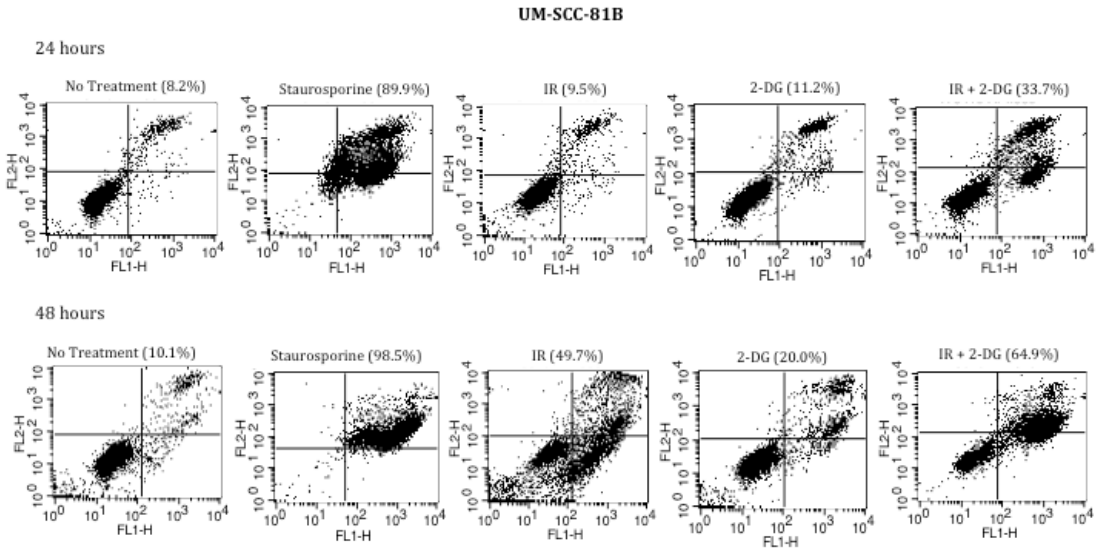

Figure 3.3.4.2: Levels of apoptosis in the panel SCCHN cells following treatment with IR with and without 2-DG. Following treatment with 6Gy IR alone, 25mM 2-DG alone or combined treatment, cells were stained with annexin V and PI and analysed by flow cytometry as described in section 2.8. at 24 and 48 hours. Results are first shown for wild-type *TP53* SCCHN cell lines (A) and subsequently for mutant *TP53* SCCHN cell lines (B). Results shown are representative of typical experiments, which were performed at least in duplicate. Percentages shown represent the proportion of apoptotic cells (early and late combined), which is the proportion of cells in the upper and lower right quadrants combined. Discernible increases in the proportion of apoptotic cells were observed following treatment with IR + 2-DG compared with IR alone in mutant but not wild-type *TP53* SCCHN cells, most evident at either 24 or 48 hours depending on individual cell line.

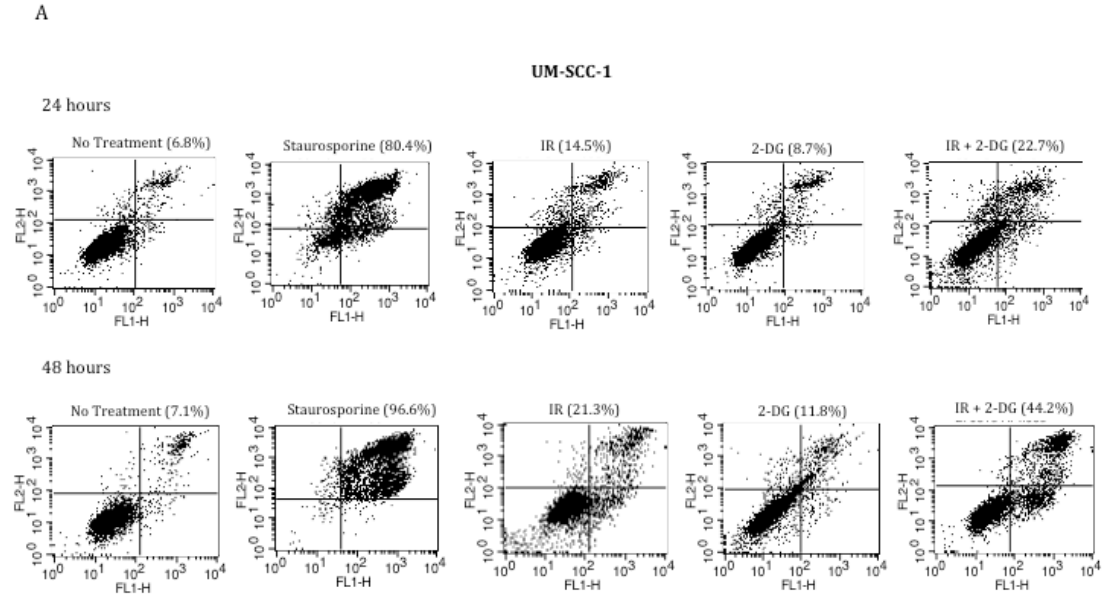

UM-SCC-1 pBABE

24 hours

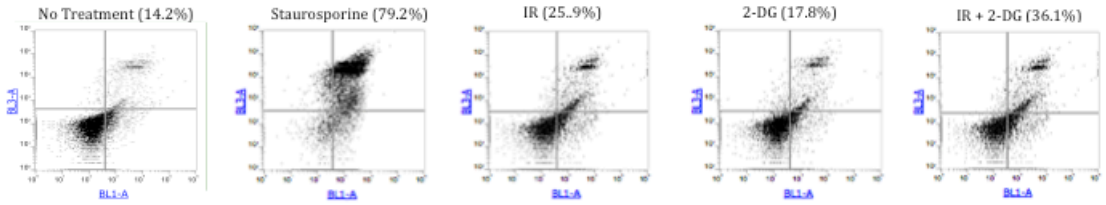

48 hours

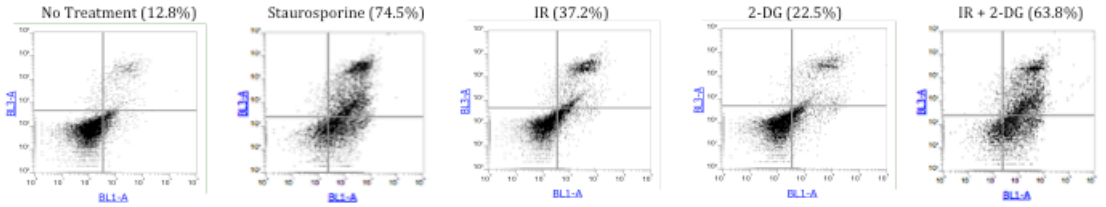

UM-SCC-1 wtp53

24 hours

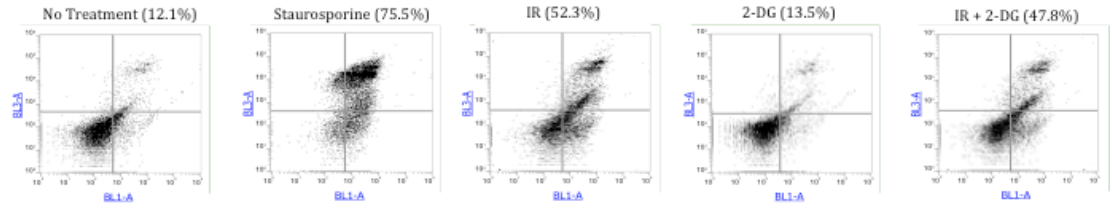

48 hours

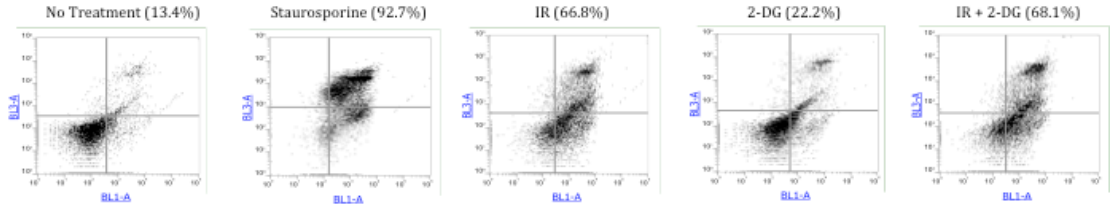

B

UM-SCC-17A

24 hours

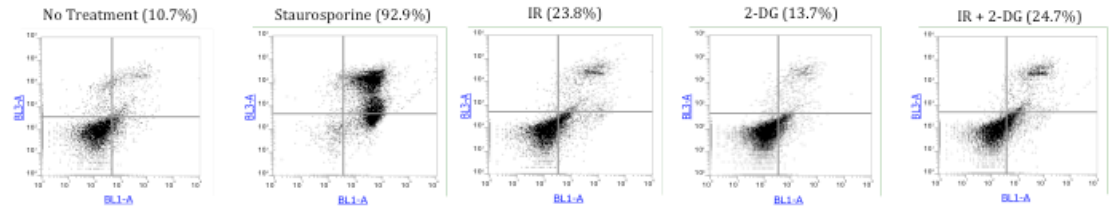

48 hours

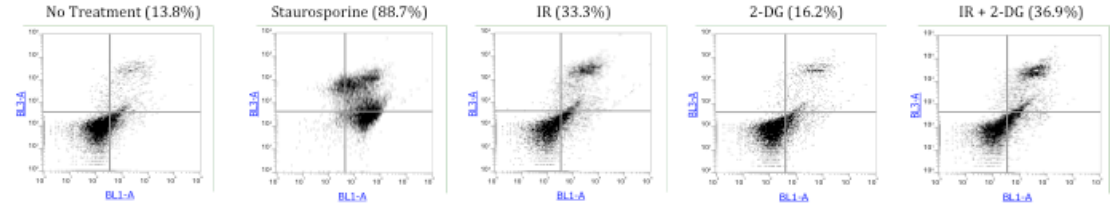

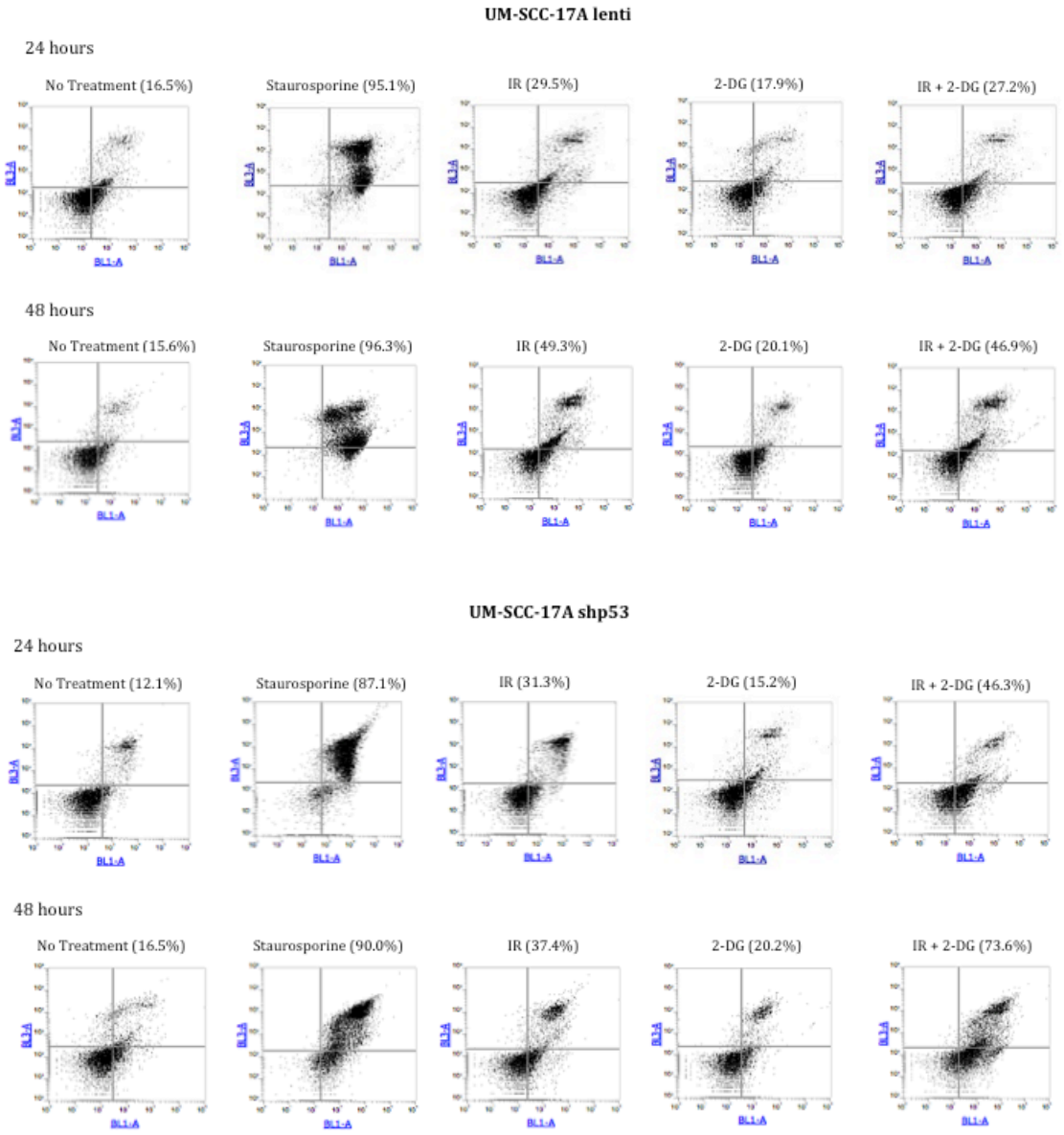

Figure 3.3.4.3: Levels of apoptosis in isogenic SCCHN cells following treatment with IR with and without 2-DG. Following treatment with 6Gy IR alone, 25mM 2-DG alone or combined treatment, cells were stained with annexin V and PI and analysed by flow cytometry as described in section 2.8. at 24 and 48 hours. Results are first shown for UM-SCC-1 and derivative cell lines (A) and subsequently for UM-SCC-17A and derivative cell lines (B). Results shown are representative of typical experiments, which were performed at least in duplicate. Percentages shown represent the proportion of apoptotic cells (early and late combined), which is the proportion of cells in the upper and lower right quadrants combined. Discernible increases in the proportion of apoptotic cells were observed following treatment with IR + 2-DG compared with IR alone in UM-SCC-1 and the empty vector control (pBABE), while forced expression of wild-type p53 in UM-SCC-1 resulted in a loss of this effect. Similarly, UM-SCC-17A and the empty vector control (lenti) displayed no difference in levels of apoptosis between IR and IR + 2-DG

conditions, while in the stable wild-type p53 knockdown cell line there was an obvious increase in apoptosis following treatment with IR + 2-DG compared with IR alone.

Intriguingly, a clear increase in the proportion of apoptotic cells was observed following IR in the presence of glycolytic inhibition relative to IR alone exclusively in SCCHN cells harbouring *TP53* mutations or wild-type p53 knock-down, and thus is the likely mechanism of cell-death correlating with the potentiating effects of 2-DG on IR observed earlier. Consistent with this, a previous study examining the effects of 2-DG on several cancer cell lines of diverse origin demonstrated that although response was variable among cell lines, moderate to high levels of apoptosis were present, characterised by morphological modifications, altered nuclear morphology, sub-G1 peak occurrence, caspase-3 activation and PARP cleavage(357). Moreover, a similar study also investigating the effects of glycolytic inhibition on a number of human tumour cell lines, demonstrated the activation of death receptor-induced apoptosis, related to increased processing of apical procaspase-8 at the DISC upon death receptor activation(415). In terms of deciphering a link between glycolytic inhibition and the induction of apoptosis, a role for hexokinase has been suggested. Danial et al reported that hexokinase IV interacts with the pro-apoptotic protein Bad in a mitochondrial complex, where the phosphorylation status of Bad is regulated, which in turn regulates both apoptosis and glycolysis(422). Similarly, a subsequent study reported that inhibition of hexokinase with 3-BP resulted in dephosphorylation of Bad, leading to translocation of the pro-apoptotic factor Bax to the mitochondria, thereby activating the release of cytochrome c and the caspase cascade(423). Alternatively, and in line with our ROS data, a number of studies have implicated cellular redox state in coupling glycolytic inhibition and apoptosis. In a study of c-Myc-transformed cells, potent induction of apoptosis was observed following glycolytic inhibition, mediated by induction of LDH-A activity, that led to constitutive generation of NAD and lactate and a decrease in the regeneration of NADH, which the authors proposed to alter the cellular redox state increasing susceptibility to apoptosis(424). Interestingly, these effects also appeared to be independent of wild-type p53 activity(424). Similarly, in a study of tumour necrosis factor (TNF)-induced cytotoxicity of fibrosarcoma cells, the absence of glucose increased production of ROS, sensitising the cells to death receptor-mediated apoptosis(425). More recently, Vaughn and Deshmukh showed that the pro-apoptotic activity of cytochrome c is influenced by its redox state: cytochrome c is held in its reduced and inactive form by intracellular GSH, generated as a result of glycolysis and the PPP, while increases in ROS lead to the oxidation and activation of cytochrome c(192).

3.4. Investigating the mechanisms underpinning the metabolic shift in mutant *TP53* SCCHN

3.4.1. Introduction

Having established in section 3.1. that in SCCHN the metabolic profile differs markedly on the basis of *TP53* status, with the loss of functional wild-type p53 conferring loss of metabolic diversity and glycolytic dependence, and having correlated this with anti-metabolic therapeutic potential in sections 3.2. and 3.3., we next sought to explore the mechanistic basis underpinning this *TP53*-dependent metabolic switch.

p53 plays a fundamental role in regulating metabolic homeostasis, balancing mitochondrial respiration and glycolysis. True to its role as a tumour suppressor and in keeping with our findings, p53 is thought to counteract metabolic alterations characteristically associated with cancer development, with loss of wild-type p53 function, therefore, leading to acquisition of a glycolytic phenotype at the expense of mitochondrial respiration(247, 267, 294). As discussed in depth earlier in section 1.3.2., p53 exerts influence over glycolysis through multiple mechanisms, which may also modulate activity of related subsidiary pathways. p53 is known to down-regulate the expression of the glycolytic transporters, including GLUT1, GLUT4, and MCT-1(298, 299), as well as influence the activity of the following glycolytic enzymes: hexokinase-II(318); PGAM(295); PDK(297); and PFK-1 through transcription of TIGAR, which acts as a bisphosphatase that dephosphorylates fructose-2,6-bisphosphate – a potent allosteric activator of PFK-1(205). Complementary to these actions to restrict glycolytic flux, p53 is also coupled to the maintenance of mitochondrial biomass, integrity, and quality control(300-303), as well as the promotion of oxidative phosphorylation, through transcriptional activation of Parkin(304) and genes involved in the assembly of the ETC complexes(286, 305-308), as well as transcription independent assembly of the ATP synthase complex(309). Given the paucity of published data concerning the mechanisms by which *TP53* status may influence metabolism in SCCHN specifically, our investigation into the mechanistic basis underpinning the *TP53*-dependent metabolic switch was focused around the above evidence of the influence of p53 on metabolic homeostasis.

3.4.2. Depressed ETC complex activity is involved in the TP53-dependent metabolic switch in SCCHN cells

Although contemporary studies have revealed that mitochondrial function is frequently unimpaired in cancer cells and many tumours retain the capacity for oxidative phosphorylation(249, 258-261), as discussed previously p53 is crucially involved in maintenance of mitochondrial function (see section 1.3.2.), and thus loss of wild-type p53 function could conceivably result in disruption to oxidative phosphorylation. Furthermore, our earlier findings that maximal respiration and ATP-linked respiration is consistently reduced in SCCHN cells with abrogated wild-type p53 function compared with wild-type *TP53* cells (section 3.1.3.) is suggestive of compromised ETC function in these cells. We, therefore, interrogated the activity of individual ETC complexes in SCCHN cells using the Seahorse Bioscience microplate-based XF24 experimental platform in combination with a selective plasma membrane permeabiliser (XF PMP) and specific oxidisable substrates, as outlined in section 2.4.9.

Many oxidisable substrates are unable to cross the plasma membrane freely, preventing control over which substrates the mitochondria are oxidising(385, 386) (see figure 2.3.9.1.). Recognising the fact that specific substrates feed differentially into mitochondrial pathways, permeabilising cells using XF PMP and supplying specific oxidisable substrates and ETC complex inhibitors affords this experimental control, and enables identification of any defects in function of ETC complexes responsible for the altered OCR originally observed in intact cells(385, 386). As detailed in section 2.4.9., cells were subjected to mitochondrial stress tests (section 2.3.7.) in the presence of 1nM XF PMP and various oxidisable substrates to assess the activity of individual ETC complexes. Substrates bypassing potentially defective ETC complexes were sequentially added, along with relevant inhibitors, in each new experiment for each individual cell line to determine whether any OCR defects could be rescued. In initial experiments, the NADH-linked complex I substrates pyruvate (10mM) and glutamate (10mM) were added. Subsequently, in order to bypass ETC complexes and analyse OCRs attributable to the remaining ETC complexes, the following substrates and inhibitors were supplied: succinate (10mM) with rotenone (2μM) to bypass and inhibit complex I; glycerol-3-phosphate (10mM) with malonate (20mM) to bypass and inhibit complex II; and ascorbate (10mM) and TMPD (100μM) with antimycin A (2μM) to bypass and inhibit complex III. As these experiments were designed to attempt to rescue any originally identified defects in the function of mitochondrial respiration, only those cell lines with

identified defects were included – i.e. cells lines with abrogation of wild-type p53 function. Results are shown in figures 3.4.2.1.

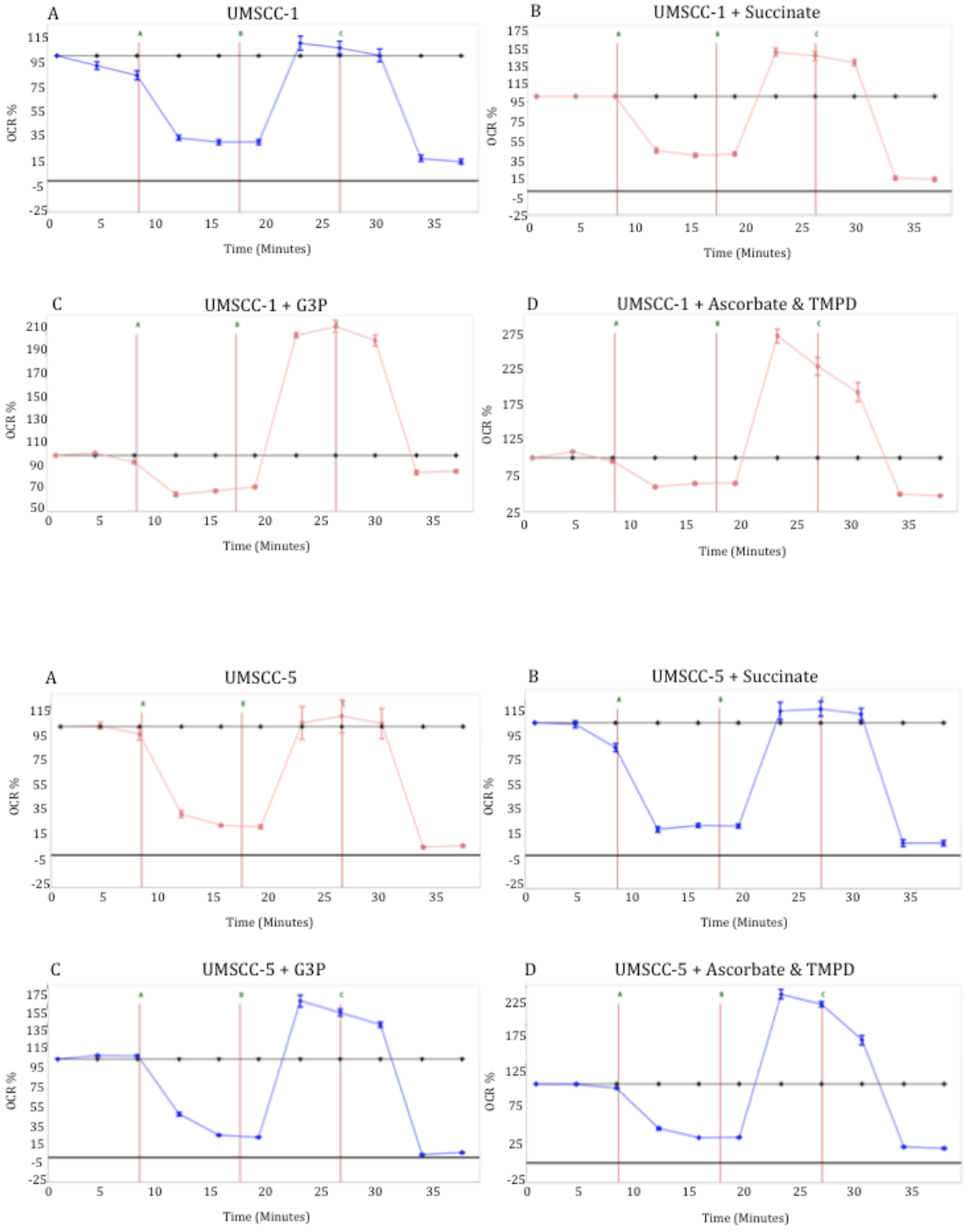

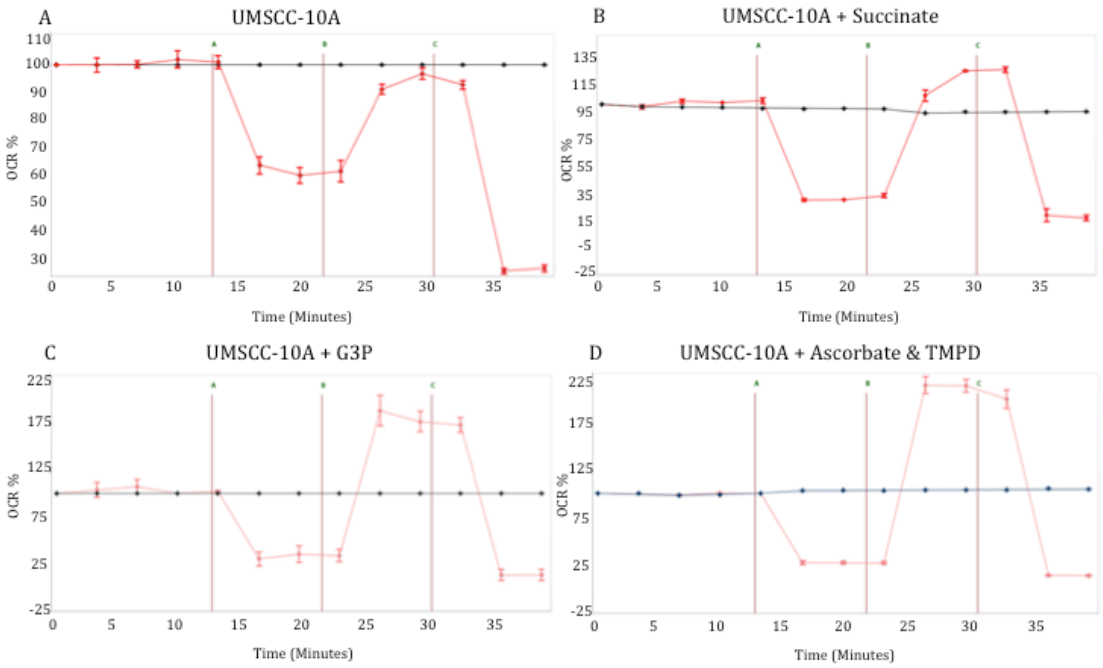
A
UMSCC-10A
B
UMSCC-10A + Succinate
C
UMSCC-10A + G3P
D
UMSCC-10A + Ascorbate & TMPD
OCR %
Time (Minutes)

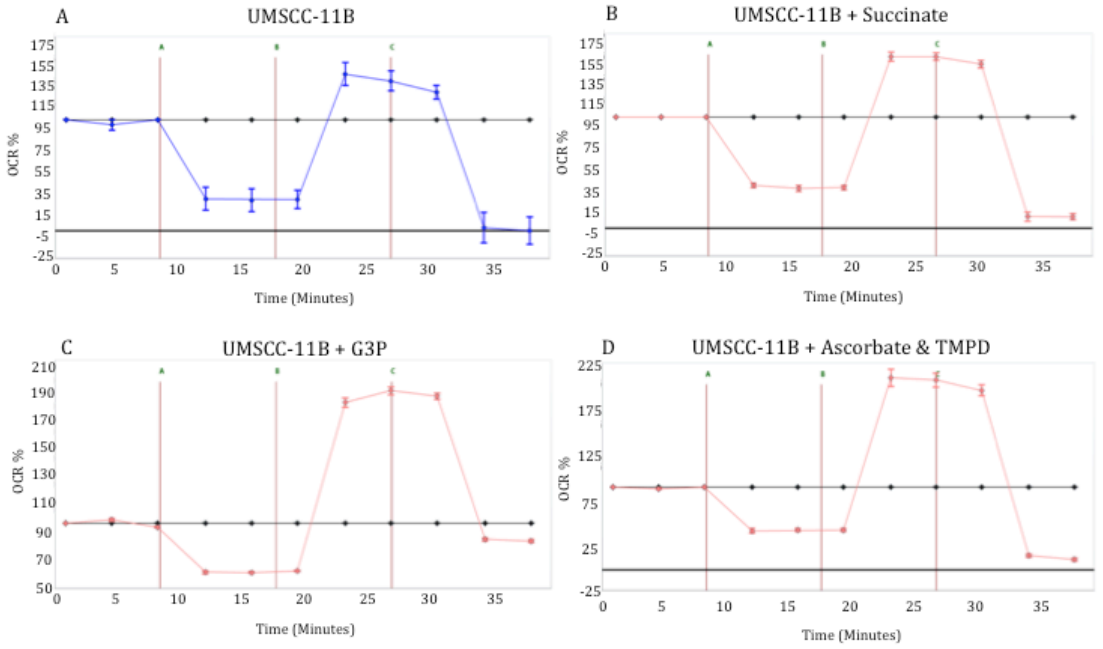
A
UMSCC-11B
B
UMSCC-11B + Succinate
C
UMSCC-11B + G3P
D
UMSCC-11B + Ascorbate & TMPD
OCR %
Time (Minutes)

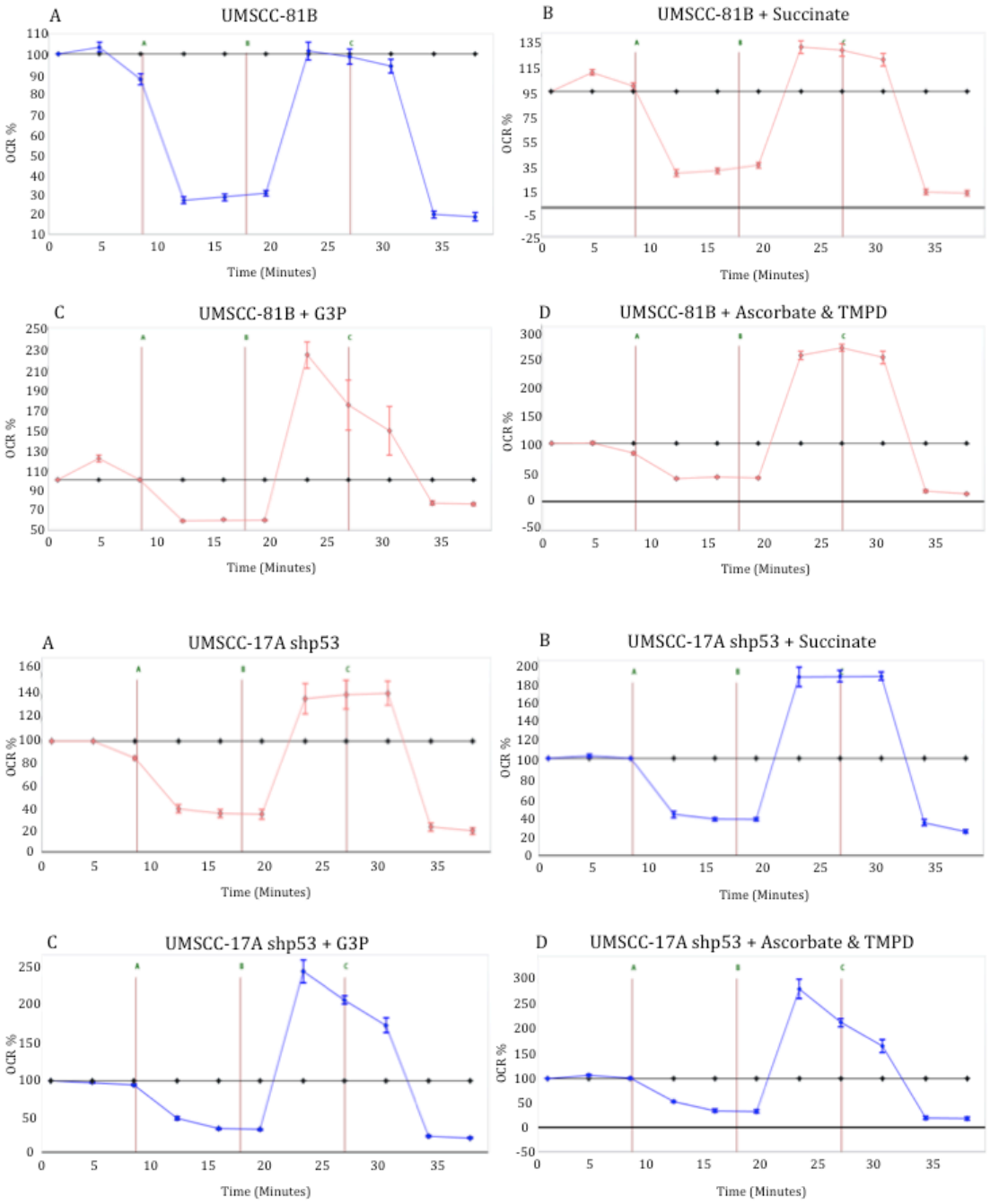

Figure 3.4.2.1: Metabolic profiles of SCCHN cell lines in mitochondrial stress tests following sequential addition of specific oxidisable substrates. Cells were permeabilised with 1nM XF PMP and subjected to mitochondrial stress tests in the presence of the following substrates and inhibitors: pyruvate (10mM) and glutamate (10mM) (A); succinate (10mM) with rotenone (2µM) (B); glycerol-3-phosphate (G3P) (10mM) with malonate (20mM) (C); TMPD (100µM) and ascorbate (10mM) with antimycin A (2µM) (D). As before, points A, B, and C on the graphs refer to the injections of oligomycin 1.25µM, FCCP 1.5µM, and rotenone and antimycin-A 1µM respectively. Data is presented as percentage increases or decreases in OCR relative to baseline measurements. The baseline is shown as the black line at 100% on the graphs. Although results varied slightly between cell lines, the sequential addition of oxidisable substrates to

bypass potentially defective ETC complexes resulted in a marked increase in spare respiratory capacity, with maximal effects generally seen with the addition of TMPD and ascorbate with antimycin A. Error bars represent SEM for each measurement.

The sequential addition of oxidisable substrates with relevant inhibitors, which systematically bypassed ETC complexes, rescued the profile of mitochondrial respiration in all of these cell lines, restoring relative maximal respiration and spare respiratory capacity to that observed earlier in SCCHN cell lines harbouring functional wild-type p53. As would be expected, results varied slightly between cell lines, with differing degrees of rescue observed when bypassing ETC complexes. For instance, in UM-SCC-5 there was minimal rescue of maximal respiration and spare respiratory capacity with the addition of succinate with rotenone, and thus the bypassing of ETC complex I, while in the other cell lines partial rescue was seen. Nonetheless, the most marked effects were observed with the addition of either glycerol-3-phosphate with malonate and/or TMPD and ascorbate with antimycin A in all cell lines. Having established that the capacity for maximal respiration, and by association spare respiratory capacity, could be rescued by bypassing potentially defective ETC complexes, we next examined whether this had resulted in any effect on rates of basal respiration by extracting absolute values. Results are depicted in figure 3.4.2.2. In accordance with the above results demonstrating rescue of the profile of mitochondrial respiration in all cell lines, the addition of oxidisable substrates and inhibitors also resulted in discernible increases in basal respiration, suggesting not only restoration of mitochondrial capacity but a switch back towards a metabolic phenotype in which oxidative phosphorylation predominates as a means of glucose catabolism and utilisation. Again, results varied slightly between cell lines, tending to reflect the degrees of rescue observed with maximal respiration and spare respiratory capacity.

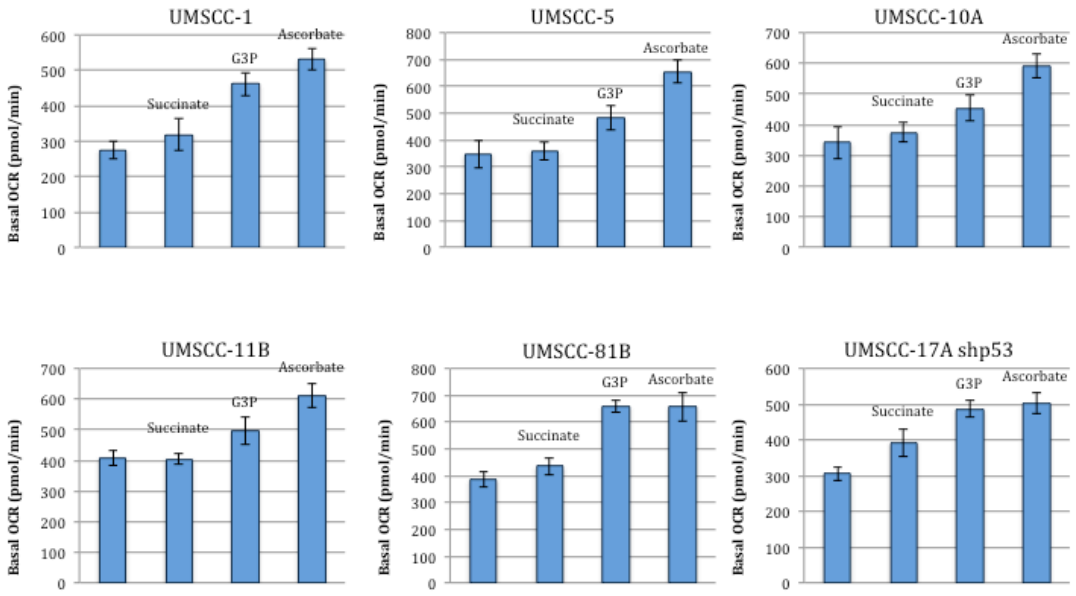

Figure 3.4.2.2: Absolute basal respiration derived from mitochondrial stress tests following sequential addition of specific oxidisable substrates. Absolute values for basal respiration for each cell line were extracted from the mitochondrial stress tests performed on permeabilised cells in the presence of specific oxidisable substrates shown in figure 3.4.2.1. The histograms are labelled to indicate which substrates had been sequentially added. Error bars represent SEM for each measurement. Again, although results varied slightly between cell lines, the sequential addition of oxidisable substrates to bypass potentially defective ETC complexes resulted in a marked increase in basal respiration.

Although bypassing of ETC complexes I, II, and III resulted in marked increases in both basal mitochondrial respiration and the capacity for maximal respiration, the inability to bypass complex IV in this experimental design (figure 2.4.9.1.) prevented assessment of whether complex IV itself was also defective and partly attributable to the *TP53*-dependent metabolic shift. Whilst we thought it unlikely that complex IV would be defective given that bypassing of ETC complexes I, II, and III had resulted in rescue of mitochondrial respiration to levels akin to those observed in intact SCCHN cells harbouring functional wild-type p53, complex IV-linked respiration, as determined by supplying permeabilised cells with TMPD and ascorbate and inhibiting complex III-driven respiration with antimycin A, was compared in the isogenic cell lines to ascertain whether any differences existed in SCCHN cells with and without the presence of functional wild-type p53. Results are shown in figure 3.4.2.3.

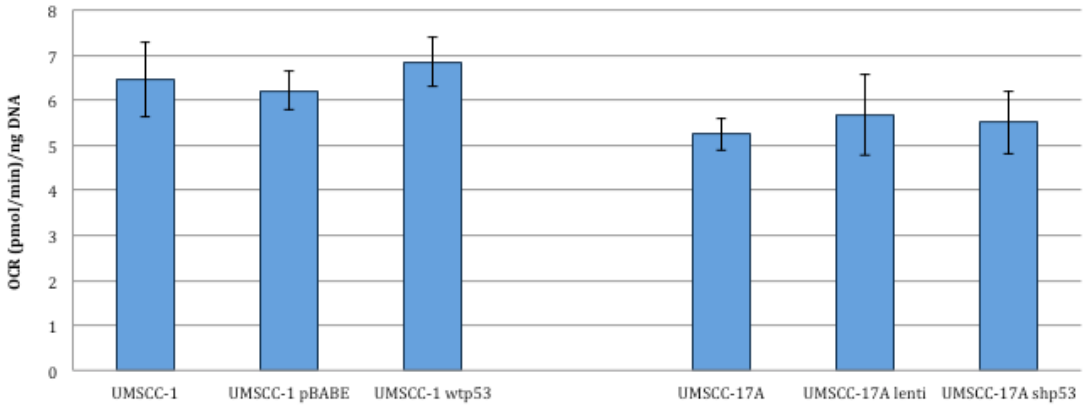

Figure 3.4.2.3: Complex IV-linked respiration in isogenic SCCHN cell lines. Absolute values for basal respiration for each isogenic cell line were extracted from mitochondrial stress tests performed on permeabilised cells in the presence of TMPD (100μM) and ascorbate (10mM) with antimycin A (2μM). These values were normalised to DNA content as described in section 2.3.8. Error bars represent SEM for each measurement. There were no consistent differences in complex IV-linked respiration between SCCHN cells with or without functional wild-type p53.

Consistent with our previous findings that bypassing of ETC complexes I, II, and III resulted in rescue of mitochondrial respiration to levels similar to those observed in intact SCCHN cells harbouring functional wild-type p53, there were no clear differences in complex IV-linked respiration between SCCHN cell lines irrespective of *TP53* status, indicative of no clear defects in complex IV function.

Considering the above findings for individual ETC complexes in permeabilised cells collectively, these results suggest that in SCCHN loss of wild-type p53 function results in global defective functioning of ETC complexes, most marked for complexes II and III, which is at least partly responsible for a metabolic shift away from oxidative phosphorylation towards glycolysis. These findings are in keeping with evidence demonstrating p53 as a promoter of oxidative phosphorylation, which as discussed in section 1.3.2., has linked p53 with the general maintenance of mitochondrial biomass, integrity, quality control, and fidelity of mitochondrial DNA replication (300-303), as well as with several aspects of ETC complex function(286, 305-309). Furthermore, the limited data specific to SCCHN on *TP53* status and ETC activity, which is derived from one previous study(360), is broadly consistent with our findings. In that study, although gene array analysis of all nuclear encoded mitochondrial-related genes demonstrated no significant differences between wild-type and mutant *TP53* SCCHN cells, the comparison of a pair of isogenic cell lines divergent on *TP53* status revealed significant reductions in

ETC complex activity in the mutant *TP53* cell line, with specific defects identified in the activity of complexes II, III, and IV(360). Notably, citrate synthase activity levels were similar in both cell lines, suggesting similar mitochondrial biomass(360).

3.4.3. Differential expression of glycolysis-related transporters and enzymes is involved in the TP53-dependent metabolic switch in SCCHN cells

Although in the previous section we demonstrated that in SCCHN cells loss of wild-type p53 function results in defective ETC complex function, which is at least partly responsible for a metabolic shift away from oxidative phosphorylation towards glycolysis, we also sought to examine whether any *TP53*-dependent differential expression of glycolytic transporters and/or enzymes may also contribute to the metabolic re-programming. As outlined in section 1.3.2., wild-type p53 is known to down-regulate the expression of several glycolytic transporters, including GLUTs and MCT-1(298, 299), as well as influence the activity of the glycolytic enzymes hexokinase-II(318), PGAM(295), PDK(297), and PFK-1(205). As such, our investigation was centred on these proteins. Cells were harvested and lysed for each SCCHN cell line, and samples prepared as described in section 2.11. Western blot analyses were then performed on cell lysates, again as described in section 2.11., with the appropriate antibodies used for protein detection as listed in section 2.1.4.. The resulting western blots are shown in figure 3.4.3.1.

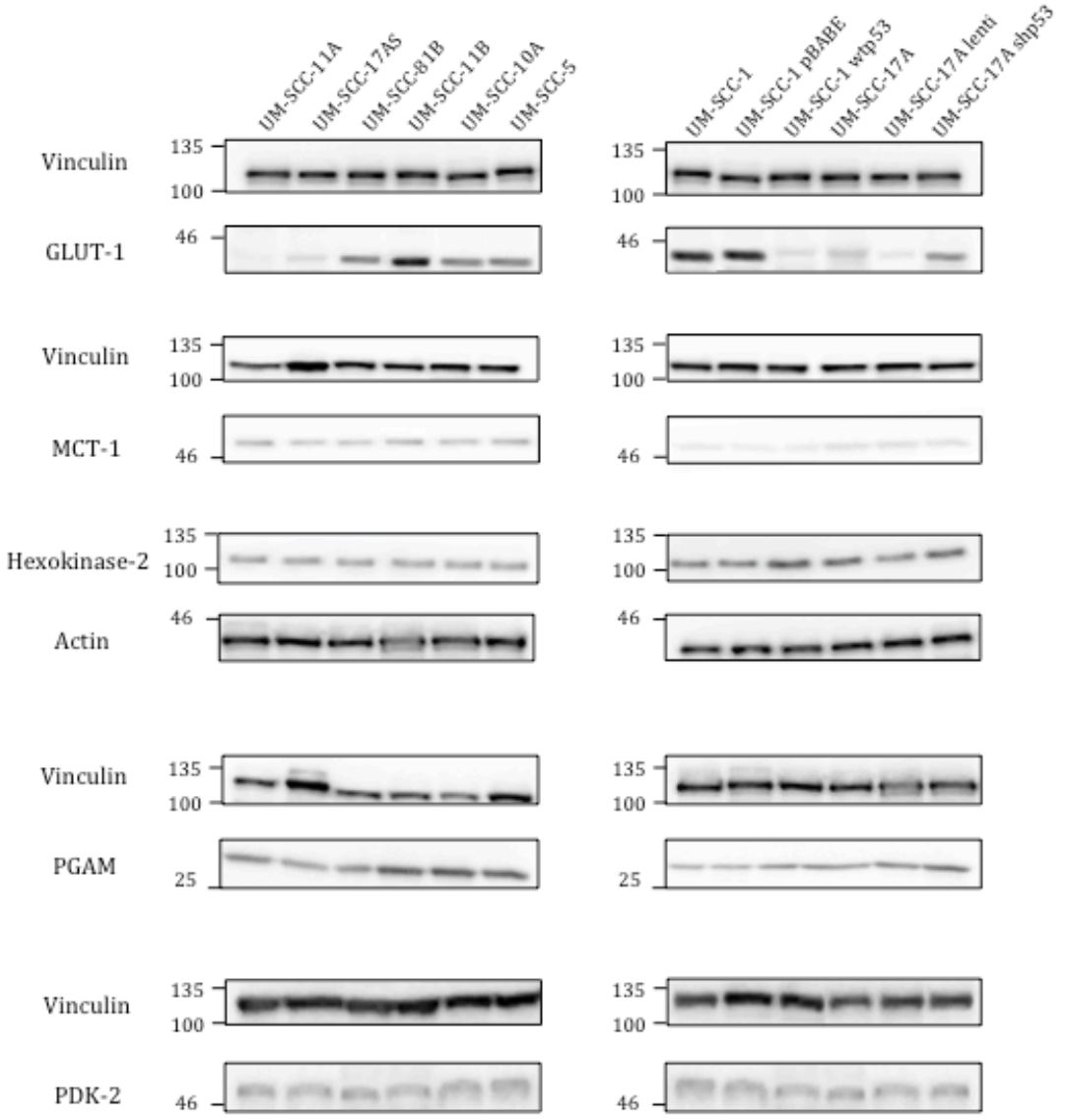

Figure 3.4.3.1: Western blot analyses of relative levels of glycolysis-related transporters and enzymes known to be controlled by p53 in SCCHN cells. Cells from each cell line were harvested and lysed as described in section 2.11. 20μg of protein was analysed in each lane and antibodies used for detection are detailed in section 2.1.4. Vinculin or actin were used a loading controls, dependent on the molecular weight of the proteins being probed for. The migration of protein standards of the indicated approximate molecular weights are shown in kDa. Blots for the panel of SCCHN cell lines are shown on the left and for the isogenic cell lines on the right. Analysis of GLUT-1 demonstrated increased protein levels in SCCHN cell lines with abrogation of wild-type p53 function compared with cells with functional wild-type p53. No clear patterns were observed for the other proteins probed for.

Although there were no obvious differences between SCCHN cells in the expression of the glycolytic enzymes examined, a clear pattern was identified for GLUT-1 expression.

Specifically, SCCHN cells harbouring mutant *TP53* expressed GLUT-1 to a greater extent than wild-type *TP53* cells and this held true when analysing the isogenic cell lines, in which greater GLUT-1 expression was observed in cell lines with abrogated wild-type p53 function. This suggests that loss of wild-type p53 function in SCCHN cells results in an increase in GLUT-1 expression and is partly attributable to the observed *TP53*-dependent switch in metabolism towards glycolysis. This finding is in keeping with the previous report that wild-type p53 acts to repress GLUT-1 gene transcription, and that mutations within the DNA-binding domain of p53 impair this repressive effect on the transcriptional activity of the GLUT1 gene promoters, thereby resulting in increased glucose metabolism(298). As discussed in section 1.3.3., several retrospective pathological studies have investigated GLUT-1 expression in SCCHN and have consistently shown overexpression relative to normal mucosa and/or benign squamous lesions(324-328), and have also demonstrated that GLUT-1 expression correlates with surrogates of disease severity(329). Furthermore, GLUT-1 expression has been shown to be an independent negative prognosticator in both oral cavity and hypopharyngeal SCC(330, 331), and a marker of radioresistance in oral cavity SCC(332), findings that have been paralleled in ^{18}F-FDG-PET studies, the biochemical and clinically utilised correlate of GLUT expression, which have shown ^{18}F-FDG avidity, as measured by standard uptake value, as a reliable predictor of long-term survival in SCCHN(335). Interestingly, despite these findings, the only other study to date examining GLUT-1 expression in SCCHN relative to *TP53* status observed equivalent expression of GLUT-1 in wild-type and mutant *TP53* cells(360). The reason for this disparity in findings is not clear, and may simply relate to the specific cell lines investigated. Indeed, whilst our findings were consistently demonstrated in a panel of SCCHN cell lines, including isogenic pairs divergent on *TP53* status, the earlier study examined GLUT-1 expression only in one mutant and one wild-type *TP53* SCCHN cell line.

3.4.4. Expression of TIGAR becomes uncoupled from p53 transcriptional regulation in the context of loss of wild-type p53 function in SCCHN cells

Having examined the differential expression of glycolysis-related transporters and enzymes that p53 is known to regulate directly, we then sought to investigate TIGAR expression given its close relationship with regulation of glycolysis and the fact that it is under the transcriptional control of p53(205). As discussed previously (see section 1.3.1.), TIGAR acts principally as a bisphosphatase that reduces the concentration of intracellular fructose-2,6-bisphosphate, which is a potent allosteric activator of PFK-1(205). PFK-1 is an essential glycolytic enzyme that catalyses conversion of fructose-6-

phosphate to fructose-1,6-bisphosphate, which represents a key regulatory point in the glycolytic pathway, and p53 regulates glycolysis at this critical point by inducing the transcription of TIGAR(205). Thus, by decreasing PFK-1 activity TIGAR limits glycolytic flux downstream of this point. TIGAR expression levels were examined using western blot analyses on cell lysates, again performed as described in section 2.11. Resulting western blots are shown in figure 3.4.4.1.

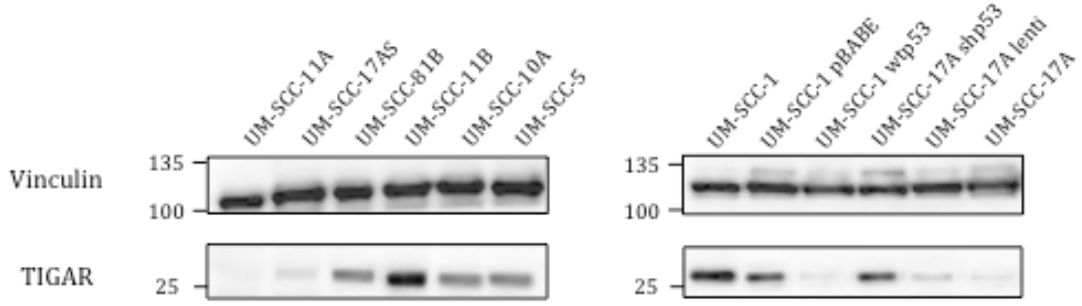

Figure 3.4.4.1: Western blot analyses of baseline TIGAR expression levels in SCCHN cells. Cells from each cell line were harvested and lysed as described in section 2.11. 20μg of protein was analysed in each lane and the α-TIGAR antibody used for detection is detailed in section 2.1.4. Vinculin was used as a loading control. The migration of protein standards of the indicated approximate molecular weights are shown in kDa. Blots for the panel of SCCHN cell lines are shown on the left and for the isogenic cell lines on the right. TIGAR expression levels were observed to be greater in SCCHN cell lines with abrogation of wild-type p53 function compared with cells with functional wild-type p53.

Curiously, baseline TIGAR expression levels were clearly greater in mutant *TP53* SCCHN cells than in wild-type *TP53* cells and in the isogenic cell lines expression was greater in those cell lines with abrogation of wild-type p53 function. Considering that TIGAR is involved in the p53 tumour suppressor pathway, with p53 inducing the transcription of TIGAR to dampen glycolysis, these findings seem counter-intuitive. Similar findings, however, have been reported in several models for other tumour types(286-288), raising the possibility that TIGAR expression becomes de-regulated, or at least uncoupled from p53 regulation, in cancer cells. In order to investigate this further in SCCHN, we examined TIGAR expression relative to expression of both p53 and known downstream targets (p21 and MDM2) using western blot analyses of lysates of selected mutant and wild-type *TP53* cell lines as well as the isogenic cell lines. These analyses

were performed both at baseline and at various time points following administration of 6Gy IR to induce p53 stabilisation. Results are shown in figures 3.4.4.2 and 3.4.4.3.

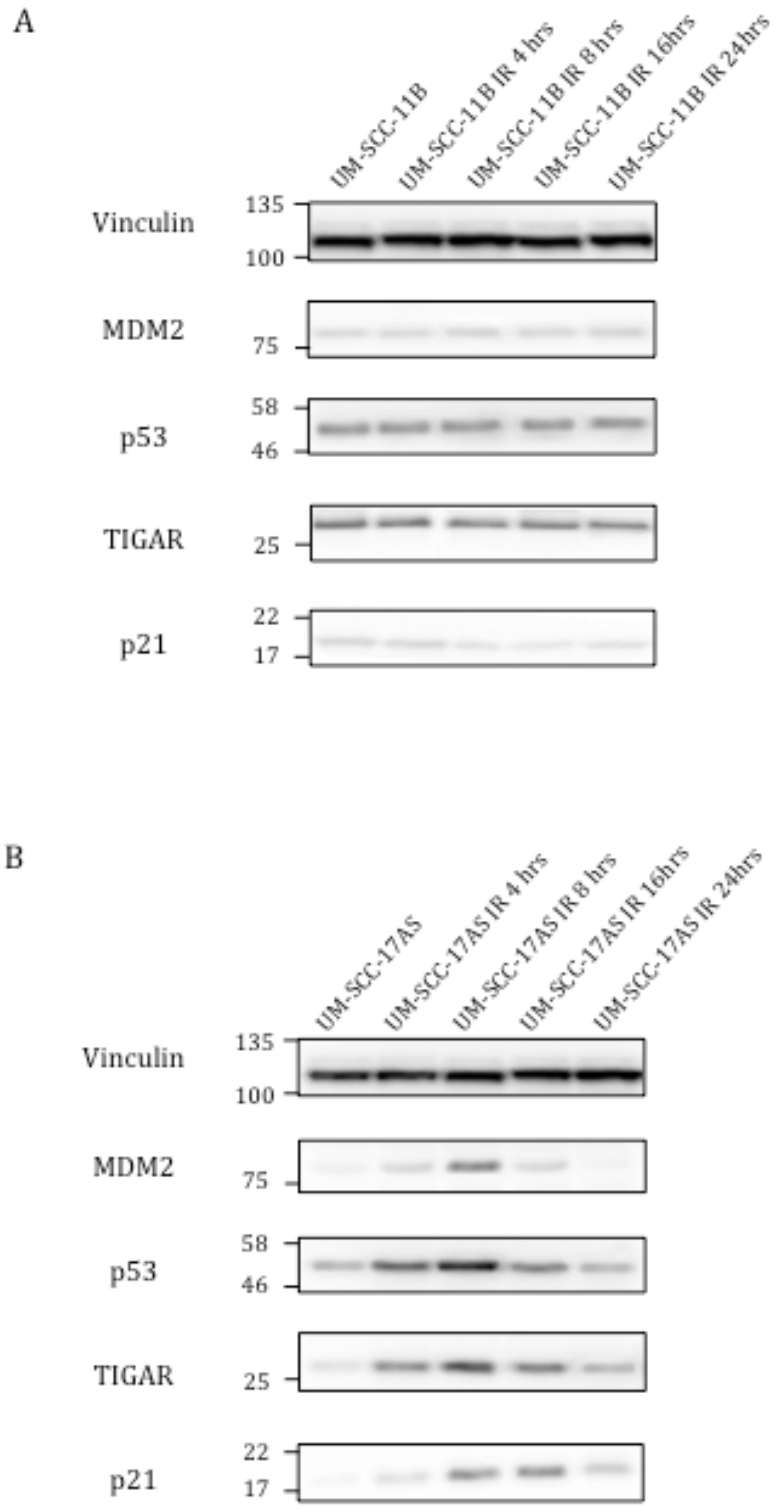

Figure 3.4.4.2: Western blot analyses of TIGAR, p53, p21, and MDM2 expression levels in selected mutant and wild-type *TP53* SCCHN cells. Cells from each cell line were harvested and

lysed as described in section 2.11. 20µg of protein was analysed in each lane and antibodies used for detection are detailed in section 2.1.4. Vinculin was used as a loading control. The migration of protein standards of the indicated approximate molecular weights are shown in kDa. Blots for the mutant *TP53* cell line UM-SCC-11B are shown first (A) and subsequently for the wild-type *TP53* cell line UM-SCC-17AS (B). In the wild-type TP53 cell line, 6Gy IR induced p53 stabilisation and consequent increases in expression of MDM2, p21, and TIGAR, while in the mutant *TP53* cell line, although there was expression of p53, this was unchanged in response to 6Gy IR, and there was no observed relationship with MDM2, p21, or TIGAR expression.

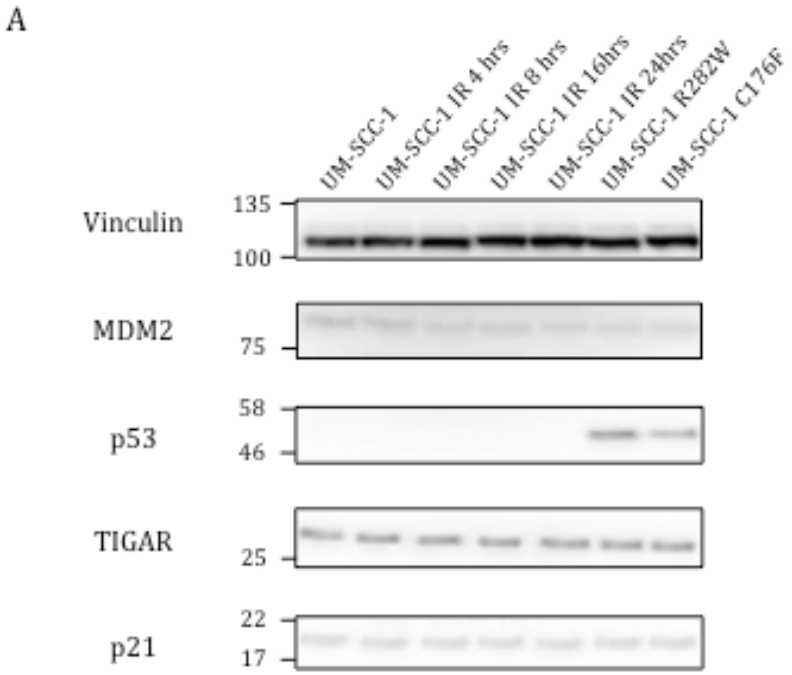

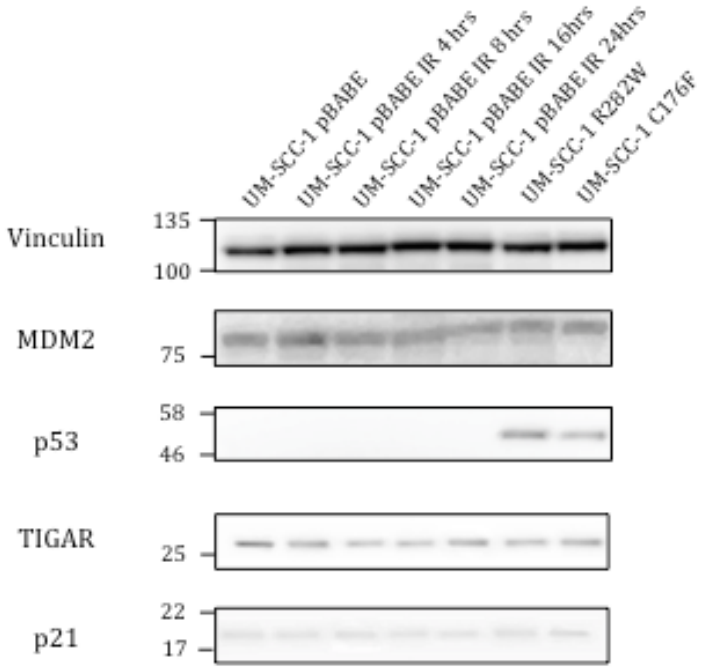

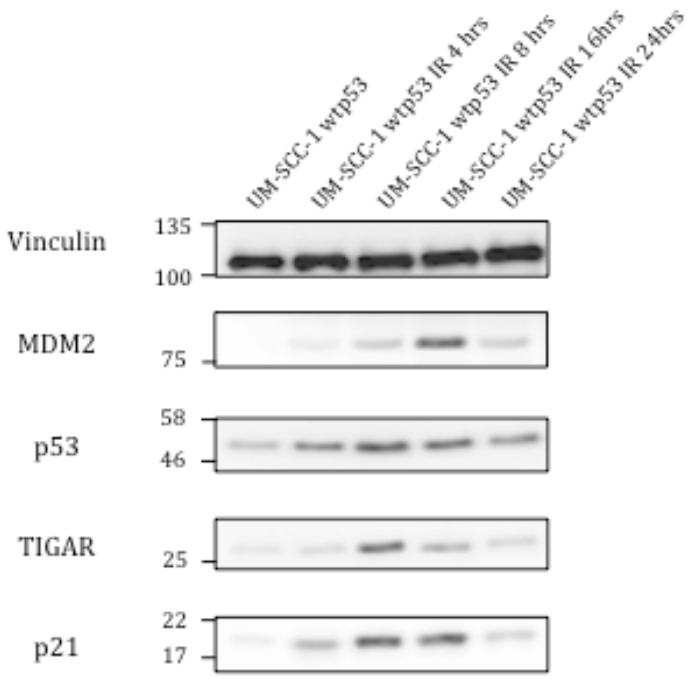
UM-SCC-1 wtp53
UM-SCC-1 wtp53 IR 4 hrs
UM-SCC-1 wtp53 IR 8 hrs
UM-SCC-1 wtp53 IR 16hrs
UM-SCC-1 wtp53 IR 24hrs
Vinculin
135
100
MDM2
75
p53
58
46
TIGAR
25
p21
22
17

B

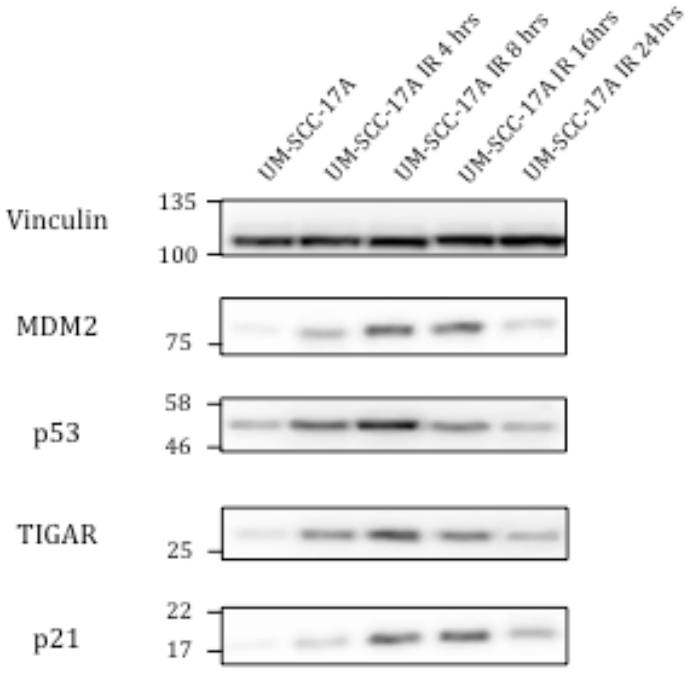
UM-SCC-17A
UM-SCC-17A IR 4 hrs
UM-SCC-17A IR 8 hrs
UM-SCC-17A IR 16hrs
UM-SCC-17A IR 24hrs
Vinculin
135
100
MDM2
75
p53
58
46
TIGAR
25
p21
22
17

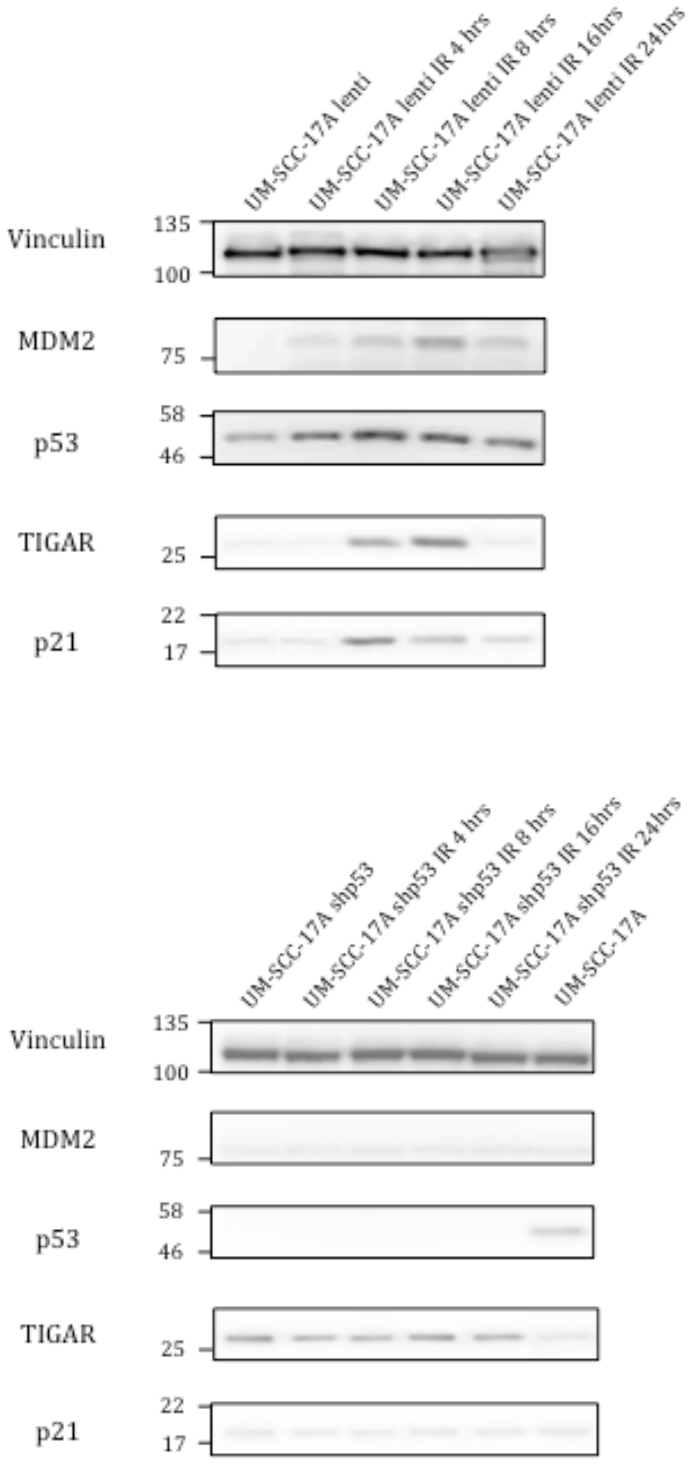

Figure 3.4.4.3: Western blot analyses of TIGAR, p53, p21, and MDM2 expression levels in isogenic SCCHN cells. Cells from each cell line were harvested and lysed as described in section 2.11. 20µg of protein was analysed in each lane and antibodies used for detection are detailed in section 2.1.4. Vinculin was used as a loading control. The migration of protein standards of the indicated approximate molecular weights are shown in kDa. Blots for UM-SCC-1 and derivate cell lines are shown first (A) and subsequently for UM-SCC-17A and derivative cell lines (B). Blots for

UM-SCC-1 included two derivative lines transduced with *TP53* mutations to provide a positive control for p53 expression, and in blots for UM-SCC-17A shp53 the parental cell line UM-SCC-17A was included as a positive control for p53 expression. In cell lines harbouring functional wild-type p53 (UM-SCC-1 wtp53, UM-SCC-17A, UM-SCC-17A lenti) 6Gy IR induced p53 stabilisation and consequent increases in expression of MDM2, p21, and TIGAR. In cell lines with loss of functional wild-type p53 there was no expression of p53 in response to 6Gy IR, and no observed relationship with MDM2, p21, or TIGAR expression.

As would be expected, in cell lines harbouring functional wild-type p53, p53-activating stress induced p53 stabilisation, which resulted in an increase in expression of known transcriptional targets MDM2 and p21. Importantly, there was also a clear direct relationship between p53 expression and TIGAR expression, consistent with TIGAR being under tight p53-dependent transcriptional control. In stark contrast, in the *TP53* mutant cell line, UM-SCC-11B, whilst there was p53 expression, there was no change to expression levels in response to IR, nor was there any relationship with MDM2, p21, or TIGAR expression. Similarly, in the p53 null cell lines UM-SCC-1 and UM-SCC-1 pBABE, as well as in the stable p53 knock-down in UM-SCC-17A, p53 expression was not detectable under any conditions and despite this high levels of TIGAR expression were observed, which were unaffected by treatment with IR. This corroborates the hypothesis that in the absence of functional wild-type p53 in SCCHN cells TIGAR expression is increased and uncoupled from the transcriptional regulation of p53. As alluded to earlier in this section, this is a notion supported by an ever-increasing body of evidence and will be discussed in greater depth subsequently in section 4. Although on initial consideration TIGAR overexpression may seem counter-intuitive as glycolytic flux would be slowed secondary to reduction in PFK-1 activity, this would be expected to facilitate shunting of carbon into subsidiary metabolic pathways, chiefly the PPP, which would generate NADPH, in turn enabling the upregulation of cellular antioxidant systems to combat oxidative stress and promote survival(280). In support of this, several studies have shown that the downregulation of TIGAR is associated with decreased levels of NADPH(426, 427), lower levels of GSH, and in turn an increase in ROS levels and cell death(205, 288, 427).

3.4.5. Uncoupling of TIGAR expression from p53 regulation in SCCHN cells with loss of wild-type p53 function results in increased PPP flux

In the previous section we established that in the context of loss of wild-type p53 function in SCCHN cells TIGAR is highly expressed and its expression becomes uncoupled from the transcriptional regulation of p53. As discussed in the previous

section, the anticipated outcome of this is that PPP flux would be heightened, resulting in increased generation of NADPH allowing for upregulation of cellular antioxidant defences. In this section we sought to investigate this hypothesis. In order to do so, we first examined the expression of two key PPP enzymes – G6PD and 6-PGD. G6PD catalyses the first and rate-limiting step in the oxidative branch of the PPP, generating the first molecule of NADPH, while 6-PGD drives the second NADPH producing step in the oxidative phase of PPP(280). G6PD and 6-PGD expression levels were examined using western blot analyses on cell lysates, again performed as described in section 2.11. Resulting western blots are shown in figure 3.4.5.1.

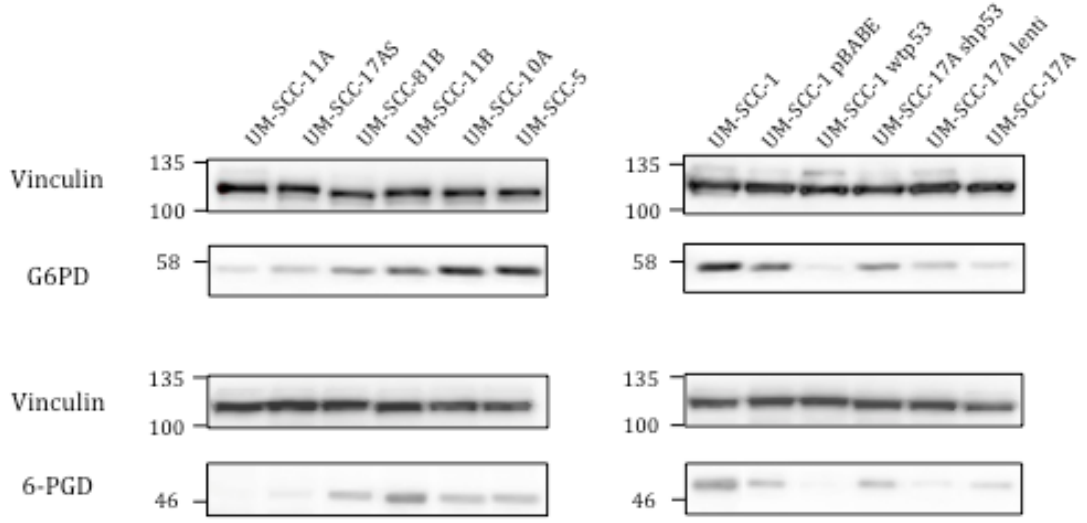

Figure 3.4.5.1: Western blot analyses of PPP enzyme expression levels in SCCHN cells. Cells from each cell line were harvested and lysed as described in section 2.11. 20µg of protein was analysed in each lane and the antibodies used for detection are detailed in section 2.1.4. Vinculin was used as a loading control. The migration of protein standards of the indicated approximate molecular weights are shown in kDa. Blots for the panel of SCCHN cell lines are shown on the left and for the isogenic cell lines on the right. Expression levels of both G6PD and 6-PGD were observed to be higher in SCCHN cell lines with abrogation of wild-type p53 function compared with cells with functional wild-type p53.

In keeping with our earlier results in relation to TIGAR expression, expression levels of both PPP oxidative branch enzymes were discernibly higher in SCCHN cells harbouring *TP53* mutations relative to those harbouring wild-type *TP53*, and in the isogenic cell lines higher expression levels were observed in cells with loss of wild-type p53 function. Whilst these findings of increased PPP enzyme expression are suggestive of increased PPP activity mediated through TIGAR-dependent shunting, other factors may directly

influence expression of these enzymes. For instance, wild-type p53 can interact directly with G6PD and suppress its activity by inhibiting the assembly of G6PD monomers into active dimers(428). In order to explore the relationship with PPP activity further, we next examined intracellular NADP and NADPH levels. Cells were either left untreated or were treated with 5μM 6-AN, and measurement of intracellular NADP and NADPH levels performed using the NADP/NADPH quantification kit as described in section 2.10. Resulting NADPH/NADP ratios are depicted in figure 3.4.5.2.

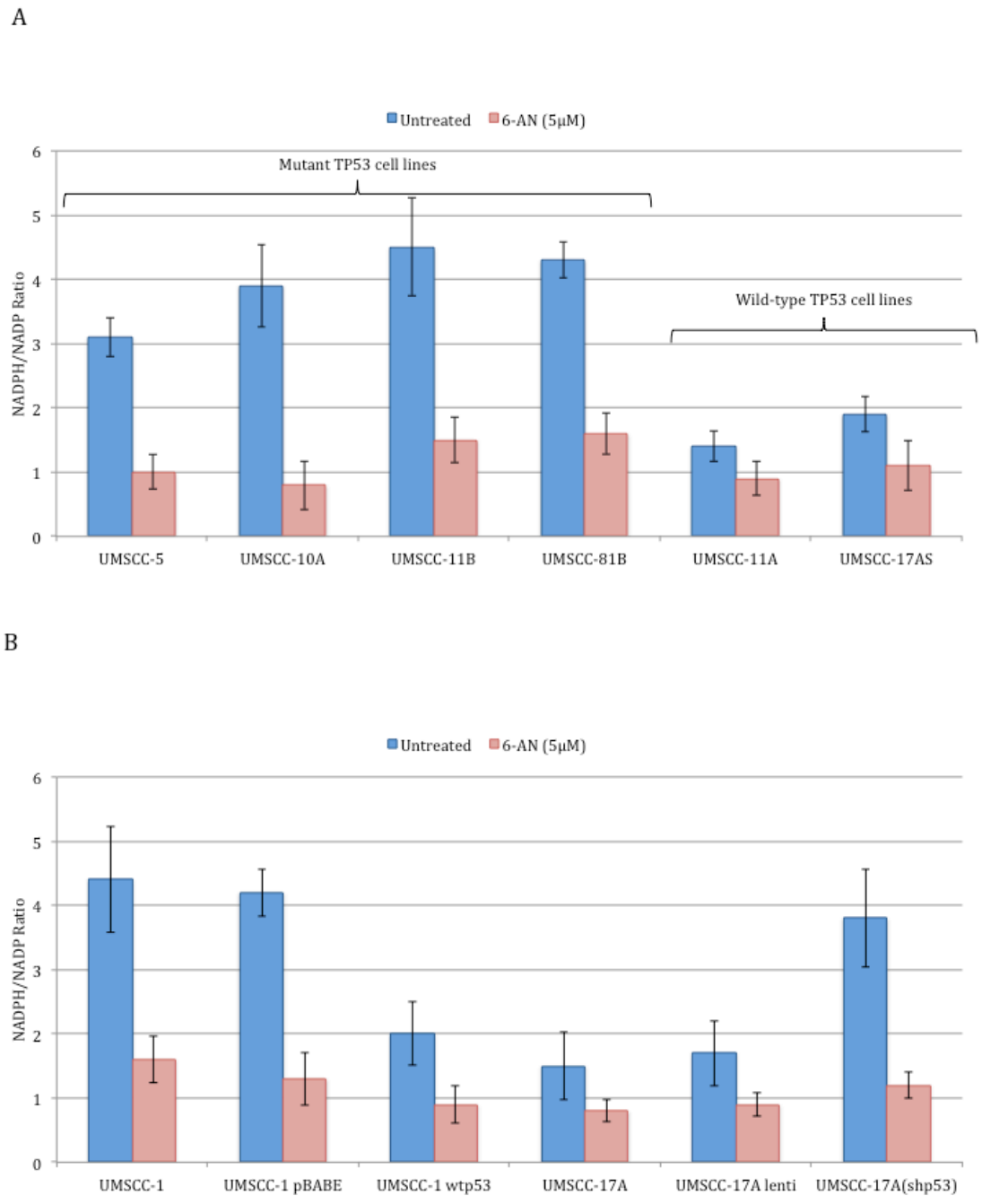

Figure 3.4.5.2: NADPH/NADP ratios in SCCHN cells at baseline and following treatment with 6-AN. Following either no treatment or treatment with 5μM 6-AN, measurement of

intracellular NADP and NADPH levels performed using the NADP/NADPH quantification kit as described in section 2.10. Results are first shown for the panel of SCCHN cell lines (A) and subsequently for the isogenic SCCHN cell lines (B). Experiments were performed in duplicate with mean values depicted in the histograms and SEMs represented by error bars. NADPH/NADP ratios were consistently higher in mutant *TP53* compared with wild-type *TP53* SCCHN cells (A). Similarly, in the isogenic cell lines NADPH/NADP ratios were higher in those cell lines with loss of wild-type p53 function (B). In all cases the PPP inhibitor 6-AN reduced NADPH/NADP ratios, with greatest effects seen in cells with loss of wild-type p53 function.

Again in keeping with our previous results in relation to TIGAR and PPP enzyme expression, NADPH/NADP ratios were clearly higher in SCCHN cell lines with abrogation of wild-type p53 function, indicating that NADPH production is greater in these cell lines. Importantly, in all cases the PPP inhibitor 6-AN reduced NADPH/NADP ratios, with greatest effects seen in cells with abrogation of wild-type p53 function, supporting the fact that the NADPH production is principally derived from PPP flux. Taken together, these findings suggest that higher levels of TIGAR expression, resulting from uncoupling from p53 transcriptional regulation, do indeed translate into increased diversion into the PPP, which in turn supports the upregulation of cellular antioxidant systems through NADPH generation. Consistent with this, several studies have shown that the downregulation of TIGAR is associated with decreased levels of NADPH(426, 427), lower levels of GSH, and in turn an increase in ROS levels and cell death(205, 288, 427). Specific to SCCHN, only one previous study has examined TIGAR expression and its relationship with PPP activity. In that study, which sought to examine the reprogramming of metabolism associated with the development of radioresistance using a matched model of radio-resistant and -sensitive SCCHN cells, radioresistant cells were observed to exhibit increased levels of TIGAR and G6PD expression, as well as increased production of NADPH(277). Unfortunately, as discussed previously in reference to this study, information on the *TP53* status of these cell lines was lacking, which hinders meaningful comparison with our findings. However, it may have been the case that sequential treatment of the parental radiation-sensitive cell line with several fractions of IR to generate the radio-resistant cell line would have resulted in acquisition of a *TP53* mutation, in which case the reported findings would be highly congruous with ours.

4. Discussion

As outlined in section 1.4., the primary aims of this thesis were to examine the metabolic phenotype exhibited by SCCHNs, whether this was related to *TP53* status, and to determine whether tailored anti-metabolic treatment might have potential therapeutic value, specifically in enhancing the effects of radiation treatment. The rationale behind these research aims was three-fold. Firstly, survival outcomes for HPV-negative SCCHN have not improved significantly over the last 20-30 years, largely because currently available treatment regimes fail to induce a response in those with advanced disease. Approximately two-thirds of patients with SCCHN present with advanced disease(1), and overall survival rates for such patients remain as low as 35%(128, 429). Thus, there is a pressing need to develop more effective and personalised treatment strategies. A major focus of this is to identify ways of sensitising these tumours to the effects of IR, particularly given the fact that RT is indicated in almost 75% of all SCCHN cases(107), resistance to RT remains a significant concern(369), and RT dosage escalation is generally not a feasible option because of normal tissue toxicity(80, 128, 129, 429). Secondly, in recent years cancer cell metabolism has come into the forefront of cancer research because of increasing links between tumour metabolism and the causal changes determining the cancer phenotype(247), yet has received relatively little attention in the context of SCCHN. Renewed interest in this field in cancer research more generally has led to the development of new drugs and re-purposing of existing drugs that target cell metabolism, which, when combined with standard therapies can offer a selective therapeutic gain(reviewed in (395, 430)). Until now, the potential of this approach in the context of SCCHN had not been fully realised. Thirdly, loss of wild-type p53 is fundamental to SCCHN oncogenesis (see sections 1.1.3. and 1.2.7.), p53 is known to be an important metabolic mediator (see section 1.3.2.), and two relatively recent studies have implicated *TP53* status as a potential determinant of the metabolic phenotype in SCCHN(359, 360). Moreover, it is widely recognised that *TP53* mutation is linked to particularly poor clinical outcomes and treatment resistance in SCCHN(56-58, 238, 239), yet to date there are no clinically available treatment strategies that stratify on this basis. The proposed therapeutic paradigm presented here specifically addresses these issues, and this, together with planned future work, will be the focus of discussion in this section.

Data presented in section 3.1. begins to address the primary aims of this study by exploring the metabolic phenotype in a panel of SCCHN cell lines using real-time microplate-based XF analysis during specifically designed mitochondrial and glycolytic pharmacological stress tests. The results presented in this section revealed that mutant SCCHN cell lines reliably and consistently exhibited a distinct metabolic phenotype to that of wild-type *TP53* cell lines, whereby wild-type *TP53* cells maintained metabolic diversity, displaying robust mitochondrial and glycolytic reserves, while mutant *TP53* cells exhibited markedly reduced mitochondrial and glycolytic reserves, functioning near or at capacity under basal conditions.

Although in general metabolic studies in SCCHN have been somewhat lacking and simplistic (discussed in depth in section 1.3.3.), two relatively recent and more robust studies from the same research group have observed a similar relationship between *TP53* status and metabolic phenotype(359, 360). Findings from those studies revealed that although SCCHN cells exhibited a general dependence on glycolysis over glutaminolysis, there was significant heterogeneity among cell lines, which was shown to relate to *TP53* status(359). Specifically, initial studies showed that wild-type *TP53* cells were relatively resistant to glucose deprivation and glycolytic inhibition compared with mutant *TP53* cells(359), and follow-on studies demonstrated that mutant *TP53* cell lines displayed markedly reduced spare respiratory capacity relative to wild-type *TP53* cell lines, using the same microplate-based XF analysis as in this thesis(360). Although both of these studies were limited in the number of cell lines analysed with respect to the differences between mutant and wild-type *TP53* cells, the consistency with the findings presented here in a larger panel of SCCHN cell lines is striking. Furthermore, recapitulation of these findings using isogenic SCCHN cell lines engineered with regards to their expression of wild-type p53, both in the work presented here and in the aforementioned studies, corroborates a functional dependence on p53. Additionally, these studies utilising shRNA knock-down of wild-type p53 demonstrate that the observed switch in metabolic profile is the result of loss of wild-type p53 function rather than any oncogenic GOF properties harboured by a particular *TP53* mutation.

The microplate-based XF data demonstrating that loss of wild-type p53 function results in reduced respiratory and glycolytic reserves in SCCHN cells was reported by the authors of the previous study as globalised loss of metabolic flexibility, but also as a dependence on glycolysis(360). However, closer scrutiny reveals that these data can be interpreted in one of two ways. Firstly, in cells with loss of wild-type p53 function

mitochondrial oxidative phosphorylation and/or glycolysis is compromised in some way, preventing cells from mounting a compensatory response to metabolic stressors; or alternatively, mutant *TP53* cells have significantly elevated rates of oxidative phosphorylation and/or glycolysis at baseline that represent maximal cellular rates. Further work presented in section 3.1 of this thesis addressed this ambiguity, providing a clearer overall metabolic picture, which has important potential therapeutic implications. Unlike the previous reports, we conducted specific glycolytic stress tests rather than extrapolating data from mitochondrial stress tests, and our XF data was normalised to DNA content to allow for calculation of absolute values for each of the metabolic parameters derived during the stress test and enable more reliable comparison across cell lines. These data revealed that under basal conditions wild-type p53 SCCHN cells catabolise glucose primarily through oxidative phosphorylation and maintain robust mitochondrial function, thus are able to mount a maximal increase in ETC activity when exposed to mitochondrial stressors. In contrast, in SCCHN cells that have lost wild-type p53 function glycolysis predominates under basal conditions, with levels elevated to maximal capacity leaving little or no reserve, while mitochondrial activity is compromised, with reduced oxidative phosphorylation under basal conditions and a diminished ability to mount an increase in activity in response to mitochondrial stressors. Following on from this, additional work presented in section 3.1. showed that this p53-dependent metabolic re-programming away from oxidative phosphorylation in favour of glycolysis does indeed represent a specific survival dependence on glycolysis, which again has attractive therapeutic implications.

It is widely acknowledged that there is a need for more selective and personalised therapeutic approaches in the wider field of cancer research, and currently much research effort is focused on this key strategy. Such molecularly targeted therapies have as yet had limited translation into the treatment of SCCHN patients. In recent years, only the EGFR inhibitor cetuximab has been approved and introduced into clinical practice for the treatment of SCCHN(87) (see section 1.1.3.), although subsequent studies have raised questions over clinical applicability(431-433). Thus, it remains a major challenge in SCCHN to develop such targeted treatments. Novel therapeutic approaches are generally predicated on a discernible therapeutic index of the chosen agent, either in isolation or in combination with other treatment regimes. Considering this, in contrast to traditional cytotoxic agents, which largely target pathways that exist in normal cells, metabolic targeting can exploit the fact that tumour cells become predominantly dependent on a particular metabolic pathway providing a selective therapeutic gain

while sparing most normal cells, which maintain metabolic diversity. Importantly, subsequent work presented in section 3.2. demonstrated that the observed glucose "addiction" of mutant *TP53* SCCHN cells does indeed correlate with radiation response after glycolytic inhibition. Specifically, 2-DG consistently potentiated radiation effects in SCCHN cells harbouring *TP53* mutations but not in those harbouring wild-type *TP53*. These findings present the opportunity for a tailored anti-metabolic approach to the treatment of SCCHN that takes into account *TP53* mutational status, whereby 2-DG could be used as a selective radiosensitiser specifically to treat mutant *TP53* SCCHN.

Currently, therapeutic decision-making for SCCHN patients is based predominantly on TNM classification and the associated UICC/AJCC staging system, which rely largely on clinical and radiological findings, although as outlined in section 1.1.4. additional factors such as HPV status have been included in the most updated versions(50). Whilst these systems have fulfilled their original mandate remarkably over the years, owing to time-tested consistency and user-friendliness, many have criticised their lack of predictive power and failure to account for numerous potentially important prognostic and/or predictive tumour factors(434). Fundamental to successful development of more personalised treatment for SCCHN will be the identification of these tumour factors that reliably predict which patients will actually derive benefit so that these treatments can be effectively deployed. As such, the potential opportunity to utilise *TP53* status as predictive biomarker to inform delivery of more personalised therapy, rather than simply a prognostic biomarker, is of particular interest. Since its discovery, p53 has been at the forefront of cancer research, is one of the most extensively studied genes in biomedicine/life sciences (having been the subject of more than 85,000 published articles listed on PubMed), and is recognised as the most common molecular alteration found in human cancers(133). Despite this, therapeutic translation into the clinical setting has been almost non-existent, with chronic lymphocytic leukemia the only cancer to date for which clinically available treatment strategies stratify on the basis of *TP53* status(435). The proposed therapeutic approach presented here would for the first time stratify SCCHN patients for treatment on the basis of *TP53* mutational status, and would also be preferentially effective in overcoming cellular resistance to radiation treatment in patients with the treatment-resistant disease typically associated with *TP53* mutation(56, 57). Moreover, this approach would be applicable to the majority of SCCHN patients given that 60-85% of SCCHNs harbour *TP53* mutations(51-53).

This use of glycolytic inhibitor treatment in the context of SCCHN has been examined previously. A small number of *in vitro* studies generally focusing on 2-DG and using homotypic cell culture experiments have demonstrated a selective sensitivity to glycolytic inhibition, particularly when combined with conventional treatments(354, 355, 359, 360). However, findings have not been universal(357) and few of these previous studies have accounted for *TP53* status, which in light of the findings presented here seems highly relevant and conceivably could explain variability in results. Consistent with this, and in keeping with our results, the study detailed above examining effects of *TP53* status on metabolism and response to glycolytic inhibition demonstrated potentiation of IR effects in the presence of 2-DG exclusively in SCCHN cells with loss of wild-type p53 function(360). Moreover, a relatively recent study specifically examining the differential cytotoxic effects of 2-DG in isogenic cell lines differing in *TP53* status also reported a significantly greater sensitivity in mutant *TP53* cells(355). Only one previous study has examined the effects of glycolytic inhibition in SCCHN in the *in vivo* setting, in which 2-DG was observed to potentiate the anti-tumorigenic effects of cisplatin on cell proliferation and survival, inhibiting growth of SCCHN xenografts both in isolation and in a combined-modality approach with IR(356). Interestingly, although this study did not seek to examine any relationship with *TP53* status, both xenografts used were derived from SCCHN cell lines documented to harbour *TP53* mutations.

Following on from these pre-clinical studies, two clinical studies, both originating in Italy in the mid 1990s, have evaluated the role of glycolytic inhibition in SCCHN(436, 437). These clinical trials both examined the effects of oral administration of the glycolytic inhibitor lonidamine, which is thought to inhibit hexokinase as well as glucose uptake and lactate efflux(395). One trial investigated lonidamine in combination with chemotherapy (methotrexate) in 89 patients with recurrent SCCHN using a phase II randomised design(437), while the other examined lonidamine in combination with RT in 96 patients with advanced primary SCCHN as a phase III, double-blind, randomised, placebo-controlled trial(436). Intriguingly, results suggested that the addition of lonidamine in either instance improved clinical outcomes, and was seemingly tolerable, with only minor side effects and relatively low attrition rates reported(436, 437). Specifically, in the phase III study although there was negligible difference in initial disease control rates (66% in the lonidamine group versus 65% in the placebo group), the addition of lonidamine resulted in a lower subsequent treatment-failure rate following initial disease clearance (50% versus 77%), and significantly improved loco-

regional control and disease-free survival at three and five years(436). Considering these findings in light of those presented in this thesis, it is perhaps surprising that such favourable outcomes were observed given that neither trial utilised *TP53* status as a predictive biomarker. However, if rates of *TP53* mutation in SCCHN from recent sequencing studies (65-80%)(51-53) are extrapolated to these patient groups it is likely that only a small minority of tumours would have harboured wild-type p53, and that any potential resistance to glycolytic inhibition in these tumours would have been masked by the effects observed in mutant *TP53* disease. What is perhaps more surprising given these promising findings is the absence of subsequent clinical studies further investigating this issue. Findings from other solid tumour types, however, highlight that whilst in many instances initial pre-clinical and/or clinical results have been therapeutically promising, responses have been inconsistent, even when combined with conventional therapies(438). Whilst these discrepancies may simply reflect differing metabolic profiles in different tumour types, and thus variable responses to glycolytic inhibition, another possible explanation relates to a lack of available predictors to define patient populations most likely to derive therapeutic benefit. For instance, in keeping with our findings presented here, it is conceivable that tumours harbouring *TP53* mutations would be sensitive to glycolytic inhibition, while those expressing wild-type p53 may be resistant, requiring a broader anti-metabolic approach, and thus attributable to the variable results.

Based on the findings and proposed therapeutic paradigm presented in this thesis, ultimately we anticipate conducting a phase II/III clinical trial in SCCHN patients that would investigate the efficacy of a tailored anti-metabolic therapeutic approach in mutant *TP53* disease. Specifically, we envisage that SCCHN patients for whom RT was indicated as part of their treatment regime would be first identified, and of these patients those with mutant *TP53* disease would be further identified through sequencing of pre-treatment biopsy specimens. Following selection on the basis of these inclusion criteria, the trial would take the form of a randomised, controlled, parallel-group, superiority study, in which all patients would receive their proposed RT regime but would be randomised to receive either 2-DG or placebo prior to each RT fraction. Oncological outcome measures of interest would include loco-regional disease control, disease specific survival, and overall survival. Functional outcome measures with regards to swallowing and voice would also be included. In the first instance, for the sake of simplicity and to minimise heterogeneity, we suggest that recruitment include only those SCCHN patients planned to have single-modality RT as their recommended

treatment. Recruitment could then be expanded to patients who were having multi-modality treatment, for example surgical resection with adjuvant RT or primary CRT.

Although no previous clinical studies have been conducted using 2-DG in SCCHN patients, 2-DG in combination with RT has been evaluated more extensively in patients with cerebral gliomas. Consequently, these data could be extrapolated to inform dosing schedules and safety profiles in SCCHN patients, potentially obviating the need for phase I/II trials before proceeding to the phase II/III trial design as described above. The clinical trials and dosage escalation studies in cerebral glioma patients conducted so far suggest that the oral administration of 2-DG following overnight fasting and immediately prior to RT in doses between 250 and 300mg/kg body weight is feasible, efficacious, and safe. The clinical side effect profile reflects that of hypoglycaemia and is predictable on the basis of the cell types that depend most on glycolysis, such as cerebral and cardiac tissues. Diaphoresis, generalised warmth, flushing, drowsiness, and hypothermia have been observed but have not been severe, have been transient lasting approximately 90 minutes, and can be reversed by the administration of glucose. The predictability of the source of these adverse effects is favourable insofar as potential toxicities could be monitored for on a proactive rather than reactive basis.

Although the likely method of delivery of 2-DG in SCCHN patients would be oral administration, in line with previous studies in cerebral glioma, topical delivery may be an option in the context of patients receiving adjuvant RT following surgical resection of their disease, and may further minimise any systemic toxicities. In this paradigm, topical 2-DG could be applied onto the tumour bed following resection in order to maximise the efficacy of RT in eliminating any residual disease, although the temporal relationship between surgical resection and administration of adjuvant RT may limit the effectiveness of this approach.

Prior to any translation into clinical practice, however, our findings, and in particular our proposed therapeutic approach, would require validation in further experiments in a pre-clinical environment. Indeed, one of the frailties of the work presented in this thesis is that experiments have been conducted exclusively using homotypic, monolayer cell culture of immortalised cell lines derived from SCCHN tumours. Although such cultured cancer cell lines are the most widely used model systems and have formed the basis for much of our current understanding of cancer biology, the clinical relevance of these models has been questioned(439). One of the major concerns over immortalised

cell lines is that of clonal evolution, whereby cells adapt to the culture environment *in vitro* as they grow and may develop genetic and phenotypic differences from the original tumour(439). Genetic and molecular cytogenetic data for SCCHN cells lines in culture, however, has shown a close resemblance to those in the primary tumours(371). In addition, to counteract clonal evolution as best possible, our experiments were performed with relatively low passage number cell lines. Nonetheless, to mitigate against this issue more definitively future pre-clinical experiments could be conducted using short-term, fresh, primary cell cultures depending on availability and feasibility.

A further potential drawback of monolayer cell culture is failure to model potential complex interactions between the tumour and surrounding stroma as well as tumour and its host because monolayer cultures lack the cell-to-cell interactions characteristic of tumours *in vivo*(371). A possible solution to this in future experiments would be to utilise a three-dimensional spheroidal culture system. Such systems are composed of an outer layer of proliferating cells, an inside layer of quiescent cells, and an inner core of necrotic cells. This arrangement reflects the growth pattern and the irregular distribution of oxygen and nutrients found in solid tumours, and may be a better representation of the *in vivo* cellular complexity and heterogeneity than monolayer culture(440, 441). To this end, microplates specifically designed for use with spheroid cultures in the XF experimental platform we utilised for our metabolic profiling studies have recently been developed, which would support this experimental design going forward. A limiting factor to the use of spheroidal culture, however, is the difficulty of establishing cell lines that can associate into spheroid clusters. Indeed, of almost 300 well-characterised and widely utilised SCCHN cell lines, so far only 11 have been reported as being capable of associating into spheroidal clusters(371).

The issue of oxygen supply is of particular relevance when considering cellular metabolism. In monolayer cell culture cells are usually maintained in conditions of 20% oxygen, whereas the *in vivo* tumour microenvironment is typically hypoxic due to lack of oxygen diffusion to the centre of a growing tumour. Hypoxia can regulate the metabolic activity of cells and induce glycolysis through the activation of HIF-1α, which, as the major transcription factor involved in regulating the adaption of cells to hypoxic conditions, regulates the expression of many glycolytic genes(442). Nevertheless, HIF-1α can be activated in cancers even under normoxic (or pseudohypoxic) conditions in response to oncogenic signalling pathways, including *TP53* mutation(443). Indeed, as

discussed in section 1.3.3., normoxic stabilisation of HIF-1α has been reported in SCCHN cells(338, 339).

An alternative pre-clinical model system that could also be applied to more effectively mimic tumour heterogeneity and the *in vivo* milieu is a microfluidic system. Purpose-built microfluidic devices allow a small sample of tumour to be maintained alive *ex vivo* in a pseudo–*in vivo* microenvironment(444). Specifically, biopsies of tissue can remain in a viable state for periods of up to seven days in a heterogenic and dynamic molecular ecosystem, in which variables such as laminar flow, perfusion, and diffusion rates can all be manipulated, enabling close control of the chemical and physical environment(444). Response of the tumour specimen to treatment regimens in this environment can subsequently be assessed. Although to date use of microfluidic systems has been relatively limited in the context of SCCHN, recent studies have successfully maintained both SCCHN primary tumour and regional lymph node metastases tissue in such systems while assessing differential response to external beam IR to personalise therapy(445).

Despite the potential utility of these pre-clinical *in vitro* and *ex vivo* model systems, in-vivo xenograft animal models are still widely regarded as the most valid and clinically relevant experimental platforms to accurately predict the activity of anti-cancer drugs or demonstrate the oncogenic properties of solid tumours(371, 446). As such, further pre-clinical validation of the findings and proposed therapeutic approach presented in this thesis would almost certainly be conducted in this setting. We envisage use of athymic nude mice with xenografts established from the SCCHN cell lines used in this study. Indeed, a number of these cell lines have previously been used to successfully establish xenografts in such mice(371), and athymic nude mice have been more thoroughly characterised and used more widely than other immunodeficient mouse models, such as the severe combined immunodeficiency (SCID) mouse. Furthermore, athymic nude mice are logistically more favourable models insofar as they are less susceptible to thymic lymphomas and life-threatening infection than SCID mice(371, 446). We would also foresee using an orthotopic xenograft system, in which the SCCHN cells are injected into the mylohyoid muscle in the floor of the mouse oral cavity, rather than the traditional xenograft technique of subcutaneous or tail vein injection. This facilitates tumour development from the natural anatomical site and thus is more likely to mimic the *in vivo* pathology and microenvironment of SCCHN(447). Once tumour cell implantations became established and palpable, mice could be then given either oral

doses or intra-peritoneal injections of 2-DG prior to exposure to fractionised IR given in 2-Gy fractions. Changes in tumour volume to assess response could be then assessed through caliper measurement and calculation of tumour volume, direct removal of the tumour, or through imaging techniques. As alluded to above, one potentially attractive application of 2-DG would be topical delivery to the tumour bed following surgical resection with the goal of enhancing the efficacy of adjuvant RT. This approach could also be first explored in the mouse xenograft model by performing macroscopic excisions of tumour xenografts with the intent of leaving a small burden of residual disease. 2-DG could then be delivered topically to these tumour margins, in conjunction with a fractionated IR regime, and marginal biopsies could subsequently be taken from these areas and monitored for any remaining tumour tissue after a suitable time frame. A comparison could then be made against administration of IR alone following the tumour xenograft resection.

As mentioned previously, one previous study has examined the potential therapeutic effects of 2-DG in SCCHN using a xenograft mouse model derived from SCCHN cell lines(356). In that study, 2-DG was observed to potentiate the effects of cisplatin with respect to inhibiting growth of SCCHN xenografts both in isolation and in a combined-modality approach with IR(356). However, the effect of 2-DG in the absence of cisplatin was not examined, only two SCCHN cell lines were xenografted, both of which were mutant *TP53* cell lines, and the xenograft technique used was subcutaneous injection.

Whilst the findings presented here, which demonstrate that in SCCHN cells loss of wild-type p53 function confers a loss of metabolic flexibility and a survival dependence on glycolysis, appear compelling and are consistent with other recent SCCHN metabolic studies(359, 360), as discussed in section 1.3.3. one research group has offered an alternative model of SCCHN metabolism. Based on functional biomarker analysis of SCCHN resection specimens, a model of metabolic symbiosis with three metabolically and morphologically distinct cell populations was proposed(366). In this paradigm non-proliferative glycolytic stromal and cancer epithelial cells generate catabolites which are released into the tumour microenvironment and subsequently taken up and utilised by the mitochondrial rich cancer cells to drive energy production and proliferation through oxidative phosphorylation(366). Close examination of these findings, however, raises questions over the conclusions drawn. MCT-1, which was the biomarker employed to indicate catabolite influx in support of mitochondrial respiration, is capable of adapting to facilitate both inward and outward lactate flux depending on glucose

availability(299), while LDH-B, which was used as a glycolytic marker, is an isoenzyme of LDH that drives conversion of lactate back to pyruvate, and is thus more indicative of catabolite influx and reverse glycolysis. Moreover, only in a subset of specimens examined were both non-proliferative compartments noted to be highly glycolytic and observed to represent a significant proportion of the tumour(366). Given that there was conspicuous absence of *TP53* characterisation, it is possible that this subset of tumours displaying a significant glycolytic compartment were those harbouring mutant *TP53*. Similar findings of metabolic coupling, however, have been reported for other tumour types(367, 368), and further exploration in SCCHN using one of the aforementioned experimental systems that models for the tumour microenvironment is warranted to help reconcile these discrepancies. This is particularly pertinent given that our findings and those of others demonstrating a generalised glycolytic phenotype of SCCHN cells(359, 360) have been derived from experiments using monolayer cell line culture, and given the important therapeutic implications of these discrepant models of SCCHN metabolism. According to the model of metabolic symbiosis therapeutic targeting would focus on MCT-1 and MCT-4 inhibition, while with the model presented here upstream glycolytic inhibition is the focus.

As touched on above, findings presented in sections 3.1. and 3.2. revealed that in contrast to mutant *TP53* disease, in SCCHN cells harbouring wild-type *TP53* metabolic diversity is maintained, and thus a broader anti-metabolic approach was required to potentiate the effects of IR. Specifically, administration of 2-DG alone did not sensitise these cells to the effects of IR and combined administration of 2-DG and metformin (a biguanide with demonstrated activity against ETC complex I(405)) was required to achieve this effect. Similar results were also observed for HPV-positive SCCHN cell lines. This was perhaps surprising given the role of the HPV E6 oncoprotein in targeting p53 for proteasomal degradation (detailed in section 1.1.3.). However, these results are consistent with the only other study to date investigating metabolism in HPV-positive SCCHN, which reported that both HPV-positive SCCHN resection specimens and a HPV-positive SCCHN cell line expressed increased levels of proteins indicative of oxidative phosphorylation and a relatively lower level of extracellular lactate accumulation(361). It may be the case, therefore, that E6-mediated inactivation of p53 is incomplete, leaving sufficient functional wild-type p53 to maintain a balanced and diversified metabolic phenotype. In accordance with this, genome-wide microarray data from a recent study examining radiation response in HPV-positive and HPV-negative SCCHN cell lines suggested that low levels of wild-type p53 remain in HPV-positive cell lines, that this

p53 can be activated by exogenous stress such as IR, and that this effect can be overcome by more complete knockdown of p53 using shRNA(381). This also raises the issue of the validity of HPV-positive SCCHN cell lines as clinically relevant model systems, several of which have been derived from patients with backgrounds of cigarette smoking and alcohol excess, and from SCCHN subsites outside the oropharynx(371, 378). Nonetheless, recent comprehensive characterisation of the reportedly HPV-positive established cell lines revealed transcriptionally active integrated and/or episomal viral DNA in seven cell lines, suggesting that these may represent suitable model systems of HPV-positive SCCHN in the absence of feasible alternatives(378). However, until E6/7 manipulation of cells is accomplished there will not be a truly reliable link to HPV and functional studies, and this is part of on-going work by other researchers in our laboratory.

From a therapeutic perspective, although the proposed combination of 2-DG and metformin to augment IR effects in wild-type *TP53* SCCHN is enticing, it has the potential to carry a narrower therapeutic index than the strategy proposed for mutant *TP53* disease. Because wild-type *TP53* SCCHN cells (HPV-positive disease included) do not depend so heavily on one isolated metabolic pathway, and thus require a broader anti-metabolic approach, sparing of normal cells is less likely. Indeed, in this instance it seems that the therapeutic gain largely stems from the fact that tumour cells have a requirement for fluxing greater quantities of glucose through both glycolysis and oxidative phosphorylation. Metformin, however, has been used widely in clinical practice in the treatment of type II diabetes for approximately 30 years with minimal toxicity and there has been an ever-increasing interest in re-purposing metformin as a anti-cancer treatment(406), an interest which stems from several epidemiological studies demonstrating a lower cancer incidence in diabetic patients taking metformin than in the general diabetic population(407). Moreover, metformin users have higher rates of disease control when treated with neoadjuvant chemotherapy for breast cancer(408). Regardless, given that our proposed radiosensitising approach of 2-DG combined with metformin has not been investigated previously in patients, extensive further validation in the pre-clinical setting using the experimental systems described above would certainly be required. In particular, *in vivo* studies determining dose-limiting toxicity of the combination of compounds would be required initially, followed by optimisation of the dosing schedule. Factors to be optimised would include the dose of compounds, timing and frequency of administration of the drugs, and possibly staggering each drug as a way of limiting toxicity. Should these prove successful, similar

thorough safety testing would be required in the setting of a phase I clinical trial. As discussed in sections 1.1.5. and 3.2.5., the prospect of radiosensitisation is particularly attractive in HPV-positive oropharyngeal SCC, given the current interest in treatment de-intensification for these patients, as this would potentially facilitate reduction in total RT dose. The rationale behind this concept of de-intensification relates to reducing the impact of treatment on long-term function, which is key in these patients who have a favourable prognosis(94-96, 102) and tend to be younger and otherwise medically fit at presentation(30), and thus more likely to experience the functional ramifications of their treatment long-term.

Following on from characterising the *TP53* mutation-induced glycolytic switch in SCCHN cells, and demonstrating the associated anti-metabolic therapeutic implications, secondary aims of this thesis were to explore the mechanistic basis underlying both the metabolic re-programming and anti-metabolic therapeutic effects. Findings presented in section 3.3. showed that the mechanism underlying the potentiating effects of glycolytic inhibition on IR in SCCHN cell lines with loss of wild-type p53 function involves oxidative stress-mediated activation of apoptosis. Specifically, the addition of 2-DG to IR resulted in a marked increase in both intracellular ROS and levels of apoptosis compared to IR alone in such cells, effects that were reversed by the further addition of NAC. Accordingly, the addition of NAC also consistently reversed the potentiating effects of 2-DG on IR in terms of clonogenic survival. As discussed in section 3.3.2., these findings are consistent with those of numerous studies of pharmacological glycolytic inhibition in cancer cells of various origin(402, 411, 412), and also with those of the paucity of studies in SCCHN(354, 359, 360). For instance, in studies specific to SCCHN glycolytic inhibition has been shown to cause perturbations in parameters indicative of oxidative stress, including decreased intracellular total glutathione with a reduced proportion of GSH(354), lessened cellular reducing potential(359), and significantly elevated ROS levels(360). Furthermore, simultaneous treatment with NAC has been shown to inhibit such parameters and reverse the cytotoxic effects of glycolytic inhibition(354, 359, 360).

These findings implicating induction of oxidative stress as the mechanism underlying glycolytic inhibition in SCCHN provide further support for a selective therapeutic advantage in the context of potentiating the effects of IR. IR induces DNA damage through a mechanism that relies to a considerable extent on free radical formation(369), and consequently intracellular redox status is thought be a crucial determinant of

sensitivity to IR and may alter the outcome of radiation therapy(448). Therefore, normal cells, which do not carry such a high burden of oxidative stress, are less likely to be susceptible to the potentiating effects of glycolytic inhibition on IR. In addition, recovery following IR-induced damage requires activation of DNA damage repair pathways and is energetically demanding, rendering tumour cells yet more vulnerable to anti-metabolic therapeutic strategies. Interestingly, cisplatin, which constitutes another mainstay of non-surgical management of advanced SCCHN (see section 1.1.5.), is inactivated by GSH and other thiol-containing proteins(449). Thus, glycolytic inhibitors such as 2-DG may also potentiate its effects. Indeed, this has been observed in two previous studies in SCCHN and presents another interesting area for further study and potential clinical translation(354, 356).

Our findings implicating oxidative stress as the mechanism underlying glycolytic inhibition in SCCHN also lend support to the hypothesis that the impetus driving cancer cells (in this case specifically mutant *TP53* SCCHN cells) towards glycolysis is at least partly to regulate cellular redox status and evade excessive ROS accumulation (see section 1.3.1.). Moreover, further findings presented in section 3.4. also support this by demonstrating that the increase in glycolysis seen in mutant *TP53* SCCHN cells also facilitates increased PPP flux. As discussed in section 1.3.1., the PPP is the major source of intracellular NADPH, which is critical to cellular redox control, and our findings demonstrate that PPP enzyme expression and associated intracellular NADPH/NADP ratios were greater in mutant *TP53* compared to wild-type SCCHN cells, indicative of increased PPP flux. Interestingly, in addition to heightening flux through subsidiary carbohydrate metabolic pathways simply by virtue of increased glycolysis, we also observed a potential mechanism that might lead to PPP diversion – specifically overexpression of TIGAR. Again as outlined in section 1.3.1., TIGAR exerts influence at a key regulatory point in the glycolytic pathway by acting to indirectly reduce PFK-1 activity and slow glycolytic flux, thus facilitating PPP diversion with resultant NADPH generation and upregulation of cellular antioxidant systems to combat oxidative stress(280). Overexpression of TIGAR, related to its role in balancing redox state in cancer cells, has been implicated in a number of tumour types. As discussed in section 1.3.3., one previous study in SCCHN, which sought to examine the reprogramming of metabolism associated with the development of radioresistance, demonstrated that radioresistant SCCHN cells displayed higher levels of TIGAR expression, as well as elevated expression of key PPP enzymes and increased production of NADPH(277). Glioma cells have also been reported to display a higher level of TIGAR expression

compared to normal brain tissue(288), and knock-down of TIGAR resulted in radiosensitisation via accumulation of ROS, leading to DNA damage and cellular senescence(450). Moreover, TKTL1 inhibition reversed the beneficial effects of TIGAR in glioma cells (in terms of GSH generation, preventing ROS accumulation, and limiting cell death during conditions of metabolic stress), further supporting the role of PPP flux(288). In multiple myeloma cells inhibition of the key oncoprotein MUC1-C resulted in downregulation of TIGAR, lower levels of NADPH, and in turn an increase in ROS and cell death(427). Similarly, in nasopharyngeal cancer cells inhibition of c-Met tyrosine kinase, the overexpression of which has been linked with poor survival outcomes and metastasis(451), resulted in lower TIGAR expression, decreased NADPH, and increased apoptosis(426). Finally, in an intestinal adenoma/carcinoma mouse model, TIGAR was found to be highly expressed when compared to surrounding normal tissue, and mice deficient in TIGAR exhibited a reduction in total tumour burden and average tumour size, associated with an enhanced survival, compared to TIGAR-competent mice(287). *In vitro*, this defective growth could be rescued with antioxidants and nucleosides(287).

This well-documented role of TIGAR overexpression in promoting cancer development through the induction of metabolic changes to counteract oxidative stress seems counterintuitive given that TIGAR is a p53-activated transcriptional target involved in the p53 tumour suppressor pathway(205, 285). However, we observed unexpectedly greater levels of baseline TIGAR expression in those SCCHN cells with abrogated p53 function, suggestive of uncoupling of TIGAR expression from p53 transcription regulation. Further time course analyses following exposure to p53-activating genotoxic stress also supported this notion, in that there was a clear direct relationship between p53 and TIGAR expression in wild-type *TP53* cells, but no such relationship in cells with abrogated p53 function, which displayed high levels of TIGAR expression at all times. Although not anticipated, this notion of uncoupling of TIGAR regulation is supported by an ever-increasing body of evidence: for instance, p53-independent expression of TIGAR has been observed in several human cancer cell lines(287), while its expression in human breast cancer has been inversely correlated with the expression of p53(286).

Whilst little is known currently about p53-independent regulation of TIGAR, the capacity for a p53-target protein to become oncogenic when no longer tightly controlled has also been described for other mediators of the p53 survival response. Specifically, p53-independent overexpression of carnitine palmitoyltransferase 1C (CPT1C), which is normally a p53-activated transcript, has been reported in lung cancers in response to

metabolic stress to increase fatty acid oxidation and ATP production(452). Interestingly, regulation of CPT1C in this instance depends on a mechanism that involves activated AMPK(452), which as a key metabolic mediator may be implicated in p53-independent regulation of TIGAR. Notably, other members of the p53 family, p63 and p73, can activate promoters of several p53 target genes(453, 454), and could conceivably, therefore, also be capable of regulating TIGAR expression. Alternatively, other transcription factors may be involved: in particular another transcription factor, SP1, has also been found to regulate the basal level of TIGAR expression in liver cancer cell lines(455). Future work investigating TIGAR expression in this context may, therefore, be centred on these possibilities. Additionally, mutant forms of p53 can display oncogenic GOF properties that can also involve modulation of tumour metabolism(319), and it is plausible that certain mutant forms of p53 retain the ability to influence the expression of TIGAR. Our findings, however, do not support this given that high levels of TIGAR expression were observed in p53 null cell lines and when a stable wild-type p53 knock-down was engineered in a *TP53* wild-type cell line. Nonetheless, p53-independent regulation of TIGAR may be transcriptional, translational, or through post-translational modifications of the protein and this will be an interesting area for further study. In the first instance this could take the form of co-immunoprecipitaion and chromatin immunoprecipitaion to explore possible protein-protein and protein-DNA interactions respectively. It will also be important to explore TIGAR expression levels under conditions of hypoxia as although TIGAR expression is not controlled by hypoxia, the activity of TIGAR is modulated under conditions of low oxygen. Specifically, it has been reported that during hypoxia, a fraction of TIGAR relocates to the mitochondria and associates with and enhances the activity of hexokinase-II(289). Perhaps of greater priority in terms of future study, however, is to examine further the contribution and importance of TIGAR overexpression to survival in mutant *TP53* SCCHN cells as this may have therapeutic implications. To begin to address this, shRNAs designed to knock-down TIGAR could be developed and transfected into mutant *TP53* SCCHN cell lines, and the impact on proliferation and sensitivity to IR assessed. Should this have significant effects on proliferation and/or radiosensitisation it would suggest that development of an inhibitor of TIGAR would be a promising novel therapeutic avenue, which may offer yet greater selectivity over glycolytic inhibition.

Importantly, identifying that a major impetus for metabolic re-programming towards glycolysis in SCCHN cells with abrogated p53 function was to upregulate cellular antioxidant systems by heightening of PPP flux also revealed a further potential

therapeutic gain. The addition of the PPP inhibitor 6-AN significantly augmented effects of IR in these cells over and above the potentiating effects of glycolytic inhibition alone. As discussed in section 3.2.4., although investigation of 6-AN in SCCHN has been limited to studies by only two research groups, findings are consistent with those presented here, in that combining 2-DG with 6-AN enhanced cytotoxicity over 2-DG alone(277, 403, 456). No previous studies, however, have examined this effect with respect to *TP53* status. Although 6-AN is an inhibitor of the key PPP enzyme 6-PGD, and thus would inhibit NADPH production and upregulation of cellular anti-oxidant systems, on initial consideration it is perhaps surprising that 6-AN provided further therapeutic gain over 2-DG given that 2-DG inhibits glycolysis upstream of PPP branching. However, it has been reported that 2-deoxy-D-glucose-6-phosphate (phosphorylated product of 2-DG by hexokinase) can be oxidised to 2-deoxygluconate-6-phosphate by G6PD, leading to the regeneration of one molecule of NADPH and subsequent regeneration of GSH from glutathione disulfide(404). Additionally, the products of gluconeogenesis feeding into the PPP may still occur in 2-DG treated cells. Thus, inhibition of glycolysis and PPP by 2-DG alone does not inhibit NADPH regeneration maximally, and distinct PPP inhibition is required to restrict NADPH production and upregulation of cellular anti-oxidant systems. There are concerns, however, over potentially toxic side-effects, in particular neurotoxicity(457). Yet, in studies to date selective cytotoxicity for cancer cells has been observed, with no significant loss of viability or clonogenicity in non-malignantly transformed human embryonic kidney cells and human lung fibroblasts following treatment with 2-DG + 6-AN + IR(456, 458). Nonetheless, 6-AN has yet to be subjected to clinical evaluation. As such, whilst the *in vitro* results presented here are compelling, extensive further validation in the pre-clinical setting using the experimental systems described above would again be required before contemplating clinical trials, particularly focusing on *in vivo* dose-escalation and dose-limiting toxicity studies.

In addition to identifying increased PPP flux mediated through de-regulated TIGAR overexpression as mechanisms underlying the metabolic shift in mutant *TP53* SCCHN, we also demonstrated ETC complex dysfunction and GLUT-1 overexpression. Analysis of individual ETC complexes in permeabilised cells presented in section 3.4.2. suggests that in SCCHN cells loss of wild-type p53 function results in global defective functioning of ETC complexes, most marked for complexes II and III. These findings are broadly consistent with the only previous study in SCCHN examining ETC complex integrity, which reported defects in the activity of complexes II, III, and IV in mutant *TP53* SCCHN cells(360). However, these findings are at odds with contemporary opinion that tumour

metabolism is a dynamic process adopted by cancer cells to fit the requirements of rapid cell proliferation, rather than a self-correcting secondary consequence to, for example, energy deficiency resulting from defective mitochondrial respiration. Indeed, findings with regards to ETC function in the wider field of cancer research have been conflicting, with some reports suggesting dysfunction in oxidative phosphorylation(459, 460) and others indicating that the capacity for oxidative phosphorylation is retained and oxygen is consumed at rates similar to those observed in normal tissues(249, 259). Notwithstanding, because ROS are natural by-products of mitochondrial respiration, it may be the case that dampening oxidative phosphorylation represents another mechanism to protect cancer cells from excessive ROS accumulation and oxidative stress(461). Moreover, our findings specific to loss of wild-type p53 function and ETC dysfunction are in keeping with evidence demonstrating p53 as a promoter of oxidative phosphorylation. As discussed in greater depth in section 1.3.2., p53 has been linked with the general maintenance of mitochondrial biomass, integrity, quality control, and fidelity of mitochondrial DNA replication (300-303), as well as with several aspects of ETC complex function(286, 305-309). The fact that in mutant *TP53* SCCHN there is global dysfunction of ETC complexes is also an important consideration from a therapeutic standpoint insofar as therapeutic strategies predicated on inhibition of oxidative phosphorylation, such as metformin, are likely to have limited efficacy in these tumours. This is highly relevant given the current interest in re-purposing metformin as an anti-cancer agent, as discussed above, and should inform any future work to this end.

That levels of GLUT-1 expression were demonstrated to be partly attributable to the observed p53-dependent switch in metabolism towards glycolysis, with loss of wild-type p53 function resulting in relative GLUT-1 overexpression, was an expected finding in light of our initial metabolic profiling results. Considering that SCCHN cells with loss of wild-type p53 function adopted a glycolytic phenotype, and that glycolysis is a relatively energetically inefficient process (yielding only two molecules of ATP per molecule of glucose consumed as opposed to up to 36 with oxidative phosphorylation), these cells would need to drastically increase rates of glycolysis to maintain sufficient ATP production, which would require a corresponding upregulation of glucose transporters. Consistent with this, in addition to sustaining higher basal levels of glycolysis, these cells also exhibited higher overall glycolytic capacities. Furthermore, as discussed previously in section 3.4.3., this finding is in keeping with the fact that *TP53* mutation diminishes the repressive effect of p53 on GLUT-1 transcription (298), and with several previous reports of GLUT-1 expression in SCCHN relative to normal tissues

(324-329). Curiously, however, in the only other study to date examining GLUT-1 expression in SCCHN relative to *TP53* status no difference in expression of GLUT-1 in wild-type and mutant *TP53* cells was observed(360). The reason for this disparity is unclear, and most likely relates to the specific cell lines investigated. Whilst our findings were consistently demonstrated across a panel of SCCHN cell lines, the earlier study examined GLUT-1 expression only in one mutant and one wild-type *TP53* SCCHN cell line.

By analogy to our expectation of differential GLUT-1 expression, its was perhaps surprising that no obvious differences were observed between mutant and wild-type *TP53* SCCHN cells in the expression of the other glycolysis-related enzymes and transporters examined. Our investigation of this, however, was limited to western blot analyses of the glycolysis-related proteins previously reported to be under the direct influence of p53, which may have been too narrow and simplistic an approach. For instance, p53 may mediate the activity and/or expression of other metabolic proteins in the context of SCCHN that have yet to be elucidated, the differential expression of which would not have been captured using our approach. Furthermore, as discussed in section 1.3.2., there is also a substantial degree of cross-talk between the p53 system and several other key metabolic mediating pathways – including PI3K/Akt(310), mTOR(310, 311), HIF-1α(315), and NF-kβ(316) pathways – resulting in indirect p53 regulation. Again, any alterations in these indirect links may have been missed in our analysis. Our decision to centre our investigation on glycolysis-related proteins known to be under the influence of wild-type p53, however, was taken largely due to time and resource constraints on the project, cognizant of the anticipated limitations. Future experiments directed at more extensive profiling would be interesting to pursue to potentially elucidate further mechanisms underpinning the p53-dependent metabolic switch in SCCHN. These experiments could be conducted using either a gene array analysis platform, with a panel reflecting genes involved in cellular metabolism, or using a next-generation sequencing approach. Complementary examination of metabolite levels using NMR spectroscopy or mass spectrometry could also be utilised, as flux is not only a reflection of steady state levels of gene expression.

These experimental systems could also be utilised to examine metabolism in SCCHN more globally. Indeed, the work in this thesis focused exclusively on carbohydrate metabolism. Whilst this was predicated on the fact that alterations in carbohydrate metabolism remain chief among the recognised metabolic perturbations of the cancer

phenotype and that glucose catabolism has been identified as the predominant metabolic pathway on which SCCHN cells depend(359), future work exploring other metabolic avenues may reveal other potential therapeutic windows to exploit. In accordance with this, the aforementioned study aiming to identify metabolic alterations related to the development of radioresistance in SCCHN reported alterations in lipid metabolism with associated therapeutic implications(277). Specifically, increased expression and activity of fatty acid synthase (FASN) was reported in a radioresistant SCCHN cell line, suggestive of increased utilisation of endogenous fatty acids for energy production, and FASN inhibition with orlistat increased cytotoxicity and radiosensitised these cells(277). Furthermore, a recent study identified a subpopulation of cells in oral cavity SCC implicated in initiating metastases that are predominantly defined by a signature of lipid metabolism, and of particular interest, blocking lipid uptake resulted in almost complete inhibition of metastases in orthotopic oral SCC mouse models(462).

Ultimately, the work presented in this thesis is of potential interest from a translational research perspective because it explores the possibility of therapeutically targeting a fundamental area of cancer cell biology to induce radiosensitisation, an area that for SCCHN is relatively uncharted. Our initial studies demonstrated that the metabolic phenotype in SCCHN is p53-dependent, with mutational loss of wild-type p53 function resulting in a loss of metabolic diversity and conferring a survival dependence on glycolysis. Further work showed that upregulation of cellular antioxidant systems to quench excessive ROS accumulation underlies this glycolytic switch, which is achieved by heightening PPP flux to produce NADPH through GLUT-1 overexpression and uncoupling of TIGAR regulation with resultant overexpression. Critically, subsequent therapeutic studies correlated with these findings, which has led us to propound a novel, tailored anti-metabolic therapeutic paradigm for SCCHN, which not only carries a selective therapeutic index, but is also informed by *TP53* status as a predictive biomarker. Specifically, we propose that in mutant *TP53* SCCHNs glycolytic inhibition with 2-DG, possibly in combination with 6-AN-induced PPP inhibition, would result in significant radiosensitisation through oxidative stress-mediated activation of apoptotic signalling. This strategy would be applicable in upwards of 60-85% of SCCHN tumours(51-53) and would be preferentially effective in patients with the aggressive and treatment-resistant disease typically associated with *TP53* mutation(56-58, 238, 239). SCCHNs harbouring wild-type *TP53* (HPV-positive disease included) are likely to be resistant to this approach, reflecting their more metabolically diverse phenotype. In these cases, therefore, we suggest the combination of 2-DG with mitochondrial

inhibition, using metformin. This strategy may also provide an attractive platform for the treatment de-intensification of carefully selected HPV-positive cases by facilitating RT dose reduction to minimise the impact of treatment on long-term function. The efficacy and safety of these strategies will require further validation in pre-clinical models prior to translation into the clinical setting, and future work will be directed in this regard. Nevertheless, we have presented a novel approach to the treatment of SCCHN, together with mechanistic insights, that takes into account *TP53* mutational status in determining selection of radiosensitising anti-metabolic agents, and which provides a rationale for initiating clinical trials.

5. Appendix

5.1. Mycoplasma contamination

As part of an effort to optimise the cell lines used in this thesis, all cell lines were tested for the presence of mycoplasma contamination as described in section 2.3.2. During the course of this testing several of the cell lines were found to be contaminated, examples of which are shown in figure 5.1.1.

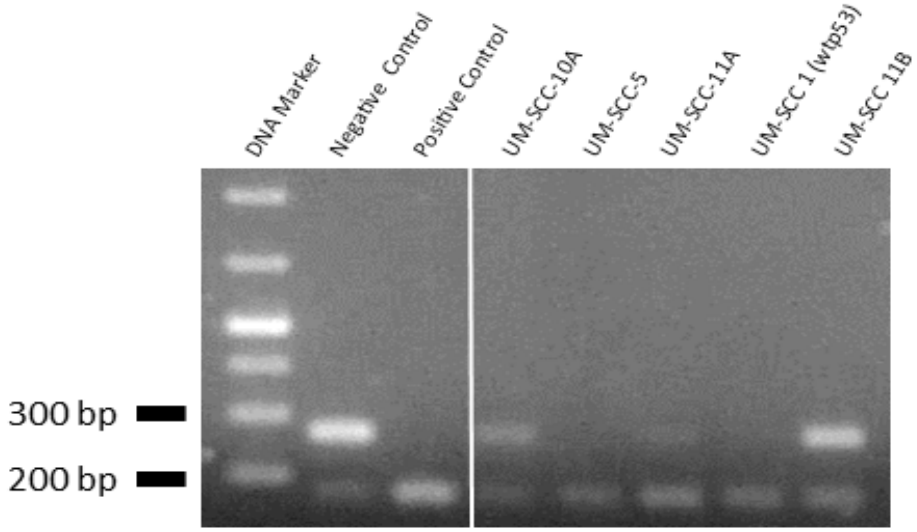

Figure 5.1.1: An example of mycoplasma contamination. The output from the e-Myco™ mycoplasma PCR detection kit (ChemBio) demonstrating presence of mycoplasma-specific DNA sequences in UM-SCC-10A, UM-SCC-11A, and UM-SCC-11B. Mycoplasm positive sequences are found at 268-277 bp as sizes of the PCR product depend on the individual species. There is also an internal control band at 160bp to confirm quality of PCR.

5.2. Mycoplasma eradication

If no negative stocks of contaminated cell lines could be sourced these cells were then treated to eradicate the contamination. Initially a decision was made to attempt eradication with the aminoglycoside antibiotic geneticin. This decision was based on the findings that one of our cell lines (UM-SCC-12) was mycoplasma positive, while genetically engineered cell lines derived from this line that were selected for with

geneticin were negative for mycoplasma. MTT assays (section 2.5.2.) were used to determine drug sensitivity to geneticin. Specifically, the concentration to be used for treating the cell lines was the maximal concentration that minimally affected growth and viability. Examples for three cell lines are depicted in figure 5.2.1. The chosen concentration for treatment was 100µg/ml.

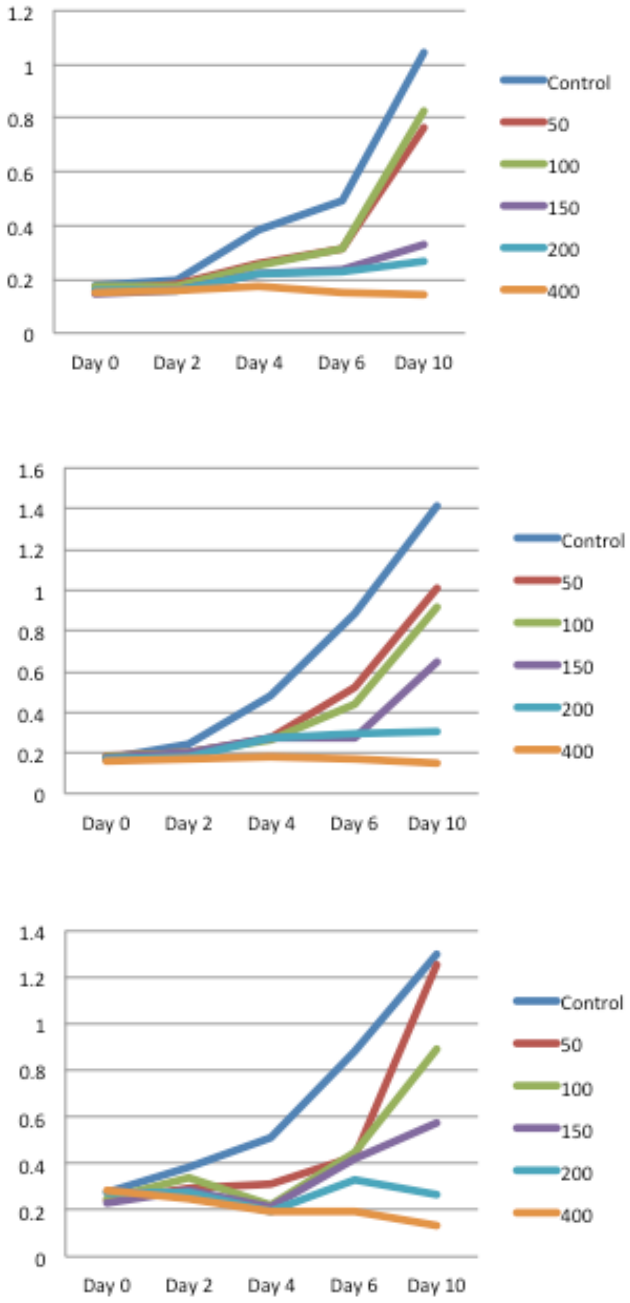

Figure 5.2.1: Examples of MTT assays used to determine treatment concentration of geneticin. MTT assays were performed as described in section 2.5.2. and are shown for UM-SCC-

10A, UM-SCC-11A, and UM-SCC-11B. All concentrations shown are in µg/ml. The optimal concentration chosen to treat the cell lines was 100µg/ml.

Following two weeks of treatment with 100µg/ml geneticin all treated cell lines remained positive for mycoplasma contamination. Consequently, it was then decided to treat these lines with a commercially available and well-established mycoplasma eradication reagent – Plasmocin™ (Invivogen)(463). Contaminated cell lines were treated for two-three weeks at a concentration of 25µg/ml. This successfully eradicated the mycoplasma contamination in all cell lines. All cell lines were continually tested every six-eight weeks to ensure no further contamination.

6. References

1. Argiris A, Karamouzis MV, Raben D, Ferris RL. Head and neck cancer. Lancet. 2008;371(9625):1695-709.
2. Mehanna H, Paleri V, West CM, Nutting C. Head and neck cancer--Part 1: Epidemiology, presentation, and prevention. Bmj. 2010;341:c4684.
3. Bosch FX, Ritter D, Enders C, Flechtenmacher C, Abel U, Dietz A, et al. Head and neck tumor sites differ in prevalence and spectrum of p53 alterations but these have limited prognostic value. Int J Cancer. 2004;111(4):530-8.
4. Timar J, Csuka O, Remenar E, Repassy G, Kasler M. Progression of head and neck squamous cell cancer. Cancer Metastasis Rev. 2005;24(1):107-27.
5. Watkinson JCG, R.W. Stell & Maran's Textbook of Head and Neck Surgery and Oncology. 5th ed. London, U.K.: Hodder Arnold; 2012.
6. Wei WI, Sham JS. Nasopharyngeal carcinoma. Lancet. 2005;365(9476):2041-54.
7. Foundation T. The Head & Neck Cancer Guide [Available from: http://www.headandneckcancerguide.org/teens/cancer-basics/explore-cancer-types/throat-cancer/laryngopharyngeal-cancer/hypopharyngeal-cancer/.
8. Schache AG, Lieger O, Rogers P, Kelly A, Newman L, Kalavrezos N. Predictors of swallowing outcome in patients treated with surgery and radiotherapy for advanced oral and oropharyngeal cancer. Oral Oncol. 2009;45(9):803-8.
9. Nicoletti G, Soutar DS, Jackson MS, Wrench AA, Robertson G. Chewing and swallowing after surgical treatment for oral cancer: functional evaluation in 196 selected cases. Plastic and reconstructive surgery. 2004;114(2):329-38.
10. Ferlay JS, I.; Ervik, M.; Dikshit, R.; Eser, S.; Mathers, C.; Rebelo, M.; Parkin, D.M.; Forman, D.; Bray, F. GLOBOCAN 2012 v1.0, Cancer Incidence and Mortality Worldwide Lyon, France: IARC CancerBase; 2012 [Available from: http://globocan.iarc.fr.
11. UK CR. Cancer Statistics for the UK London, UK: Cancer Research UK; 2016 [Available from: http://www.cancerresearchuk.org/health-professional/cancer-statistics.
12. Boyle PL, B. World cancer report. International Agency for Research on Cancer. 2008:1-503.
13. Conway DI, Hashibe M, Boffetta P, consortium I, Wunsch-Filho V, Muscat J, et al. Enhancing epidemiologic research on head and neck cancer: INHANCE - The international head and neck cancer epidemiology consortium. Oral Oncol. 2009;45(9):743-6.
14. Maier H, Dietz A, Gewelke U, Heller WD, Weidauer H. Tobacco and alcohol and the risk of head and neck cancer. Clin Investig. 1992;70(3-4):320-7.
15. Lewin F, Norell SE, Johansson H, Gustavsson P, Wennerberg J, Biorklund A, et al. Smoking tobacco, oral snuff, and alcohol in the etiology of squamous cell carcinoma of the head and neck: a population-based case-referent study in Sweden. Cancer. 1998;82(7):1367-75.
16. Boffetta P, Hecht S, Gray N, Gupta P, Straif K. Smokeless tobacco and cancer. Lancet Oncol. 2008;9(7):667-75.
17. Hashibe M, Brennan P, Benhamou S, Castellsague X, Chen C, Curado MP, et al. Alcohol drinking in never users of tobacco, cigarette smoking in never

drinkers, and the risk of head and neck cancer: pooled analysis in the International Head and Neck Cancer Epidemiology Consortium. J Natl Cancer Inst. 2007;99(10):777-89.
18. Hashibe M, Boffetta P, Zaridze D, Shangina O, Szeszenia-Dabrowska N, Mates D, et al. Evidence for an important role of alcohol- and aldehyde-metabolizing genes in cancers of the upper aerodigestive tract. Cancer Epidemiol Biomarkers Prev. 2006;15(4):696-703.
19. Druesne-Pecollo N, Tehard B, Mallet Y, Gerber M, Norat T, Hercberg S, et al. Alcohol and genetic polymorphisms: effect on risk of alcohol-related cancer. Lancet Oncol. 2009;10(2):173-80.
20. Humans IWGotEoCRt. Human papillomaviruses. IARC Monographs on the Evaluation of Carcinogenic Risks to Humans. 2007;90:1-670.
21. Tommasino M. The human papillomavirus family and its role in carcinogenesis. Semin Cancer Biol. 2014;26:13-21.
22. Syrjanen K, Syrjanen S, Lamberg M, Pyrhonen S, Nuutinen J. Morphological and immunohistochemical evidence suggesting human papillomavirus (HPV) involvement in oral squamous cell carcinogenesis. Int J Oral Surg. 1983;12(6):418-24.
23. Kreimer AR, Clifford GM, Boyle P, Franceschi S. Human papillomavirus types in head and neck squamous cell carcinomas worldwide: a systematic review. Cancer Epidemiol Biomarkers Prev. 2005;14(2):467-75.
24. Hobbs CG, Sterne JA, Bailey M, Heyderman RS, Birchall MA, Thomas SJ. Human papillomavirus and head and neck cancer: a systematic review and meta-analysis. Clinical otolaryngology : official journal of ENT-UK ; official journal of Netherlands Society for Oto-Rhino-Laryngology & Cervico-Facial Surgery. 2006;31(4):259-66.
25. Mehanna H, Beech T, Nicholson T, El-Hariry I, McConkey C, Paleri V, et al. Prevalence of human papillomavirus in oropharyngeal and nonoropharyngeal head and neck cancer--systematic review and meta-analysis of trends by time and region. Head Neck. 2013;35(5):747-55.
26. Gillison ML, Koch WM, Capone RB, Spafford M, Westra WH, Wu L, et al. Evidence for a causal association between human papillomavirus and a subset of head and neck cancers. J Natl Cancer Inst. 2000;92(9):709-20.
27. Begum S, Cao D, Gillison M, Zahurak M, Westra WH. Tissue distribution of human papillomavirus 16 DNA integration in patients with tonsillar carcinoma. Clin Cancer Res. 2005;11(16):5694-9.
28. Kreimer AR, Clifford GM, Snijders PJ, Castellsague X, Meijer CJ, Pawlita M, et al. HPV16 semiquantitative viral load and serologic biomarkers in oral and oropharyngeal squamous cell carcinomas. Int J Cancer. 2005;115(2):329-32.
29. Braakhuis BJ, Snijders PJ, Keune WJ, Meijer CJ, Ruijter-Schippers HJ, Leemans CR, et al. Genetic patterns in head and neck cancers that contain or lack transcriptionally active human papillomavirus. J Natl Cancer Inst. 2004;96(13):998-1006.
30. Fakhry C, Gillison ML. Clinical implications of human papillomavirus in head and neck cancers. Journal of clinical oncology : official journal of the American Society of Clinical Oncology. 2006;24(17):2606-11.
31. Heck JE, Berthiller J, Vaccarella S, Winn DM, Smith EM, Shan'gina O, et al. Sexual behaviours and the risk of head and neck cancers: a pooled analysis in the

International Head and Neck Cancer Epidemiology (INHANCE) consortium. Int J Epidemiol. 2010;39(1):166-81.
32. Pavia M, Pileggi C, Nobile CG, Angelillo IF. Association between fruit and vegetable consumption and oral cancer: a meta-analysis of observational studies. Am J Clin Nutr. 2006;83(5):1126-34.
33. Zheng W, Blot WJ, Shu XO, Diamond EL, Gao YT, Ji BT, et al. Risk factors for oral and pharyngeal cancer in Shanghai, with emphasis on diet. Cancer Epidemiol Biomarkers Prev. 1992;1(6):441-8.
34. Chang JS, Lo HI, Wong TY, Huang CC, Lee WT, Tsai ST, et al. Investigating the association between oral hygiene and head and neck cancer. Oral Oncol. 2013;49(10):1010-7.
35. Maier H, Tisch M. [Occupation and cancer of the head-neck area]. HNO. 1999;47(12):1025-37.
36. Gustavsson P, Jakobsson R, Johansson H, Lewin F, Norell S, Rutkvist LE. Occupational exposures and squamous cell carcinoma of the oral cavity, pharynx, larynx, and oesophagus: a case-control study in Sweden. Occup Environ Med. 1998;55(6):393-400.
37. Mathers CD, Loncar D. Projections of global mortality and burden of disease from 2002 to 2030. PLoS Med. 2006;3(11):e442.
38. Institute SNC. Surveillance epidemiology and end results [Available from: http://seer.cancer.gov/faststats/selections.php - Output,.
39. Network NCI. Profile of head and neck cancers 2010 [Available from: http://library.ncin.org.uk/docs/100504-OCIU Head_and_Neck_Profi- les.pdf.
40. Ramqvist T, Dalianis T. An epidemic of oropharyngeal squamous cell carcinoma (OSCC) due to human papillomavirus (HPV) infection and aspects of treatment and prevention. Anticancer Res. 2011;31(5):1515-9.
41. Schache AG, Powell NG, Cuschieri KS, Robinson M, Leary S, Mehanna H, et al. HPV-Related Oropharynx Cancer in the United Kingdom: An Evolution in the Understanding of Disease Etiology. Cancer research. 2016;76(22):6598-606.
42. Leemans CR, Braakhuis BJ, Brakenhoff RH. The molecular biology of head and neck cancer. Nat Rev Cancer. 2011;11(1):9-22.
43. Hanahan D, Weinberg RA. The hallmarks of cancer. Cell. 2000;100(1):57-70.
44. Hanahan D, Weinberg RA. Hallmarks of cancer: the next generation. Cell. 2011;144(5):646-74.
45. Chung CH, Parker JS, Karaca G, Wu J, Funkhouser WK, Moore D, et al. Molecular classification of head and neck squamous cell carcinomas using patterns of gene expression. Cancer Cell. 2004;5(5):489-500.
46. Smeets SJ, Brakenhoff RH, Ylstra B, van Wieringen WN, van de Wiel MA, Leemans CR, et al. Genetic classification of oral and oropharyngeal carcinomas identifies subgroups with a different prognosis. Cell Oncol. 2009;31(4):291-300.
47. Smeets SJ, Braakhuis BJ, Abbas S, Snijders PJ, Ylstra B, van de Wiel MA, et al. Genome-wide DNA copy number alterations in head and neck squamous cell carcinomas with or without oncogene-expressing human papillomavirus. Oncogene. 2006;25(17):2558-64.
48. Slebos RJ, Yi Y, Ely K, Carter J, Evjen A, Zhang X, et al. Gene expression differences associated with human papillomavirus status in head and neck squamous cell carcinoma. Clin Cancer Res. 2006;12(3 Pt 1):701-9.

49. Lechner M, Frampton GM, Fenton T, Feber A, Palmer G, Jay A, et al. Targeted next-generation sequencing of head and neck squamous cell carcinoma identifies novel genetic alterations in HPV+ and HPV- tumors. Genome Med. 2013;5(5):49.
50. Huang SH, O'Sullivan B. Overview of the 8th Edition TNM Classification for Head and Neck Cancer. Curr Treat Options Oncol. 2017;18(7):40.
51. Agrawal N, Frederick MJ, Pickering CR, Bettegowda C, Chang K, Li RJ, et al. Exome sequencing of head and neck squamous cell carcinoma reveals inactivating mutations in NOTCH1. Science. 2011;333(6046):1154-7.
52. Stransky N, Egloff AM, Tward AD, Kostic AD, Cibulskis K, Sivachenko A, et al. The mutational landscape of head and neck squamous cell carcinoma. Science. 2011;333(6046):1157-60.
53. Cancer Genome Atlas N. Comprehensive genomic characterization of head and neck squamous cell carcinomas. Nature. 2015;517(7536):576-82.
54. Petitjean A, Mathe E, Kato S, Ishioka C, Tavtigian SV, Hainaut P, et al. Impact of mutant p53 functional properties on TP53 mutation patterns and tumor phenotype: lessons from recent developments in the IARC TP53 database. Hum Mutat. 2007;28(6):622-9.
55. Muller PA, Vousden KH. p53 mutations in cancer. Nat Cell Biol. 2013;15(1):2-8.
56. Poeta ML, Manola J, Goldwasser MA, Forastiere A, Benoit N, Califano JA, et al. TP53 mutations and survival in squamous-cell carcinoma of the head and neck. The New England journal of medicine. 2007;357(25):2552-61.
57. Skinner HD, Sandulache VC, Ow TJ, Meyn RE, Yordy JS, Beadle BM, et al. TP53 disruptive mutations lead to head and neck cancer treatment failure through inhibition of radiation-induced senescence. Clin Cancer Res. 2012;18(1):290-300.
58. Neskey DM, Osman AA, Ow TJ, Katsonis P, McDonald T, Hicks SC, et al. Evolutionary Action Score of TP53 Identifies High-Risk Mutations Associated with Decreased Survival and Increased Distant Metastases in Head and Neck Cancer. Cancer research. 2015;75(7):1527-36.
59. Boyle JO, Hakim J, Koch W, van der Riet P, Hruban RH, Roa RA, et al. The incidence of p53 mutations increases with progression of head and neck cancer. Cancer research. 1993;53(19):4477-80.
60. Nees M, Homann N, Discher H, Andl T, Enders C, Herold-Mende C, et al. Expression of mutated p53 occurs in tumor-distant epithelia of head and neck cancer patients: a possible molecular basis for the development of multiple tumors. Cancer research. 1993;53(18):4189-96.
61. Tjebbes GW, Leppers vd Straat FG, Tilanus MG, Hordijk GJ, Slootweg PJ. p53 tumor suppressor gene as a clonal marker in head and neck squamous cell carcinoma: p53 mutations in primary tumor and matched lymph node metastases. Oral Oncol. 1999;35(4):384-9.
62. Braakhuis BJ, Leemans CR, Brakenhoff RH. A genetic progression model of oral cancer: current evidence and clinical implications. J Oral Pathol Med. 2004;33(6):317-22.
63. Miller DL, Puricelli MD, Stack MS. Virology and molecular pathogenesis of HPV (human papillomavirus)-associated oropharyngeal squamous cell carcinoma. Biochem J. 2012;443(2):339-53.

64. Westra WH, Taube JM, Poeta ML, Begum S, Sidransky D, Koch WM. Inverse relationship between human papillomavirus-16 infection and disruptive p53 gene mutations in squamous cell carcinoma of the head and neck. Clin Cancer Res. 2008;14(2):366-9.
65. Huibregtse JM, Scheffner M, Howley PM. A cellular protein mediates association of p53 with the E6 oncoprotein of human papillomavirus types 16 or 18. EMBO J. 1991;10(13):4129-35.
66. Lechner MS, Laimins LA. Inhibition of p53 DNA binding by human papillomavirus E6 proteins. J Virol. 1994;68(7):4262-73.
67. Nevins JR. The Rb/E2F pathway and cancer. Hum Mol Genet. 2001;10(7):699-703.
68. Park HW, Song SY, Lee TJ, Jeong D, Lee TY. Abrogation of the p16-retinoblastoma-cyclin D1 pathway in head and neck squamous cell carcinomas. Oncol Rep. 2007;18(1):267-72.
69. Rayess H, Wang MB, Srivatsan ES. Cellular senescence and tumor suppressor gene p16. Int J Cancer. 2012;130(8):1715-25.
70. Schache AG, Liloglou T, Risk JM, Filia A, Jones TM, Sheard J, et al. Evaluation of human papilloma virus diagnostic testing in oropharyngeal squamous cell carcinoma: sensitivity, specificity, and prognostic discrimination. Clin Cancer Res. 2011;17(19):6262-71.
71. Bova RJ, Quinn DI, Nankervis JS, Cole IE, Sheridan BF, Jensen MJ, et al. Cyclin D1 and p16INK4A expression predict reduced survival in carcinoma of the anterior tongue. Clin Cancer Res. 1999;5(10):2810-9.
72. Reed AL, Califano J, Cairns P, Westra WH, Jones RM, Koch W, et al. High frequency of p16 (CDKN2/MTS-1/INK4A) inactivation in head and neck squamous cell carcinoma. Cancer research. 1996;56(16):3630-3.
73. Smith EM, Wang D, Kim Y, Rubenstein LM, Lee JH, Haugen TH, et al. P16INK4a expression, human papillomavirus, and survival in head and neck cancer. Oral Oncol. 2008;44(2):133-42.
74. Lee SY, Kumano K, Nakazaki K, Sanada M, Matsumoto A, Yamamoto G, et al. Gain-of-function mutations and copy number increases of Notch2 in diffuse large B-cell lymphoma. Cancer Sci. 2009;100(5):920-6.
75. Weng AP, Ferrando AA, Lee W, Morris JPt, Silverman LB, Sanchez-Irizarry C, et al. Activating mutations of NOTCH1 in human T cell acute lymphoblastic leukemia. Science. 2004;306(5694):269-71.
76. Talora C, Sgroi DC, Crum CP, Dotto GP. Specific down-modulation of Notch1 signaling in cervical cancer cells is required for sustained HPV-E6/E7 expression and late steps of malignant transformation. Genes Dev. 2002;16(17):2252-63.
77. Devgan V, Mammucari C, Millar SE, Brisken C, Dotto GP. p21WAF1/Cip1 is a negative transcriptional regulator of Wnt4 expression downstream of Notch1 activation. Genes Dev. 2005;19(12):1485-95.
78. Niimi H, Pardali K, Vanlandewijck M, Heldin CH, Moustakas A. Notch signaling is necessary for epithelial growth arrest by TGF-beta. J Cell Biol. 2007;176(5):695-707.
79. Rangarajan A, Talora C, Okuyama R, Nicolas M, Mammucari C, Oh H, et al. Notch signaling is a direct determinant of keratinocyte growth arrest and entry into differentiation. EMBO J. 2001;20(13):3427-36.

80. Mehanna H, West CM, Nutting C, Paleri V. Head and neck cancer--Part 2: Treatment and prognostic factors. Bmj. 2010;341:c4690.
81. Marur S, Forastiere AA. Head and Neck Squamous Cell Carcinoma: Update on Epidemiology, Diagnosis, and Treatment. Mayo Clin Proc. 2016;91(3):386-96.
82. Grandis JR, Tweardy DJ. Elevated levels of transforming growth factor alpha and epidermal growth factor receptor messenger RNA are early markers of carcinogenesis in head and neck cancer. Cancer research. 1993;53(15):3579-84.
83. Ang KK, Berkey BA, Tu X, Zhang HZ, Katz R, Hammond EH, et al. Impact of epidermal growth factor receptor expression on survival and pattern of relapse in patients with advanced head and neck carcinoma. Cancer research. 2002;62(24):7350-6.
84. Herbst RS. Review of epidermal growth factor receptor biology. Int J Radiat Oncol Biol Phys. 2004;59(2 Suppl):21-6.
85. Lin SY, Makino K, Xia W, Matin A, Wen Y, Kwong KY, et al. Nuclear localization of EGF receptor and its potential new role as a transcription factor. Nat Cell Biol. 2001;3(9):802-8.
86. Rubin Grandis J, Tweardy DJ, Melhem MF. Asynchronous modulation of transforming growth factor alpha and epidermal growth factor receptor protein expression in progression of premalignant lesions to head and neck squamous cell carcinoma. Clin Cancer Res. 1998;4(1):13-20.
87. Ferreira MB, Lima JP, Cohen EE. Novel targeted therapies in head and neck cancer. Expert Opin Investig Drugs. 2012;21(3):281-95.
88. Bonner JA, Harari PM, Giralt J, Azarnia N, Shin DM, Cohen RB, et al. Radiotherapy plus cetuximab for squamous-cell carcinoma of the head and neck. The New England journal of medicine. 2006;354(6):567-78.
89. Vermorken JB, Mesia R, Rivera F, Remenar E, Kawecki A, Rottey S, et al. Platinum-based chemotherapy plus cetuximab in head and neck cancer. The New England journal of medicine. 2008;359(11):1116-27.
90. Roland NJP, V. Head and Neck Cancer: Multidisciplinary Management Guidelines. 4th ed. London, UK: ENT UK; 2011.
91. Leibel SA, Scott CB, Mohiuddin M, Marcial VA, Coia LR, Davis LW, et al. The effect of local-regional control on distant metastatic dissemination in carcinoma of the head and neck: results of an analysis from the RTOG head and neck database. Int J Radiat Oncol Biol Phys. 1991;21(3):549-56.
92. Ghosh SK, Roland NJ, Kumar A, Tandon S, Lancaster JL, Jackson SR, et al. Detection of synchronous lung tumors in patients presenting with squamous cell carcinoma of the head and neck. Head Neck. 2009;31(12):1563-70.
93. Czernin J, Benz MR, Allen-Auerbach MS. PET/CT imaging: The incremental value of assessing the glucose metabolic phenotype and the structure of cancers in a single examination. Eur J Radiol. 2010;73(3):470-80.
94. Fakhry C, Westra WH, Li S, Cmelak A, Ridge JA, Pinto H, et al. Improved survival of patients with human papillomavirus-positive head and neck squamous cell carcinoma in a prospective clinical trial. J Natl Cancer Inst. 2008;100(4):261-9.
95. Ang KK, Harris J, Wheeler R, Weber R, Rosenthal DI, Nguyen-Tan PF, et al. Human papillomavirus and survival of patients with oropharyngeal cancer. The New England journal of medicine. 2010;363(1):24-35.
96. Licitra L, Perrone F, Bossi P, Suardi S, Mariani L, Artusi R, et al. High-risk human papillomavirus affects prognosis in patients with surgically treated

oropharyngeal squamous cell carcinoma. Journal of clinical oncology : official journal of the American Society of Clinical Oncology. 2006;24(36):5630-6.
97. Robinson M, Schache A, Sloan P, Thavaraj S. HPV specific testing: a requirement for oropharyngeal squamous cell carcinoma patients. Head Neck Pathol. 2012;6 Suppl 1:S83-90.
98. Robinson M, Sloan P, Shaw R. Refining the diagnosis of oropharyngeal squamous cell carcinoma using human papillomavirus testing. Oral Oncol. 2010;46(7):492-6.
99. Westra WH. The changing face of head and neck cancer in the 21st century: the impact of HPV on the epidemiology and pathology of oral cancer. Head Neck Pathol. 2009;3(1):78-81.
100. Mellin H, Friesland S, Lewensohn R, Dalianis T, Munck-Wikland E. Human papillomavirus (HPV) DNA in tonsillar cancer: clinical correlates, risk of relapse, and survival. Int J Cancer. 2000;89(3):300-4.
101. Ragin CC, Taioli E. Survival of squamous cell carcinoma of the head and neck in relation to human papillomavirus infection: review and meta-analysis. Int J Cancer. 2007;121(8):1813-20.
102. Lassen P, Eriksen JG, Hamilton-Dutoit S, Tramm T, Alsner J, Overgaard J. Effect of HPV-associated p16INK4A expression on response to radiotherapy and survival in squamous cell carcinoma of the head and neck. Journal of clinical oncology : official journal of the American Society of Clinical Oncology. 2009;27(12):1992-8.
103. Brandwein-Gensler M, Smith RV. Prognostic indicators in head and neck oncology including the new 7th edition of the AJCC staging system. Head Neck Pathol. 2010;4(1):53-61.
104. Shaw RJ, Lowe D, Woolgar JA, Brown JS, Vaughan ED, Evans C, et al. Extracapsular spread in oral squamous cell carcinoma. Head Neck. 2010;32(6):714-22.
105. Dunne AA, Muller HH, Eisele DW, Kessel K, Moll R, Werner JA. Meta-analysis of the prognostic significance of perinodal spread in head and neck squamous cell carcinomas (HNSCC) patients. Eur J Cancer. 2006;42(12):1863-8.
106. Pathologists RCo. Standards and datasets for reporting cancers: datasets for histopathology reports on head and neck carcinomas and salivary neoplasms. 2nd ed. London, UK: The Royal College of Pathologists; 2005.
107. Delaney G, Jacob S, Barton M. Estimation of an optimal external beam radiotherapy utilization rate for head and neck carcinoma. Cancer. 2005;103(11):2216-27.
108. Montero PH, Patel SG. Cancer of the oral cavity. Surg Oncol Clin N Am. 2015;24(3):491-508.
109. Jones AS, Fish B, Fenton JE, Husband DJ. The treatment of early laryngeal cancers (T1-T2 N0): surgery or irradiation? Head Neck. 2004;26(2):127-35.
110. Monnier Y, Simon C. Surgery Versus Radiotherapy for Early Oropharyngeal Tumors: a Never-Ending Debate. Curr Treat Options Oncol. 2015;16(9):42.
111. Hartl DM, Brasnu DF. Contemporary Surgical Management of Early Glottic Cancer. Otolaryngologic clinics of North America. 2015;48(4):611-25.
112. Ambrosch P. The role of laser microsurgery in the treatment of laryngeal cancer. Curr Opin Otolaryngol Head Neck Surg. 2007;15(2):82-8.

113. Grant DG, Hinni ML, Salassa JR, Perry WC, Hayden RE, Casler JD. Oropharyngeal cancer: a case for single modality treatment with transoral laser microsurgery. Arch Otolaryngol Head Neck Surg. 2009;135(12):1225-30.
114. Kutter J, Lang F, Monnier P, Pasche P. Transoral laser surgery for pharyngeal and pharyngolaryngeal carcinomas. Arch Otolaryngol Head Neck Surg. 2007;133(2):139-44.
115. Bhalavat RL, Fakih AR, Mistry RC, Mahantshetty U. Radical radiation vs surgery plus post-operative radiation in advanced (resectable) supraglottic larynx and pyriform sinus cancers: a prospective randomized study. Eur J Surg Oncol. 2003;29(9):750-6.
116. Induction chemotherapy plus radiation compared with surgery plus radiation in patients with advanced laryngeal cancer. The Department of Veterans Affairs Laryngeal Cancer Study Group. The New England journal of medicine. 1991;324(24):1685-90.
117. Bernier J, Domenge C, Ozsahin M, Matuszewska K, Lefebvre JL, Greiner RH, et al. Postoperative irradiation with or without concomitant chemotherapy for locally advanced head and neck cancer. The New England journal of medicine. 2004;350(19):1945-52.
118. Cooper JS, Pajak TF, Forastiere AA, Jacobs J, Campbell BH, Saxman SB, et al. Postoperative concurrent radiotherapy and chemotherapy for high-risk squamous-cell carcinoma of the head and neck. The New England journal of medicine. 2004;350(19):1937-44.
119. Adelstein DJ, Li Y, Adams GL, Wagner H, Jr., Kish JA, Ensley JF, et al. An intergroup phase III comparison of standard radiation therapy and two schedules of concurrent chemoradiotherapy in patients with unresectable squamous cell head and neck cancer. Journal of clinical oncology : official journal of the American Society of Clinical Oncology. 2003;21(1):92-8.
120. Patterson JM, McColl E, Carding PN, Hildreth AJ, Kelly C, Wilson JA. Swallowing in the first year after chemoradiotherapy for head and neck cancer: clinician- and patient-reported outcomes. Head Neck. 2014;36(3):352-8.
121. Trotti A, Pajak TF, Gwede CK, Paulus R, Cooper J, Forastiere A, et al. TAME: development of a new method for summarising adverse events of cancer treatment by the Radiation Therapy Oncology Group. Lancet Oncol. 2007;8(7):613-24.
122. Ferlito A, Devaney KO, Devaney SL, Rinaldo A. What is the incidence of occult metastasis in patients with stage N(0) cancers of the head and neck? ORL J Otorhinolaryngol Relat Spec. 2001;63(1):1-5.
123. Tateya I, Shiotani A, Satou Y, Tomifuji M, Morita S, Muto M, et al. Transoral surgery for laryngo-pharyngeal cancer - The paradigm shift of the head and cancer treatment. Auris, nasus, larynx. 2016;43(1):21-32.
124. Mendenhall WM, Amdur RJ, Palta JR. Intensity-modulated radiotherapy in the standard management of head and neck cancer: promises and pitfalls. Journal of clinical oncology : official journal of the American Society of Clinical Oncology. 2006;24(17):2618-23.
125. Nutting CM, Morden JP, Harrington KJ, Urbano TG, Bhide SA, Clark C, et al. Parotid-sparing intensity modulated versus conventional radiotherapy in head and neck cancer (PARSPORT): a phase 3 multicentre randomised controlled trial. Lancet Oncol. 2011;12(2):127-36.

126. Fu KK, Pajak TF, Trotti A, Jones CU, Spencer SA, Phillips TL, et al. A Radiation Therapy Oncology Group (RTOG) phase III randomized study to compare hyperfractionation and two variants of accelerated fractionation to standard fractionation radiotherapy for head and neck squamous cell carcinomas: first report of RTOG 9003. Int J Radiat Oncol Biol Phys. 2000;48(1):7-16.
127. Siegel RL, Miller KD, Jemal A. Cancer statistics, 2015. CA: a cancer journal for clinicians. 2015;65(1):5-29.
128. Forastiere AA, Trotti A, Pfister DG, Grandis JR. Head and neck cancer: recent advances and new standards of care. Journal of clinical oncology : official journal of the American Society of Clinical Oncology. 2006;24(17):2603-5.
129. Forastiere AA. Chemotherapy in the treatment of locally advanced head and neck cancer. Journal of surgical oncology. 2008;97(8):701-7.
130. Rackley T, Palaniappan N, Owens D, Evans M. Adjuvant treatment decisions for oropharyngeal cancer - is it time for a change? Clinical otolaryngology : official journal of ENT-UK ; official journal of Netherlands Society for Oto-Rhino-Laryngology & Cervico-Facial Surgery. 2014;39(5):316-21.
131. Mehanna H, Olaleye O, Licitra L. Oropharyngeal cancer - is it time to change management according to human papilloma virus status? Curr Opin Otolaryngol Head Neck Surg. 2012;20(2):120-4.
132. Vogelstein B, Lane D, Levine AJ. Surfing the p53 network. Nature. 2000;408(6810):307-10.
133. Hollstein M, Sidransky D, Vogelstein B, Harris CC. p53 mutations in human cancers. Science. 1991;253(5015):49-53.
134. Nigro JM, Baker SJ, Preisinger AC, Jessup JM, Hostetter R, Cleary K, et al. Mutations in the p53 gene occur in diverse human tumour types. Nature. 1989;342(6250):705-8.
135. Joerger AC, Fersht AR. Structural biology of the tumor suppressor p53. Annu Rev Biochem. 2008;77:557-82.
136. Dawson R, Muller L, Dehner A, Klein C, Kessler H, Buchner J. The N-terminal domain of p53 is natively unfolded. J Mol Biol. 2003;332(5):1131-41.
137. Walker KK, Levine AJ. Identification of a novel p53 functional domain that is necessary for efficient growth suppression. Proc Natl Acad Sci U S A. 1996;93(26):15335-40.
138. Liu X, Miller CW, Koeffler PH, Berk AJ. The p53 activation domain binds the TATA box-binding polypeptide in Holo-TFIID, and a neighboring p53 domain inhibits transcription. Mol Cell Biol. 1993;13(6):3291-300.
139. Truant R, Xiao H, Ingles CJ, Greenblatt J. Direct interaction between the transcriptional activation domain of human p53 and the TATA box-binding protein. J Biol Chem. 1993;268(4):2284-7.
140. Teufel DP, Freund SM, Bycroft M, Fersht AR. Four domains of p300 each bind tightly to a sequence spanning both transactivation subdomains of p53. Proc Natl Acad Sci U S A. 2007;104(17):7009-14.
141. Marine JC, Jochemsen AG. Mdmx as an essential regulator of p53 activity. Biochem Biophys Res Commun. 2005;331(3):750-60.
142. Kussie PH, Gorina S, Marechal V, Elenbaas B, Moreau J, Levine AJ, et al. Structure of the MDM2 oncoprotein bound to the p53 tumor suppressor transactivation domain. Science. 1996;274(5289):948-53.

143. Lin J, Wu X, Chen J, Chang A, Levine AJ. Functions of the p53 protein in growth regulation and tumor suppression. Cold Spring Harb Symp Quant Biol. 1994;59:215-23.
144. Cho Y, Gorina S, Jeffrey PD, Pavletich NP. Crystal structure of a p53 tumor suppressor-DNA complex: understanding tumorigenic mutations. Science. 1994;265(5170):346-55.
145. Pavletich NP, Chambers KA, Pabo CO. The DNA-binding domain of p53 contains the four conserved regions and the major mutation hot spots. Genes Dev. 1993;7(12B):2556-64.
146. Jeffrey PD, Gorina S, Pavletich NP. Crystal structure of the tetramerization domain of the p53 tumor suppressor at 1.7 angstroms. Science. 1995;267(5203):1498-502.
147. Malecka KA, Ho WC, Marmorstein R. Crystal structure of a p53 core tetramer bound to DNA. Oncogene. 2009;28(3):325-33.
148. Blattner C. Regulation of p53: the next generation. Cell cycle. 2008;7(20):3149-53.
149. Vousden KH. Activation of the p53 tumor suppressor protein. Biochim Biophys Acta. 2002;1602(1):47-59.
150. Wu X, Bayle JH, Olson D, Levine AJ. The p53-mdm-2 autoregulatory feedback loop. Genes Dev. 1993;7(7A):1126-32.
151. Lohrum MA, Woods DB, Ludwig RL, Balint E, Vousden KH. C-terminal ubiquitination of p53 contributes to nuclear export. Mol Cell Biol. 2001;21(24):8521-32.
152. Oliner JD, Pietenpol JA, Thiagalingam S, Gyuris J, Kinzler KW, Vogelstein B. Oncoprotein MDM2 conceals the activation domain of tumour suppressor p53. Nature. 1993;362(6423):857-60.
153. Kobet E, Zeng X, Zhu Y, Keller D, Lu H. MDM2 inhibits p300-mediated p53 acetylation and activation by forming a ternary complex with the two proteins. Proc Natl Acad Sci U S A. 2000;97(23):12547-52.
154. Okamoto K, Taya Y, Nakagama H. Mdmx enhances p53 ubiquitination by altering the substrate preference of the Mdm2 ubiquitin ligase. FEBS Lett. 2009;583(17):2710-4.
155. Sabbatini P, McCormick F. MDMX inhibits the p300/CBP-mediated acetylation of p53. DNA Cell Biol. 2002;21(7):519-25.
156. Lakin ND, Hann BC, Jackson SP. The ataxia-telangiectasia related protein ATR mediates DNA-dependent phosphorylation of p53. Oncogene. 1999;18(27):3989-95.
157. Canman CE, Lim DS, Cimprich KA, Taya Y, Tamai K, Sakaguchi K, et al. Activation of the ATM kinase by ionizing radiation and phosphorylation of p53. Science. 1998;281(5383):1677-9.
158. Hirao A, Kong YY, Matsuoka S, Wakeham A, Ruland J, Yoshida H, et al. DNA damage-induced activation of p53 by the checkpoint kinase Chk2. Science. 2000;287(5459):1824-7.
159. Maya R, Balass M, Kim ST, Shkedy D, Leal JF, Shifman O, et al. ATM-dependent phosphorylation of Mdm2 on serine 395: role in p53 activation by DNA damage. Genes Dev. 2001;15(9):1067-77.
160. Shinozaki T, Nota A, Taya Y, Okamoto K. Functional role of Mdm2 phosphorylation by ATR in attenuation of p53 nuclear export. Oncogene. 2003;22(55):8870-80.

161. Sakaguchi K, Herrera JE, Saito S, Miki T, Bustin M, Vassilev A, et al. DNA damage activates p53 through a phosphorylation-acetylation cascade. Genes Dev. 1998;12(18):2831-41.
162. Zhang Y, Xiong Y. Control of p53 ubiquitination and nuclear export by MDM2 and ARF. Cell Growth Differ. 2001;12(4):175-86.
163. Sherr CJ. Tumor surveillance via the ARF-p53 pathway. Genes Dev. 1998;12(19):2984-91.
164. Kruse JP, Gu W. Modes of p53 regulation. Cell. 2009;137(4):609-22.
165. Ryan KM, Phillips AC, Vousden KH. Regulation and function of the p53 tumor suppressor protein. Curr Opin Cell Biol. 2001;13(3):332-7.
166. Vousden KH. Outcomes of p53 activation--spoilt for choice. J Cell Sci. 2006;119(Pt 24):5015-20.
167. Riley T, Sontag E, Chen P, Levine A. Transcriptional control of human p53-regulated genes. Nat Rev Mol Cell Biol. 2008;9(5):402-12.
168. Lu X. p53: a heavily dictated dictator of life and death. Curr Opin Genet Dev. 2005;15(1):27-33.
169. Laptenko O, Prives C. Transcriptional regulation by p53: one protein, many possibilities. Cell Death Differ. 2006;13(6):951-61.
170. el-Deiry WS, Kern SE, Pietenpol JA, Kinzler KW, Vogelstein B. Definition of a consensus binding site for p53. Nat Genet. 1992;1(1):45-9.
171. Bennett M, Macdonald K, Chan SW, Luzio JP, Simari R, Weissberg P. Cell surface trafficking of Fas: a rapid mechanism of p53-mediated apoptosis. Science. 1998;282(5387):290-3.
172. Vousden KH. Apoptosis. p53 and PUMA: a deadly duo. Science. 2005;309(5741):1685-6.
173. Miller SJ, Suthiphongchai T, Zambetti GP, Ewen ME. p53 binds selectively to the 5' untranslated region of cdk4, an RNA element necessary and sufficient for transforming growth factor beta- and p53-mediated translational inhibition of cdk4. Mol Cell Biol. 2000;20(22):8420-31.
174. Vousden KH, Prives C. Blinded by the Light: The Growing Complexity of p53. Cell. 2009;137(3):413-31.
175. Norbury C, Nurse P. Animal cell cycles and their control. Annu Rev Biochem. 1992;61:441-70.
176. Pines J, Hunter T. Cyclin-dependent kinases: a new cell cycle motif? Trends Cell Biol. 1991;1(5):117-21.
177. Lodish HB, A.; Zipursky, S.L.; Matsudaira, P.; Baltimore, D.; Darnell, J. Molecular Cell Biology. 4th ed. New York, NY: W. H. Freeman; 2000.
178. el-Deiry WS, Tokino T, Velculescu VE, Levy DB, Parsons R, Trent JM, et al. WAF1, a potential mediator of p53 tumor suppression. Cell. 1993;75(4):817-25.
179. Abbas T, Dutta A. p21 in cancer: intricate networks and multiple activities. Nat Rev Cancer. 2009;9(6):400-14.
180. Waga S, Hannon GJ, Beach D, Stillman B. The p21 inhibitor of cyclin-dependent kinases controls DNA replication by interaction with PCNA. Nature. 1994;369(6481):574-8.
181. Zhan Q, Antinore MJ, Wang XW, Carrier F, Smith ML, Harris CC, et al. Association with Cdc2 and inhibition of Cdc2/Cyclin B1 kinase activity by the p53-regulated protein Gadd45. Oncogene. 1999;18(18):2892-900.
182. Mhawech P. 14-3-3 proteins--an update. Cell Res. 2005;15(4):228-36.

183. Ohki R, Nemoto J, Murasawa H, Oda E, Inazawa J, Tanaka N, et al. Reprimo, a new candidate mediator of the p53-mediated cell cycle arrest at the G2 phase. J Biol Chem. 2000;275(30):22627-30.
184. Taylor RC, Cullen SP, Martin SJ. Apoptosis: controlled demolition at the cellular level. Nat Rev Mol Cell Biol. 2008;9(3):231-41.
185. Elmore S. Apoptosis: a review of programmed cell death. Toxicol Pathol. 2007;35(4):495-516.
186. Brown JM, Attardi LD. The role of apoptosis in cancer development and treatment response. Nat Rev Cancer. 2005;5(3):231-7.
187. Savill J, Fadok V. Corpse clearance defines the meaning of cell death. Nature. 2000;407(6805):784-8.
188. Westphal D, Kluck RM, Dewson G. Building blocks of the apoptotic pore: how Bax and Bak are activated and oligomerize during apoptosis. Cell Death Differ. 2014;21(2):196-205.
189. Happo L, Strasser A, Cory S. BH3-only proteins in apoptosis at a glance. J Cell Sci. 2012;125(Pt 5):1081-7.
190. Boldin MP, Goncharov TM, Goltsev YV, Wallach D. Involvement of MACH, a novel MORT1/FADD-interacting protease, in Fas/APO-1- and TNF receptor-induced cell death. Cell. 1996;85(6):803-15.
191. Polyak K, Xia Y, Zweier JL, Kinzler KW, Vogelstein B. A model for p53-induced apoptosis. Nature. 1997;389(6648):300-5.
192. Vaughn AE, Deshmukh M. Glucose metabolism inhibits apoptosis in neurons and cancer cells by redox inactivation of cytochrome c. Nat Cell Biol. 2008;10(12):1477-83.
193. Vlatkovic N, Crawford K, Rubbi CP, Boyd MT. Tissue-specific therapeutic targeting of p53 in cancer: one size does not fit all. Curr Pharm Des. 2011;17(6):618-30.
194. Miyashita T, Reed JC. Tumor suppressor p53 is a direct transcriptional activator of the human bax gene. Cell. 1995;80(2):293-9.
195. Oda E, Ohki R, Murasawa H, Nemoto J, Shibue T, Yamashita T, et al. Noxa, a BH3-only member of the Bcl-2 family and candidate mediator of p53-induced apoptosis. Science. 2000;288(5468):1053-8.
196. Nakano K, Vousden KH. PUMA, a novel proapoptotic gene, is induced by p53. Mol Cell. 2001;7(3):683-94.
197. Oda K, Arakawa H, Tanaka T, Matsuda K, Tanikawa C, Mori T, et al. p53AIP1, a potential mediator of p53-dependent apoptosis, and its regulation by Ser-46-phosphorylated p53. Cell. 2000;102(6):849-62.
198. Owen-Schaub LB, Zhang W, Cusack JC, Angelo LS, Santee SM, Fujiwara T, et al. Wild-type human p53 and a temperature-sensitive mutant induce Fas/APO-1 expression. Mol Cell Biol. 1995;15(6):3032-40.
199. Fukazawa T, Fujiwara T, Morimoto Y, Shao J, Nishizaki M, Kadowaki Y, et al. Differential involvement of the CD95 (Fas/APO-1) receptor/ligand system on apoptosis induced by the wild-type p53 gene transfer in human cancer cells. Oncogene. 1999;18(13):2189-99.
200. Wu GS, Burns TF, McDonald ER, 3rd, Jiang W, Meng R, Krantz ID, et al. KILLER/DR5 is a DNA damage-inducible p53-regulated death receptor gene. Nat Genet. 1997;17(2):141-3.
201. Berube C, Boucher LM, Ma W, Wakeham A, Salmena L, Hakem R, et al. Apoptosis caused by p53-induced protein with death domain (PIDD) depends on

the death adapter protein RAIDD. Proc Natl Acad Sci U S A. 2005;102(40):14314-20.
202. Robles AI, Bemmels NA, Foraker AB, Harris CC. APAF-1 is a transcriptional target of p53 in DNA damage-induced apoptosis. Cancer research. 2001;61(18):6660-4.
203. MacLachlan TK, El-Deiry WS. Apoptotic threshold is lowered by p53 transactivation of caspase-6. Proc Natl Acad Sci U S A. 2002;99(14):9492-7.
204. Liu B, Chen Y, St Clair DK. ROS and p53: a versatile partnership. Free Radic Biol Med. 2008;44(8):1529-35.
205. Bensaad K, Tsuruta A, Selak MA, Vidal MN, Nakano K, Bartrons R, et al. TIGAR, a p53-inducible regulator of glycolysis and apoptosis. Cell. 2006;126(1):107-20.
206. Miyashita T, Krajewski S, Krajewska M, Wang HG, Lin HK, Liebermann DA, et al. Tumor suppressor p53 is a regulator of bcl-2 and bax gene expression in vitro and in vivo. Oncogene. 1994;9(6):1799-805.
207. Chipuk JE, Maurer U, Green DR, Schuler M. Pharmacologic activation of p53 elicits Bax-dependent apoptosis in the absence of transcription. Cancer Cell. 2003;4(5):371-81.
208. Tomita Y, Marchenko N, Erster S, Nemajerova A, Dehner A, Klein C, et al. WT p53, but not tumor-derived mutants, bind to Bcl2 via the DNA binding domain and induce mitochondrial permeabilization. J Biol Chem. 2006;281(13):8600-6.
209. Roos WP, Kaina B. DNA damage-induced cell death by apoptosis. Trends Mol Med. 2006;12(9):440-50.
210. Fricker M, Papadia S, Hardingham GE, Tolkovsky AM. Implication of TAp73 in the p53-independent pathway of Puma induction and Puma-dependent apoptosis in primary cortical neurons. J Neurochem. 2010;114(3):772-83.
211. Jullig M, Zhang WV, Ferreira A, Stott NS. MG132 induced apoptosis is associated with p53-independent induction of pro-apoptotic Noxa and transcriptional activity of beta-catenin. Apoptosis. 2006;11(4):627-41.
212. Kim SG, Ravi G, Hoffmann C, Jung YJ, Kim M, Chen A, et al. p53-Independent induction of Fas and apoptosis in leukemic cells by an adenosine derivative, Cl-IB-MECA. Biochem Pharmacol. 2002;63(5):871-80.
213. Seol DW. p53-Independent up-regulation of a TRAIL receptor DR5 by proteasome inhibitors: a mechanism for proteasome inhibitor-enhanced TRAIL-induced apoptosis. Biochem Biophys Res Commun. 2011;416(1-2):222-5.
214. Urist M, Tanaka T, Poyurovsky MV, Prives C. p73 induction after DNA damage is regulated by checkpoint kinases Chk1 and Chk2. Genes Dev. 2004;18(24):3041-54.
215. Rudolf E, Rudolf K, Cervinka M. Camptothecin induces p53-dependent and -independent apoptogenic signaling in melanoma cells. Apoptosis. 2011;16(11):1165-76.
216. Bauer MK, Vogt M, Los M, Siegel J, Wesselborg S, Schulze-Osthoff K. Role of reactive oxygen intermediates in activation-induced CD95 (APO-1/Fas) ligand expression. J Biol Chem. 1998;273(14):8048-55.
217. Schmitt CA, Fridman JS, Yang M, Lee S, Baranov E, Hoffman RM, et al. A senescence program controlled by p53 and p16INK4a contributes to the outcome of cancer therapy. Cell. 2002;109(3):335-46.

218. Campisi J, d'Adda di Fagagna F. Cellular senescence: when bad things happen to good cells. Nat Rev Mol Cell Biol. 2007;8(9):729-40.
219. Debacq-Chainiaux F, Erusalimsky JD, Campisi J, Toussaint O. Protocols to detect senescence-associated beta-galactosidase (SA-betagal) activity, a biomarker of senescent cells in culture and in vivo. Nat Protoc. 2009;4(12):1798-806.
220. Hayflick L. The Limited in Vitro Lifetime of Human Diploid Cell Strains. Exp Cell Res. 1965;37:614-36.
221. Itahana K, Dimri G, Campisi J. Regulation of cellular senescence by p53. Eur J Biochem. 2001;268(10):2784-91.
222. Olsen CL, Gardie B, Yaswen P, Stampfer MR. Raf-1-induced growth arrest in human mammary epithelial cells is p16-independent and is overcome in immortal cells during conversion. Oncogene. 2002;21(41):6328-39.
223. Michaloglou C, Vredeveld LC, Soengas MS, Denoyelle C, Kuilman T, van der Horst CM, et al. BRAFE600-associated senescence-like cell cycle arrest of human naevi. Nature. 2005;436(7051):720-4.
224. Passos JF, Von Zglinicki T. Oxygen free radicals in cell senescence: are they signal transducers? Free Radic Res. 2006;40(12):1277-83.
225. Passos JF, Nelson G, Wang C, Richter T, Simillion C, Proctor CJ, et al. Feedback between p21 and reactive oxygen production is necessary for cell senescence. Mol Syst Biol. 2010;6:347.
226. Inoue T, Kato K, Kato H, Asanoma K, Kuboyama A, Ueoka Y, et al. Level of reactive oxygen species induced by p21Waf1/CIP1 is critical for the determination of cell fate. Cancer Sci. 2009;100(7):1275-83.
227. Takahashi A, Ohtani N, Yamakoshi K, Iida S, Tahara H, Nakayama K, et al. Mitogenic signalling and the p16INK4a-Rb pathway cooperate to enforce irreversible cellular senescence. Nat Cell Biol. 2006;8(11):1291-7.
228. Hussain SP, Harris CC. Molecular epidemiology of human cancer: contribution of mutation spectra studies of tumor suppressor genes. Cancer research. 1998;58(18):4023-37.
229. Knudson AG, Jr. Mutation and cancer: statistical study of retinoblastoma. Proc Natl Acad Sci U S A. 1971;68(4):820-3.
230. Shaulian E, Zauberman A, Ginsberg D, Oren M. Identification of a minimal transforming domain of p53: negative dominance through abrogation of sequence-specific DNA binding. Mol Cell Biol. 1992;12(12):5581-92.
231. Kern SE, Pietenpol JA, Thiagalingam S, Seymour A, Kinzler KW, Vogelstein B. Oncogenic forms of p53 inhibit p53-regulated gene expression. Science. 1992;256(5058):827-30.
232. Milner J, Medcalf EA. Cotranslation of activated mutant p53 with wild type drives the wild-type p53 protein into the mutant conformation. Cell. 1991;65(5):765-74.
233. Greenblatt MS, Bennett WP, Hollstein M, Harris CC. Mutations in the p53 tumor suppressor gene: clues to cancer etiology and molecular pathogenesis. Cancer research. 1994;54(18):4855-78.
234. Kato S, Han SY, Liu W, Otsuka K, Shibata H, Kanamaru R, et al. Understanding the function-structure and function-mutation relationships of p53 tumor suppressor protein by high-resolution missense mutation analysis. Proc Natl Acad Sci U S A. 2003;100(14):8424-9.

235. Cao Y, Gao Q, Wazer DE, Band V. Abrogation of wild-type p53-mediated transactivation is insufficient for mutant p53-induced immortalization of normal human mammary epithelial cells. Cancer research. 1997;57(24):5584-9.
236. Chene P. In vitro analysis of the dominant negative effect of p53 mutants. J Mol Biol. 1998;281(2):205-9.
237. Erber R, Conradt C, Homann N, Enders C, Finckh M, Dietz A, et al. TP53 DNA contact mutations are selectively associated with allelic loss and have a strong clinical impact in head and neck cancer. Oncogene. 1998;16(13):1671-9.
238. Sano D, Xie TX, Ow TJ, Zhao M, Pickering CR, Zhou G, et al. Disruptive TP53 mutation is associated with aggressive disease characteristics in an orthotopic murine model of oral tongue cancer. Clin Cancer Res. 2011;17(21):6658-70.
239. Osman AA, Neskey DM, Katsonis P, Patel AA, Ward AM, Hsu TK, et al. Evolutionary Action Score of TP53 Coding Variants Is Predictive of Platinum Response in Head and Neck Cancer Patients. Cancer research. 2015;75(7):1205-15.
240. Finlay CA, Hinds PW, Tan TH, Eliyahu D, Oren M, Levine AJ. Activating mutations for transformation by p53 produce a gene product that forms an hsc70-p53 complex with an altered half-life. Mol Cell Biol. 1988;8(2):531-9.
241. Halevy O, Michalovitz D, Oren M. Different tumor-derived p53 mutants exhibit distinct biological activities. Science. 1990;250(4977):113-6.
242. Lang GA, Iwakuma T, Suh YA, Liu G, Rao VA, Parant JM, et al. Gain of function of a p53 hot spot mutation in a mouse model of Li-Fraumeni syndrome. Cell. 2004;119(6):861-72.
243. Olive KP, Tuveson DA, Ruhe ZC, Yin B, Willis NA, Bronson RT, et al. Mutant p53 gain of function in two mouse models of Li-Fraumeni syndrome. Cell. 2004;119(6):847-60.
244. Hanel W, Marchenko N, Xu S, Yu SX, Weng W, Moll U. Two hot spot mutant p53 mouse models display differential gain of function in tumorigenesis. Cell Death Differ. 2013;20(7):898-909.
245. Zhu J, Sammons MA, Donahue G, Dou Z, Vedadi M, Getlik M, et al. Gain-of-function p53 mutants co-opt chromatin pathways to drive cancer growth. Nature. 2015;525(7568):206-11.
246. Warburg O. On the origin of cancer cells. Science. 1956;123(3191):309-14.
247. Levine AJ, Puzio-Kuter AM. The control of the metabolic switch in cancers by oncogenes and tumor suppressor genes. Science. 2010;330(6009):1340-4.
248. Christofk HR, Vander Heiden MG, Harris MH, Ramanathan A, Gerszten RE, Wei R, et al. The M2 splice isoform of pyruvate kinase is important for cancer metabolism and tumour growth. Nature. 2008;452(7184):230-3.
249. Fantin VR, St-Pierre J, Leder P. Attenuation of LDH-A expression uncovers a link between glycolysis, mitochondrial physiology, and tumor maintenance. Cancer Cell. 2006;9(6):425-34.
250. Yuneva MO, Fan TW, Allen TD, Higashi RM, Ferraris DV, Tsukamoto T, et al. The metabolic profile of tumors depends on both the responsible genetic lesion and tissue type. Cell Metab. 2012;15(2):157-70.
251. Maddocks OD, Berkers CR, Mason SM, Zheng L, Blyth K, Gottlieb E, et al. Serine starvation induces stress and p53-dependent metabolic remodelling in cancer cells. Nature. 2013;493(7433):542-6.

252. DeBerardinis RJ, Mancuso A, Daikhin E, Nissim I, Yudkoff M, Wehrli S, et al. Beyond aerobic glycolysis: transformed cells can engage in glutamine metabolism that exceeds the requirement for protein and nucleotide synthesis. Proc Natl Acad Sci U S A. 2007;104(49):19345-50.
253. Wise DR, DeBerardinis RJ, Mancuso A, Sayed N, Zhang XY, Pfeiffer HK, et al. Myc regulates a transcriptional program that stimulates mitochondrial glutaminolysis and leads to glutamine addiction. Proc Natl Acad Sci U S A. 2008;105(48):18782-7.
254. Hatzivassiliou G, Zhao F, Bauer DE, Andreadis C, Shaw AN, Dhanak D, et al. ATP citrate lyase inhibition can suppress tumor cell growth. Cancer Cell. 2005;8(4):311-21.
255. Altenberg B, Greulich KO. Genes of glycolysis are ubiquitously overexpressed in 24 cancer classes. Genomics. 2004;84(6):1014-20.
256. Yeh CS, Wang JY, Chung FY, Lee SC, Huang MY, Kuo CW, et al. Significance of the glycolytic pathway and glycolysis related-genes in tumorigenesis of human colorectal cancers. Oncol Rep. 2008;19(1):81-91.
257. Vander Heiden MG, Cantley LC, Thompson CB. Understanding the Warburg effect: the metabolic requirements of cell proliferation. Science. 2009;324(5930):1029-33.
258. Moreno-Sanchez R, Rodriguez-Enriquez S, Marin-Hernandez A, Saavedra E. Energy metabolism in tumor cells. FEBS J. 2007;274(6):1393-418.
259. Rossignol R, Gilkerson R, Aggeler R, Yamagata K, Remington SJ, Capaldi RA. Energy substrate modulates mitochondrial structure and oxidative capacity in cancer cells. Cancer research. 2004;64(3):985-93.
260. Frezza C, Gottlieb E. Mitochondria in cancer: not just innocent bystanders. Semin Cancer Biol. 2009;19(1):4-11.
261. Yan H, Parsons DW, Jin G, McLendon R, Rasheed BA, Yuan W, et al. IDH1 and IDH2 mutations in gliomas. The New England journal of medicine. 2009;360(8):765-73.
262. Gottschalk S, Anderson N, Hainz C, Eckhardt SG, Serkova NJ. Imatinib (STI571)-mediated changes in glucose metabolism in human leukemia BCR-ABL-positive cells. Clin Cancer Res. 2004;10(19):6661-8.
263. Elstrom RL, Bauer DE, Buzzai M, Karnauskas R, Harris MH, Plas DR, et al. Akt stimulates aerobic glycolysis in cancer cells. Cancer research. 2004;64(11):3892-9.
264. Meng MB, Wang HH, Guo WH, Wu ZQ, Zeng XL, Zaorsky NG, et al. Targeting pyruvate kinase M2 contributes to radiosensitivity of non-small cell lung cancer cells in vitro and in vivo. Cancer Lett. 2015;356(2 Pt B):985-93.
265. Yizhak K, Le Devedec SE, Rogkoti VM, Baenke F, de Boer VC, Frezza C, et al. A computational study of the Warburg effect identifies metabolic targets inhibiting cancer migration. Mol Syst Biol. 2014;10:744.
266. Pfeiffer T, Schuster S, Bonhoeffer S. Cooperation and competition in the evolution of ATP-producing pathways. Science. 2001;292(5516):504-7.
267. Cairns RA, Harris IS, Mak TW. Regulation of cancer cell metabolism. Nat Rev Cancer. 2011;11(2):85-95.
268. Schafer ZT, Grassian AR, Song L, Jiang Z, Gerhart-Hines Z, Irie HY, et al. Antioxidant and oncogene rescue of metabolic defects caused by loss of matrix attachment. Nature. 2009;461(7260):109-13.

269. Giannoni E, Buricchi F, Raugei G, Ramponi G, Chiarugi P. Intracellular reactive oxygen species activate Src tyrosine kinase during cell adhesion and anchorage-dependent cell growth. Mol Cell Biol. 2005;25(15):6391-403.
270. Lee SR, Yang KS, Kwon J, Lee C, Jeong W, Rhee SG. Reversible inactivation of the tumor suppressor PTEN by H2O2. J Biol Chem. 2002;277(23):20336-42.
271. Valko M, Leibfritz D, Moncol J, Cronin MT, Mazur M, Telser J. Free radicals and antioxidants in normal physiological functions and human disease. Int J Biochem Cell Biol. 2007;39(1):44-84.
272. DeNicola GM, Karreth FA, Humpton TJ, Gopinathan A, Wei C, Frese K, et al. Oncogene-induced Nrf2 transcription promotes ROS detoxification and tumorigenesis. Nature. 2011;475(7354):106-9.
273. O'Donnell-Tormey J, Nathan CF, Lanks K, DeBoer CJ, de la Harpe J. Secretion of pyruvate. An antioxidant defense of mammalian cells. J Exp Med. 1987;165(2):500-14.
274. Long LH, Halliwell B. Artefacts in cell culture: alpha-Ketoglutarate can scavenge hydrogen peroxide generated by ascorbate and epigallocatechin gallate in cell culture media. Biochem Biophys Res Commun. 2011;406(1):20-4.
275. Long LH, Halliwell B. The effects of oxaloacetate on hydrogen peroxide generation from ascorbate and epigallocatechin gallate in cell culture media: potential for altering cell metabolism. Biochem Biophys Res Commun. 2012;417(1):446-50.
276. Fruehauf JP, Meyskens FL, Jr. Reactive oxygen species: a breath of life or death? Clin Cancer Res. 2007;13(3):789-94.
277. Mims J, Bansal N, Bharadwaj MS, Chen X, Molina AJ, Tsang AW, et al. Energy metabolism in a matched model of radiation resistance for head and neck squamous cell cancer. Radiat Res. 2015;183(3):291-304.
278. Lucarelli G, Galleggiante V, Rutigliano M, Sanguedolce F, Cagiano S, Bufo P, et al. Metabolomic profile of glycolysis and the pentose phosphate pathway identifies the central role of glucose-6-phosphate dehydrogenase in clear cell-renal cell carcinoma. Oncotarget. 2015;6(15):13371-86.
279. Fang M, Shen Z, Huang S, Zhao L, Chen S, Mak TW, et al. The ER UDPase ENTPD5 promotes protein N-glycosylation, the Warburg effect, and proliferation in the PTEN pathway. Cell. 2010;143(5):711-24.
280. Patra KC, Hay N. The pentose phosphate pathway and cancer. Trends Biochem Sci. 2014;39(8):347-54.
281. Mazurek S, Boschek CB, Hugo F, Eigenbrodt E. Pyruvate kinase type M2 and its role in tumor growth and spreading. Semin Cancer Biol. 2005;15(4):300-8.
282. Schneider J, Neu K, Grimm H, Velcovsky HG, Weisse G, Eigenbrodt E. Tumor M2-pyruvate kinase in lung cancer patients: immunohistochemical detection and disease monitoring. Anticancer Res. 2002;22(1A):311-8.
283. Christofk HR, Vander Heiden MG, Wu N, Asara JM, Cantley LC. Pyruvate kinase M2 is a phosphotyrosine-binding protein. Nature. 2008;452(7184):181-6.
284. Mazurek S, Zwerschke W, Jansen-Durr P, Eigenbrodt E. Metabolic cooperation between different oncogenes during cell transformation: interaction between activated ras and HPV-16 E7. Oncogene. 2001;20(47):6891-8.
285. Jen KY, Cheung VG. Identification of novel p53 target genes in ionizing radiation response. Cancer research. 2005;65(17):7666-73.

286. Won KY, Lim SJ, Kim GY, Kim YW, Han SA, Song JY, et al. Regulatory role of p53 in cancer metabolism via SCO2 and TIGAR in human breast cancer. Hum Pathol. 2012;43(2):221-8.
287. Cheung EC, Athineos D, Lee P, Ridgway RA, Lambie W, Nixon C, et al. TIGAR is required for efficient intestinal regeneration and tumorigenesis. Dev Cell. 2013;25(5):463-77.
288. Wanka C, Steinbach JP, Rieger J. Tp53-induced glycolysis and apoptosis regulator (TIGAR) protects glioma cells from starvation-induced cell death by up-regulating respiration and improving cellular redox homeostasis. J Biol Chem. 2012;287(40):33436-46.
289. Cheung EC, Ludwig RL, Vousden KH. Mitochondrial localization of TIGAR under hypoxia stimulates HK2 and lowers ROS and cell death. Proc Natl Acad Sci U S A. 2012;109(50):20491-6.
290. Lee P, Vousden KH, Cheung EC. TIGAR, TIGAR, burning bright. Cancer Metab. 2014;2(1):1.
291. Yuneva M, Zamboni N, Oefner P, Sachidanandam R, Lazebnik Y. Deficiency in glutamine but not glucose induces MYC-dependent apoptosis in human cells. J Cell Biol. 2007;178(1):93-105.
292. Kim MH, Kim H. Oncogenes and tumor suppressors regulate glutamine metabolism in cancer cells. J Cancer Prev. 2013;18(3):221-6.
293. Bieging KT, Mello SS, Attardi LD. Unravelling mechanisms of p53-mediated tumour suppression. Nat Rev Cancer. 2014;14(5):359-70.
294. Berkers CR, Maddocks OD, Cheung EC, Mor I, Vousden KH. Metabolic regulation by p53 family members. Cell Metab. 2013;18(5):617-33.
295. Kondoh H, Lleonart ME, Gil J, Wang J, Degan P, Peters G, et al. Glycolytic enzymes can modulate cellular life span. Cancer research. 2005;65(1):177-85.
296. Mikawa T, Maruyama T, Okamoto K, Nakagama H, Lleonart ME, Tsusaka T, et al. Senescence-inducing stress promotes proteolysis of phosphoglycerate mutase via ubiquitin ligase Mdm2. J Cell Biol. 2014;204(5):729-45.
297. Contractor T, Harris CR. p53 negatively regulates transcription of the pyruvate dehydrogenase kinase Pdk2. Cancer research. 2012;72(2):560-7.
298. Schwartzenberg-Bar-Yoseph F, Armoni M, Karnieli E. The tumor suppressor p53 down-regulates glucose transporters GLUT1 and GLUT4 gene expression. Cancer research. 2004;64(7):2627-33.
299. Boidot R, Vegran F, Meulle A, Le Breton A, Dessy C, Sonveaux P, et al. Regulation of monocarboxylate transporter MCT1 expression by p53 mediates inward and outward lactate fluxes in tumors. Cancer research. 2012;72(4):939-48.
300. Lebedeva MA, Eaton JS, Shadel GS. Loss of p53 causes mitochondrial DNA depletion and altered mitochondrial reactive oxygen species homeostasis. Biochim Biophys Acta. 2009;1787(5):328-34.
301. Kulawiec M, Ayyasamy V, Singh KK. p53 regulates mtDNA copy number and mitocheckpoint pathway. J Carcinog. 2009;8:8.
302. Bourdon A, Minai L, Serre V, Jais JP, Sarzi E, Aubert S, et al. Mutation of RRM2B, encoding p53-controlled ribonucleotide reductase (p53R2), causes severe mitochondrial DNA depletion. Nat Genet. 2007;39(6):776-80.
303. Kitamura N, Nakamura Y, Miyamoto Y, Miyamoto T, Kabu K, Yoshida M, et al. Mieap, a p53-inducible protein, controls mitochondrial quality by repairing or eliminating unhealthy mitochondria. PLoS One. 2011;6(1):e16060.

304. Zhang C, Lin M, Wu R, Wang X, Yang B, Levine AJ, et al. Parkin, a p53 target gene, mediates the role of p53 in glucose metabolism and the Warburg effect. Proc Natl Acad Sci U S A. 2011;108(39):16259-64.
305. Okamura S, Ng CC, Koyama K, Takei Y, Arakawa H, Monden M, et al. Identification of seven genes regulated by wild-type p53 in a colon cancer cell line carrying a well-controlled wild-type p53 expression system. Oncol Res. 1999;11(6):281-5.
306. Matoba S, Kang JG, Patino WD, Wragg A, Boehm M, Gavrilova O, et al. p53 regulates mitochondrial respiration. Science. 2006;312(5780):1650-3.
307. Wanka C, Brucker DP, Bahr O, Ronellenfitsch M, Weller M, Steinbach JP, et al. Synthesis of cytochrome C oxidase 2: a p53-dependent metabolic regulator that promotes respiratory function and protects glioma and colon cancer cells from hypoxia-induced cell death. Oncogene. 2012;31(33):3764-76.
308. Stambolsky P, Weisz L, Shats I, Klein Y, Goldfinger N, Oren M, et al. Regulation of AIF expression by p53. Cell Death Differ. 2006;13(12):2140-9.
309. Bergeaud M, Mathieu L, Guillaume A, Moll UM, Mignotte B, Le Floch N, et al. Mitochondrial p53 mediates a transcription-independent regulation of cell respiration and interacts with the mitochondrial F(1)F0-ATP synthase. Cell cycle. 2013;12(17):2781-93.
310. Feng Z, Hu W, de Stanchina E, Teresky AK, Jin S, Lowe S, et al. The regulation of AMPK beta1, TSC2, and PTEN expression by p53: stress, cell and tissue specificity, and the role of these gene products in modulating the IGF-1-AKT-mTOR pathways. Cancer research. 2007;67(7):3043-53.
311. Feng Z, Zhang H, Levine AJ, Jin S. The coordinate regulation of the p53 and mTOR pathways in cells. Proc Natl Acad Sci U S A. 2005;102(23):8204-9.
312. Budanov AV, Karin M. p53 target genes sestrin1 and sestrin2 connect genotoxic stress and mTOR signaling. Cell. 2008;134(3):451-60.
313. Faubert B, Boily G, Izreig S, Griss T, Samborska B, Dong Z, et al. AMPK is a negative regulator of the Warburg effect and suppresses tumor growth in vivo. Cell Metab. 2013;17(1):113-24.
314. Marin-Hernandez A, Gallardo-Perez JC, Ralph SJ, Rodriguez-Enriquez S, Moreno-Sanchez R. HIF-1alpha modulates energy metabolism in cancer cells by inducing over-expression of specific glycolytic isoforms. Mini Rev Med Chem. 2009;9(9):1084-101.
315. Choy MK, Movassagh M, Bennett MR, Foo RS. PKB/Akt activation inhibits p53-mediated HIF1A degradation that is independent of MDM2. J Cell Physiol. 2010;222(3):635-9.
316. Kawauchi K, Araki K, Tobiume K, Tanaka N. p53 regulates glucose metabolism through an IKK-NF-kappaB pathway and inhibits cell transformation. Nat Cell Biol. 2008;10(5):611-8.
317. Ruiz-Lozano P, Hixon ML, Wagner MW, Flores AI, Ikawa S, Baldwin AS, Jr., et al. p53 is a transcriptional activator of the muscle-specific phosphoglycerate mutase gene and contributes in vivo to the control of its cardiac expression. Cell Growth Differ. 1999;10(5):295-306.
318. Mathupala SP, Heese C, Pedersen PL. Glucose catabolism in cancer cells. The type II hexokinase promoter contains functionally active response elements for the tumor suppressor p53. J Biol Chem. 1997;272(36):22776-80.

319. Zhou G, Wang J, Zhao M, Xie TX, Tanaka N, Sano D, et al. Gain-of-function mutant p53 promotes cell growth and cancer cell metabolism via inhibition of AMPK activation. Mol Cell. 2014;54(6):960-74.
320. Reitzer LJ, Wice BM, Kennell D. Evidence that glutamine, not sugar, is the major energy source for cultured HeLa cells. J Biol Chem. 1979;254(8):2669-76.
321. Bonuccelli G, Tsirigos A, Whitaker-Menezes D, Pavlides S, Pestell RG, Chiavarina B, et al. Ketones and lactate "fuel" tumor growth and metastasis: Evidence that epithelial cancer cells use oxidative mitochondrial metabolism. Cell cycle. 2010;9(17):3506-14.
322. Jitschin R, Hofmann AD, Bruns H, Giessl A, Bricks J, Berger J, et al. Mitochondrial metabolism contributes to oxidative stress and reveals therapeutic targets in chronic lymphocytic leukemia. Blood. 2014;123(17):2663-72.
323. Gambhir SS. Molecular imaging of cancer with positron emission tomography. Nat Rev Cancer. 2002;2(9):683-93.
324. Reisser C, Eichhorn K, Herold-Mende C, Born AI, Bannasch P. Expression of facilitative glucose transport proteins during development of squamous cell carcinomas of the head and neck. Int J Cancer. 1999;80(2):194-8.
325. Mellanen P, Minn H, Grenman R, Harkonen P. Expression of glucose transporters in head-and-neck tumors. Int J Cancer. 1994;56(5):622-9.
326. Chandan VS, Faquin WC, Wilbur DC, Khurana KK. The utility of GLUT-1 immunolocalization in cell blocks: An adjunct to the fine needle aspiration diagnosis of cystic squamous lesions of the head and neck. Cancer. 2006;108(2):124-8.
327. Weiner MF, Miranda RN, Bardales RH, Mukunyadzi P, Baker SJ, Korourian S, et al. Diagnostic value of GLUT-1 immunoreactivity to distinguish benign from malignant cystic squamous lesions of the head and neck in fine-needle aspiration biopsy material. Diagn Cytopathol. 2004;31(5):294-9.
328. Starska K, Forma E, Jozwiak P, Brys M, Lewy-Trenda I, Brzezinska-Blaszczyk E, et al. Gene and protein expression of glucose transporter 1 and glucose transporter 3 in human laryngeal cancer-the relationship with regulatory hypoxia-inducible factor-1alpha expression, tumor invasiveness, and patient prognosis. Tumour Biol. 2015;36(4):2309-21.
329. Li SJ, Guo W, Ren GX, Huang G, Chen T, Song SL. Expression of Glut-1 in primary and recurrent head and neck squamous cell carcinomas, and compared with 2-[18F]fluoro-2-deoxy-D-glucose accumulation in positron emission tomography. Br J Oral Maxillofac Surg. 2008;46(3):180-6.
330. Kunkel M, Reichert TE, Benz P, Lehr HA, Jeong JH, Wieand S, et al. Overexpression of Glut-1 and increased glucose metabolism in tumors are associated with a poor prognosis in patients with oral squamous cell carcinoma. Cancer. 2003;97(4):1015-24.
331. Mineta H, Miura K, Takebayashi S, Misawa K, Araki K, Misawa Y, et al. Prognostic value of glucose transporter 1 expression in patients with hypopharyngeal carcinoma. Anticancer Res. 2002;22(6B):3489-94.
332. Kunkel M, Moergel M, Stockinger M, Jeong JH, Fritz G, Lehr HA, et al. Overexpression of GLUT-1 is associated with resistance to radiotherapy and adverse prognosis in squamous cell carcinoma of the oral cavity. Oral Oncol. 2007;43(8):796-803.

333. Ayala FR, Rocha RM, Carvalho KC, Carvalho AL, da Cunha IW, Lourenco SV, et al. GLUT1 and GLUT3 as potential prognostic markers for Oral Squamous Cell Carcinoma. Molecules. 2010;15(4):2374-87.
334. Estilo CL, P Oc, Talbot S, Socci ND, Carlson DL, Ghossein R, et al. Oral tongue cancer gene expression profiling: Identification of novel potential prognosticators by oligonucleotide microarray analysis. BMC Cancer. 2009;9:11.
335. Xie P, Li M, Zhao H, Sun X, Fu Z, Yu J. 18F-FDG PET or PET-CT to evaluate prognosis for head and neck cancer: a meta-analysis. J Cancer Res Clin Oncol. 2011;137(7):1085-93.
336. Deron P, Vermeersch H, Mees G, Vangestel C, Pauwels P, Van de Wiele C. Expression and prognostic value of glucose transporters and hexokinases in tonsil and mobile tongue squamous cell carcinoma. Histol Histopathol. 2011;26(9):1165-72.
337. Chen J, Zhang S, Li Y, Tang Z, Kong W. Hexokinase 2 overexpression promotes the proliferation and survival of laryngeal squamous cell carcinoma. Tumour Biol. 2014;35(4):3743-53.
338. McFate T, Mohyeldin A, Lu H, Thakar J, Henriques J, Halim ND, et al. Pyruvate dehydrogenase complex activity controls metabolic and malignant phenotype in cancer cells. J Biol Chem. 2008;283(33):22700-8.
339. Sun W, Zhou S, Chang SS, McFate T, Verma A, Califano JA. Mitochondrial mutations contribute to HIF1alpha accumulation via increased reactive oxygen species and up-regulated pyruvate dehydrogenease kinase 2 in head and neck squamous cell carcinoma. Clin Cancer Res. 2009;15(2):476-84.
340. Wigfield SM, Winter SC, Giatromanolaki A, Taylor J, Koukourakis ML, Harris AL. PDK-1 regulates lactate production in hypoxia and is associated with poor prognosis in head and neck squamous cancer. Br J Cancer. 2008;98(12):1975-84.
341. Ervens J, Fuchs H, Niemann VT, Hoffmeister B. Pyruvate kinase isoenzyme M2 is not of diagnostic relevance as a marker for oral cancer. J Craniomaxillofac Surg. 2008;36(2):89-94.
342. Wong TS, Liu XB, Chung-Wai Ho A, Po-Wing Yuen A, Wai-Man Ng R, Ignace Wei W. Identification of pyruvate kinase type M2 as potential oncoprotein in squamous cell carcinoma of tongue through microRNA profiling. Int J Cancer. 2008;123(2):251-7.
343. Desai S, Ding M, Wang B, Lu Z, Zhao Q, Shaw K, et al. Tissue-specific isoform switch and DNA hypomethylation of the pyruvate kinase PKM gene in human cancers. Oncotarget. 2014;5(18):8202-10.
344. Brizel DM, Schroeder T, Scher RL, Walenta S, Clough RW, Dewhirst MW, et al. Elevated tumor lactate concentrations predict for an increased risk of metastases in head-and-neck cancer. Int J Radiat Oncol Biol Phys. 2001;51(2):349-53.
345. Blatt S, Voelxen N, Sagheb K, Pabst AM, Walenta S, Schroeder T, et al. Lactate as a predictive marker for tumor recurrence in patients with head and neck squamous cell carcinoma (HNSCC) post radiation: a prospective study over 15 years. Clin Oral Investig. 2016.
346. Quennet V, Yaromina A, Zips D, Rosner A, Walenta S, Baumann M, et al. Tumor lactate content predicts for response to fractionated irradiation of human squamous cell carcinomas in nude mice. Radiother Oncol. 2006;81(2):130-5.

347. Sattler UG, Meyer SS, Quennet V, Hoerner C, Knoerzer H, Fabian C, et al. Glycolytic metabolism and tumour response to fractionated irradiation. Radiother Oncol. 2010;94(1):102-9.
348. Ziebart T, Walenta S, Kunkel M, Reichert TE, Wagner W, Mueller-Klieser W. Metabolic and proteomic differentials in head and neck squamous cell carcinomas and normal gingival tissue. J Cancer Res Clin Oncol. 2011;137(2):193-9.
349. Sun W, Zhang X, Ding X, Li H, Geng M, Xie Z, et al. Lactate dehydrogenase B is associated with the response to neoadjuvant chemotherapy in oral squamous cell carcinoma. PLoS One. 2015;10(5):e0125976.
350. Grimm M, Alexander D, Munz A, Hoffmann J, Reinert S. Increased LDH5 expression is associated with lymph node metastasis and outcome in oral squamous cell carcinoma. Clin Exp Metastasis. 2013;30(4):529-40.
351. Tripathi P, Kamarajan P, Somashekar BS, MacKinnon N, Chinnaiyan AM, Kapila YL, et al. Delineating metabolic signatures of head and neck squamous cell carcinoma: phospholipase A2, a potential therapeutic target. Int J Biochem Cell Biol. 2012;44(11):1852-61.
352. Somashekar BS, Kamarajan P, Danciu T, Kapila YL, Chinnaiyan AM, Rajendiran TM, et al. Magic angle spinning NMR-based metabolic profiling of head and neck squamous cell carcinoma tissues. J Proteome Res. 2011;10(11):5232-41.
353. Bag S, Banerjee DR, Basak A, Das AK, Pal M, Banerjee R, et al. NMR ((1)H and (13)C) based signatures of abnormal choline metabolism in oral squamous cell carcinoma with no prominent Warburg effect. Biochem Biophys Res Commun. 2015;459(4):574-8.
354. Simons AL, Ahmad IM, Mattson DM, Dornfeld KJ, Spitz DR. 2-Deoxy-D-glucose combined with cisplatin enhances cytotoxicity via metabolic oxidative stress in human head and neck cancer cells. Cancer research. 2007;67(7):3364-70.
355. Vibhuti A, Muralidhar K, Dwarakanath BS. Differential cytotoxicity of the glycolytic inhibitor 2-deoxy-D-glucose in isogenic cell lines varying in their p53 status. J Cancer Res Ther. 2013;9(4):686-92.
356. Simons AL, Fath MA, Mattson DM, Smith BJ, Walsh SA, Graham MM, et al. Enhanced response of human head and neck cancer xenograft tumors to cisplatin combined with 2-deoxy-D-glucose correlates with increased 18F-FDG uptake as determined by PET imaging. Int J Radiat Oncol Biol Phys. 2007;69(4):1222-30.
357. Zhang XD, Deslandes E, Villedieu M, Poulain L, Duval M, Gauduchon P, et al. Effect of 2-deoxy-D-glucose on various malignant cell lines in vitro. Anticancer Res. 2006;26(5A):3561-6.
358. Ralser M, Wamelink MM, Struys EA, Joppich C, Krobitsch S, Jakobs C, et al. A catabolic block does not sufficiently explain how 2-deoxy-D-glucose inhibits cell growth. Proc Natl Acad Sci U S A. 2008;105(46):17807-11.
359. Sandulache VC, Ow TJ, Pickering CR, Frederick MJ, Zhou G, Fokt I, et al. Glucose, not glutamine, is the dominant energy source required for proliferation and survival of head and neck squamous carcinoma cells. Cancer. 2011;117(13):2926-38.
360. Sandulache VC, Skinner HD, Ow TJ, Zhang A, Xia X, Luchak JM, et al. Individualizing antimetabolic treatment strategies for head and neck squamous cell carcinoma based on TP53 mutational status. Cancer. 2012;118(3):711-21.

361. Krupar R, Robold K, Gaag D, Spanier G, Kreutz M, Renner K, et al. Immunologic and metabolic characteristics of HPV-negative and HPV-positive head and neck squamous cell carcinomas are strikingly different. Virchows Arch. 2014;465(3):299-312.
362. Bansal N, Mims J, Kuremsky JG, Olex AL, Zhao W, Yin L, et al. Broad phenotypic changes associated with gain of radiation resistance in head and neck squamous cell cancer. Antioxid Redox Signal. 2014;21(2):221-36.
363. Sun W, Liu Y, Glazer CA, Shao C, Bhan S, Demokan S, et al. TKTL1 is activated by promoter hypomethylation and contributes to head and neck squamous cell carcinoma carcinogenesis through increased aerobic glycolysis and HIF1alpha stabilization. Clin Cancer Res. 2010;16(3):857-66.
364. Smith IM, Glazer CA, Mithani SK, Ochs MF, Sun W, Bhan S, et al. Coordinated activation of candidate proto-oncogenes and cancer testes antigens via promoter demethylation in head and neck cancer and lung cancer. PLoS One. 2009;4(3):e4961.
365. Volker HU, Scheich M, Schmausser B, Kammerer U, Eck M. Overexpression of transketolase TKTL1 is associated with shorter survival in laryngeal squamous cell carcinomas. Eur Arch Otorhinolaryngol. 2007;264(12):1431-6.
366. Curry JM, Tuluc M, Whitaker-Menezes D, Ames JA, Anantharaman A, Butera A, et al. Cancer metabolism, stemness and tumor recurrence: MCT1 and MCT4 are functional biomarkers of metabolic symbiosis in head and neck cancer. Cell cycle. 2013;12(9):1371-84.
367. Witkiewicz AK, Whitaker-Menezes D, Dasgupta A, Philp NJ, Lin Z, Gandara R, et al. Using the "reverse Warburg effect" to identify high-risk breast cancer patients: stromal MCT4 predicts poor clinical outcome in triple-negative breast cancers. Cell cycle. 2012;11(6):1108-17.
368. Martinez-Outschoorn UE, Sotgia F, Lisanti MP. Power surge: supporting cells "fuel" cancer cell mitochondria. Cell Metab. 2012;15(1):4-5.
369. Perri F, Pacelli R, Della Vittoria Scarpati G, Cella L, Giuliano M, Caponigro F, et al. Radioresistance in head and neck squamous cell carcinoma: Biological bases and therapeutic implications. Head Neck. 2015;37(5):763-70.
370. Krause CJ, Carey TE, Ott RW, Hurbis C, McClatchey KD, Regezi JA. Human squamous cell carcinoma. Establishment and characterization of new permanent cell lines. Arch Otolaryngol. 1981;107(11):703-10.
371. Lin CJ, Grandis JR, Carey TE, Gollin SM, Whiteside TL, Koch WM, et al. Head and neck squamous cell carcinoma cell lines: established models and rationale for selection. Head Neck. 2007;29(2):163-88.
372. Bradford CR, Zacks SE, Androphy EJ, Gregoire L, Lancaster WD, Carey TE. Human papillomavirus DNA sequences in cell lines derived from head and neck squamous cell carcinomas. Otolaryngology--head and neck surgery : official journal of American Academy of Otolaryngology-Head and Neck Surgery. 1991;104(3):303-10.
373. Hauser U, Balz V, Carey TE, Grenman R, Van Lierop A, Scheckenbach K, et al. Reliable detection of p53 aberrations in squamous cell carcinomas of the head and neck requires transcript analysis of the entire coding region. Head Neck. 2002;24(9):868-73.
374. Brenner JC, Graham MP, Kumar B, Saunders LM, Kupfer R, Lyons RH, et al. Genotyping of 73 UM-SCC head and neck squamous cell carcinoma cell lines. Head Neck. 2010;32(4):417-26.

375. Friedman J, Nottingham L, Duggal P, Pernas FG, Yan B, Yang XP, et al. Deficient TP53 expression, function, and cisplatin sensitivity are restored by quinacrine in head and neck cancer. Clin Cancer Res. 2007;13(22 Pt 1):6568-78.
376. Yan B, Yang X, Lee TL, Friedman J, Tang J, Van Waes C, et al. Genome-wide identification of novel expression signatures reveal distinct patterns and prevalence of binding motifs for p53, nuclear factor-kappaB and other signal transcription factors in head and neck squamous cell carcinoma. Genome Biol. 2007;8(5):R78.
377. Frank CJ, McClatchey KD, Devaney KO, Carey TE. Evidence that loss of chromosome 18q is associated with tumor progression. Cancer research. 1997;57(5):824-7.
378. Olthof NC, Huebbers CU, Kolligs J, Henfling M, Ramaekers FC, Cornet I, et al. Viral load, gene expression and mapping of viral integration sites in HPV16-associated HNSCC cell lines. Int J Cancer. 2015;136(5):E207-18.
379. Tang AL, Hauff SJ, Owen JH, Graham MP, Czerwinski MJ, Park JJ, et al. UM-SCC-104: a new human papillomavirus-16-positive cancer stem cell-containing head and neck squamous cell carcinoma cell line. Head Neck. 2012;34(10):1480-91.
380. Rieckmann T, Tribius S, Grob TJ, Meyer F, Busch CJ, Petersen C, et al. HNSCC cell lines positive for HPV and p16 possess higher cellular radiosensitivity due to an impaired DSB repair capacity. Radiother Oncol. 2013;107(2):242-6.
381. Kimple RJ, Smith MA, Blitzer GC, Torres AD, Martin JA, Yang RZ, et al. Enhanced radiation sensitivity in HPV-positive head and neck cancer. Cancer research. 2013;73(15):4791-800.
382. Young L, Sung J, Stacey G, Masters JR. Detection of Mycoplasma in cell cultures. Nat Protoc. 2010;5(5):929-34.
383. Divakaruni AS, Paradyse A, Ferrick DA, Murphy AN, Jastroch M. Analysis and interpretation of microplate-based oxygen consumption and pH data. Methods Enzymol. 2014;547:309-54.
384. Wu M, Neilson A, Swift AL, Moran R, Tamagnine J, Parslow D, et al. Multiparameter metabolic analysis reveals a close link between attenuated mitochondrial bioenergetic function and enhanced glycolysis dependency in human tumor cells. Am J Physiol Cell Physiol. 2007;292(1):C125-36.
385. Salabei JK, Gibb AA, Hill BG. Comprehensive measurement of respiratory activity in permeabilized cells using extracellular flux analysis. Nat Protoc. 2014;9(2):421-38.
386. Divakaruni AS, Rogers GW, Murphy AN. Measuring Mitochondrial Function in Permeabilized Cells Using the Seahorse XF Analyzer or a Clark-Type Oxygen Electrode. Curr Protoc Toxicol. 2014;60:25 2 1-16.
387. Divakaruni AS, Wiley SE, Rogers GW, Andreyev AY, Petrosyan S, Loviscach M, et al. Thiazolidinediones are acute, specific inhibitors of the mitochondrial pyruvate carrier. Proc Natl Acad Sci U S A. 2013;110(14):5422-7.
388. Altman SA, Randers L, Rao G. Comparison of trypan blue dye exclusion and fluorometric assays for mammalian cell viability determinations. Biotechnol Prog. 1993;9(6):671-4.
389. Berridge MV, Tan AS. Characterization of the cellular reduction of 3-(4,5-dimethylthiazol-2-yl)-2,5-diphenyltetrazolium bromide (MTT): subcellular

localization, substrate dependence, and involvement of mitochondrial electron transport in MTT reduction. Arch Biochem Biophys. 1993;303(2):474-82.
390. Franken NA, Rodermond HM, Stap J, Haveman J, van Bree C. Clonogenic assay of cells in vitro. Nat Protoc. 2006;1(5):2315-9.
391. Schlegel RA, Williamson P. Phosphatidylserine, a death knell. Cell Death Differ. 2001;8(6):551-63.
392. Koopman G, Reutelingsperger CP, Kuijten GA, Keehnen RM, Pals ST, van Oers MH. Annexin V for flow cytometric detection of phosphatidylserine expression on B cells undergoing apoptosis. Blood. 1994;84(5):1415-20.
393. Steensma DP, Timm M, Witzig TE. Flow cytometric methods for detection and quantification of apoptosis. Methods Mol Med. 2003;85:323-32.
394. Eruslanov E, Kusmartsev S. Identification of ROS using oxidized DCFDA and flow-cytometry. Methods Mol Biol. 2010;594:57-72.
395. Jones NP, Schulze A. Targeting cancer metabolism--aiming at a tumour's sweet-spot. Drug Discov Today. 2012;17(5-6):232-41.
396. Scheffner M, Werness BA, Huibregtse JM, Levine AJ, Howley PM. The E6 oncoprotein encoded by human papillomavirus types 16 and 18 promotes the degradation of p53. Cell. 1990;63(6):1129-36.
397. Huang SH, Xu W, Waldron J, Siu L, Shen X, Tong L, et al. Refining American Joint Committee on Cancer/Union for International Cancer Control TNM stage and prognostic groups for human papillomavirus-related oropharyngeal carcinomas. Journal of clinical oncology : official journal of the American Society of Clinical Oncology. 2015;33(8):836-45.
398. Gupta AK, Lee JH, Wilke WW, Quon H, Smith G, Maity A, et al. Radiation response in two HPV-infected head-and-neck cancer cell lines in comparison to a non-HPV-infected cell line and relationship to signaling through AKT. Int J Radiat Oncol Biol Phys. 2009;74(3):928-33.
399. Spanos WC, Nowicki P, Lee DW, Hoover A, Hostager B, Gupta A, et al. Immune response during therapy with cisplatin or radiation for human papillomavirus-related head and neck cancer. Arch Otolaryngol Head Neck Surg. 2009;135(11):1137-46.
400. DeWeese TL, Walsh JC, Dillehay LE, Kessis TD, Hedrick L, Cho KR, et al. Human papillomavirus E6 and E7 oncoproteins alter cell cycle progression but not radiosensitivity of carcinoma cells treated with low-dose-rate radiation. Int J Radiat Oncol Biol Phys. 1997;37(1):145-54.
401. Pelicano H, Martin DS, Xu RH, Huang P. Glycolysis inhibition for anticancer treatment. Oncogene. 2006;25(34):4633-46.
402. Lin X, Zhang F, Bradbury CM, Kaushal A, Li L, Spitz DR, et al. 2-Deoxy-D-glucose-induced cytotoxicity and radiosensitization in tumor cells is mediated via disruptions in thiol metabolism. Cancer research. 2003;63(12):3413-7.
403. Varshney R, Dwarakanath B, Jain V. Radiosensitization by 6-aminonicotinamide and 2-deoxy-D-glucose in human cancer cells. Int J Radiat Biol. 2005;81(5):397-408.
404. Suzuki M, O'Dea JD, Suzuki T, Agar NS. 2-Deoxyglucose as a substrate for glutathione regeneration in human and ruminant red blood cells. Comp Biochem Physiol B. 1983;75(2):195-7.
405. El-Mir MY, Nogueira V, Fontaine E, Averet N, Rigoulet M, Leverve X. Dimethylbiguanide inhibits cell respiration via an indirect effect targeted on the respiratory chain complex I. J Biol Chem. 2000;275(1):223-8.

406. Pollak MN. Investigating metformin for cancer prevention and treatment: the end of the beginning. Cancer Discov. 2012;2(9):778-90.
407. Noto H, Goto A, Tsujimoto T, Noda M. Cancer risk in diabetic patients treated with metformin: a systematic review and meta-analysis. PLoS One. 2012;7(3):e33411.
408. Jiralerspong S, Palla SL, Giordano SH, Meric-Bernstam F, Liedtke C, Barnett CM, et al. Metformin and pathologic complete responses to neoadjuvant chemotherapy in diabetic patients with breast cancer. Journal of clinical oncology : official journal of the American Society of Clinical Oncology. 2009;27(20):3297-302.
409. Anedda A, Rial E, Gonzalez-Barroso MM. Metformin induces oxidative stress in white adipocytes and raises uncoupling protein 2 levels. J Endocrinol. 2008;199(1):33-40.
410. Muaddi H, Chowdhury S, Vellanki R, Zamiara P, Koritzinsky M. Contributions of AMPK and p53 dependent signaling to radiation response in the presence of metformin. Radiother Oncol. 2013;108(3):446-50.
411. Lee YJ, Galoforo SS, Berns CM, Chen JC, Davis BH, Sim JE, et al. Glucose deprivation-induced cytotoxicity and alterations in mitogen-activated protein kinase activation are mediated by oxidative stress in multidrug-resistant human breast carcinoma cells. J Biol Chem. 1998;273(9):5294-9.
412. Ahmad IM, Aykin-Burns N, Sim JE, Walsh SA, Higashikubo R, Buettner GR, et al. Mitochondrial O2*- and H2O2 mediate glucose deprivation-induced stress in human cancer cells. J Biol Chem. 2005;280(6):4254-63.
413. Eriksson D, Stigbrand T. Radiation-induced cell death mechanisms. Tumour Biol. 2010;31(4):363-72.
414. Kim R, Emi M, Tanabe K. The role of apoptosis in cancer cell survival and therapeutic outcome. Cancer Biol Ther. 2006;5(11):1429-42.
415. Munoz-Pinedo C, Ruiz-Ruiz C, Ruiz de Almodovar C, Palacios C, Lopez-Rivas A. Inhibition of glucose metabolism sensitizes tumor cells to death receptor-triggered apoptosis through enhancement of death-inducing signaling complex formation and apical procaspase-8 processing. J Biol Chem. 2003;278(15):12759-68.
416. Halicka HD, Ardelt B, Li X, Melamed MM, Darzynkiewicz Z. 2-Deoxy-D-glucose enhances sensitivity of human histiocytic lymphoma U937 cells to apoptosis induced by tumor necrosis factor. Cancer research. 1995;55(2):444-9.
417. Ben Sahra I, Laurent K, Giuliano S, Larbret F, Ponzio G, Gounon P, et al. Targeting cancer cell metabolism: the combination of metformin and 2-deoxyglucose induces p53-dependent apoptosis in prostate cancer cells. Cancer research. 2010;70(6):2465-75.
418. Lehmann BD, McCubrey JA, Jefferson HS, Paine MS, Chappell WH, Terrian DM. A dominant role for p53-dependent cellular senescence in radiosensitization of human prostate cancer cells. Cell cycle. 2007;6(5):595-605.
419. Jung YS, Qian Y, Chen X. Examination of the expanding pathways for the regulation of p21 expression and activity. Cell Signal. 2010;22(7):1003-12.
420. Back JH, Rezvani HR, Zhu Y, Guyonnet-Duperat V, Athar M, Ratner D, et al. Cancer cell survival following DNA damage-mediated premature senescence is regulated by mammalian target of rapamycin (mTOR)-dependent Inhibition of sirtuin 1. J Biol Chem. 2011;286(21):19100-8.

421. Brady CA, Jiang D, Mello SS, Johnson TM, Jarvis LA, Kozak MM, et al. Distinct p53 transcriptional programs dictate acute DNA-damage responses and tumor suppression. Cell. 2011;145(4):571-83.
422. Danial NN, Gramm CF, Scorrano L, Zhang CY, Krauss S, Ranger AM, et al. BAD and glucokinase reside in a mitochondrial complex that integrates glycolysis and apoptosis. Nature. 2003;424(6951):952-6.
423. Xu RH, Pelicano H, Zhou Y, Carew JS, Feng L, Bhalla KN, et al. Inhibition of glycolysis in cancer cells: a novel strategy to overcome drug resistance associated with mitochondrial respiratory defect and hypoxia. Cancer research. 2005;65(2):613-21.
424. Shim H, Chun YS, Lewis BC, Dang CV. A unique glucose-dependent apoptotic pathway induced by c-Myc. Proc Natl Acad Sci U S A. 1998;95(4):1511-6.
425. Goossens V, Grooten J, Fiers W. The oxidative metabolism of glutamine. A modulator of reactive oxygen intermediate-mediated cytotoxicity of tumor necrosis factor in L929 fibrosarcoma cells. J Biol Chem. 1996;271(1):192-6.
426. Lui VW, Wong EY, Ho K, Ng PK, Lau CP, Tsui SK, et al. Inhibition of c-Met downregulates TIGAR expression and reduces NADPH production leading to cell death. Oncogene. 2011;30(9):1127-34.
427. Yin L, Kosugi M, Kufe D. Inhibition of the MUC1-C oncoprotein induces multiple myeloma cell death by down-regulating TIGAR expression and depleting NADPH. Blood. 2012;119(3):810-6.
428. Jiang P, Du W, Wang X, Mancuso A, Gao X, Wu M, et al. p53 regulates biosynthesis through direct inactivation of glucose-6-phosphate dehydrogenase. Nat Cell Biol. 2011;13(3):310-6.
429. Forastiere A, Weber R, Ang K. Treatment of head and neck cancer. The New England journal of medicine. 2008;358(10):1076; author reply 7-8.
430. Galluzzi L, Kepp O, Vander Heiden MG, Kroemer G. Metabolic targets for cancer therapy. Nat Rev Drug Discov. 2013;12(11):829-46.
431. Ang KK, Zhang Q, Rosenthal DI, Nguyen-Tan PF, Sherman EJ, Weber RS, et al. Randomized phase III trial of concurrent accelerated radiation plus cisplatin with or without cetuximab for stage III to IV head and neck carcinoma: RTOG 0522. Journal of clinical oncology : official journal of the American Society of Clinical Oncology. 2014;32(27):2940-50.
432. Shapiro LQ, Sherman EJ, Riaz N, Setton J, Koutcher L, Zhang Z, et al. Efficacy of concurrent cetuximab vs. 5-fluorouracil/carboplatin or high-dose cisplatin with intensity-modulated radiation therapy (IMRT) for locally-advanced head and neck cancer (LAHNSCC). Oral Oncol. 2014;50(10):947-55.
433. Magrini SM, Buglione M, Corvo R, Pirtoli L, Paiar F, Ponticelli P, et al. Cetuximab and Radiotherapy Versus Cisplatin and Radiotherapy for Locally Advanced Head and Neck Cancer: A Randomized Phase II Trial. Journal of clinical oncology : official journal of the American Society of Clinical Oncology. 2016;34(5):427-35.
434. Patel SG, Lydiatt WM. Staging of head and neck cancers: is it time to change the balance between the ideal and the practical? Journal of surgical oncology. 2008;97(8):653-7.
435. Pettitt AR, Jackson R, Carruthers S, Dodd J, Dodd S, Oates M, et al. Alemtuzumab in combination with methylprednisolone is a highly effective induction regimen for patients with chronic lymphocytic leukemia and deletion

of TP53: final results of the national cancer research institute CLL206 trial. Journal of clinical oncology : official journal of the American Society of Clinical Oncology. 2012;30(14):1647-55.
436. Magno L, Terraneo F, Bertoni F, Tordiglione M, Bardelli D, Rosignoli MT, et al. Double-blind randomized study of lonidamine and radiotherapy in head and neck cancer. Int J Radiat Oncol Biol Phys. 1994;29(1):45-55.
437. Colella E, Merlano M, Blengio F, Angelini F, Ausili Cefaro GP, Scasso F, et al. Randomised phase II study of methotrexate (MTX) versus methotrexate plus lonidamine (MTX + LND) in recurrent and/or metastatic carcinoma of the head and neck. Eur J Cancer. 1994;30A(7):928-30.
438. Dwarakanath BS, Singh D, Banerji AK, Sarin R, Venkataramana NK, Jalali R, et al. Clinical studies for improving radiotherapy with 2-deoxy-D-glucose: present status and future prospects. J Cancer Res Ther. 2009;5 Suppl 1:S21-6.
439. Gillet JP, Varma S, Gottesman MM. The clinical relevance of cancer cell lines. J Natl Cancer Inst. 2013;105(7):452-8.
440. Schwachofer JH, Acker H, Crooijmans RP, Van Gasteren JJ, Holtermann G, Hoogenhout J, et al. Oxygen tensions in two human tumor cell lines grown and irradiated as multicellular spheroids. Anticancer Res. 1991;11(1):273-9.
441. Freyer JP. Role of necrosis in regulating the growth saturation of multicellular spheroids. Cancer research. 1988;48(9):2432-9.
442. Majmundar AJ, Wong WJ, Simon MC. Hypoxia-inducible factors and the response to hypoxic stress. Mol Cell. 2010;40(2):294-309.
443. Semenza GL. HIF-1: upstream and downstream of cancer metabolism. Curr Opin Genet Dev. 2010;20(1):51-6.
444. Tanweer F, Green VL, Stafford ND, Greenman J. Application of microfluidic systems in management of head and neck squamous cell carcinoma. Head Neck. 2013;35(5):756-63.
445. Cheah R, Srivastava R, Stafford ND, Beavis AW, Green V, Greenman J. Measuring the response of human head and neck squamous cell carcinoma to irradiation in a microfluidic model allowing customized therapy. Int J Oncol. 2017;51(4):1227-38.
446. Lu SL, Herrington H, Wang XJ. Mouse models for human head and neck squamous cell carcinomas. Head Neck. 2006;28(10):945-54.
447. Simon C, Nemechek AJ, Boyd D, O'Malley BW, Jr., Goepfert H, Flaitz CM, et al. An orthotopic floor-of-mouth cancer model allows quantification of tumor invasion. The Laryngoscope. 1998;108(11 Pt 1):1686-91.
448. Zhivotovsky B, Joseph B, Orrenius S. Tumor radiosensitivity and apoptosis. Exp Cell Res. 1999;248(1):10-7.
449. Cepeda V, Fuertes MA, Castilla J, Alonso C, Quevedo C, Perez JM. Biochemical mechanisms of cisplatin cytotoxicity. Anticancer Agents Med Chem. 2007;7(1):3-18.
450. Pena-Rico MA, Calvo-Vidal MN, Villalonga-Planells R, Martinez-Soler F, Gimenez-Bonafe P, Navarro-Sabate A, et al. TP53 induced glycolysis and apoptosis regulator (TIGAR) knockdown results in radiosensitization of glioma cells. Radiother Oncol. 2011;101(1):132-9.
451. Comoglio PM, Giordano S, Trusolino L. Drug development of MET inhibitors: targeting oncogene addiction and expedience. Nat Rev Drug Discov. 2008;7(6):504-16.

452. Zaugg K, Yao Y, Reilly PT, Kannan K, Kiarash R, Mason J, et al. Carnitine palmitoyltransferase 1C promotes cell survival and tumor growth under conditions of metabolic stress. Genes Dev. 2011;25(10):1041-51.
453. Yang A, Kaghad M, Wang Y, Gillett E, Fleming MD, Dotsch V, et al. p63, a p53 homolog at 3q27-29, encodes multiple products with transactivating, death-inducing, and dominant-negative activities. Mol Cell. 1998;2(3):305-16.
454. Lee CW, La Thangue NB. Promoter specificity and stability control of the p53-related protein p73. Oncogene. 1999;18(29):4171-81.
455. Zou S, Gu Z, Ni P, Liu X, Wang J, Fan Q. SP1 plays a pivotal role for basal activity of TIGAR promoter in liver cancer cell lines. Mol Cell Biochem. 2012;359(1-2):17-23.
456. Sharma PK, Bhardwaj R, Dwarakanath BS, Varshney R. Metabolic oxidative stress induced by a combination of 2-DG and 6-AN enhances radiation damage selectively in malignant cells via non-coordinated expression of antioxidant enzymes. Cancer Lett. 2010;295(2):154-66.
457. Penkowa M, Quintana A, Carrasco J, Giralt M, Molinero A, Hidalgo J. Metallothionein prevents neurodegeneration and central nervous system cell death after treatment with gliotoxin 6-aminonicotinamide. J Neurosci Res. 2004;77(1):35-53.
458. Bhardwaj R, Sharma PK, Jadon SP, Varshney R. A combination of 2-deoxy-D-glucose and 6-aminonicotinamide induces cell cycle arrest and apoptosis selectively in irradiated human malignant cells. Tumour Biol. 2012;33(4):1021-30.
459. Cuezva JM, Krajewska M, de Heredia ML, Krajewski S, Santamaria G, Kim H, et al. The bioenergetic signature of cancer: a marker of tumor progression. Cancer research. 2002;62(22):6674-81.
460. Isidoro A, Martinez M, Fernandez PL, Ortega AD, Santamaria G, Chamorro M, et al. Alteration of the bioenergetic phenotype of mitochondria is a hallmark of breast, gastric, lung and oesophageal cancer. Biochem J. 2004;378(Pt 1):17-20.
461. Brand KA, Hermfisse U. Aerobic glycolysis by proliferating cells: a protective strategy against reactive oxygen species. FASEB J. 1997;11(5):388-95.
462. Pascual G, Avgustinova A, Mejetta S, Martin M, Castellanos A, Attolini CS, et al. Targeting metastasis-initiating cells through the fatty acid receptor CD36. Nature. 2017;541(7635):41-5.
463. Uphoff CC, Denkmann SA, Drexler HG. Treatment of mycoplasma contamination in cell cultures with Plasmocin. J Biomed Biotechnol. 2012;2012:267678.